FROST ACTION MITIGATION THROUGH ENGINEERED WATER REPELLENCY: UPSCALING FROM LABORATORY TO FIELD APPLICATION

by

Emmanuel Dotun Adeyanju

A dissertation submitted to the faculty of
The University of North Carolina at Charlotte
in partial fulfillment of the requirements
for the degree of Doctor of Philosophy in
Civil Engineering

Charlotte

2024

Approved by

Dr. John L. Daniels

Dr. Vincent O. Ogunro

Dr. Milind Khire

Dr. Bora Cetin (MSU)

Dr. Tara Cavalline

Dr. Yunesh Saulick (uOttawa)

ABSTRACT

EMMANUEL DOTUN ADEYANJU. Frost Action Mitigation Through Engineered Water Repellency: Upscaling From Laboratory to Field Application.
(Under the direction of DR. JOHN L. DANIELS)

This dissertation presents an in-depth investigation into the performance of Engineered Water Repellent (EWR) soils for mitigating frost action, particularly in pavement subgrade applications. EWR involves the permanent bonding of soil particles with organosilanes (OS), a silica-based organic coupling agent that modifies the soil surface without forming bonding properties. This modification is achieved by replacing the -OH groups, which absorb water, with a stable alkyl siloxane. The study evaluates the ability of EWR-treated soils to withstand hydrostatic pressure, both in laboratory breakthrough tests and in the field through capillary rise from high water table. The research bridges the gap between laboratory tests and field applications by optimizing OS concentrations, EWR penetration and placement depth, and its water resistance for creating capillary breaks. Field evaluations were conducted at the MnROAD facility in Minnesota, where two test sections were constructed and monitored. In addition to performance testing, the research includes a comprehensive Life Cycle Assessment (LCA) and Life Cycle Cost Analysis (LCCA) of frost-resistant gravel road treatments and flexible pavements in Minnesota.

The breakthrough pressure (BP) was measured using a modified water-ponding method combined with a triaxial setup and FlowTRAC system for precise volume and pressure control. BP was defined as the pressure at which 0.02 cc of water permeated the soil within one minute. The study evaluates the effects of sustained water pressure and key factors such as density, water-repellent treatment dosage concentration, confining pressure, loading rate, and duration on the water resistance behavior of EWR-treated samples. The impact of extreme environmental conditions, including repetitive loading, repeat wetting-drying, and inundation, on the durability and resistance of hydrophobic soils was assessed. Furthermore, six different soil types were analyzed using various approaches, including mixing at optimum moisture content (OMC) for compacted EWR lifts, and simulated field spraying (at 0.55, 0.33, and 0.22 OS liters/m² on untreated

soils). The results were then used to design a capillary barrier system. A physics-based model was used to calculate the most effective EWR placement depth, positioned between the frost depth and the water table. Contact Angle (CA) tests were performed to determine the optimal OS dosage required for each soil. The study also evaluates the performance of EWR-treated samples under various environmental conditions, including air drying, cyclic wet-dry (W-D) cycles, and prolonged immersion, by assessing their unconfined compressive strength (UCS). X-ray scans were used to analyze porosity changes and internal pore structures after exposure to drastic environmental conditions.

Two field test sections were constructed and instrumented at the MnROAD facility in Otsego, MN, where a commercially available organosilane was sprayed at three different depths at predetermined rates. These test cells were instrumented to monitor soil volumetric water content, temperature, suction, frost heave-thaw settlement, and pavement quality. The study also evaluated typical gravel roads (2-lane, 1-mile) and four frost-resistant alternatives using Life Cycle Assessment (LCA) and Life Cycle Cost Analysis (LCCA). The scenarios included standard gravel (regraded), gravel with a macadam base, chemically stabilized roadstone, and two EWR treatments (spray and compacted). Primary data were collected from the County Engineering Office, with LCA modeling performed using the FHWA LCA PAVE tool, and economic impact was assessed via Net Present Value (NPV) following ISO 15686-5 standards. A similar study was conducted for the MnROAD test sections, evaluating the environmental and economic impacts of typical flexible pavement structures used in Minnesota, as well as three EWR-treated variants. The LCCA was performed using MnDOT's tool to calculate NPV, following ISO 15686-5 standards.

The study revealed that soil densification and molding moisture content play significant roles in enhancing BP, increasing from 7.4 kPa to 21.25 kPa (a threefold increase) when comparing loosely (13.2 kN/m^3) to densely (14.69 kN/m^3) compacted soils. Additionally, as the fine content decreased from 100% to 63%, BP values dropped threefold. Confining pressure also significantly influenced BP, indicating changes in hydraulic conductivity and interparticle voids. The curing period was crucial, with BP increasing over seven days. The results showed that increasing the loading rate reduced BP, while increasing the time

interval between loading steps significantly improved the soil's resistance to water infiltration. After durability testing, BP values decreased due to microstructural changes and unused OS. UCS results showed that OS treatment reduced the optimum moisture content (OMC) while having minimal impact on maximum dry density (MDD). However, mechanical strength decreased as OS concentration increased, likely due to the organic moiety of the OS molecule (siloxane bond formation), which reduced compressive strength. Despite this, EWR-treated soils maintained structural integrity during extended immersion, with higher OS concentrations offering better resistance to W-D cycles. Over 120 days of soaking, both soils experienced strength reductions of up to 98% due to increased porosity and excess unbound OS. X-ray analysis confirmed volumetric changes correlated with water infiltration and pore expansion. While EWR enhanced moisture resistance, a reduction in mechanical strength was observed.

CA test results showed that lower OS concentrations decreased CA values, but they remained above 90° (hydrophobic) for most soils at a 1:40 (OS: Soil) ratio. Sprayed CA tests showed penetration depths were generally limited to less than 2 mm for soils at OMC but increased to 4.2 mm for air-dried and 4.7 mm for oven-dried samples, indicating that drier conditions enhance OS penetration. BP testing, simulating field water pressures, revealed that higher OS concentrations (0.55 liters/m^2) provided the greatest water resistance. However, limitations in penetration depth and molding solution volume pose challenges for field applications. The study concludes that while laboratory tests provide valuable insights into OS application efficiency, real-world conditions require adjustments to OS concentrations and application methods to achieve optimal hydrophobic performance.

Field simulations showed that a 50% reduction in frost heave was achieved at a placement depth of 1.2 meters. Preliminary results indicated that treated sections experienced settlement and maintained consistent volumetric water content, while control sections showed measurable heave and full saturation. The study presents a methodology for utilizing EWR as an engineering solution for moisture migration mitigation within pavement structures alongside relevant field performance assessments. Gravel roads treated with chemical stabilizers emerged as the most sustainable and cost-effective option, with regrade

being 45% more expensive and generating 47% more emissions. OS-related activities in EWR-treated gravel roads accounted for 13-20% of emissions and 34-49% of total costs. In the flexible pavement LCCA and LCA evaluation, the MnDOT Soil Replacement Method (SRM) with EWR showed a 23% reduction in global warming potential (GWP) compared to traditional SRM methods. OS-related activities accounted for 10% of the total emissions in EWR variants and 14% of the total costs, including excavation and granular material.

For field applications, several questions remain, including optimizing OS to improve efficiency and reduce costs. Although OS-treated soils are expected to be non-leachable, further testing should include leaching experiments before and after activation. Drying time optimization for field applications should also be explored to ensure effective EWR treatment. Future studies should investigate combining EWR with other methods, such as wicking fabrics, to manage near-surface moisture content more effectively. Additional field tests across different soil types and environmental conditions are necessary to further validate the performance and application of EWR treatments.

ACKNOWLEDGMENTS

To the One to whom I belong and whom I serve, my Lord and Savior, Jesus Christ, and our Almighty Father, the giver of life, I offer my deepest gratitude. To His most Holy Spirit, I remain eternally thankful for blessings beyond what words can express.

My overwhelming appreciation goes to my advisor, Dr. John L. Daniels, for his firm support, invaluable guidance, and steadfast support throughout my academic endeavor at UNC at Charlotte. I also extend my sincere gratitude to the distinguished members of my dissertation committee, Dr. Vincent O. Ogunro, Dr. Milind Khire, Dr. Bora Cetin, Dr. Yunesh Saulick, and Dr. Tara Cavalline—for their insightful feedback and meaningful contributions to my research. Their expertise and thorough reviews have significantly enhanced the excellence and depth of my work.

A heartfelt thank you also goes to my supervisor at MnDOT, Dr. Emil Bautista, and the MnDOT and MnROAD teams, including Dr. Raul Velasquez, Dr. Bernard Izevbekhai, Jacob Calvert, Steven Olson, and Daniel Roushar. I deeply appreciate their support and technical assistance throughout this research. Similarly, I am grateful to the engineers and technical staff of the Keokuk County Engineer's Office, especially Andrew J. McGuire, P.E., for providing data and valuable technical support.

I would also like to express my sincere appreciation to Daniels Research Lab team—Dr. Micheal Uduebor, Adams Familusi, Dr. Rui He, and Mackenzie—for creating a collaborative and supportive research environment. Their friendship, insightful conversations, and knowledge have been instrumental in advancing my growth as a researcher.

I am grateful for the financial support that enabled this research such as the National Science Foundation (NSF) and the Iowa Highway Research Board (IHRB) awards. Also, the National Road Research Alliance (NRRA) deserves special recognition for their funding contributions.

Finally, I appreciate my family for their moral and financial support. I say a big thank you and God bless you.

DEDICATION

To God and that stubborn aunty, Atinuke.

TABLE OF CONTENTS

LIST OF TABLES

LIST OF FIGURES

LIST OF ABBREVIATIONS

AASHO - American Association of State Highway Officials

AASHTO - American Association of State Highway and Transportation Officials

ASTM - American Society for Testing and Materials

BP - Breakthrough testing

CA - Contact angles

CBR - California Bearing Ratio

CPD - Control Pavement Design

CRM - Capillary rise methods

CST - Critical surface tension

DOT - Department of Transportation

EC - Electrical conductivity

EPS, XPS - Polystyrene

ESALs - Equivalent Single-Axle Loads

EWR - Engineered Water Repellency

FFM – “Frost-Free” Material

FWD - Falling weight deflectometer.

FHWA - Federal Highway Administration

FSS - Frost-susceptible soil

GCBD - Geocomposite capillary barrier drain

GWP - Global Warming Potential

GCE - Generalized Clapeyron Equation

HDPE: High-Density Polyethylene

HRBC - Highway Research Board Committee

JDAAF - Joint Departments of the Army and Air Force USA

LCA - Life Cycle Assessment

LCCA - Life Cycle Cost Analysis

LVR - Low-Volume Road

MDUW - Maximum Dry Unit Weight

MED - Molarity of an Ethanol Drop test.

MICP - Microbially induced carbonate precipitation.

Mn - Minnesota

MnDOT - Minnesota Department of Transportation

NCHRP - National Cooperative Highway Research Program

NPV - Net Present Value

NFSS - Non-frost susceptible soil

HMA - Hot Mix Asphalt

OMC - Optimum moisture content

OS - Organo-silanes

PU - Polyurethane

RAP - Recycled Asphalt Pavement

SDM - Sessile drop methods

SFCC - Soil Freezing Characteristics Curve

SRM - Soil Replacement Method

SWCC - Soil Water Characteristic Curve

SWR - Soil Water Repellency

TRIP - The Road Information Program

UCS: Unconfined Compressive Strength

USACE - U.S. Army Corps of Engineers

USCS - Unified Soil Classification System

W-D: Wet-Dry

WDPT - Water drop penetration test.

WEP - Water Entry Pressure

WP - water-ponding method

X-ray CT: X-ray computed tomography.

CHAPTER 1: INTRODUCTION

1.1 Background

Frost action, the combination of frost heaving and frost boil displayed in Figure 1.1, is an international problem encountered in temperate regions, causing pavement distress and significant road damage because of continuous changes in pavement resilient modulus. From the American Association of State Highway Officials (AASHO) Road Test, Oman and Lund (2018) discovered that frost action accounted for 60 % of pavement failure during spring. According to the Federal Highway Administration [FHWA] (1999), The Road Information Program [TRIP] estimates that frost action-related damage costs the USA about two billion dollars annually in maintenance (FHWA, 1999). Similarly, another FHWA reported that 20 % of the Department of Transportation [DOT] budget goes to winter road maintenance (FHWA, 2023). To extend pavement life and reduce maintenance costs, different countries and DOTs utilize spring load restrictions of up to 50 %, which extend the useful life of asphalt roads (up to 95 %) (USACE, 1993; Ovik et al., 2000; Kestler et al., 2007; Daniel et al., 2017) but impose significant economic costs on road users (Levinson, 2005). Furthermore, when sustainability is considered, the cost is higher, as maintenance of roads contributes 5 to 6 % of the total greenhouse pollution throughout the lifecycle of a road (Wu et al., 2014).

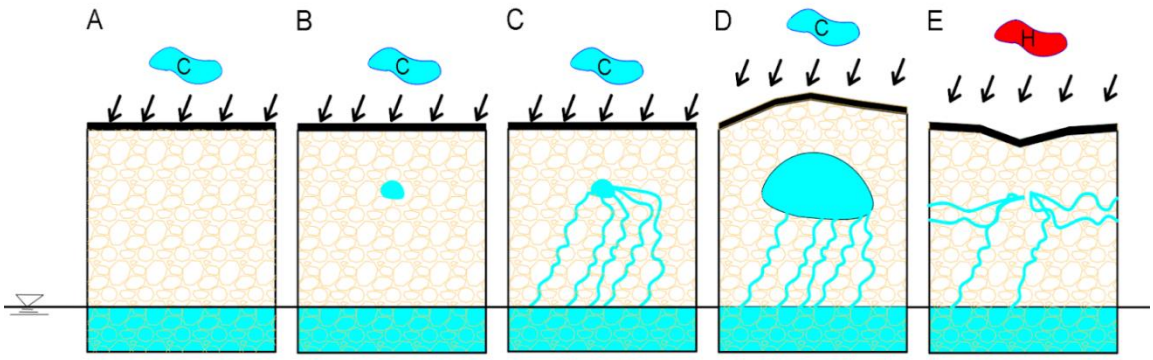

Figure 1.1: Frost action in the pavement.

While the detrimental impact (pavement deflection, cracks, stone splinters, etc.) on engineering structures is well documented (White & Coree, 1990; St-Laurent & Roy, 1995; Janoo, 2002; Dore, 2004), there are still many unknowns about ice lens growth. Studies have shown that several factors influence ice

lens development, including soil properties (i.e., particle size distribution, porosity, and permeability), temperature gradients, and water availability (Linell & Kaplar, 1959; Chamberlain, 1981; Lai et al., 2014; Bing et al., 2015; Naqvi et al., 2022; Sadiq et al., 2023). It is widely recognized that three fundamental conditions are required for frost action to occur: the presence of frost-susceptible soil (FSS), surface temperatures that fluctuate above and below 32°F (0°C), and sufficient water availability for the formation of ice lenses. Consequently, several models have been developed to quantify frost heave and thaw weakening (frost boils), with varying levels of success.

While a fully validated model for ice lens formation does not exist, there are various mitigation methods currently used to prevent or mitigate frost action; with diverse approaches and several critical limitations (Zhang et al., 2014; Edgar et al., 2015; Zornberg et al., 2017; Guo et al., 2018; Galinmoghadan et al., 2019; Gowthaman et al., 2020; Baldovino et al., 2021; Nourmohamadi et al., 2022). Accordingly, developing an alternative mitigation method that can be applied to various engineering projects is essential. One such approach is Engineered Water Repellency (EWR) which can be implemented with conventional expertise and equipment. A laboratory study by Uduebor et al. (2022) demonstrated the potential of EWR to prevent associated road damage effectively by hindering moisture migration, as displayed in Figure 1.2. However, studies on the field application of EWR still need to be conducted. EWR is an engineered soil layer that is water-repellent, i.e., hydrophobic. Soil becomes hydrophobic when treated with organo-silanes (OS) (Daniels et al., 2009; Jerez et al., 2018; Mahedi et al., 2020). OS is a silica-based organic coupling agent that covers soil particles without rendering any interparticle bonding.

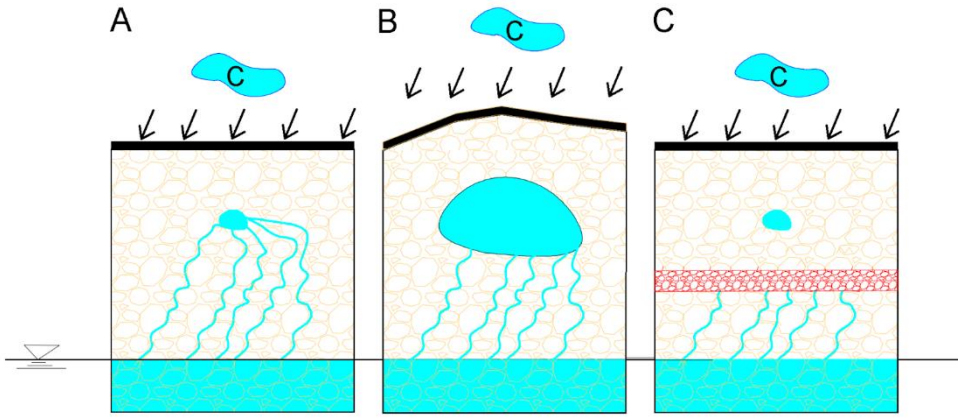

Figure 1.2: EWR methodology.

Unfortunately, there is no standardization on the testing and characterizing of hydrophobic soils because it is an emerging field for frost heave mitigation. Even though naturally occurring hydrophobicity has been well documented, the closest existing methodologies are geared towards materials such as sand (Leelamanie & Karube, 2012; Bachmann et al., 2013; Wijewardana et al., 2015; Movasat & Tomac, 2021), glass beads (Xing et al., 2020; Huang & Gates, 2020) or Fly Ash (Feyyisa et al., 2017; Keatts et al., 2018), which differ immensely from silty or frost susceptible soils [FSS]. Furthermore, these tests are not performance-based testing; hence, the need to develop Water Entry Pressure (WEP) testing and cast as field application indices. Different studies have shown that WEP depends on density, OS concentration, and fines content; however, there is no correlation between WEP and other hydrophobic tests for FSS.

Therefore, this study will examine different field trial runs based on laboratory testing to evaluate EWR performance and optimize its potential application for frost mitigation. Optimizing EWR for frost heave mitigation depends on the depth of placement and OS application; this will be achieved through a Physics-based Model and statistical analysis of frost depth to create an optimized EWR placement model. Furthermore, a life cycle assessment of frost action and different mitigation methods, including EWR, will be done.

1.2 Research Hypothesis

Although different laboratory experiments (Uduebor et al., 2022) and setups have indicated the potential of EWR transforming FSS to frost-resistant soil, upscaling laboratory work to field implementation is yet to be carried out to evaluate the performance of EWR under real-time seasonal conditions. This research primarily aims to evaluate organo-silane (OS) used to mitigate frost heave-thaw settlement of frost susceptible soils under granular and flexible roadways. Understanding the underlying principles that would affect future applications of EWR in different engineering projects, especially granular roadways, is necessary.

Hypothesis (1) states that water-repellent additives (OS) reduce frost heave-thaw settlement.

- Sub-hypothesis (1a) is that EWR will hinder water movement into the ice lens.
- Sub-hypothesis (1b) is that the EWR will continuously be water-repellent independent of changes in seasonal weather and capillary rise.

Hypothesis (2) states that EWR is a more viable option than other mitigation methods.

- Sub-hypothesis (2a) is that EWR application will ensure soil stiffness stability year around.
- Sub-hypothesis (2b) is that the EWR application on the field will remain more viable than alternative methods.

To test these hypotheses, this research study will focus on these central themes:

EWR placement depth optimization

- Determine optimal dosage for field acceptance based on cost, maximum repellency, and field application constraints.

- Determine the optimal placement depth for EWR and explore the correlation between laboratory results and field performance to enhance the design.

Life Cycle Assessment (LCA)

· Explore the LCA of EWR and alternatives methods.

· Evaluate the cost-effectiveness of EWR compared to other common frost mitigation methods used by State Departments of Transportation (DOTs)

1.3 Intellectual Merit

This research highlights that densification is as critical to the performance of engineered water repellency (EWR) as the organosilane treatments used to induce hydrophobicity. Furthermore, the study emphasizes the importance of connecting laboratory tests—such as contact angle (CA) and breakthrough pressure (BP) testing—with physics-based modeling to optimize the placement depth for field applications. Lessons learned from both lab testing and field trials have led to significant insights into improving EWR technology. Preliminary results demonstrate that EWR can effectively mitigate frost action, building upon small-scale control tests conducted thus far. EWR shows potential to enhance the performance, economic efficiency, and service lifespan of granular roads through frost action mitigation. Additionally, this research explores whether organosilane (OS) treatment offers a cost-effective solution for counties and departments of transportation (DOTs). The findings from this project will provide a valuable foundation for developing decision-making tools to optimize mitigating frost action.

1.4 Dissertation Outline

This dissertation includes several chapters which successively serve to upscale from the laboratory toward field application of engineered water repellency. The chapters that follow are structured as outlined below:

Chapter 2: Literature Review (page 13). This chapter provides a comprehensive historical background on frost action, highlighting the primary factors influencing ice lens growth and the criteria for ice lens initiation. The review also explores existing frost action mitigation techniques, their limitations, and presents engineered water repellency (EWR) as an innovative alternative. Additionally, the chapter discusses the principles and methods behind hydrophobic soil treatments. The chapter concludes by identifying critical knowledge gaps in the current body of research, setting the stage for further investigation.

Chapter 3: Performance Evaluation of Hydrophobic Soils **(2 Articles, page 66)**

This chapter presents an in-depth performance evaluation of hydrophobic soils, with a focus on their water resistance and mechanical behavior through experimental testing. The chapter encompasses the following articles:

Article 1: Factors Affecting the Water Resistance of Frost-Susceptible Hydrophobic Soils.

This study investigated the water resistance performance of engineered water-repellent (EWR) soils under hydrostatic pressure, specifically measured through breakthrough pressure (BP). The research explores the effects of sustained water pressure and key factors such as soil density, water-repellent treatment dosage, confining pressure, loading rate, and duration on the behavior of EWR-treated soils. Additionally, the durability of these soils is evaluated under extreme environmental conditions, including repetitive loading, cyclic wetting-drying, and prolonged inundation.

Article 2: Investigation of the Compressive Strength of Engineered Water-Repellent Soils Under Varying Environmental Conditions.

This study assesses the compressive strength of EWR-treated soils (IA-BV and MnRD) under different environmental stressors, including air drying, cyclic wetting-drying (W-D) cycles, and extended immersion. X-ray scans are employed to analyze changes in porosity and internal pore structure following exposure to these conditions. The study provides critical insights into the structural integrity of EWR-treated soils under real-world environmental exposures.

Chapter 4: FIELD EVALUATION OF ENGINEERED WATER REPELLENCY. (2 Articles, page 142).

This chapter bridges the gap between laboratory testing and field implementation, focusing on the design philosophy and construction of active test sites at MnROAD. It outlines the design, construction methodology, sensor instrumentation plan, and current results from the most recent frost action monitoring.

Article 1: Translating Laboratory Water Repellency Tests to Field Design: Developing a Capillary Break System for Frost Action Mitigation in Pavement Foundations at MnROAD.

This study focuses on optimizing organosilane (OS) applications for field conditions, using contact angle (CA) measurements and breakthrough pressure tests. Both compaction and spray methods for applying the OS treatments were simulated, with the breakthrough pressure results guiding the design of a capillary barrier system. The field design aims to mitigate frost action by enhancing water resistance in the subgrade.

Article 2: Design and Construction of Engineered Water Repellency (EWR) at MnROAD

This study demonstrates how frost action can be mitigated through the application of EWR to reduce large deformations in frost-susceptible soils. The research uses a physics-based model to determine the optimal depth for placing the EWR treatment, targeting the area between the frost line and water table. Two test sections were constructed and instrumented at MnROAD's low-volume road facility in Otsego, MN, to monitor key performance indicators such as volumetric water content, temperature, matric suction, frost heave-thaw settlement, and overall pavement quality.

Chapter 5: Life Cycle Assessment (LCA) and Life Cycle Cost Analysis (LCCA) of EWR Applications (2 Articles, page 209).

This chapter presents the environmental and economic evaluations of frost action mitigation methods using Life Cycle Assessment (LCA) and Life Cycle Cost Analysis (LCCA) techniques based on actual field test sites constructed at Iowa and MnROAD. It highlights the environmental impact and cost of EWR treatments, providing insights into their long-term viability.

Article 1: Comparative LCA and LCCA of Frost-Resistant Gravel Road Treatments in Rural Iowa

This study evaluates the environmental and economic impacts of various frost-resistant gravel road treatments over a typical two-lane, one-mile road section. The alternatives considered include standard gravel (regrade), gravel with a macadam base, chemically stabilized roadstone, and two EWR treatments (sprayed and compacted). Primary data were gathered from local county engineering offices, and the LCA was modeled using the FHWA LCA PAVE tool. The LCCA, performed following ISO 15686-5, provides a comprehensive comparison of the economic and environmental costs.

Article 2: Environmental and Economic Assessment of Engineered Water Repellency for Frost Mitigation in Low-Volume Flexible Pavements in Minnesota

This study evaluates the environmental and economic performance of standard flexible pavements in Minnesota, alongside three variations treated with EWR. Using the MnDOT LCCA tool, Net Present Value (NPV) was calculated in compliance with ISO 15686-5. The study was modeled after test sections in Cells 2305 and 2306 at MnROAD's low-volume road (LVR) facility, offering insights into the long-term benefits of EWR in frost-prone regions.

The research presented in these chapters advances the understanding of EWR for mitigating frost action in field applications, providing a foundation for future innovations in pavement foundation design.

1.5 Reference

Adeinola, O.S., & Nnochiri, E.S. (2017). Stabilizing lateritic soil using terrasil solution. SSP - Journal of Civil Engineering. 12(1), 19–27. DOI: 10.1515/sspjce-2017-0002.

Bachmann, J., Goebel, M. O., & Woche S. K. (2013). Small-scale contact angle mapping on undisturbed soil surfaces. Journal of Hydrology and Hydromechanics. 61:3–8. DOI:10.2478/johh-2013-0002.

Daniels, J. L., & Hourani, M. S. (2009). Soil Improvement with Organo-Silane. American Society of Civil Engineers U.S.-China Workshop on Ground Improvement Technologies 2009 - Orlando, Florida, United States (March 14, 2009) Advances in Ground Improvement. 217–224. doi:10.1061/41025(338)23.

de Jesús Arrieta Baldovino, J., dos Santos Izzo, R. L., & Rose, J. L. (2021). Effects of Freeze–thaw Cycles and Porosity/cement index on Durability, Strength and Capillary Rise of a Stabilized Silty Soil Under Optimal Compaction Conditions. Geotechnical and Geological Engineering, 39(1), 481–498. https://doi.org/10.1007/S10706-020-01507-Y/FIGURES/12.

Drelich, Jaroslaw W. (2019). Contact angles: From past mistakes to new developments through liquid-solid adhesion measurements. Advances in Colloid and Interface Science, (), S0001868618303658–. DOI:10.1016/j.cis.2019.02.002.

Edgar, T., Potter, C., & Mathis, R. (2015). Frost Heave Mitigation Using Polymer Injection and Frost Depth Prediction. Proceedings of the International Conference on Cold Regions Engineering, 2015-January (January), pp. 416–427. https://doi.org/10.1061/9780784479315.037.

Feyyisa, J. L., Daniels, J. L., & Pando, M. A. (2017). Contact Angle Measurements for Use in Specifying Organosilane-Modified Coal Combustion Fly Ash. Journal of Materials in Civil Engineering, 29(9). https://doi.org/10.1061/(asce)mt.1943-5533.0001943.

FHWA (1999). A Quarter Century of Geotechnical Research, Chapter 4: Soil and Rock Behavior. Federal Highway Administration (FHWA), Report Number: FHWA-RD-98-139, Turner-Fairbank Highway Research Center, McLean, VA, USA.

Galinmoghadan, J., Zhang, X., & Lin, C. (2019). A Bio-Wicking System to Prevent Frost Heave in Alaskan Pavements: Phase II Implementation. https://scholarworks.alaska.edu/handle/11122/10746.

Guo, F., Shi, H., Cheng, M., Gao, W., Yang, H., & Miao, Q. (2018). A study of polystyrene boards' insulation mechanism and anti-frost heave effects in seasonal frozen soil. Water (Switzerland), 10(8). https://doi.org/10.3390/W10080979.

Gowthaman, S., Nakashima, K., & Kawasaki, S. (2020). Freeze-thaw durability and shear responses of cemented slope soil treated by microbial induced carbonate precipitation. Soils and Foundations, 60(4), 840–855. https://doi.org/10.1016/J.SANDF.2020.05.012.

Huang, X., Gates, I. (2020). Apparent Contact Angle around the Periphery of a Liquid Drop on Roughened Surfaces. Sci Rep 10, 8220. https://doi.org/10.1038/s41598-020-65122-w.

Keatts, M. I., Daniels, J. L., Langley, W. G., Pando, M. A., & Ogunro, V. O. (2018). Apparent Contact Angle and Water Entry Head Measurements for Organo-Silane Modified Sand and Coal Fly Ash. Journal of Geotechnical and Geoenvironmental Engineering, 144(6). https://doi.org/10.1061/(asce)gt.1943-5606.0001887.

Jerez, Laura Daniela; Gómez, Orlando Elías; Murillo, & Carol Andrea. (2018). Stabilization of Colombian lateritic soil with a hydrophobic compound (organosilane). International Journal of Pavement Research and Technology, S1996681417302213 doi: 10.1016/j.ijprt.2018.06.001.

Leelamanie, D.A.L., & J. Karube. (2012). Drop size dependence of soil-water contact angle in relation to the droplet geometry and line tension. Soil Sci. Plant Nutr. 58, 675–683. doi:10.1080/00380768.2012.745798.

Liyanage, T.D.P. & Leelamanie, D.A.L. (2016). Influence of organic manure amendments on water repellency, water entry value, and water retention of soil samples from a tropical Ultisol. Journal of Hydrology and Hydromechanics, 64(2), 160-166. https://doi.org/10.1515/johh-2016-0025.

Mahedi, M., Satvati, S., Cetin, B., & Daniels, J. L. (2020). Chemically Induced Water Repellency and the Freeze–Thaw Durability of Soils. Journal of Cold Regions Engineering, 34(3). https://doi.org/10.1061/(asce)cr.1943-5495.0000223.

Movasat M, Tomac I. (2021). Assessment of physical properties of water-repellent soils. J Geotech Geoenviron Eng 147:06021010. https://doi.org/10.1061/(asce)gt.1943-5606.0002604.

Nourmohamadi, M., Abtahi, S. M., Hashemolhosseini, H., & Hejazi, S. M. (2022). Control of frost effects in susceptible soils using a novel sandwich geocomposite composed of geotextile-soil-nano silica aerogel-geotextile liners. Transportation Geotechnics, 33, 100718. https://doi.org/10.1016/J.TRGEO.2022.100718.

Oman, M. S., & Lund, Neil G. (2018). Designing Base and Subbase to Resist Environmental Effects on Pavements – (MN/RC 2018-06). Minnesota Department of Transportation Research Services & Library 395 John Ireland Boulevard, MS 330 St. Paul, Minnesota 55155-1899. http:// mndot.gov/research/reports/2018/201806.pdf.

Saulick, Y., Lourenço, S. D. N., & Baudet, B. A. (2017). A Semi-Automated Technique for Repeatable and Reproducible Contact Angle Measurements in Granular Materials using the Sessile Drop Method. Soil Science Society of America Journal, 81(2). https://doi.org/10.2136/sssaj2016.04.0131.

Uduebor M., Adeyanju E., Saulick Y., Daniels J., Cetin B. (2022). A review of innovative frost heave mitigation techniques for road pavements. International Conference on Transportation and Development 2022, Pavements Wei H American Society of Civil Engineers Reston, VA, USA, pp. 95, 106. https://ascelibrary.org/doi/10.1061/9780784484357.009.

Wijewardana, N.S., K. Kawamoto, P. Moldrup, T. Komatsu, L.C. Kurukulasuriya, & Priyankara, N. H. (2015). Characterization of water repellency for hydrophobized grains with different geometries and sizes. Environ. Earth Sci. 74:5525–5539. doi:10.1007/s12665-015-4565-6.

Wu, P. Xia, Bo. & Zhao, Xianbo. (2014). The importance of use and end-of-life phases to the life cycle greenhouse gas (GHG) emissions of concrete – A review. Renewable and Sustainable Energy Reviews, 37, 360–369. doi: 10.1016/j.rser.2014.04.070.

Xing, Y. Zhang, Youfei. Ding, S. Zheng, Xi. Xu, Mengdi. Cao, Yijun. & Gui, Xiahui. (2019). Effect of surface roughness on the detachment between bubble and glass beads with different contact angles. Powder Technology, S0032591019309994–. doi: 10.1016/j.powtec.2019.11.040.

Zhang, X., Presler, W., Li, L., Jones, D., & Odgers, B. (2014). Use of Wicking Fabric to Help Prevent Frost Boils in Alaskan Pavements. Journal of Materials in Civil Engineering, 26(4), 728–740. https://doi.org/10.1061/(ASCE)MT.1943-5533.0000828.

Zornberg, J. G., Azevedo, M., Sikkema, M., & Odgers, B. (2017). Geosynthetics with enhanced lateral drainage capabilities in roadway systems. Transportation Geotechnics, 12, 85–100. https://doi.org/10.1016/J.TRGEO.2017.08.008.

CHAPTER 2: LITERATURE REVIEW

2.1 Introduction

Frost action, a combination of heaving and thawing, accounts for more than 60 % of pavement distress in temperate regions (Oman & Lund, 2018), which occurs when there is a subfreezing temperature, frost-susceptible soil (FSS) and water supply near the ground surface. This damage is due to the alternating cycle of ice lens continuous growth in spring and the subsequent thawing in summer and results in continuous seasonal variation of subgrade and base course modulus (Richter, 2006; Papuc, 2021), as illustrated in Figure 2.1. Different theories were formulated to explain ice lens formation development and growth; however, our understanding of mechanisms around the ice lens is still lacking.

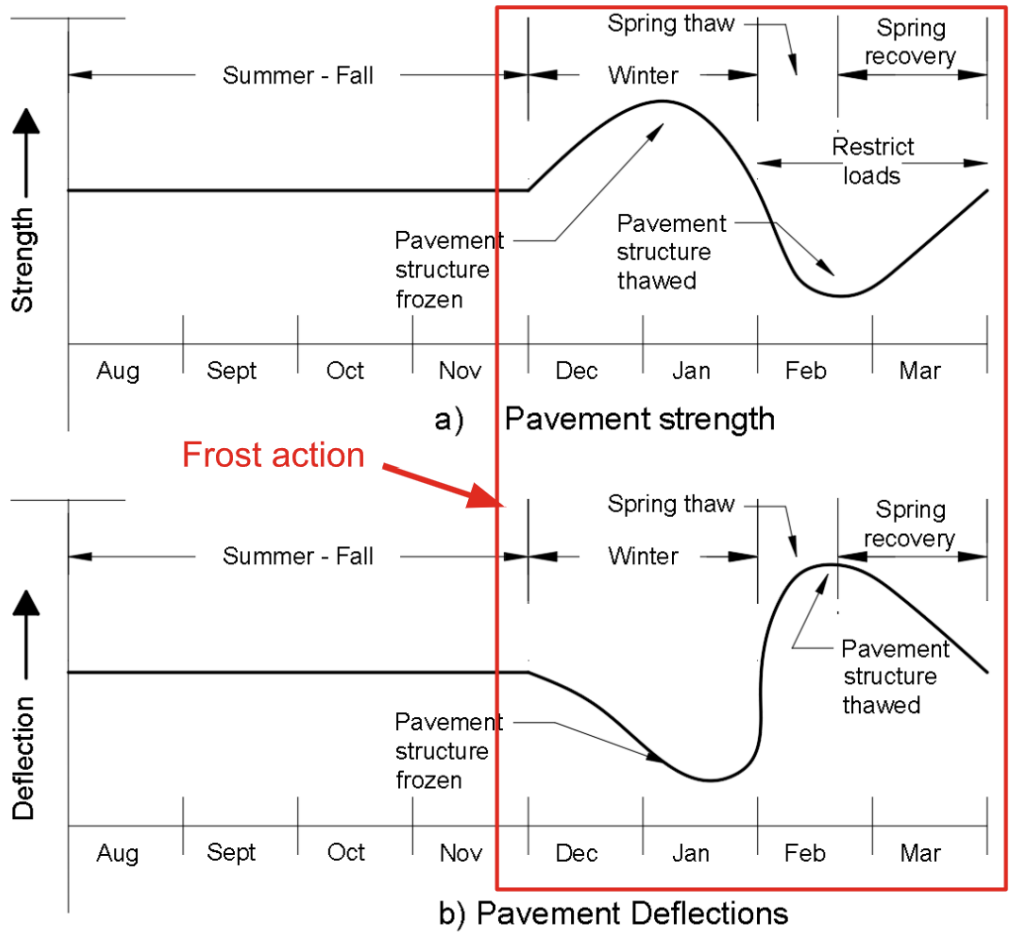

Figure 2.1: Typical Pavement seasonal changes (Adapted from Mahoney et al., 1986).

There are currently a handful of mitigation methods, such as hindering water supply, reducing frost depth and frost action impact, replacing FSS, or increasing subgrade stiffness, to prevent frost action

(Mackey et al., 1992; Uduebor et al., 2022). However, these methods suffer from different corresponding pitfalls, including increased energy consumption, raw materials, and greenhouse gas emissions, making these methods expensive and unsustainable.

There is a need to understand how to incorporate EWR into engineering design to solve different engineering problems relating to moisture content variation. To achieve this, there is a need to develop a testing protocol and standardization index, which can be directly used in engineering design. Furthermore, there is no environmental impact assessment for frost action impact on pavement. Furthermore, the life cycle analysis of all possible methods, including EWR, must provide a sustainability benchmark.

This chapter highlights the historical perspective of frost action, the three fundamental conditions essential for it, and the existing methodology used to mitigate it. In addition, a critical appraisal of ice lens initiation and growth was performed. Lastly, the EWR application, its existing testing methodologies, and Life Cycle Analysis (LCA) were evaluated.

2.2 Historical Background of Frost Action

Frost action has been documented as far back as the 1600s and was referred to as “pipkrake” and “freezing up of stones from the ground” (Beskow, 1935, p. no 1). Although it was not understood, it was observed and documented (Hiarne, 1694; Runeberg, 1765, cited in Beskow, 1935). Frost action is the combination of frost heave and frost boil, i.e., the effect of freezing and thawing in soils (U.S. Army Corps of Engineers [USACE], 1984). Frost heave is the rising of the ground surface due to the formation and growth of ice lenses within the soil strata. In contrast, frost boil is the softening and loosening of upper soil layers during thawing, resulting in the settlement as segregated ice melts (USACE, 1984).

The demand for highways in the 20th century due to the automobile boom, especially in the north temperate region, necessitated understanding the mysteries of frost action because of highway pavement distresses. Earlier works started from field observations to laboratory experiments and later to modeling. They focused on the fundamental mechanism behind frost action. Field observation by Taber (1916, 1918a,

b) showed that heaving was due to ice segregation of water from the unfrozen zone against just the in-situ moisture content and supported by other studies (e.g., Wyckoff, 1918). This marks the first fundamental understanding of frost heaving. Further laboratory studies (Taber, 1928 and 1930) showed that frost heave developed in the direction of heat loss and started the concept of frozen fringe theory. In 1931, the generally accepted Criterion of FSS was introduced (Casagrande, 1931). Other fundamental concepts were introduced by Beskow (1935), which include the establishment of the similarities between soil freezing and soil drying, i.e., water evaporation in soil drying is like ice formation occurring in soil freezing and presented a soil freezing characteristics curve (SFCC) and instituted the impact of capillary action on the frost action.

In the 1950s and 1960s, different mechanisms of frost heaving were proposed but significantly failed to explain it, as most of these mechanisms were based on Taber's concept, explained from different perspectives, such as kinetics of solidification (Jackson & Chalmers, 1958), surface tension at the ice and water interface (Gold, 1957), and osmotic effect (Cass & Miller, 1959). Everett (1961) initiated the capillary theory of water migration and concluded that the maximum heaving pressure depends on pore size and the interfacial energy between ice and water. This mechanism ignored the soil particle surface effects. i.e., only focused on mechanical equilibrium. This theory, also called primary heave, consists of an ice lens resting on unfrozen soil. Water flows from the unfrozen soil into the ice, as shown in Figure 2.2. In this theory, no frozen fringe exists, and all heave results in a surface bulge that overestimates the frost heave.

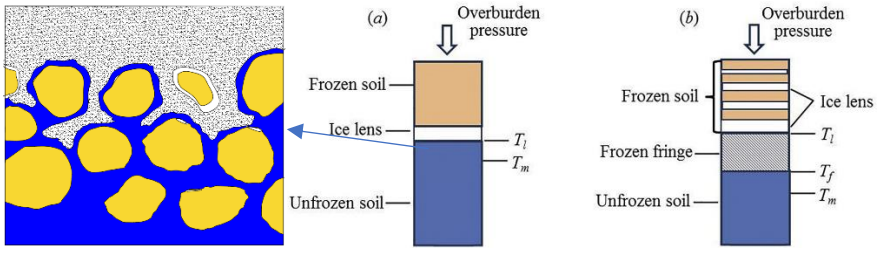

Figure 2.2: Schematic of freezing soils without (a) and with (b) a frozen fringe. ("T_m is the freezing point of bulk water, T_f is the temperature at the freezing front, and T_l is the temperature at the warmer boundary of the warmest ice lens" -adapted from Zhou & Wei, 2020)

That study highlighted the role of water migration earlier, mentioned by Taber, as the reason for frost action, as water needs to keep flowing to the ice for frost heaving. This led to subsequent studies focusing on water migration to explain frost heave (Harlan, 1973; Taylor & Luthin, 1978; Michalowski, 1993; Michalowski & Zhu, 2006). However, they all still have significant limitations in explaining frost action. For instance, Harlan's model requires "tuning," i.e., an arbitrary correction function to modify the model for the current condition. Studies such as Miller et al. (1960) and Miller et al. (1975) improved Everett's thermodynamics analysis and utilized the generalized Clapeyron equation (GCE) to account for the osmotic effect. Within this period, the resultant movement of soil particles as the ice grows became the center of attention (Koopmans & Millet, 1966; Romkens & Miller, 1973; Dirksen & Miller, 1966).

These studies introduced regelation to explain soil particles' movement. Regelation is ice melting, moving around soil grains through the absorbed films, and refreezing (Henry, 2000), as shown in Figure 2.3. Within this period, the fringe theory also called the secondary heave theory, introduced ice beneath the ice lens moved by relegation (Miller, 1977). This theory was somehow confirmed by Loch and Miller (1975) (as cited in Black, 1991). Building on the fringe theory practicality, the rigid ice model was established (Miller, 1978; O'Neill & Miller, 1985), forming the basis for models such as Sheng (1994) – PC-Heave. Other researchers developed models, including (Gilpin, 1980; Konrad & Morgenstern, 1980; Nixon, 1991), which gained varied levels of popularity. All these models do not have thermo-hydro-mechanical interaction and assume freezing soil as incompressible, i.e., only heat and mass transport are examined. Also, most of these models require specific thermodynamic inputs such as segregation-freezing temperature Ts and the frozen fringe permeability.

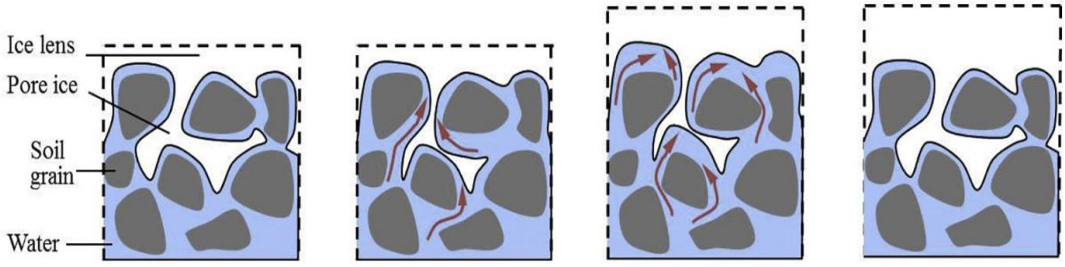

Figure 2.3: Regelation in the frozen fringe (Adapted from Zhou & Wei, 2020).

The frozen fringe is the zone of an interconnected network of pore ice, extending from the warmest ice (i.e., deepest ice) to the frost depth or where ice has penetrated the narrowest part of the largest pores. This theory is more practical because, within the frozen fringe, more than one ice lens can be formed, and heaving is not based on one ice lens but on the accumulation of all. Therefore, the initial theoretical maximum heaving pressure transits from primary to secondary heaving. However, different mechanisms are at play in the frozen fringe, ranging from water transport even though the zone is frozen (i.e., temperature lower than 0^{o}C) and the growth of a new ice lens due to transported water. At the warmest ice lens interface, water is sucked toward the lens while water tries to force the ice and soil apart (Gilpin, 1980; Vignes-Adler, 1977).

A phase change occurs within the frozen fringe, increasing pore pressure within the unfrozen pores. A cryogenic suction gradient is developed at the ice/water interface because the applied temperature gradient causes pore water from the unfrozen soil to flow to the ice lens (Thomas et al., 2009). Furthermore, Suction is affected by soil properties and temperature gradient (Wang et al., 2017). To quantify the cryogenic suction, the Clapeyron equation has been used by different research and is estimated to be around 1.56 to 18 psi (Konrad & Morgenstern, 1980; Thomas et al., 2009). Most studies focus on temperature and heave data while ignoring water migration and suction measurement. In addition, the ionic concentration around the ice lens is estimated by certain studies as around 80 times the initial concentration in the sand (Kay & Groenevelt, 1983).

All these studies have significantly shown that such factors as soil texture, pore size (Beskow, 1935; Penner, 1968), rate of heat removal and temperature gradient (Henry, 2000; Sadiq et al., 2023), moisture condition/water availability (Taber 1916, 1918a, b; Penner, 1959), overburden stress (Lai et al., 2014; Wang et al., 2018), and number of freeze-thaw cycles affect frost action. However, three fundamental conditions are essential for frost action to occur:

1. FSS,

2. Surface temperature that drops below and rises above 32°F (0°C),

3. Water availability to ice lens.

2.3 Fundamentals about FSS

According to the Highway Research Board Committee on Frost Heave and Frost Action in Soil [HRBC] (1955), "A frost-susceptible soil is one in which significant ice segregation will occur when the requisite moisture and freezing conditions are present" (HRBC, 1955). Earlier works have shown that FSS has high permeability and capillary potential (Beskow, 1935). Silt is the most suitable of all soil types (as indicated in Figure 2.4) as its hydraulic conductivity ranges from 10^{-6} to 10^{-4} cm/s and can experience capillary height up to 2 m. Clay has a higher capillary potential than silty soil but has a far lower hydraulic conductivity, i.e., water supply would be slow; therefore, frost heaving is not as severe in clay soils. Also, large voids in sand and coarse soils allow water to freeze without segregation into ice lenses, hence no frost action, as listed in Table 2-1.

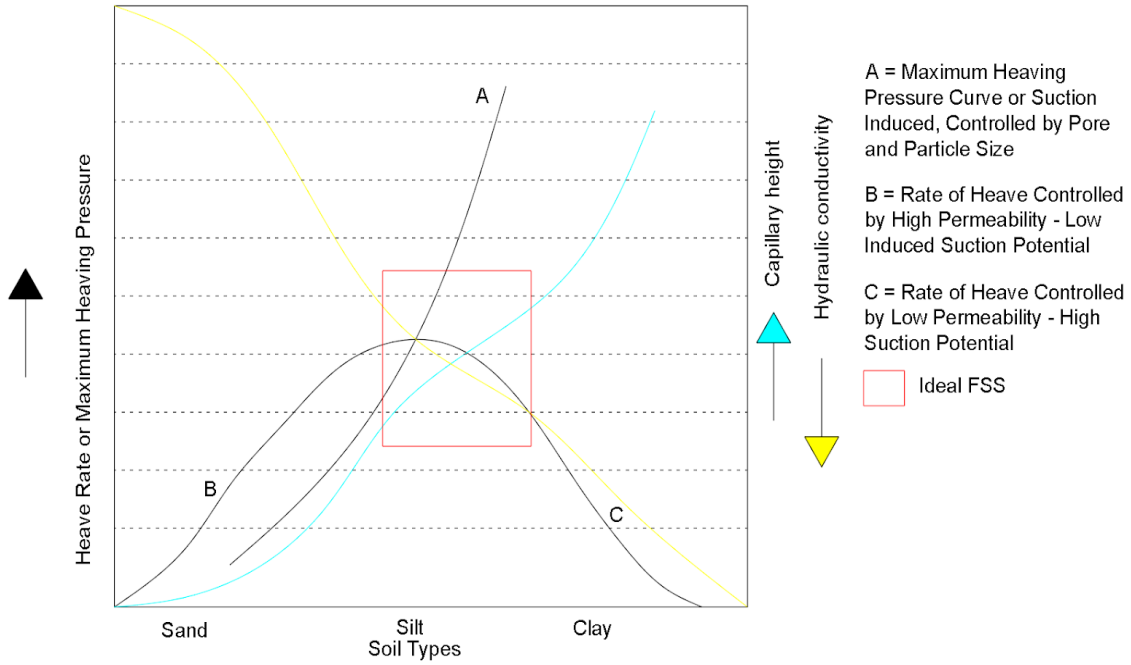

Figure 2.4: Schematic representation of the relationship between heaving rate, pressure, capillary rise, particle size, and hydraulic conductivity resulting from ice lens growth (Adapted from Penner, 1968).

Table 2-1: Frost susceptibility classification (NCHRP 1-37A)

Frost Group	Degree of susceptibility	Type of soil	Percentage Finer than 0.02 mm	Typical Soil Classification (Unified)
NFS	Negligible	Gravels, Sands	0 - 3	GW, GP, SW, SP
PFS	Low	Gravels, Sands	1.5 - 10	GW, GP, SW, SP
S1	Very Low to Medium	Gravelly soils	3 - 6	GW, GP, GW-GM, GP-GM
S2	Negligible to Low	Sandy soils	3 - 6	SW, SP, SW-SM, SP-SM
F1	Very Low to Medium	Gravelly soils	6 - 10.	GM, GW-GM, GP-GM
F2	Low to Medium	Gravelly soils	10 - 20.	GM, GW-GM, GP-GM
		Sands	6 - 15.	SM, SW-SM, SP-SM
F3	High	Gravelly soils	> 20	GM, GC
		Sands, except very fine, silty sands	> 15	SM, SC
		Clays (PI>12)	-	CL, CH
F4	Very High	All silts	-	ML, MH

	Very fine silty sands	> 15	SM
	Clays (PI<12)	-	CL, CL-ML
	Varved clays and other fine-grained, banded sediments	-	CL, ML, CH, SM

There are lots of location-specific criteria for FSS. However, the universally accepted criteria for FSS were defined by Casagrande (1932):

> Under natural freezing conditions and with sufficient water supply, one should expect considerable ice segregation in non-uniform soils containing-more than 3% of grains smaller than 0.02 mm, and in very uniform soils containing more than 10 percent smaller than 0.02 mm. No ice segregation was observed in soils containing less than 1 percent of grains smaller than 0.02 mm, even if the groundwater level is as high as the frost line. (as cited in Chamberlain, 1981, p. 1)

Other local or regional criteria are based primarily on particle distribution analysis (usually done for any typical project). However, they are inadequate as it does not fully address susceptibility. Consequently, the best existing criteria include other soil properties ranging from mineralogy to moisture condition to surcharge. Other tests used in determining FFS include pore size characteristics, soil/water interaction, soil/water/ice interaction, and frost heave (Chamberlain, 1981). Still, the most reliable method for FSS identification is yet to be established (Oman & Lund, 2018).

2.4 Freezing Temperatures

Weather conditions, especially air temperature, lead to a thermal gradient within the soil layer or pavement structure, which is then transmitted to the subgrade, i.e., as the surface temperature freezes, there is top-down freezing within the soil. This freezing front progresses downward rapidly when the steep temperature gradient slows as it gets to lower and wetter soil strata (Oman & Lund, 2018). Subsequently, there is a limit to this progression, at which the cooling, i.e., a negative temperature (Celsius) reading, ends, and the soil warms up. This interface is the frost line, and the soil depth from the surface to this interface is

referred to as frost depth or frost penetration. This frost penetration is the soil depth that can be frozen, i.e., at or below O°C, and it is ultimately a function of the thermal properties of all impacted layers and the duration and magnitude of the freezing ambient temperatures.

Several maps provide the typical average or maximum frost penetration, such as Figure 2.5. Also, there are a lot of empirical formulas that can be used to calculate frost depth, which include the Neumann formula (Neumann, 1860), Stefan formula (Stefan, 1891), Modified Berggren Formula (Aldrich & Paynter, 1953), and General frost depth calculation. The Stefan formula is an improvement on the Neumann formula that is implicit and requires a constant surface temperature (Kurylyk & Hayashi, 2016). However, the Stefan equation tends to overestimate and does not include the volumetric heat capacity of the soil and water. Hence, the development of the Modified Berggren Formula. Nevertheless, the modified Berggren equation assumes that the entire soil is at its mean temperature at the start of the freezing season and that the surface temperature change is rapid from mean to freezing.

However, this can only be applied to a cycle or a season, i.e., daily frost depth cannot be directly calculated. Furthermore, to use these formulas, specific soil properties (e.g., thermal conductivity, volumetric latent heat of fusion, specific heat, and thermal resistance) and weather conditions (e.g., freezing and thawing indexes) are necessary (Joint Departments of the Army and Air Force USA [JDAAF], 1988).

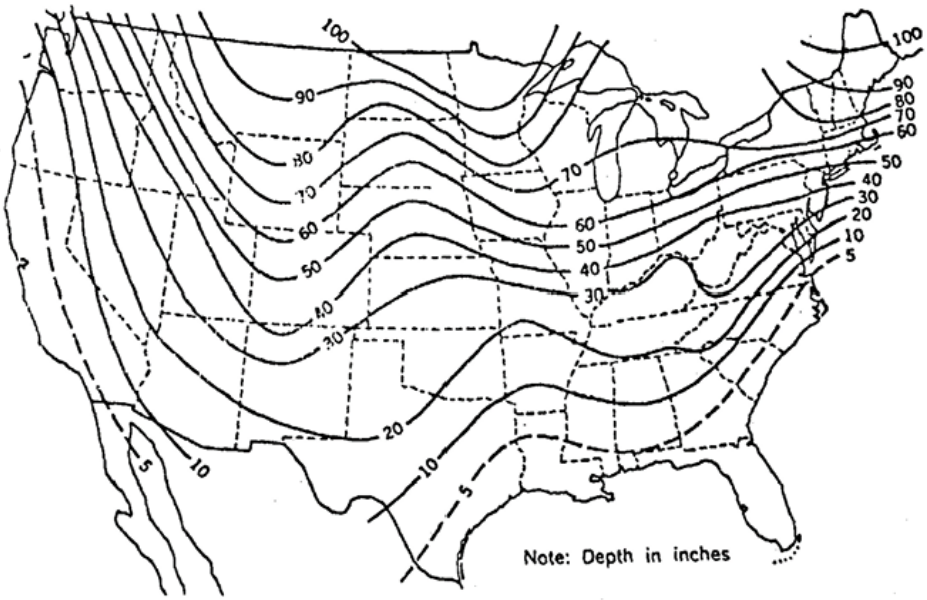

Figure 2.5: Maximum Depth of frost penetration in the USA (Adapted from FHWA, 1980).

2.5 Subsurface Water

FSS has high hydraulic conductivity and capillary potential properties, which take effect only when a water source is nearby, as shown in Figure 2.6. A water table within 3 m (10 ft) depletes high frost hazard potential; consequently, it is a low hazard potential when the water table is greater than 6 m (20 ft) (Christopher et al., 2006). Therefore, a water table within 3 m is ideal for frost action as its capillary height will increase the water level closer to the surface. Hence, the ice lens will keep growing through the capillary rise and thicken in the direction of heat transfer until the water supply is depleted or until freezing conditions at the freezing interface cannot support further crystallization. Soils, such as carrier barriers (Henry, 1998) or EWR, can impede this water supply.

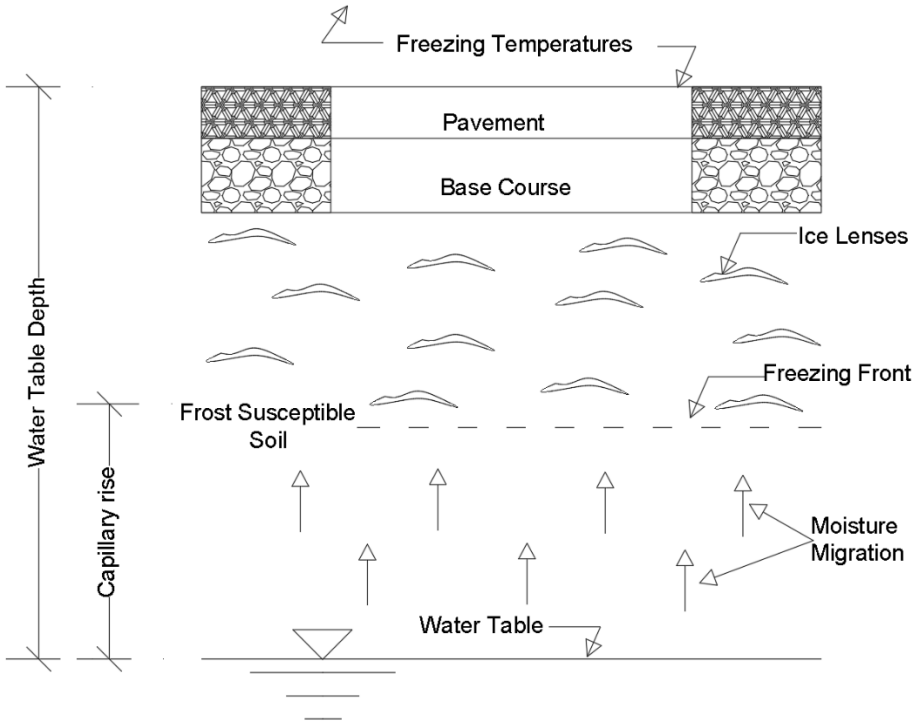

Figure 2.6: Capillary Moisture migrating toward the freezing front to feed the growth of ice lenses.

2.6 Ice Lens Initiation Criteria

Laboratory and empirical studies have discovered different criteria for defining new ice lens formation and its location. Also, field observation has noticed one or two phenomena that have led to many criteria; for example, a new ice lens is formed when effective stress is equal to zero (Bishop, 1959). Similarly, O'Neill and Miller (1980) describe the same condition; however, the relationship between maximum neutral stress (sum of water and ice pressure) and overburden pressure was used to define effective stress. Conversely, Miller (1972, 1978) stated that a new ice lens is formed when pore water pressure is strong enough to separate soil particles.

Likewise, a new ice lens is created when maximum ice pressure equals separation pressure (Gilpin, 1980). Within the same light, a new ice lens can be formed when ice pressure is greater than overburden pressure and the freezing soil tensile strength (Akagawa et al., 2007), as shown in Figure 2.7. In comparison, Konrad and Duquennoi (1993) suggested that an ice lens is formed when the vertical strain in the frozen soil reaches the instantaneous tensile failure strain.

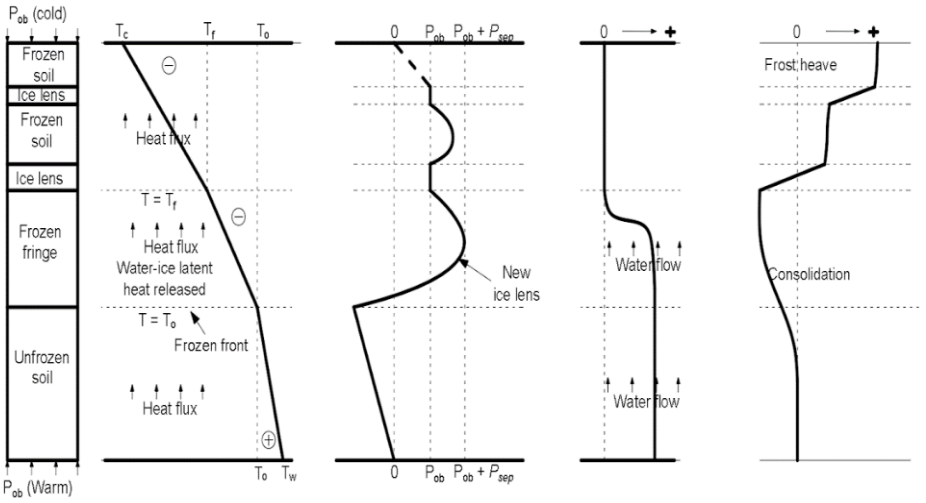

Figure 2.7: Schematic representation of a freezing soil with ice segregation (T_c, T_w, temperature at cold and warm ends, respectively; T_f, temperature at the base of ice lens; T_0, freezing point; p_{ob}, surface overburden load; p_{sep}, separation strength).

Another widespread criterion was developed by Konrad and Morgenstern (1980), which states that segregation temperature defines ice formation, which ties in with the secondary theory. New ice is formed when the permeability around an existing ice lens is low; therefore, a new one is formed at a favorable location. Recently, some studies have shown that soil crack precedes ice lens formation, as shown in Figure 2.8 (Konrad & Duquennoi, 1993; Azmatch et al., 2011). This criterion was improved and clearly defined the initiation temperature as the temperature corresponding to the Ice Entry Value (i.e., point of crack formation from soil freezing characteristics curve (SFCC)) (Azmatch et al., 2012).

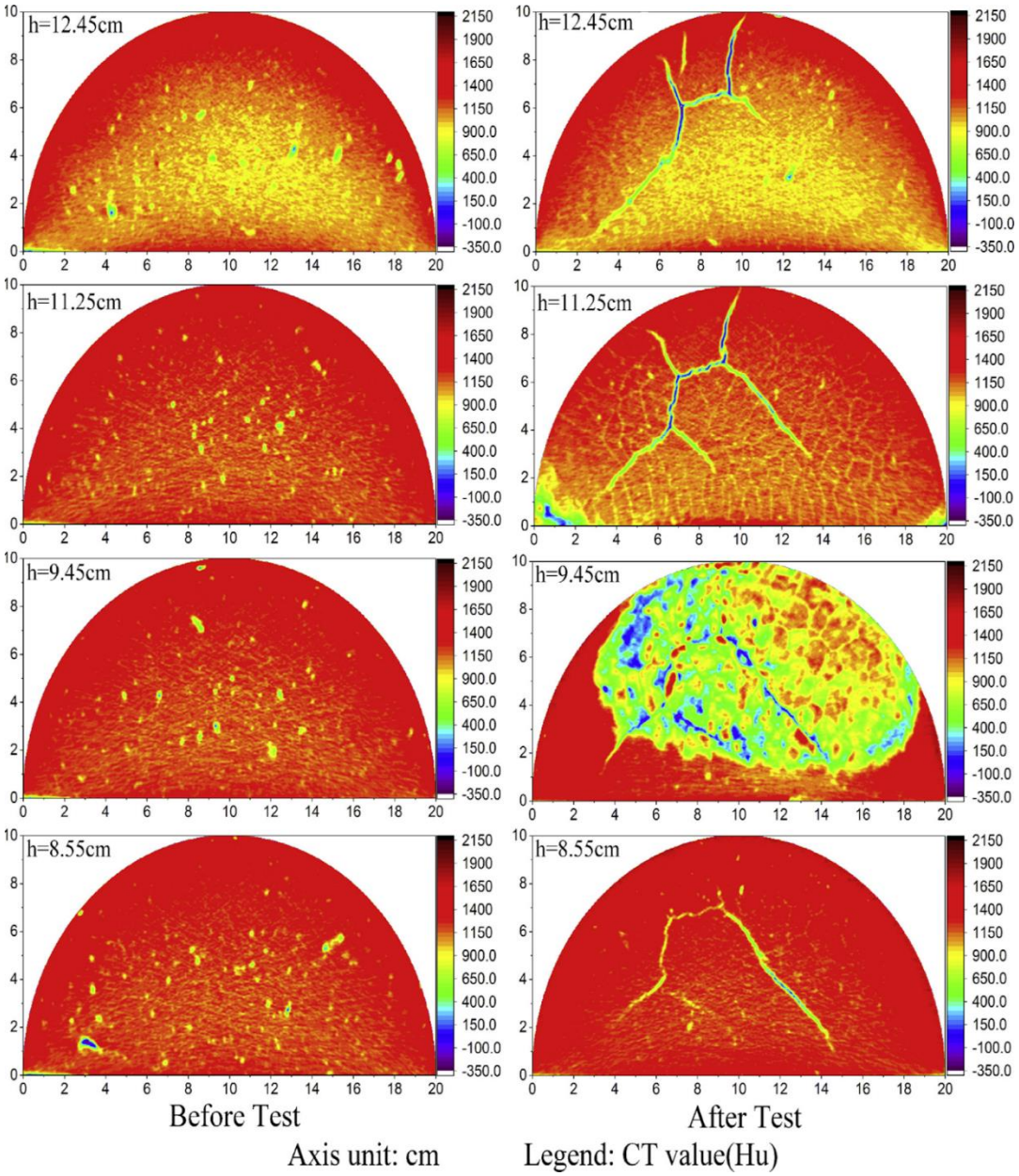

Figure 2.8: Crack formation preceding ice lens formation (Wang et al., 2018).

Similarly, a new ice lens is formed when porosity exceeds the separating porosity (Lai et al., 2014). All this theory can be nominalized to ice lens initiation temperature (Azmatch et al., 2012). Zhou et al. (2014) suggested that the ice lens initiates and grows when the volumetric water content equals or exceeds one. These initiation criteria are used in computer modeling to study and predict frost heave, although supported with little or no experiment validation. Any validated initiation criteria would help improve the

frost heave study. However, these criteria inputs are immeasurable, but temperature can be measured easily during laboratory and field testing.

Almost all laboratory studies on frost heave effectively measure temperature, heave, and water intake (Konrad, 1987; Hermansson & Guthrie, 2005; Zhang et al., 2017; Naqvi et al., 2022; Sadiq, 2023). Continuous improvement in soil properties measurement sensors now allows the collection of complementing data relating to volumetric water content, matric suction, and electrical conductivity [EC]. All these measurements allow a better understanding of water migration to the ice lens as wall soil behavior within fringe and unfrozen zones. A similar idea was explored by Uduebor et al. (2022), which showed moisture, EC, and matric suction variations with corresponding temperature changes in FSS. All this enables a proper understanding of what is happening within the soil. Combining all these soil properties measurements will shed more light on what leads to ice lens initiation and growth.

Studies have avoided investigating these properties, especially around the ice lens. The first problem is where the ice will be formed. A change in porosity is expected around the ice lens, leading to compression downwards and budging upwards (Lai et al., 2014). Other properties, such as moisture content, Electrical conductivity (EC), and suction, are challenging to measure. However, understanding the soil column's suction provides an understanding of the suitable capillary barrier that can be designed to prevent water from flowing to the ice lens.

2.7 Existing Frost Action Mitigation Methods

Different strategies are currently used to either minimize or prevent frost heaving. These strategies vary from region to region based on experience rather than rigorous theoretical analysis (Christopher et al., 2006). The underlying concept that controls which strategy is used depends on whether surface deformation prevention or adequate bearing capacity is essential (Pavement Interactive [PI], 2023). These strategies encompass one or two methods and are centered around altering one of three fundamental conditions for

frost heave. The method includes hindering water supply, reducing frost depth and frost action impact, replacing FSS, or increasing subgrade stiffness.

Hindering water supply includes improved deep/subsurface drainage and capillary barriers. This strategy utilizes materials of larger pore sizes relative to FSS and materials that can absorb moisture and drain it out or increase the evaporation of water (Rengmark, 1963; Allen et al., 1983; Henry, 1990; Henry & Holtz, 2001). Ideal materials have high wettability (ability to absorb water from unsaturated soils) and high permittivity (Zhang, 2014). Therefore, capillary flow around them is reduced, i.e., capillary break. These materials are placed above the water table and below the penetration depth (Shoop & Henry, 1991). This strategy ensures that the water table is deep and that no infiltrating water is sufficiently available for the ice lens. It is usually utilized alongside increased pavement depth or FSS replacement. Capillary barriers include geosynthetic drains, such as geocomposite drains and wicking fabric, open-graded coarse soils (usually gravel), or a combination of both coarse soil and geosynthetics (Oman & Lund, 2018). To prevent clogging, especially with sand or geosynthetics, filters are used around it (Henry, 1996).

There are multiple evaluations on drainage and capillary barrier use in frost action mitigation. Different investigations have utilized coarse soil as capillary barriers (Kisch, 1959; Rengmark, 1963); however, it was replaced with geosynthetics, which also showed a reduction in frost heave (Hoover et al., 1981; Henry, 1988; Henry et al., 1989; Henry, 1991). Allen et al. (1983) recorded a reduction of up to 60 %. For geotextile, these studies indicate that properties such as wettability, pore size, and thickness significantly affect the result. Additional advantages of using geotextile include added reinforcement, separation, and filtration when adequately installed (Andersson & Freden, 1977; Andersson, 1977; Hoover et al., 1981; Clough & French, 1982; Henry, 1996). Both full-scale physical model tests and field studies (Zhang et al., 2014; Lin et al., 2015; Zornberg et al., 2017; Zaman et al., 2022) have shown the variability of wick fabric in frost heave mitigation. However, more studies are needed to understand its mechanisms and establish it as a top option. Another geosynthetics-related method, put forward by Henry and Stormont (2002), is the geocomposite capillary barrier drain (GCBD), which consists of “a capillary barrier layer

sandwiched between transport layers." Theoretically, it is an effective mitigation method (Zornberg et al., 2010), but others have not thoroughly investigated it.

The use of Polymer materials, such as polystyrene (XPS), polyurethane (PU), and polystyrene (EPS), to reduce frost depth is another strategy being implemented. A study showed that 1 cm of PU application equals 14 cm frost depth reduction (Zhang, 2013). Likewise, an ESP of 6 cm results in a 50 % reduction in frozen depth (Zhang, 2003). Similarly, the placement of ESP at the optimum depth can increase the ground temperature by 0.7°C per cm thickness (Guo et al., 2018; Liu & Liu, 2012). All these studies and others observed frost heave reduction with polymer insulation (Sheng et al., 2006; Zhang, 2009; Ivanov & Korotkov, 2017; Valtseva et al., 2018). Numerous DOTs utilize this method and have developed guidance specifying the minimum compressive strength, the maximum water absorption by volume, the minimum amount of fill that must be placed above it, and the transition limits. This method requires substantial FSS removal, placement of polymer, and gravel fill. Unfortunately, this will consume much energy, add greenhouse gas, and utilize new raw materials, which makes this method expensive and unsustainable.

Another unsustainable but well-utilized method is the FSS removal and replacement with non-frost susceptible soil (NFSS) to the depth of expected frost penetration. Many DOTs support this method; however, FSS removal depth varies (Schaus & Popik, 2011). The design approach governs the depth of FSS removal. A complete protection approach will demand total FSS replacement, although this is usually utilized in low frost hazard potential areas. In contrast, reduced subgrade strength will require less FSS replacement, as the pavement material is expected to support the pavement frost action impact. A study by Evan et al. (2011) indicated that the effectiveness of this method is dependent on the depth of FSS replacement. Likewise, FSS replacement of about one-third results in a 50 % reduction. FHWA also supports adding NFSS to a suitable thickness to prevent subgrade freezing. Another closely related method is increased pavement thickness. Pavement thickness is supported by different DOTs as strength reduction

due to frost action is accounted for in the design. When the replacement or addition of NFS is impossible or expensive, FSS modification can be done.

This can be achieved by physical-chemical modification or stabilization. In most cases, lime and cement are mainly used (Nourmohamadi et al., 2022). For typical lime stabilization, a pH of 12.4 is needed; however, it does not apply to all soils, especially soil with low Plasticity, sulfates, phosphates, organics, and iron, and requires a curing period (Arabi et al., 1989; Celauro et al., 2012; ASTM D6276, 2019). Cement-stabilized FSS is also effective; however, its performance in terms of strength and ductility changes with freeze-thaw cycles (Shidi & Kamei, 2014; Baldovino et al., 2020). Other major materials used include fly ash (Yarbaşı et al., 2006; Zhang et al., 2016), cotton fiber (Liu et al., 2020), jute fiber, steel fiber (Ghazavi & Roustaie, 2010; Gullu & Khudir, 2014), polypropylene (PP) (Roustaei et al., 2015; Ding et al., 2018; Kravchenko et al., 2018) and microbially induced carbonate precipitation (MICP) (Gowthaman et al., 2020; Sun et al., 2021), which significantly improve ductility and strength. Another drawback of this method is that it requires big machinery, leaching might occur, or its efficiency and durability might reduce with time.

2.8 Introduction of EWR

As an alternative to current mitigation methods, EWR is being investigated. EWR involves making the existing in-situ FSS, which is hydrophilic, become hydrophobic. Hydrophobic soil is water-repellent, i.e., it cannot absorb or allow water to flow through it without applying a positive hydrostatic head. Soil's natural affinity for water is significantly reduced, as observed in natural Soil Water Repellency (SWR) (DeBano, 2000; Smettem et al., 2021). These researchers were focused on the causes of natural SWR or to characterize and mitigate the effects on infiltration, soil moisture, and strength. In nature, SWR is caused by hydrophobic organic compounds and microbial activity which coat soil particles or join the soil matrix as interstitial particles (Bond, 1960; Tschapek, 1984; Jex et al., 1985; Hallet & Youg, 1999; Doerr et al., 2000; Doerr et al., 2005; Kawamoto et al., 2007; Doerr et al., 2009). The Persistence and intensity/severity of SWR is influenced by such factors as soil organic matter content and chemical properties (Doerr &

Thomas, 2000; Goebel et al., 2011), soil mineralogy (Lichner et al., 2006; Zavala et al., 2009), soil texture (Bachmann et al., 2006; Lichner et al., 2006; Jordán et al., 2013), vegetation type (Dekker & Ritsema, 1994; Doerr et al., 2000; Ferreira et al., 2000; Zavala et al., 2009a; Pekarova et al., 2015), soil moisture content (SMC) (Bond & Harris, 1964; Ritsema & Dekker, 1994; Berglund & Persson, 1996; Doerr & Thomas, 2000) and fire (Doerr et al., 1996; Granged et al., 2011b; Jiménez-Pinilla et al., 2016; Malvar et al., 2016; Martins et al., 2020). According to Smettem et al. (2021), SWR occurrence is due to all these combined factors, not even one at a time.

Hydrophobicity can be induced artificially using synthetic or organic compounds such as wax coatings (Bardet et al., 2014), Silanes, and fatty acids (Bardet et al., 2014; Chan & Lourenço, 2016; Ng & Lourenço, 2016). Silances include the likes of dimethyldichlorosilane (DMDCS) (Liu et al., 2012; Saulick et al., 2017) and trichloro(octadecyl)silane (OTS), which form high and stable hydrophobicity (Lin & Lorrenco, 2022), floro-chemicals (Fink, 1970), polyoxyalkylated diethylenetriamine (Alexandrova et al., 2011), polytetrafluorethylene (Dell'Avanzi et al., 2010), stearic acid (Leelamanie et al., 2008; Subedi et al., 2012; González-Peñaloza et al., 2013), and oleic acid (Subedi et al., 2012). Fatty acids include Tung Oil (Zhang et al., 2016; Lin et al., 2019; Lin & Lorrenco, 2022) and Paraffin Oils. Tung oil has the added advantage of aggregation, and it is more effective after being exposed to 100^0C and hardened (Wexler, 1964). However, Liu et al. (2015) observed that it only lasts 25 years indoors for wood preservation, so it can be significantly degraded when exposed to environmental factors. While most showed water repellency, their long-term effectiveness is not certain. Hence, the development of EWR using silances.

EWR is a permanent coating of soil particles using organosilanes (OS), a silica-based organic coupling agent that modifies the soil surface without any bonding properties (Daniels et al., 2009). This is achieved by replacing the -OH surface readily available in the soil to absorb water with stable Alkyl Siloxane (Meeravali & Rangaswamy, 2020), as shown below in Figure 2.9. Different studies have shown that the soil particles at 40 % coverage are still effectively hydrophobic (Daniels et al., 2009; Jerez et al., 2018; Mahedi et al., 2020) and that the coating is near permanent to permanent (Daniel & Hourani, 2009;

Adeinola & Nnochiri, 2017). Therefore, a significant decline in repellency and effectiveness is not expected after application; hence, there is no need for maintenance or failure. This is far more convenient than existing mitigation methods. In addition, EWR can help improve subgrade stiffness and keep it constant year-round. Also, it helps design engineers ignore potential capillary height impact on road stiffness and strength, as illustrated in Figure 2.10. To fully apply EWR in engineering projects, there is a need for standardization on severity, persistence, and engineering performance.

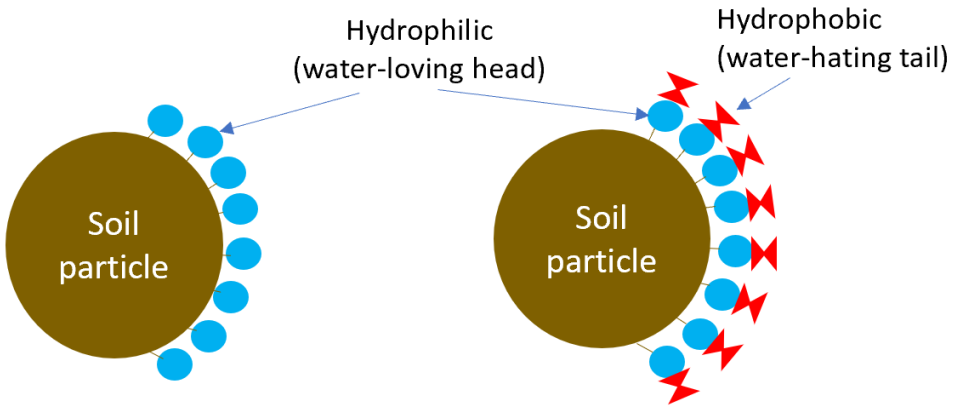

Figure 2.9: Hydrophilic modification to hydrophobicity.

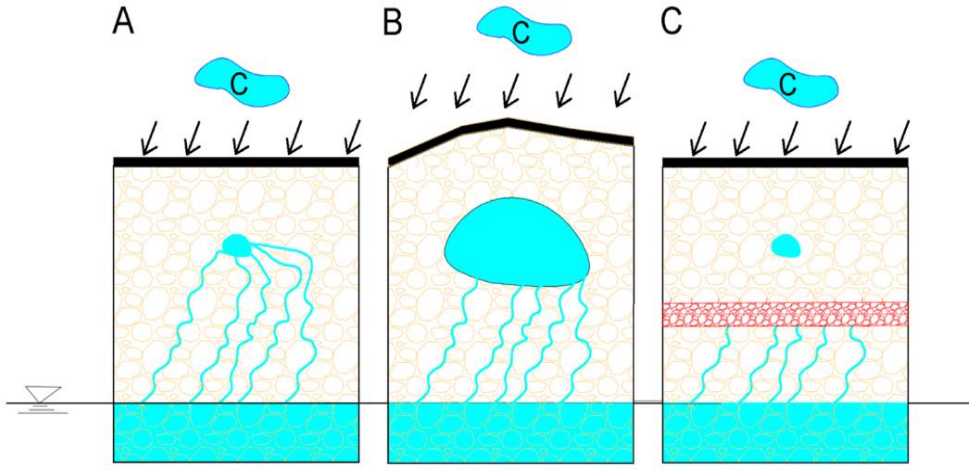

Figure 2.10: EWR application.

2.9 Laboratory Testing

After decades of studying SWR, there is still no fixed consensus on testing procedures or results interpretation, divided into severity and persistence. Severity defines the degree to which soil is hydrophobic, either wettable (i.e., super hydrophilic or hydrophilic) or non-wettable (i.e., hydrophobic or

superhydrophobic). This classification is done based on tests such as Contact Angles (CA) and Molarity of an Ethanol Drop test (MED) (also referred to as the Critical Surface Tension (CST) test) (Letey et al., 1962; Emerson & Bond 1963; Watson & Letey, 1970; Bachmann et al., 2000; Roy & McGill, 2002; Wijewardana et al., 2016; Smettem et al., 2021). For the CA test, super hydrophilic soil has a contact angle of less than 20^{o}, whereas hydrophilic soil ranges from 20 to 90^{o} (Zhang et al., 2015). Also, hydrophobic soil possesses contact angles higher than 90^{o}, and it becomes superhydrophobic at more than 150 - 160^{o} (McHale et al., 2005; Chandler, 2013).

There are different methods of CA measurement, such as sessile drop methods (SDM), Wilhelmy plate method, captive bubble, thin column wicking methods, and capillary rise methods (CRM) (Letey et al., 1962; Bachmann et al., 2000; Hajnos et al., 2013; Lourenco et al., 2015). The Wilhelmy plate method and the capillary rise method utilized bulk samples, a better improvement over utilizing the finer part of a soil or a monolayer (Bachmann et al., 2003). Wilhelmy plate method measures advancing (as the sample is inserted in water) and receding (as the sample is removed from the fluid) CA between a range of 0 and 180^{o} as water is inserted in a fluid, whereas the CRM cannot measure above 90^{o} (Adamson, 1990; Bachmann et al., 2003).

The fundamental mechanism governing both methods is fully described by Saulick (2018). Both methods utilized significant assumptions such as steady state laminar flow, zero velocity at the liquid/solid interface, no externally applied pressure, negligible gravitational differences, and liquid viscosity (Siebold et al., 1997; Ramírez-Flores et al., 2010). These methods are more laborious and time-intensive; hence, automation is needed to improve measurement; also, soil properties (e.g., bulk density swelling) must be kept constant. Although they utilize a big sample size, which is more representative of the soil sample, SDM is more pronounced as it is more straightforward and offers a direct measurement solid–liquid–vapor phase boundary from 0 to 180^{o}.

However, SDM result is influenced by different factors including sample preparation (Bachmann et al., 2000b), droplet volume (Good & Koo, 1979; Shang et al., 2008; Saulick et al., 2017), surface roughness and flatness (Bond, 1968; Murray & Darvell, 1990; Valat, 1991; Drelich, 1997; Kwok et al., 1997; Bachmann et al., 2000a; Meiron et al., 2004; Marmur, 2006; Chibowski, 2007), sample moisture (Bachmann et al., 2000a; Subedi et al., 2011; Liu et al., 2012; Chau et al., 2014), and capture technique (Saulick et al., 2017).

Local asperities on rough surfaces can cause a moving drop's interface to be pinched, leading to the appearance of a stick-slip motion. The fundamental principle for contact angles is based on Young's law, which shows the relationship between solid–liquid, solid–vapor, and liquid–vapor interfaces. However, it was designed for smooth, flat, homogenous, inert, insoluble, nonreactive, non-porous, and non-deformable surfaces. Furthermore, the CA measurement is not applicable in the fields or large areas as the level of repellency can be heterogeneous.

For MED, infiltration of ethanol less than 1 sec means low to no significant severity. In contrast, 1.2 to 2.2-sec infiltration indicates moderate severity, 2.4 to 3 shows severe repellency, and 3.2 to 10 sec signifies severe repellency. For MED, 40 µl of ethanol solution at varying concentrations of 0.2 M is used, and the corresponding penetration time is measured (Watson & Letey, 1970; King, 1981; Dekker & Ritsema, 1994; Gilboa et al., 2006).

Another variation to this approach is using 60 µl of ethanol droplet to determine the minimum liquid surface tension by examining if it ponds or infiltrates in 5 seconds (de Jonge et al., 1999). An increase in the concentration of ethanol results in the reduction of its surface tension, thereby aiding its infiltration into the sample, which indicates a higher severity of hydrophobicity. However, the formal approach is more utilized. MED is a more practical in-field application than WDPT or CA because its results can be obtained rapidly without considering the effect of water evaporation.

Persistence speaks to the time it takes water to penetrate a hydrophobic surface. The water achieves this drop penetration test (WDPT) (Doerr, 1998; Letey, 1969; Dekker & Ritsema, 1994; Doerr et al., 2000; Leelamanie et al., 2008). This test is straightforward and inexpensive, although attention must be paid to the evaporation effect for long-duration testing. The existing result interpretation of SWR (as indicated in Figure 2.11) is being used for OS-treated materials, as observed in studies using materials such as glass beads and fly ash (Feyyisa et al., 2017; Feyyisa et al., 2019; Rodríguez-Guevara et al., 2023), and sand (Leelamanie et al., 2008; Byun et al., 2011; González-Peñaloza et al., 2013; Keatts et al., 2018). However, these materials are one-graded or mono-grained. Therefore, they are incredibly different from soil, which can consist of various particle sizes.

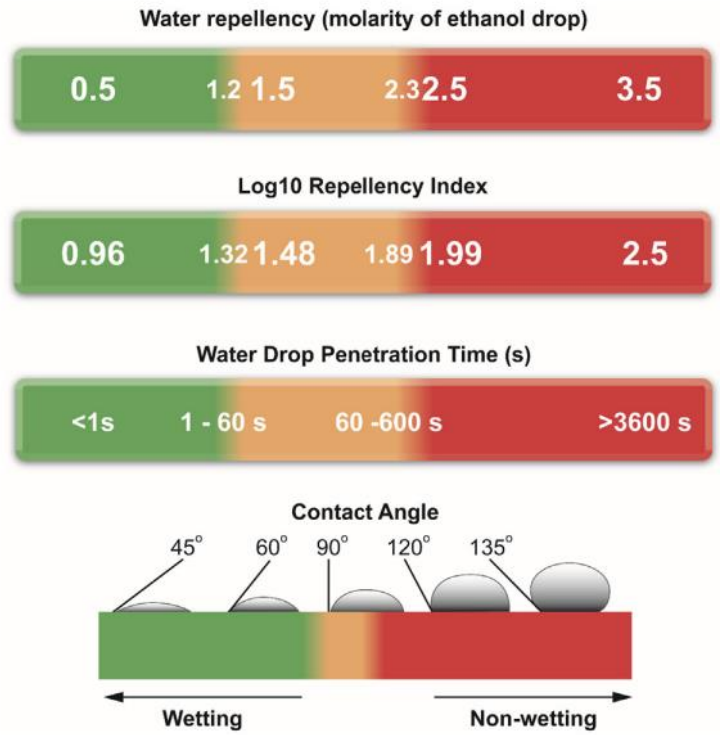

Figure 2.11: Inter-comparison of measurement scales for methods used to characterize hydrophobicity. The amber zone indicates a transition from thoroughly wetting (green) to highly non-wetting (red). Indices sourced from (a) King (1981), (b) Moody and Schlossberg (2010), and (c) Leelamanie et al. (2008) (Smettem et al., 2021).

Also, there are still issues with measurement and sample preparation testing sequences (Tillman et al., 1989; Wallis et al., 1991; Dekker et al., 1998; Moody & Schlossberg, 2010). Another major pitfall with these tests is that they are not performance-based testing because engineering design or construction cannot

be directly carried with them. Additionally, they are not hydraulic indicators of soil hydrophobicity and cannot help in understanding when failure, i.e., water flows through the EWR, is possible. Hence, the use of breakthrough testing (BP) or WEP.

WEP is the minimum hydrostatic pressure required to force water through the largest opening of a dry hydrophobic surface or film. Unlike hydrophilic soils, water flows through the smallest pores first. According to Wang et al. (2000) and Lee et al. (2015), it is the pressure at which a wettable fluid (air in this case) starts to displace a non-wetting fluid (water); the start of water infiltration. Humorously, breakthrough testing is an indirect measurement of hydrophobicity because its result is dependent on the surface tension and porosity. In hydrophilic soil, negative pressure, called air entry value, can move water through its pore (can be obtained from soil water characteristic curve [SWCC]). However, for hydrophobic soil, such as EWR, a positive head of water would be required to push water through it, which is inversely proportional to the porosity and dependent on the surface tension.

Different researchers use numerous methods to measure breakthrough pressures. Nevertheless, the only universal point across all studies is their definition of water entry testing, ensuring proper air drainage, application of static water head, and waterproofing to avoid minimizing side leakage. Different studies have measured water entry at different points. Fundamentally, water entry pressure is at the interface, at film thickness, i.e., the point at which water starts to flow into the hydrophobic soil, not at a thickness. However, it is understandable that this film measurement is complicated to measure. Currently, three methods have been documented for WEP measurement. The water-ponding method (WP) is the most common, followed by the Tension pressure infiltrometer (TPI) and the Triaxial setup.

The WP is the most common and first standardized approach. The fundamental feature of WP is the soil compaction into a tube. A cheesecloth or filter paper is placed on it to prevent surface disruption, static water ponding on the sample, proper air drainage at the base, and utilization of hydrophobic coating to avoid soil-wall preferential flow. In this method, a drop in water head or a change in measured pressure

is the critical variant for WEP. Although this method is simple and cost-effective, ensuring proper compaction, preventing side leakage, and determining the exact point of water infiltration is problematic.

This method has different variations, and researchers have varied water ponding approaches, as shown in Figure 2.12. Furthermore, a sensor can be used to measure water level changes or to determine water pressure changes within the soil. Water pressure change in the soil is always far from the soil surface; therefore, the true WEP is not measured. The closer the sensor is to the surface, the more significant the soil disruption, a big pitfall for this approach. Also, the result depends on the soil compaction around this sensor or its measurement resolution.

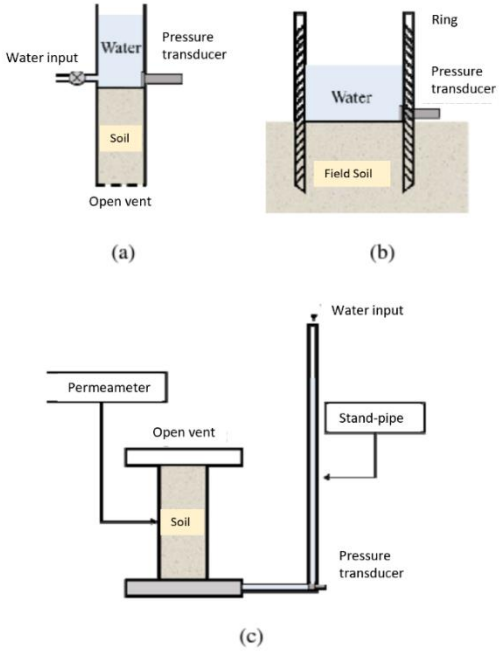

Figure 2.12: Different ponding methods (Adapted from Lourenço et al., 2021).

Tension pressure infiltrometer was introduced by Wang et al. 2000 and designed to be used for both wettable and non-wettable soil. TPI is a modified tension infiltrometer of Perroux and white, 1988 and Fallow and Elrick (1996). This method relies on water supply (usually stored in a Mariotte tube), imposed on the soil surface through a porous disk (perfect seal is essential), and suction pressure or positive hydrostatic pressure is applied by varying the air inlet position as shown in Figure 2.13.

The appealing feature is its application to both soil types (hydrophilic and hydrophobic), thus creating a fantastic means of comparing wettable and non-wettable. Other methods require another method to measure wettable soil water entry pressure. Studies that have utilized these methods have fabricated their version by relying on this principle (Annaka & Hanayama, 2005). Furthermore, this method has more moving parts, and the measurement range is complex to ascertain as there is a need to adjust the air inlet. Some studies record water entry pressure far above 1m, making this method tasking.

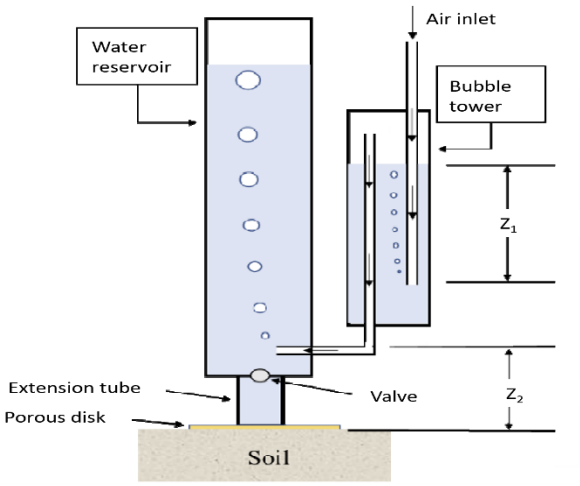

Figure 2.13: Tension pressure infiltrometer (Adapted from Lourenço et al., 2021).

To resolve the measure range issue in TPI and WP, as well as the problem of side leakage, Feyyisa (2018) developed a methodology based on the recognized triaxial flexible wall permeameter setup (ASTM D5084). A FlowTrac II apparatus from Geocomp was used to apply a wide range of water heads. This head can be applied at different rates, and its resolution is significantly high, allowing for more accuracy. This method relies on water being ramped up to a specific value, such as 138 kPa in the Dumenu (2019), at a specific rate. This test method was repeatable for fly ash but proved problematic for soil as it consists of more grain sizes.

In addition, a particular water pressure can be maintained easily or ramped up to any pressure. Also, the total water utilized at any time can be accurately monitored. However, apart from being repeatable, there is a need to ensure the criteria are the same. Hence, the development of a new methodology by Uduebour et al. 2023. Instead of targeting the interface, a measurable amount of water inflow is targeted.

Different engineering projects have different tolerances for water flow. Engineering projects like landfills and dams have specific flow rates.

Different studies have shown that breakthrough is affected by porosity and concentration (surface energy) (Wang et al., 2000; Lee et al., 2015; Xing et al., 2022). The lower the porosity, the higher the concentration; the higher the concentration, the higher the EWR. However, there might be a diminishing return after a specific concentration. There is a need to understand this concentration impact on WEP results. Also, there is a need to standardize the densification benefit of EWR into already understood standard proctor MDD used in the field. For instance, in the case of landfill or dam construction, compaction on the wet side of optimum is preferred because it offers less permeability and volume change. Furthermore, organic matter, clay content, and temperature affect WEP at a given concentration and density (Lee et al., 2015; Jordan et al., 2015; Keatts et al., 2018). It might be linked to surface energy or concentration, as more OS might be needed for soil with more fines than clay. There is little study into this, as this could help to understand optimum soils for EWR. Also, this testing approach relies on confining pressure to prevent side leakage; hence, its effects on WEP testing are also unknown. Furthermore, water ingress into the soil below WEP has been observed, with little to no scientific observation. However, specific changes in surface energy over time have been attributed to this observation. Nevertheless, water infiltration below WEP is possible if water pressure is maintained for a specific time interval. To this end, there is a need to understand this dynamic WEP concept. Lastly, the moisture content of EWR has been observed to affect its performance. Hence, its impact on WEP also needs evaluation.

Another primary concern with all this testing is correlations. There are existing models and equations on contact angle to WDPT and WEP. Such correlations include the Washburn equation. However, laboratory measurements indicated they are significantly off, especially with artificially modified EWR. It should be noted that EWR are highly hydrophobic and were not the basis for the correlation developed. Therefore, new correlations or modifications are required. The laboratory test needs to be able to document soil hydrophobic severity and durability. However, the WEP testing is time-consuming and labor-intensive.

Therefore, the correlation has been developed for breakthrough testing and contact angle for materials such as glass beads and fly ash.

2.10 Life Cycle Analysis (LCA)

Frost action is a significant problem because it is rarely uniform, leading to patchy damage. Differential frost heaving is attributable to such causes as instability of the one-dimensional freezing process, variability in the FSS, availability of moisture, the variability of the thermal regime, and the topography of the surface (Peterson & Krantz, 2003; Dore & Zubeck, 2009). It is detrimental to all types of pavements in addition to traffic loading. Studies have shown that most road networks in cold regions have relatively low traffic densities and are typically traditional hot-mix asphalt, cold mixes, surface treatments, and gravel surfaces (Dore & Zubeck, 2009; Solour & Erlingsson, 2012).

Also, it was observed that Portland cement concrete and cement-treated materials are rarely used in cold regions because of their high initial cost, lack of high traffic density, and sensitivity to differential settlement due to frost action. Furthermore, gravel pavement is the most common pavement because it is cheap to construct and has low traffic loading; however, its maintenance cost is high (Federal Highway Administration [FHWA], 2015). Different failure mechanisms exist due to traffic loading and environmental factors on different pavements.

Furthermore, spring thawing leads to bearing capacity loss because melting frozen water flows into the pavement structure (Janoo, 2002), weakening soil stiffness. The impact of thawing is a function of the amount of frost heave rate of thawing and consolidation rate (Dore, 2004). Different studies have utilized different testing approaches such as California Bearing Ratio (CBR) tests (Janoo, 2002), back-calculated modulus (Ovik et al., 2000; Saarelainen & Gustavsson, 2001), and Falling Weight Deflectometer (FWD) (Solour & Erlingsson, 2012) tests to evaluate capacity losses. They observed that bearing capacity losses vary from 20% to 60 % depending on soil properties and other factors. Hence, a relatively load-induced damage of 1.5 to 3 times the average annual damage (St-Laurent & Roy, 1995) and more deterioration

during thawing would occur (Janoo & Berg, 1990; White & Core, 1990). Similarly, Dore & Savard (1998) observed that 90 % of fatigue occurred during thaw periods, and Zhang and Macdonald (2000) observed a 60 to 75 % permanent deformation. Also, an AASHO road test showed that 60 % of pavement failure occurs during spring (White & Coree, 1990). Another study by St-Laurent, 1995 noticed that the "loss of stiffness relative to summer modulus is equal to 36, 30, and 54 percent for the granular base, subbase, and subgrade soil, respectively", as cited in p. 157), furthermore, it "takes over approximately three months for the base, four months for the subbase, and nearly five months for the clay subgrade."

As stated earlier, there are different methods to prevent or mitigate these problems, which affect the different stages of a pavement's life (i.e., design, construction, operation and maintenance, rehabilitation, and end of life). The pavement design stage considers the impact of expected frost action within the region, the soil and pavement materials, and the traffic loads. It involves conducting site-specific soil tests to determine the risk of frost damage, selecting appropriate pavement materials and thicknesses (specify thicker layers of subgrade materials, base courses, and asphalt or concrete surfacing materials), and incorporating features such as proper drainage and insulation to reduce the impact of frost action.

Some frost heave design approaches utilize either non-frost-susceptible materials within or expected frost depth and use of high-strength durable material that can withstand thaw-weakened periods and traffic loading. USACE recommends that the top fifty percent of the granular unbound base be non-frost susceptible for flexible pavement. In contrast, in rigid pavements, FSS should be replaced by non-FSS at least equal to the slab thickness (U.S. Army Corps of Engineers [USACE], 1984). The 1993 AASHTO guide for the design of pavement structures recommends FSS replacement by "one-half or more of the frost depth" (American Association of State Highway and Transportation Officials [AASHTO], 1993). Similarly, the 1993 AASHTO guide for the design of pavement-structures recommends 12 to 24 inches of granular materials over frost-susceptible roadbed soils to account for expected subgrade strength reduction. All these methods entail a considerable amount of non-FSS material; most times, sandy or granular materials are preferred. These materials must be mined, transported, laid, and compacted after removing

and hauling the in-situ FSS. All this process involves intensive energy, heavy machinery, construction time and manpower, and substantial gas emissions.

During operation, regular maintenance and inspection are carried out to detect any signs of frost damage and repair them promptly to extend the pavement's service life. The constant need to maintain different road sections leads to increased operational costs, gas emissions, traffic disruptions, and green material usage. In addition, pavement distresses such as potholes and bumps increase reduces gas millage, increase vehicular wear and tear, and increase travel time on driver seeking alternative routes (Barnes & Langworthy, 2004; Jackson, 2004; EPA, 2011; FHWA, 2011; Islam & William, 2012). Additionally, increased gas emissions can result from using energy-intensive measures to prevent or mitigate the effects of frost action, such as deicing chemicals or installing heating systems. Load restrictions are usually utilized because the pavement weakness varies from 40 to 50 days and is more pronounced in gravel pavement.

Deicing chemicals such as sodium chloride, magnesium chloride, and calcium chloride, applied during operation to remove snow for road user usage and to prevent frost cracking, result in increased pavement greenhouse gas emissions, energy consumption, and environmental fauna and flora toxicity (Lewis, 1999; Davis et al., 2012; Balakrishnan, 2015; Hintz & Relyea, 2017; LaLonde, 2019). The amount of energy required to produce deicing chemicals can vary depending on several factors, such as the type of chemical, the production process, and the source of energy used, storage, and application process of these chemicals to roads and other surfaces.

Over time, the pavement may require more substantial rehabilitation to repair or replace damaged sections. Rehabilitation methods differ significantly from region to region and depend on the severity of damage and pavement type. At the end of its service life, the pavement can be recycled or disposed of in an environmentally friendly manner. The life cycle analysis considers the pavement's environmental, social, and economic impacts of the pavement over its expected service life, including the impact of frost action. Optimizing the pavement structure for durability, safety, and environmental sustainability is possible

considering the entire life cycle, including design, construction, operation, maintenance, rehabilitation, and end-of-life.

There is no life cycle analysis of pavements in cold regions. Regarding environmental impact on low-density traffic pavements, construction accounts for 65 to 82%, while usage and transportation accounts for 10-21 and 11-20%, respectively (Santos et al., 2015). Little or no studies of the impact of frost action on gravel pavement, more widely found in cold temperate regions, exist. The closest analysis was done by Rukashaza-Mukome et al. 2003, which showed that frost action accounts for 2% of maintenance costs on gravel roads and less than 1% on Bituminous Road in Minnesota counties. However, this pavement goes through constantly reshaping snow, and ice removal. Frost action affects the road design, construction, maintenance, user usage, and pavement end of life. There is a need to understand to what extent frost action affects total pavement cost in terms of economic, human, and environmental impact.

2.11 Knowledge Gaps.

Many studies have addressed various aspects of frost mitigation, but significant limitations remain. While EWR presents a promising alternative, several areas still require further assessment, particularly in evaluating its performance through Water Entry Pressure (WEP) tests for water resistance and Unconfined Compressive Strength (UCS) for mechanical strength (Chapter 3). Practical questions about how EWR-treated soils will perform in the field, especially concerning durability and the impact of on-site compaction, need to be answered (Chapter 3 and 4). Additionally, as a relatively new method, there is a need to determine the optimal application of EWR in terms of depth, field density, and OS concentration (Chapter 4). Furthermore, while the national impact of frost action is well-documented, the localized effects of frost action and its mitigation methods, including EWR, are still unclear (Chapter 5). For example, what is the economic impact of frost action from a construction or maintenance standpoint? Finally, what is the most cost-effective method for mitigating frost action?

2.12 Reference

Aabøe, R., & Frydenlund, T. E. (40). Years of experience using EPS geofoam blocks in road construction. In Proceedings of the Fourth International Conference on Geofoam Blocks in Construction Applications, Lillestrom, Norway.

AASHTO M145-91 (2012). Classification of Soils and Soil-Aggregate Mixtures for Highway Construction Purposes. Washington DC: American Association of State Highway and Transportation Officials.

Aitken, G. W., & Berg, R. L. (1968). Digital solution of modified Berggren equation to calculate depths of freeze or thaw in multilayered systems.

Akagawa, S., Satoh, M., Kanie, S., & Mikami, T. (2006). Effect of tensile strength on ice lens initiation temperature. In Current Practices in Cold Regions Engineering (pp. 1-12).

Aldrich, H. P., & Paynter, H. M. (1953). Analytical studies of freezing and thawing of soils. Technical Rep, 42.

Alexandrova, L., Nedyalkov, M., Khristov, K., & Platikanov, D. (2011). Thin wetting film from aqueous solution of polyoxyalkylated DETA (Diethylenetriamine) polymeric surfactant. Colloids and Surfaces A: Physicochemical and Engineering Aspects, 382(1-3), 88-92.

Allen, T. M. (1983). Properties of geotextiles in cold regions applications. Transportation Research Report 83-6. Transportation Research Institute, Oregon State University, Corvallis, 1983.

Amir, A. H., & Alibaba, H. Z. (2018). Comparison between Heat Conductivity of EPS (Expanded Polystyrene) and XPS (Extruded Polystyrene). International Journal of Recent Research in Civil and Mechanical Engineering (IJRRCME), 4(2), 24-31.

Andersson, O. (1977). The use of plastic fabric for pavement protection during frost break (No. 1977: 9 Monograph).

Andersson, O., & Fredén, S. (1977). The Influence of a Plastic Fabric Upon the Pavement at Frost Break. Frost i Jord, (18).

Annaka, T., & Hanayama, S. (2005). Dynamic water-entry pressure for initially dry glass beads and sea sand. Vadose zone journal, 4(1), 127-133. https://doi.org/10.2113/4.1.127

Arabi, M., Wild, S., & Rowlands, G. O. (1989). Frost resistance of lime-stabilized clay soil. Transportation Research Record, (1219).

ASTM D6276, (2019). "Standard Test Method for Using pH to Estimate the Soil-Lime Proportion Requirement for Soil Stabilization" ASTM International, 100 Barr Harbor Drive, PO Box C700, West Conshohocken, PA 19428–2959. United States

Azmatch, T. F., Sego, D. C., Arenson, L. U., & Biggar, K. W. (2011). Tensile strength and stress–strain behavior of Devon silt under frozen fringe conditions. Cold Regions Science and Technology, 68(1-2), 85-90. https://doi:10.1016/j.coldregions.2011.05.002

Azmatch, T. F., Sego, D. C., Arenson, L. U., & Biggar, K. W. (2012). Using soil freezing characteristic curve to estimate the hydraulic conductivity function of partially frozen soils. Cold Regions Science and Technology, 83, 103–109.

Bachmann, J., Arye, G., Deurer, M., Woche, S. K., Horton, R., Hartge, K. H., & Chen, Y. (2006). Universality of a surface tension—contact-angle relation for hydrophobic soils of different texture. Journal of Plant Nutrition and Soil Science, 169(6), 745-753

Bachmann, J., Ellies, A., & Hartge, K. H. (2000). Development and application of a new sessile drop contact angle method to assess soil water repellency. Journal of Hydrology, 231, 66–75. doi:10.1016/s0022-1694(00)00184-0

Bachmann, J., Horton, R., Van Der Ploeg, R. R., & Woche, S. (2000). Modified sessile drop method for assessing initial soil–water contact angle of sandy soil. Soil Science Society of America Journal, 64(2), 564–567. https://doi.org/10.2136/sssaj2000.642564x

Balakrishnan, A. (2015). Road salt: Winter's $2.3 billion game changer. Cary Institute of Ecosystem Studies. Retrieved from http://www.caryinstitute.org/newsroom/road-salt-winters23-billion-game-changer

Baldovino, J., Izzo, R.L. & Rose, J.L. (2021). Effects of Freeze–thaw Cycles and Porosity/cement index on Durability, Strength and Capillary Rise of a Stabilized Silty Soil Under Optimal Compaction Conditions. Geotech Geol Eng 39, 481–498.

Bardet, J. P., Jesmani, M., & Jabbari, N. (2014). Permeability and compressibility of wax-coated sands. Géotechnique, 64(5), 341-350. http://dx.doi.org/10.1680/geot.13.P.118Berglund, K., & Persson, L. (1996). Water repellence of cultivated organic soils. Acta Agriculturae Scandinavica B-Plant Soil Sciences, 46(3), 145–152.

Barnes, G., & Langworthy, P. (2004). Per mile costs of operating automobiles and trucks. Transportation Research Record, 1864(1), 71–77.

Beskow, G. (1948). Soil freezing and frost heaving with special application to roads and railroads.

Bouyoucos, G. J. (1920). Degree of temperature to which soils can be cooled without freezing. Journal of agricultural research, 20(4), 267–269.

Bing, H., He, P., & Zhang, Y. (2015). Cyclic freeze–thaw as a mechanism for water and salt migration in soil. Environmental Earth Sciences, pp. 74, 675–681. https://doi.org/10.1007/s12665-015-4072-9

Bishop, A. (1959). The principle of effective stress. Tek. Ukebl. 106 (39), 859–863.

Black, P. B. (1985). A continuum approach to modeling of frost heaving. In Freezing and Thawing of Soil-Water Systems (pp. 36–45). ASCE.

Black, P.B. (1995). Rigid Ice model of secondary frost heave. USA Cold Regions Research and Engineering Laboratory, Special Report 95-12.

Black, P. B., & Hardenberg, M. J. (1991). Historical perspectives in frost heave research: the early works of S. Taber and G. Beskow (p. 37). CRREL.

Bond, R. (1968). Water-repellent sands. In: Holmes, J.W., editor, Transactions of the 9th International Congress of Soil Science, Adelaide, Australia. 6–16 Aug. 1968, Vol. 1. Elsevier, New York. p.339–347.

Bond, R. D., & Harris, J. R. (1964). The influence of the microflora on the physical properties of soils. I. Effects associated with filamentous algae and fungi. Soil Research, 2(1), 111–122.

Byun, Y. H., Tran, M. K., Yun, T. S., & Lee, J. S. (2012). Strength and stiffness characteristics of unsaturated hydrophobic granular media. ASTM International. https://doi.org/10.1520/GTJ103650.

Cass, L. A., & Miller, R. D. (1959). Role of the electric double layer in the mechanism of frost heaving.

Celauro, B., Bevilacqua, A., Bosco, D. L., & Celauro, C. (2012). Design procedures for soil-lime stabilization for road and railway embankments. Part 1-review of design methods. Procedia-Social and Behavioral Sciences, 53, 754-763. https://doi.org/10.1016/j.sbspro.2012.09.925.

Chamberlain, E. J. (1981). Frost susceptibility of soil: review of index tests (No. DOT/FAA/RD-81/91 Final Rpt.). Hanover, NH: Cold Regions Research and Engineering Laboratory.

Chan, C. S. H., & Lourenço, S. D. N. (2016). Comparison of three silane compounds to impart water repellency in an industrial sand. Géotechnique Letters, 6(4), 263-266. https://doi.org/10.1680/jgele.16.00097

Chandler D. L. (2013, July 16). Explained: Hydrophobic and hydrophilic. MIT News | Massachusetts Institute of Technology. https://news.mit.edu/2013/hydrophobic-and-hydrophilic-explained-0716#:~:text=Though%20the%20definitions%20of%20these%20terms%20are%20less,than%20about%2020%20degrees%2C%20the%20surface%20is%20superhydrophilic

Chau, H. W., Biswas, A., Vujanovic, V., & Si, B. C. (2014). Relationship between the severity, persistence of soil water repellency, and the critical soil water content in water repellent soils. Geoderma, 221, 113-120.

Chibowski, E. (2007). On some relations between advancing, receding, and Young's contact angles. Advances in Colloid and Interface Science, 133(1), 51-59.

Christopher, B. R., Schwartz, C. W., Boudreaux, R., & Berg, R. R. (2006). Geotechnical aspects of pavements (No. FHWA-NHI-05-037). United States. Federal Highway Administration.

Clough, I. R., & French, W. J. (1982, August). Laboratory and fieldwork relating to the use of geotextiles in arid regions. In Proceedings of the 2nd International Conference on Geotextiles, Las Vegas, Nev (pp. 1–6).

Crandell, J. H. (2010). Below-ground performance of rigid polystyrene foam insulation: review of effective thermal resistivity values used in ASCE standard 32-01—design and construction of frost-protected shallow foundations. Journal of Cold Regions Engineering, 24(2), 35-53.

Daniels, J. L., Mehta, P., Vaden, M., Sweem, D., Mason, M. D., Zavareh, M., & Ogunro, V. (2009). Nano-scale organo-silane applications in geotechnical and geoenvironmental engineering. Journal of Terraspace Science and Engineering, 1(1), 21–30.

Davis, J. G., Waskom, R. M., Bauder, T. A., Cardon, G. E., Follett, R. H., & Franklin, W. T. (2012). Managing sodic soils. Service in action; no. 0.504.

De Jonge, L. W., Jacobsen, O. H., & Moldrup, P. (1999). Soil water repellency: effects of water content, temperature, and particle size. Soil Science Society of America Journal, 63(3), 437-442.

DeBano, L. F. (2000). Water repellency in soils: a historical overview. Journal of Hydrology, 231, 4–32. https://doi.org/10.1016/s0022-1694(00)00180–3.

Dekker, L. W., & Ritsema, C. J. (1994). How water moves in a water-repellent sandy soil: 1. Potential and actual water repellency. Water Resources Research, 30(9), 2507-2517.

Dekker, L. W., Ritsema, C. J., Oostindie, K., & Boersma, O. H. (1998). Effect of drying temperature on the severity of soil water repellency. Soil Science, 163(10), 780-796.

Dell'Avanzi, E., Guizelini, A. P., Da Silva, W. R., Nocko, L. M., & Buzzi, O. (2010). Potential use of induced soil-water repellency techniques to improve the performance of landfill's alternative final cover systems. In Proceedings of the 4th Asia-Pacific Conference on Unsaturated Soils (UNSAT 2009) (pp. 461-466).

Ding, M., Zhang, F., Ling, X., & Lin, B. (2018). Effects of freeze-thaw cycles on mechanical properties of polypropylene fiber and cement stabilized clay. Cold Regions Science and Technology, pp. 154, 155–165. https://doi.org/10.1016/j.coldregions.2018.07.004.

Dirksen, C., & Miller, R. D. (1966). Closed-system freezing of unsaturated soil. Soil Science Society of America Journal, 30(2), 168-173.

Doerr, S. H. (1998). On standardizing the ‘water drop penetration time’ and the ‘molarity of an ethanol droplet’techniques to classify soil hydrophobicity: a case study using medium textured soils. Earth Surface Processes and Landforms: The Journal of the British Geomorphological Group, 23(7), 663–668. https://doi.org/10.1002/ (SICI)1096-9837(199807)23:73.0.CO;2-6.

Doerr, S. H., Llewellyn, C. T., Douglas, P., Morley, C. P., Mainwaring, K. A., Haskins, C., ... & Diamantis, J. (2005). Extraction of compounds associated with water repellency in sandy soils of different origin. Soil Research, 43(3), 225–237.

Doerr, S. H., Shakesby, R. A., & MacDonald, L. H. (2009). Soil water repellency: a key factor in post-fire erosion. In Fire effects on soils and restoration strategies (pp. 213–240). CRC Press.

Doerr, S. H., Shakesby, R. A., & Walsh, R. (2000). Soil water repellency: its causes, characteristics and hydro-geomorphological significance. Earth-Science Reviews, 51(1-4), 33–65.

Doerr, S. H., & Thomas, A. D. (2000). The role of soil moisture in controlling water repellency: new evidence from forest soils in Portugal. Journal of Hydrology, 231, 134–147. https://doi.org/10.1016/s0022-1694(00)00190–6.

Doré, G., & Zubeck, H. K. (2009). Cold regions pavement engineering.

Doré, G. (2004). Development and validation of the thaw-weakening index. International Journal of Pavement Engineering, 5(4), 185–192. https://doi.org/10.1080/10298430412331317464

Doré, G., and Savard, Y. 1998. Analysis of seasonal pavement deterioration. Transportation research board. Preprint No. 981046, Transportation Research Board of the National Academies, Washington, D.C.

Drelich, J. (1997). Static contact angles for liquids at heterogeneous rigid solid surfaces. Polish Journal of Chemistry, 71(5), 525–549.

Dumenu, L. (2019). Water Repellency Effect on Unsaturated Properties of Compacted Coal Combustion Residuals (Doctoral dissertation, The University of North Carolina at Charlotte).

Ekström, G., & Flodkvist, H. (1926). Hydrologiska undersökningar av åkerjord inom Örebro län. Kungl. boktryckeriet, PA Norstedt & söner.

Emerson, W. W., & Bond, R. D. (1963). The rate of water entry into dry sand and calculation of the advancing contact angle. Soil Research, 1(1), 9-16. https://doi.org/10.1071/ SR9630009.

Evans, G.L., Truebe, M.A., & Hanek, G.L. (2011). Monitoring report of Frost Heave on Warm Lake Road. Transportation Research Record: Journal of the Transportation Research Board, No. 2204, Transportation Research Board of the National Academies. Washington, D. C., 251-257.

Federal Highway Administration (FHWA); South Dakota Local Technical Assistance Program (SDLTAP) (2015), Gravel Roads Construction and Maintenance Guide,

Ferreira, A. J. D., Coelho, C. O. A., Walsh, R. P. D., Shakesby, R. A., Ceballos, A., & Doerr, S. H. (2000). Hydrological implications of soil water-repellency in Eucalyptus globulus forests, north-central Portugal. Journal of Hydrology, 231, 165–177. https://doi.org/10.1016/S0022-1694(00)00192-X.

Feyyisa, J. L., & Daniels, J. L. (2016). A dynamic contact angle measurement technique for water-repellent coal fly ash (CFA). In Geo-Chicago 2016 (pp. 925–938). https://doi.org/doi:10.1061/9780784480144.092

Feyyisa, J. L., Daniels, J. L., & Pando, M. A. (2017). Contact angle measurements for use in specifying organosilane-modified coal combustion fly ash. Journal of Materials in Civil Engineering, 29(9), 04017096. https://doi.org/doi:10.1061/(ASCE)MT.1943-5533.0001943.

Feyyisa, J. L., Daniels, J. L., Pando, M. A., & Ogunro, V. O. (2019). Relationship between breakthrough pressure and contact angle for organo-silane treated coal fly ash. Environmental technology & innovation, p. 14, 100332. https://doi.org/10.1016/j.eti.2019.100332.

Fink, D. H. (1970). Water repellency and infiltration resistance of organic-film-coated soils. Soil Science Society of America Journal, 34(2), 189–194.

Fuel Economy Guide—Model Year 2010. U.S. Environmental Protection Agency. http://www.fueleconomy.gov/feg/pdfs/guides/FEG2011. pdf. Accessed April 15, 2011.

Galinmoghadan, J., Zhang, X., & Lin, C. (2019). A Bio-Wicking System to Prevent Frost Heave in Alaskan Pavements: Phase II Implementation.

Ghazavi, M., & Roustaie, M. (2010). The influence of freeze–thaw cycles on the unconfined compressive strength of fiber-reinforced clay. Cold regions science and technology, 61(2-3), 125-131.

Gilboa, A., Bachmann, J., Woche, S. K., & Chen, Y. (2006). Applicability of interfacial theories of surface tension to water-repellent soils. Soil Science Society of America Journal, 70(5), 1417-1429.

Gilpin, R. (1980). A model for the prediction of ice lensing and frost heave in soils. Water Resources Research, 16(5), 918–930.

Glaerum, 0. (1920) Statens forsoksgaard paa Vold. Beretninger fra Statens F~rscdksstasjoner I plantekultur for 1919. Se sarsk, s. 137-138.

Goebel, M. O., Bachmann, J., Reichstein, M., Janssens, I. A., & Guggenberger, G. (2011). Soil water repellency and its implications for organic matter decomposition–is there a link to extreme climatic events? Global Change Biology, 17(8), 2640-2656. https://doi.org/10.1111/j.1365-2486.2011.02414.x

Gold, L. W. (1957). A possible force mechanism associated with the freezing of water in porous materials. High. Res. Board Bull, 168, 65-72.

González-Peñaloza, F. A., Zavala, L. M., Jordán, A., Bellinfante, N., Bárcenas-Moreno, G., Mataix-Solera, J., ... & Neto-Paixão, H. M. (2013). Water repellency as conditioned by particle size and drying in hydrophobized sand. Geoderma, 209, 31-40.

Good, R. J., & Koo, M. N. (1979). The effect of drop size on contact angle. Journal of Colloid and Interface Science, 71(2), 283-292.

Gowthaman, S., Nakashima, K., & Kawasaki, S. (2020). Freeze-thaw durability and shear responses of cemented slope soil treated by microbial-induced carbonate precipitation. Soils and Foundations.Volume 60, Issue 4, Pages 840-855, ISSN 0038-0806

Güllü, H., & Khudir, A. (2014). Effect of freeze-thaw cycles on unconfined compressive strength of fine-grained soil treated with jute fiber, steel fiber, and lime, Cold Regions Science and Technology, Volumes 106–107, Pages 55-65, ISSN 0165-232X

Guthrie, W. S., Hermansson, Å., & Woffinden, K. H. (2006). Saturation of granular base material due to water vapor flow during freezing: laboratory experimentation and numerical modeling. In Current Practices in Cold Regions Engineering (pp. 1–12).

H Güllü, H., & Khudir, A. (2014). Effect of freeze–thaw cycles on unconfined compressive strength of fine-grained soil treated with jute fiber, steel fiber, and lime. Cold Regions Science and Technology, 106, 55-65.

Hajnos, M., Calka, A., & Jozefaciuk, G. (2013). Wettability of mineral soils. Geoderma, 206, 63-69. https://doi.org/10.1016/j.geoderma.2013.04.019.

Hallett, P. D. (2008). A brief overview of the causes, impacts, and amelioration of soil water repellency–a review. Soil and Water Research, 3(1), 521-528.

Hallett, P. D., & Young, I. M. (1999). Changes to water repellence of soil aggregates caused by substrate-induced microbial activity. European Journal of Soil Science, 50(1), 35–40.

Harlan, R. L. (1973). Analysis of coupled heat-fluid transport in partially frozen soil. Water Resources Research, 9(5), 1314-1323.

Henry, K. S. (1998). The use of geosynthetics to mitigate frost heave in soils. University of Washington.

Henry, K. S. (1988, August). Use of geotextiles to mitigate frost heave in soils. In Proceedings, V International Conference on Permafrost in Trondheim, Norway (Vol. 2, pp. 1096–1011).

Henry, K. (1990). Geotextiles as capillary barriers. Geotechnical Fabrics Report, 8(2).

Henry, K. S. (2000). A review of the thermodynamics of frost heave.

Henry, K. S. Effect of Geotextiles on Water Migration in Freezing Soils and the Influence of Freezing on Performance. Proc., Geosynthetics, ’91, Atlanta, Ga., Industrial Fabrics Association International, St. Paul, Minn., 1991, pp. 469–484. 10.

Henry, K. S. Geotextiles as Capillxary Barriers. Geotechnical Fabrics Report, March/April 1990, pp. 30–36. 9.

Henry, K. S., Ingersoll, J. E., & Taylor, S. (1990). Effects of freezing on the microstructure of geotextiles. ASTM International.

Henry, K. S., & Holtz, R. D. (2001). Geocomposite capillary barriers to reduce frost heave in soils. Canadian Geotechnical Journal, 38(4), 678–694.

Hermansson, Å., & Guthrie, W. S. (2005). Frost heave, and water uptake rates in silty soil are subject to variable water table height during freezing. Cold Regions Science and Technology, 43(3), 128–139. https://doi:10.1016/j.coldregions.2005.03.003.

Highway Finance Data Collection, Our Nation's Highways: 2010. FHWA, U.S. Department of Transportation. http://www.fhwa.dot.gov/ policyinformation/pubs/hf/pl10023/fig5_1.cfm. Accessed July 20, 2011. 14Highway Research Board Committee on Frost Heave and Frost Action in Soil (1955) Highway Research Board Bulletin, no. 111, p. 107-110.

Highway Subdrainage Design. U.S. Department of Transportation Publication No. FHWA-TS-80-224, Federal Highway Administration. August 1980.

Hintz, W. D., & Relyea, R. A. (2017). Impacts of road deicing salts on the early-life growth and development of a stream salmonid: salt type matters. Environmental pollution, pp. 223, 409–415. https://doi.org/10.1016/j.envpol.2017.01.040

Hoover, J. M., Pitt, J. M., Handfelt, L. D., & Stanley, R. L. (1980). Performance of soil-aggregate-fabric systems in frost-susceptible roads, Linn County, Iowa (No. ISU-ERI-AMES-80211). Iowa State University. Dept. of Civil Engineering.

Hua, L., Fujun, N., Yonghong, N., & Xifeng, Y. (2014). Study on the thermal regime of roadbed–culvert transition section along a high-speed railway in seasonally frozen regions. Cold regions science and technology, 106, 216-231.

Islam, S., & Buttlar, W. G. (2012). Effect of pavement roughness on user costs. Transportation research record, 2285(1), 47-55. https://doi.org/10.3141/2285-06

Ivanov, K. S., & Korotkov, E. A. (2017). Investigation of the effect of a layer of granulated foam-glass ceramic on the temperature conditions of frozen soil. Soil Mechanics and Foundation Engineering, 54, 349-355.

Jackson, N. M. (2004). An Evaluation of the Relationship Between Fuel Consumption and Pavement Smoothness. University of North Florida, Jacksonville, FL.

Jackson, K. A., & Chalmers, B. (1958). Freezing of liquids in porous media with special reference to frost heave in soils. Journal of Applied Physics, 29(8), 1178-1181.

Janoo, V. C., & Berg, R. L. (1990). Thaw weakening of pavement structures in seasonal frost areas. Transportation Research Record, (1286).

Jiménez-Pinilla, P., Lozano, E., Mataix-Solera, J., Arcenegui, V., Jordán, A., & Zavala, L. M. (2016). Temporal changes in soil water repellency after a forest fire in a Mediterranean calcareous soil: Influence of ash and different vegetation type. Science of the Total Environment, 572, 1252-1260. https://doi.org/10.1016/j.scitotenv.2015.09.121.

Johansson, S. (1916) Argogeologisk undersokning av Ultuna egendom. S.G.U., Ser. C, nr. 271 (Arsbok 9) (1915); sdrsk, sid. 73–74.

Joint Departments of the Army and Air Force USA. (1988). Arctic and Subarctic Construction Calculation Methods for Determination of Depths of Freeze and Thaw in Soils., Technical Manual TM5-852-6/AFR88-19, Volume 6, Calculation Methods for Determination of Depths of Freeze and Thaw in soils.

Jordán, A., Zavala, L. M., Mataix-Solera, J., & Doerr, S. H. (2013). Soil water repellency: Origin, assessment and geomorphological consequences. Catena, 108, 1-5.

Kawamoto, K., Moldrup, P., Komatsu, T., de Jonge, L. W., & Oda, M. (2007). Water repellency of aggregate size fractions of a volcanic ash soil. Soil Science Society of America Journal, 71(6), 1658–1666. https://doi.org/10.2136/sssaj2006.0284

King, P. M. (1981). Comparison of methods for measuring the severity of water repellence of sandy soils and assessment of some factors that affect its measurement. Soil Research, 19(3), 275–285. https://doi.org/10.1071/sr9810275.

Kokkonen, P. (1926) Beobachtungen uiberdie Struktur des Bonenfrostes. Acta Forestalia Fennica, nr. 30, Helsingfors. by

Konrad, J. M., & Duquennoi, C. (1993). A model for water transport and ice lensing in freezing soils. Water Resources Research, 29(9), 3109-3124.

Koopmans, R. W. R., & Miller, R. D. (1966). Soil freezing and soil water characteristic curves. Soil Science Society of America Journal, 30(6), 680-685.

Kravchenko, E., Liu, J., Niu, W., & Zhang, S. (2018). Performance of clay soil reinforced with fibers subjected to freeze-thaw cycles. Cold Regions Science and Technology, 153, 18-24.

Kurylyk, B. L., & Hayashi, M. (2016). Improved Stefan equation correction factors to accommodate sensible heat storage during soil freezing or thawing. Permafrost and Periglacial Processes, 27(2), 189-203. https://doi: 10.1002/ppp.1865.

Kwok, D. Y., Gietzelt, T., Grundke, K., Jacobasch, H. J., & Neumann, A. W. (1997). Contact angle measurements and contact angle interpretation. 1. Contact angle measurements by axisymmetric drop shape analysis and a goniometer sessile drop technique. Langmuir, 13(10), 2880-2894.

Lai, Y., Pei, W., Zhang, M., & Zhou, J. (2014). Study on theory model of hydro-thermal–mechanical interaction process in saturated freezing silty soil. International Journal of Heat and Mass Transfer, pp. 78, 805–819. https://doi.org/10.1016/j.ijheatmasstransfer.2014.07.035

LaLonde, K. M. (2019). Highway Deicer Use in Oregon: Life Cycle Assessments of Magnesium Chloride and Sodium Chloride (Doctoral dissertation, Harvard University).

Leelamanie, D. A. L., Karube, J., & Yoshida, A. (2008). Characterizing water repellency indices: Contact angle and water drop penetration time of hydrophobized sand. Soil Science & Plant Nutrition, 54(2), 179-187. https://doi.org/10.1111/j.1747-0765.2007.00232.x.

Letey, J., (1969). Measurement of contact angle, water drop penetration time, and critical surface tension. In: LF, DeBano, Letey, J. (Eds.), Water Repellent Soils — Proceedings of the Symposium on Water Repellent Soils. University of California, Riverside, pp. 43–47.

Letey, J., Osborn, J., & Pelishek, R. E. (1962). Measurement of liquid-solid contact angles in soil and sand. Soil Science, 93(3), 149–153.

Letey, J., Osborn, J., & Pelishek, R. E. (1962). The influence of the water-solid contact angle on water movement in soil. Hydrological Sciences Journal, 7(3), 75–81. https://doi.org/10.1080/02626666209493272.

Lewis, W. M., & Analysts, W. E. (1999). Studies of environmental effects of magnesium chloride deicer in Colorado (No. CDOT-DTD-R-99-10). Colorado Department of Transportation, Research Branch.

Li, Y., Zhang, C., Chen, C., & Chen, H. (2018). Calculation of capillary rise height of soils by SWCC model. Advances in Civil Engineering, 2018. https://doi:10.1155/2018/5190354

Lichner, L., Dlapa, P., Doerr, S. H., & Mataix-Solera, J. (2006). Evaluation of different clay minerals as additives for soil water repellency alleviation. Applied Clay Science, 31(3-4), 238-248. https://doi.org/10.1016/j.clay.2005.10.012.

Lin, C., Zhang, X., & Presler, W. (2015). Application of Wicking Fabric to Reduce Damage in Alaskan Pavements. Final Project Report to TenCate Geosynthetics (North America), Alaska University of Transportation Center, University of Alaska Fairbanks, under review.

Lin, H., & Lourenço, S. D. (2022). Accelerated weathering of hydrophobized sands. Acta Geotechnica, 17(2), 377-390. https://doi.org/10.1007/s11440-021-01235-4.

Lin, H., Lourenço, S. D., Yao, T., Zhou, Z., Yeung, A. T., Hallett, P. D., ... & Cheuk, J. (2019). Imparting water repellency in completely decomposed granite with Tung oil. Journal of Cleaner Production, 230, 1316-1328.

Linell, K. A., & Kaplar, C. W. (1959). The factor of soil and material type in frost action. Highway Research Board Bulletin, (225).

Liu, H., Ju, Z., Bachmann, J., Horton, R., & Ren, T. (2012). Moisture-dependent wettability of artificial hydrophobic soils and its relevance for soil water desorption curves. Soil Science Society of America Journal, 76(2), 342-349.

Liu, Z. B., & Liu, J. J. (2012). The application of benzene plate in channel expanding. Low-temperature Construction Technology, 7, 142-144.

Liu, C., Lv, Y., Yu, X., & Wu, X. (2020). Effects of freeze-thaw cycles on the unconfined compressive strength of straw fiber-reinforced soil, Geotextiles, and Geomembranes, Volume 48, Issue 4. Pages 581-590, ISSN 0266-1144,

Liu, X. Y., Timar, M. C., Varodi, A. M., & Yi, S. L. (2015). Tung oil and linseed oil as traditional finishing materials important for furniture conservation. Pro Ligno, 11(4), 571-579.

Loch, J P.G. and R.D. Miller (1975). Test of the concept of secondary frost heaving. Soil Science Society of America, Proceedings, 39(6): 1036-1041.

Lourenço, S. D., Saulick, Y., Shuang, Z., Xing, X., Hongjie, L., Hongwei, Y., ... & Rui, Q. (2021). Hydrophobized Granular Materials for Ground Infrastructure. Materials with Extreme Wetting Properties: Methods and Emerging Industrial Applications, 153-177.

Lourenço, S. D. N., Woche, S. K., Bachmann, J., & Saulick, Y. (2015). Wettability of crushed air-dried minerals. Géotechnique Letters, 5(3), 173-177. https://doi.org/10.1680/jgele.15.00075

MacKay, M. H., Hein, D. K., & Emery, J. J. (1992). Evaluation of frost action mitigation procedures for highly frost-susceptible soils. Transportation Research Record, (1362).

Malvar, M. C., Prats, S. A., Nunes, J. P., & Keizer, J. J. (2016). Soil water repellency severity and its spatio-temporal variation in burnt eucalypt plantations in North-Central Portugal. Land Degradation & Development, 27(5), 1463-1478.

Marmur, A. (2006). Soft contact: measurement and interpretation of contact angles. Soft Matter, 2(1), 12–17.

Martins, M. A., Verheijen, F. G., Malvar, M. C., Serpa, D., González-Pelayo, O., & Keizer, J. J. (2020). Do wildfire and slope aspect affect soil water repellency in eucalypt plantations?–A two-year high-resolution temporal dataset. Catena, 189, 104471. https://doi.org/10.1016/j.catena.2020.104471.

McHale, G., Newton, M. I., & Shirtcliffe, N. J. (2005). Water-repellent soil and its relationship to granularity, surface roughness, and hydrophobicity: a materials science view. European Journal of Soil Science, 56(4), 445–452. https://doi.org/10.1111/j.1365-2389.2004.00683.x

Meeravali, K., Ruben, N., & Rangaswamy, K. (2020). Stabilization of soft-clay using nanomaterial: Terrasil. Materials Today: Proceedings, 27, 1030-1037. https://doi.org/10.1016/j.matpr.2020.01.384.

Meiron, T. S., Marmur, A., & Saguy, I. S. (2004). Contact angle measurement on rough surfaces. Journal of colloid and interface science, 274(2), 637-644.

Michalowski, R. L. (1993). A constitutive model of saturated soils for frost heave simulations. Cold regions science and technology, 22(1), 47-63.

Michalowski, R. L., & Zhu, M. (2006). Frost heave modeling using porosity rate function. International journal for numerical and analytical methods in geomechanics, 30(8), 703-722.

Miller, R. D. (1972). Freezing and heaving of saturated and unsaturated soils. Highway Research Record, 393(1), 1-11.

Miller, R. D. (1978). Frost heaving in non-colloidal soils. In Proceedings, 3rd International Conference on Permafrost, 1978.

Miller, R. D., Baker, J. H., & Kolaian, J. H. (1960). Particle size, overburden pressure, pore water pressure, and freezing temperature of ice lenses in soil. Transactions seventh int. Congr. Soil Sci., 1, 122-129.

Miller, R. D., Loch, J. P. G., & Bresler, E. (1975). Transport of water and heat in a frozen permeameter. Soil Science Society of America Journal, 39(6), 1029-1036.

Moody, D. R., & Schlossberg, M. J. (2010). Soil water repellency index prediction using the molarity of ethanol droplet test. Vadose Zone Journal, 9(4), 1046-1051. https://doi.org/10.2136/vzj2009.0119

Moussa, A., Shalaby, A., Kavanagh, L., & Maghoul, P. (2018). Use of rigid geofoam insulation to mitigate frost heave at shallow culvert installations. Journal of Cold Regions Engineering, 33(3), 05019003.

Murray, M. D., & Darvell, B. W. (1990). A protocol for contact angle measurement. Journal of Physics D: Applied Physics, 23(9), 1150.

Neumann, F., Riemann, B., & Weber, H. (1912). Lectures Given in the 1860s. Die Partiellen Differential-Gleichungen der Mthematischen Physik, 2, 17-121.

Newcomb, D., Willis, R., & Timm, D. H. (2010). Perpetual Asphalt Pavements, A Synthesis. Asphalt Pavement Alliance, Lanham, MD.

Ng, S. H. Y., & Lourenço, S. D. N. (2016). Conditions to induce water repellency in soils with dimethyldichlorosilane. Géotechnique, 66(5), 441-444. https://doi.org/10.1680/jgeot.15.T.025

Nourmohamadi, M, Abtahi, S.M., Hashemolhosseini H., & Hejazi, S.M. (2022). Control of frost effects in susceptible soils using a novel sandwich geocomposite composed of geotextile-soil-nano silica aerogel-geotextile liners, Transportation Geotechnics, Volume 33, 100718, ISSN 2214-3912,

O'Neill, K., & Miller, R. D. (1985). Exploration of a rigid ice model of frost heave. Water Resources Research, 21(3), 281–296. https://doi:10.1029/wr021i003p00281

Ovik, J. M., Birgisson, B., & Newcomb, D. (2000). Characterizing seasonal variations in pavement material properties for use in a mechanistic-empirical design procedure.

Papuc, D. (2021). Laboratory and full-scale pavement sections testing for evaluating frost action in cold regions. Rowan University.

Pavement Interactive (n.d.). Frost Action Mitigation. Pavementinteractive.org. Retrieved April 1, 2023, from https://pavementinteractive.org/reference-desk/design/design-parameters/frost-action-mitigation/

Pekárová, P., Pekár, J., & Lichner, Ľ. (2015). A new method for estimating soil water repellency index. Biologia, 70(11), 1450-1455. https://doi.org/10.1515/biolog-2015-0178.

Penner, E. (1968). Particle size as a basis for predicting frost action in soils. Soils and Foundations, 8(4), 21–29.

Penner, E. (1959). The mechanism of frost heaving in soils. Highway Research Board Bulletin, (225).

Peterson, R. A., & Krantz, W. B. (2003). A mechanism for differential frost heave and its implications for patterned-ground formation. Journal of Glaciology, 49(164), 69-80.

Rengmark, F. (1963). Highway pavement design in frost areas in Sweden. Highway Research Record, (33).

Richter, C. A. (2006). Seasonal variations in the moduli of unbound pavement layers (No.FHWA-HRT-04-079). United States. Federal Highway Administration Roach, P., Shirtcliffe, N. J., & Newton, M. I. (2008). Progress in superhydrophobic surface development. Soft Matter, 4(2), 224-240

Rodríguez-Guevara, C. M., Pando, M. A., & Larrahondo, J. M. (2022). Reduced wettability in compacted coal fly ash due to organosilane treatment. Environmental Geotechnics, 40(XXXX), 1-14.

Römkens, M. J. M., & Miller, R. D. (1973). Migration of mineral particles in ice with a temperature gradient. Journal of Colloid and Interface Science, 42(1), 103-111.

Roustaei, M., Eslami, A., & Ghazavi, M. (2015). Effects of freeze–thaw cycles on fiber-reinforced fine-grained soil in relation to geotechnical parameters. Cold Regions Science and Technology, 120, 127-137.

Roy, J. L., & McGill, W. B. (2002). Assessing soil water repellency using the molarity of ethanol droplet (MED) test. Soil Science, 167(2), 83–97.

Rukashaza-Mukome, M. C., Thorius, J. M., Jahren, C. T., Johnson, G. D., & White, D. J. (2003, August). Cost comparison of treatments used to maintain or upgrade aggregate roads. In Proceedings of the 2003 Mid-Continent Transportation Research Symposium.

Taber, S. (1916). The growth of crystals under external pressure. American Journal of Science, 4(246), 532–556.

Taber, S. (1918). Ice forming in clay soils will lift surface weights. Eng. News-Record, 80(6), 262–63.

Taber, S. (1918). Surface heaving caused by the segregation of water, forming ice crystals. Engineering News-Record, pp. 81, 683–684.

Taylor, G. S., & Luthin, J. N. (1978). A model for coupled heat and moisture transfer during soil freezing. Canadian Geotechnical Journal, 15(4), 548–555.

Thomas, H. R., Cleall, P., Li, Y. C., Harris, C., & Kern-Luetschg, M. (2009). Modeling of cryogenic processes in permafrost and seasonally frozen soils. Geotechnique, 59(3), 173-184. https://doi:10.1680/geot.2009.59.3.173.

Transportation Officials. (1993). AASHTO Guide for Design of Pavement Structures, 1993 (Vol. 1). Aashto.

Saarelainen, S., & Gustavsson, H. (2001). Thaw weakening of subgrades in Finland. In International Conference on soil mechanics and geotechnical engineering (pp. 2183-2186).

Sadiq, M. F., Naqvi, M. W., Cetin, B., & Daniels, J. (2023). Role of Temperature Gradient and Soil Thermal Properties on Frost Heave. Transportation Research Record, 03611981221147261. https://doi.org/10.1177/03611981221147261

Salour, F., & Erlingsson, S. (2012). Pavement structural behavior during spring thaw: interpretation of FWD measurements by monitoring environmental data from county road 126 at Torpsbruk. Statens väg-och transportforskningsinstitut.

Santos, J., Ferreira, A., & Flintsch, G. (2015). A life cycle assessment model for pavement management: road pavement construction and management in Portugal. International Journal of Pavement Engineering, 16(4), 315-336. https://doi.org/10.1080/10298436.2014.942862

Saulick, Y. (2018). Synthesized water-repellent granular solids. HKU Theses Online (HKUTO).

Saulick, Y., Lourenço, S. D. N., & Baudet, B. A. (2017). A semi-automated technique for repeatable and reproducible contact angle measurements in granular materials using the sessile drop method. Soil Science Society of America Journal, 81(2), 241-249. https://doi.org/10.2136/sssaj2016.04.0131

Schaus, L., & Popik, M. (2011). Frost Heaves: A Problem That Continues to Swell, Integrating Successful Mitigation of Frost Heaves Session of the 2011 Annual Conference of the Transportation Association of Canada Edmonton, Alberta, 11-14 September 2011. Transportation Association of Canada, Ottawa, ON, pp 1201-1211.

Shang, J., Flury, M., Harsh, J. B., & Zollars, R. L. (2008). Comparison of different methods to measure contact angles of soil colloids. Journal of colloid and interface science, 328(2), 299–307. https://doi.org/10.1016/j.jcis.2008.09.039.

Sheng, Y., Wen, Z., Ma, W., Liu, Y., Qi, J., & Wu, J. (2006). Long-term evaluations of insulated road in the Qinghai-Tibetan plateau. Cold regions science and technology, 45(1), 23-30.

Shibi, T., Kamei, T. (2014). Effect of freeze-thaw cycles on the strength and physical properties of cement-stabilized soil containing recycled bassanite and coal ash, Cold Regions Science and Technology, Volumes 106–107, Pages 36-45, ISSN 0165-232X,

Shoop, S. A., & Henry, K. S. (1991). Effect of a geotextile on water migration and frost heave in a large-scale test basin. Transportation Research Record, (1307).

Smettem, K. R. J., Rye, C., Henry, D. J., Sochacki, S. J., & Harper, R. J. (2021). Soil water repellency and the five spheres of influence: A review of mechanisms, measurement, and ecological implications. Science of the Total Environment, 787, 147429. https://doi.org/10.1016/j.scitotenv.2021.147429.

St-Laurent, D., and Roy, M. (1995). "Évaluation structurale des chausses souples dans un contexte climatique nordique: une étude avec le FWD (Structural evaluation of flexible pavements in a northern context: A study using the FWD)," Proceedings of the 30th Annual Conference of AQTR, Association Québécoise du Transport et des Routes, Quebec, Canada.

Stefan J. (1891). Über die Theorie der Eisbildung, insbesondere über die Eisbildung im Polarmee. Annals of Physics and Chemistry, 42: 269286

Subedi, S., Kawamoto, K., Kuroda, T., Moldrup, P., & Komatsu, T. (2011, December). Effect of water content on the water repellency for hydrophobized sands. In AGU Fall Meeting Abstracts (Vol. 2011, pp. H53A-1372).

Sun, X., Miao, L., Wang, H. (2021). Improvement of characteristics and freeze-thaw durability of solidified loess based on microbially induced carbonate precipitation. Bull Eng Geol Environ 80, 4957–4966.

Tillman, R. W., Scotter, D. R., Wallis, M. G., & Clothier, B. E. (1989). Water repellency and its measurement by using intrinsic sorptivity. Soil Research, 27(4), 637–644.

Tschapek, M. (1984). Criteria for determining the hydrophilicity-hydrophobicity of soils. Zeitschrift für pflanzenernährung und bodenkunde, 147(2), 137-149. https://doi.org/10.1002/jpln.19841470202

U.S. Army Corps of Engineers, EM 1110-3-138, "Pavement Criteria for Seasonal Frost Conditions," Department of The Army Corps of Engineers Office of The Chief of Engineers. April 1984.

Valat, B., Jouany, C., & Riviere, L. M. (1991). Characterization of the wetting properties of air-dried peats and composts. Soil Science, 152(2), 100-107. https://doi.org/10.1097/00010694-199108000-00006.

Valtseva, T., Peters, A., Kudryavtsev, S., & Alekseenko, S. (2019). Investigation of the construction of airfield pavement using extruded polystyrene foam in the cold regions of the Russian Far East. In MATEC Web of Conferences (Vol. 265, p. 02007). EDP Sciences.

Vignes-Adler. M. (1977). On the origin of the water aspiration in a freezing dispersed medium. , 60(1), 162–171. https://doi:10.1016/0021-9797(77)90267–3.

Wallis, M. G., Scotter, D. R., & Horne, D. J. (1991). An evaluation of the intrinsic sorptivity water repellency index on a range of New Zealand soils. Soil Research, 29(3), 353–362.

Wang, Y., Wang, D., Ma, W., Wen, Z., Chen, S., & Xu, X. (2018). Laboratory observation and analysis of frost heave progression in clay from the Qinghai-Tibet Plateau. Applied Thermal Engineering, 131, 381-389. https://doi:10.1016/j.applthermaleng.2017.11.052.

Wang, Z., Wu, L., & Wu, Q. J. (2000). Water-entry value as an alternative indicator of soil water-repellency and wettability. Journal of Hydrology, 231, 76–83.

Watson, C. L., & Letey, J. (1970). Indices for characterizing soil-water repellency based upon contact angle-surface tension relationships. Soil Science Society of America Journal, 34(6), 841-844. https://doi.org/10.2136/sssaj1970.03615995003400060011x

Wasif Naqvi, M., Sadiq, M. F., Cetin, B., Uduebor, M., & Daniels, J. (2022). Investigating the Frost Action in Soils. In Geo-Congress 2022 (pp. 257-267).

Wen-zhi, Z. (2003). Application of polystyrene foam plastic slabs in frost heaving prevention of canal. Journal of Water Resources and Architectural Engineering, 6(2), 56–57.

Wexler, H. (1964). Polymerization of drying oils. Chemical Reviews, 64(6), 591–611. https://doi.org/10.1021/cr60232a001.

White, T. D., & Coree, B. J. (1990, July). Threshold pavement thickness to survive spring thaw. In Proceedings of the Third International Conference on Bearing Capacity of Roads and Airfields, Trondheim, Norway (pp. 41–51).

Wijewardana, N. S., Müller, K., Moldrup, P., Clothier, B., Komatsu, T., Hiradate, S., ... & Kawamoto, K. (2016). Soil-water repellency characteristic curves for soil profiles with organic carbon gradients. Geoderma, 264, 150-159. https://doi.org/10.1016/j.geoderma.2015.10.020

Wyckoff, L. B. (1918). Some observations on the effect of frost in raising weights. Eng. News-Record, pp. 80, 628.

Yarbaşı, N., Kalkan, E., & Akbulut, S. (2007). Modification of the geotechnical properties, as influenced by freeze–thaw, of granular soils with waste additives. Cold regions science and technology, 48(1), 44-54.

Zaimoglu, A. S. (2010). Freezing–thawing behavior of fine-grained soils reinforced with polypropylene fibers. Cold regions science and technology, 60(1), 63-65. https://doi.org/10.1016/j.coldregions.2009.07.001

Zaman, Md & Han, Jie & Zhang, Xiong. (2022). Technical Review of Development and Applications from Wicking Fabric to Wicking Geotextile. 587-596. https://doi.org/10.1061/9780784484012.059.

Zavala, L. M., González, F. A., & Jordán, A. (2009). Intensity and persistence of water repellency in relation to vegetation types and soil parameters in Mediterranean SW Spain. Geoderma, 152(3-4), 361-374.

Zhang, W., & Macdonald, R. A. (1999). The Danish Road Testing Machine 1995-2000. In International Conference on Accelerated Pavement Testing. by Road Directorate, Danish Road Institute.

Zhang, H. Y., Zhu, S. B., Li, M., & Zhang, X. C. (2016). Water repellency of monument soil treated by tung oil. Geotechnical and Geological Engineering, pp. 34, 205–216. https://doi.org/10.1016/j.jclepro.2019.05.032.

Zhang, P., Wang, S., Wang, S., & Jiang, L. (2015). Superwetting surfaces under different media: effects of surface topography on wettability. Small, 11(16), 1939-1946. https://doi.org/10.1002/smll.201401869.

Zhang, M., Zhang, X., Li, S., Lu, J., & Pei, W. (2017). Effect of temperature gradients on the frost heave of a saturated silty clay with a water supply. Journal of Cold Regions Engineering, 31(4), 04017011. https://doi:10.1061/(ASCE)CR.1943-5495.0000137

Zhang, X., & Belmont, N. (2009). Use of Mirafi nylon wicking fabric to help prevent frost heaving in Alaska pavement: 1st, 2nd, 3rd, 4th, and fifth progress reports. Progress reports to TENCATE GEOSYNTHETICS (North America).

Zhang, X., Presler, W., Li, L., Jones, D., & Odgers, B. (2014). Use of wicking fabric to help prevent frost boils in Alaskan pavements. Journal of Materials in Civil Engineering, 26(4), 728–740.

Zhang, Y., Johnson, A.E., & White, D.J. (2016). Laboratory freeze–thaw assessment of cement, fly ash, and fiber-stabilized pavement foundation materials. Cold Regions Science and Technology, Volume 122, Pages 50–57, ISSN 0165-232X.

Zhang, Y. W. (2009). Application of Polystyrene Foam Plate in Pipeline Anti-freeze Technology. Gansu Water Conserv. Hydropower Technol, pp. 45, 7–9.

Zhao, X. (2017, June). Introduction to EPS and XPS two exterior insulation used. In Advances in Materials, Machinery, Electrical Engineering (AMMEE 2017) (pp. 72–74). Atlantis Press.

Zhou, J., & Wei, C. (2020). Ice lens-induced interfacial hydraulic resistance in frost heave. Cold Regions Science and Technology, p. 171, 102964. https://doi.org/10.1016/j.coldregions.2019.102964

Zhou, J., Wei, C., Wei, H., & Tan, L. (2014). Experimental and theoretical characterization of frost heave and ice lenses. Cold Regions Science and Technology, pp. 104, 76–87. https://doi:10.1016/j.coldregions.2014.05.002

Zornberg, J. G., Azevedo, M., Sikkema, M., & Odgers, B. (2017). Geosynthetics with enhanced lateral drainage capabilities in roadway systems. Transportation Geotechnics, 12, 85-100.

Zornberg, J. G., Bouazza, A., & McCartney, J. S. (2010). Geosynthetic capillary barriers: current state of knowledge. Geosynthetics International, 17(5), 273–300. https://doi:10.1680/gein.2010.17.5.273

CHAPTER 3: PERFORMANCE EVALUATION OF HYDROPHOBIC SOILS

FACTORS AFFECTING THE WATER RESISTANCE OF FROST SUSCEPTIBLE HYDROPHOBIC SOIL.

Abstract

This study presents a comprehensive investigation into the performance of engineered water-repellent (EWR) soils in withstanding hydrostatic pressure, measured through breakthrough pressure (BP). The study evaluates the effects of sustained water pressure and key factors such as density, water-repellent treatment dosage concentration, confining pressure, loading rate, and duration on the water resistance behavior of EWR-treated samples. The impact of extreme environmental conditions, including repetitive loading, repeat wetting-drying, and inundation, on the durability and resistance of hydrophobic soils was assessed. A fat clay soil from Iowa was treated with a commercial chemical compound, imparting hydrophobicity to soil particle surfaces. The BP was measured using a modified water-ponding method combined with a triaxial setup and FlowTRAC system for precise volume and pressure control. The BP was defined as the pressure at which 0.02 cc of water permeated the soil within one minute. The study revealed that soil densification plays a significant role in enhancing BP, increasing from 7.4 kPa to 21.25 kPa (by three times) when comparing loosely (13.2 kN/m^3) to densely (14.69 kN/m^3) compacted soils. BP increased progressively until the maximum dry unit weight (MDUW) was reached, followed by a sharp decline as the soil became oversaturated. Additionally, as the fine content decreased from 100% to 63%, BP values dropped threefold, indicating the importance of fine particle content in water resistance. Confining pressure also significantly influenced BP, suggesting changes in hydraulic conductivity and interparticle voids. The curing period was also crucial, with BP increasing over seven days. The results showed that increasing the loading rate reduced BP (hydrostatic pressure increment) while increasing the time interval between loading steps significantly improved the soil's resistance to water infiltration. At low hydrostatic pressures, water permeated the sample without reaching a breakthrough volume. After durability testing, BP values decreased due to microstructural changes and sample volume adjustments caused by the exposure conditions. The findings suggest that while EWR treatment in soils offers improvement to its hydrostatic

resistance, soil porosity or density is also important, if not more so, in determining their overall performance.

Keywords: Hydrophobicity, water entry pressure, durability,

Nomenclature

AASHTO: American Association of Highway and Transportation Officials

BP: Breakthrough Pressure

EWR: Engineered Water Repellency

MDD: Maximum Dry Density

OMC: Optimum Moisture Content

OS: Organosilane

SWR: Soil water repellency

USCS: Unified Soil Classification System

WEP: Water Entry Pressure

WP: Water-ponding

W-D: Wet-Dry

3.1 Introduction

According to several studies, soil water repellency (SWR) is a global phenomenon due to natural effects such as the presence of aliphatic compounds (Doerr et al., 2005; Goebel et al., 2011), wildfire (Granged et al., 2011b; Jiménez-Pinilla et al., 2016; Malvar et al., 2016; Martins et al., 2020), natural decomposition (Doerr & Thomas, 2000; Goebel et al., 2011), or even anthropogenic factors (chemical spill or burning). This is generally described as having an undesirable effect on soil properties or the prevailing hydrology, e.g., reduced soil water infiltration capacity, higher surface runoff, accelerated soil erosion, and

reduced evaporation (Terry & Shakesby, 1993; Deurer & Bachmann, 2007; Hardie et al., 2012). Naturally occurring SWR is typically classified as a function of severity or persistence.

The severity of soil hydrophobicity is determined by its wetting properties, which can range from being highly wettable (superhydrophilic or hydrophilic) to non-wettable (hydrophobic or superhydrophobic). Various tests, such as Contact Angles (CA) and the Molarity of an Ethanol Drop test (MED) (also known as the Critical Surface Tension or CST test), are employed to assess this property (Bachmann et al., 2000; Roy & McGill, 2002; Wijewardana et al., 2016; Smettem et al., 2021). In contrast, persistence relates to how long it takes for water to infiltrate a hydrophobic surface, which is evaluated through a water drop penetration time test (Dekker & Ritsema, 1994; Doerr, 1998; Letey, 1969; Doerr et al., 2000; Leelamanie et al., 2008). While these tests offer valuable insights, they do not provide a foundation for harnessing the beneficial aspects of soil hydrophobicity (water retarding capacity) for geotechnical engineering applications. For instance, they do not indicate how much a hydrophobic surface can function as a barrier to hydraulic pressure.

Hydrophobic soil has diverse uses, including mitigating frost action (Mahedi et al., 2020; Uduebor et al., 2022a), stabilizing soil moisture levels against seasonal fluctuations and changes in soil stiffness, and preventing leaching (Lin et al., 2019; Daniels, 2020; Kim et al., 2021). Consequently, there is a pressing need to evaluate a soil's capacity to withstand hydrostatic pressure effectively (i.e., its ability to resist water pressure over time). One crucial property associated with hydrostatic resistance is the Water Entry Pressure (WEP) (also referred to as Breakthrough Pressure (BP)). This parameter denotes the minimum positive hydrostatic pressure required to force water through the largest opening in hydrophobic soil. Unlike hydrophilic soils, where water initially permeates through the smallest pores, hydrophobic materials possess this distinctive characteristic (Bauters et al., 2000; Doerr et al., 2000; Bachmann et al., 2007).

Currently, three established methods are available for assessing BP. The most widely adopted technique is the water-ponding method (WP), then the tension pressure infiltrometer, and the triaxial setup

(Perroux & White, 1988; Fallow & Elrick, 1996; Annaka & Hanayama, 2005; Keatts et al., 2018; Feyyisa et al., 2019). Research in this area has revealed that a range of factors, including density, concentration of hydrophobic chemicals (e.g., organosilane, dimethyldichlorosilane, polyoxyalkylated diethylenetriamine, oleic acid, and stearic acid), and fines content, can exert an influence on the BP values of Engineered Water-Repellent (EWR) soil. Therefore, a more comprehensive understanding of these factors is crucial for effectively applying these findings. Furthermore, it is essential to note that there is a paucity of research regarding the impacts of confining pressure (such as depth placement), repetitive environmental exposures (such as full immersion, multiple loadings, and wetting-drying cycles), and prolonged exposure to hydrostatic pressure on BP values. These aspects have yet to be thoroughly investigated and represent areas that warrant further research and exploration.

This study will focus on exploring the various factors that affect the BP of EWR samples, including densification, OS concentration, fines content, hydrostatic loading rate, and prolonged hydrostatic exposure. Additionally, the study will investigate the influence of environmental factors, specifically wetting-drying cycles, and the repetitive impact of hydrostatic loading and full immersion on the BP.

3.2 Materials and Methods

3.2.1 Material

Fat clay (CH, according to the Unified Soil Classification System [USCS]) from Iowa (IA-BV) is utilized in this study. Table 3-1 summarizes basic geotechnical testing, including particle size distribution (see Figure 3.1) (ASTM D422-63, 2007; ASTM D7928, 2017), specific gravity (ASTM D854-10, 2006), Atterberg limit (i.e., liquid and plastic limit) (ASTM D 4318-00, 2000), and Standard Proctor compaction test (ASTM D698, 2012).

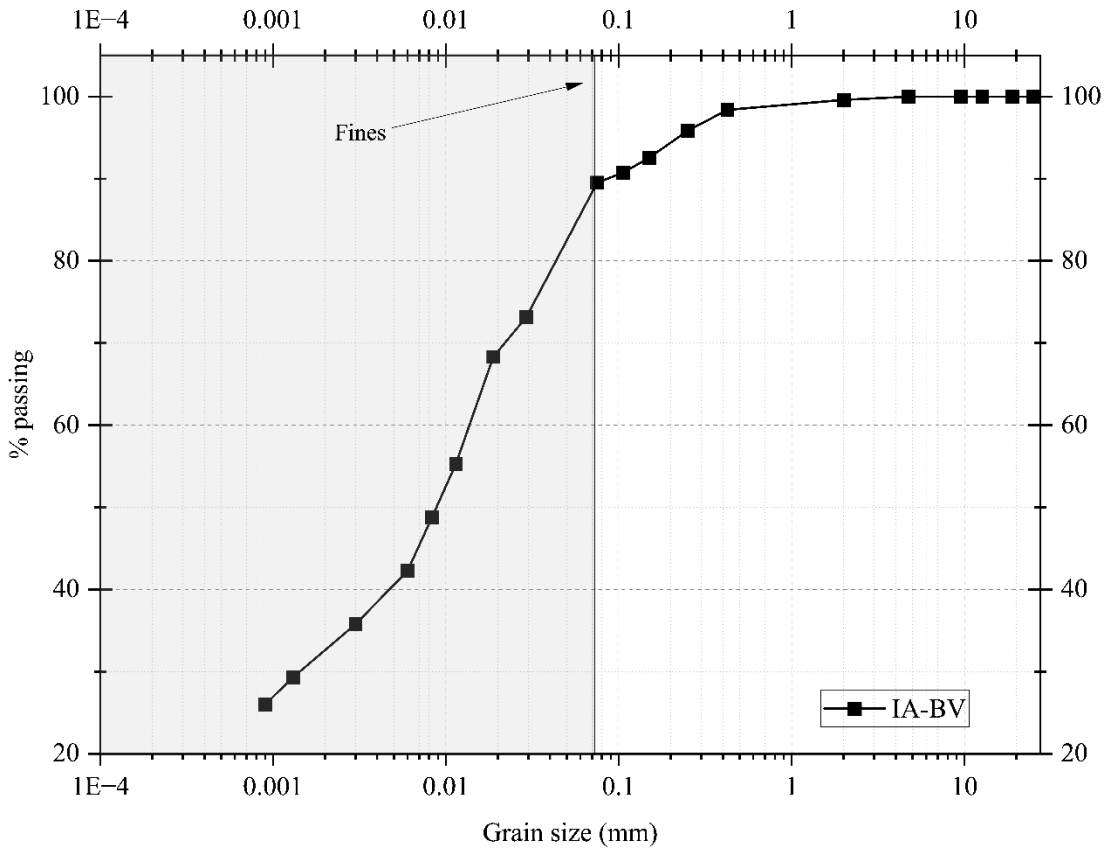

Figure 3.1. Particle size distribution of IA-BV.

Terrasil from Zydex Industries, India, a commercially available OS, was used to induce hydrophobicity. Terrasil is a non-leachable, viscous, and water-soluble chemical that modifies the soil surface by coating it without bonding properties (Daniels & Hourani, 2009a; Daniels et al., 2009b). Different studies (Uduebor et al., 2022a; Uduebor et al., 2022b; Brooks et al., 2022) have shown that soil treated with varying concentrations of OS displayed hydrophobicity has a contact angle higher than 90^0, indicating it is either hydrophobic or superhydrophobic. The results depicting the variation in the ratio of organosilane (OS) to soil are presented in Figure 3.2. This study utilized an OS: Soil ratio of 1:40, 1:10, and 1:80, batched by weight.

Table 3-1. Basic Soil properties of selected soils.

Soil properties	Characteristics	Units	IA-BV
Classification	AASTHO		A-7-6
	USCS		CH
	D_{60}		0.014
	D_{30}		0.001
Fines	Silt	%	57.24
	Clay	%	32.28
	Fines	%	89.52
Physical properties	Specific gravity		2.69
Atterberg limits	Liquid limit	%	66.54
	Plastic limit	%	26
	Plasticity index	%	40.54
Proctor test	Optimum Moisture Content (OMC)	%	27.60
	Maximum Dry Density (MDD)	kN/m^3	13.50

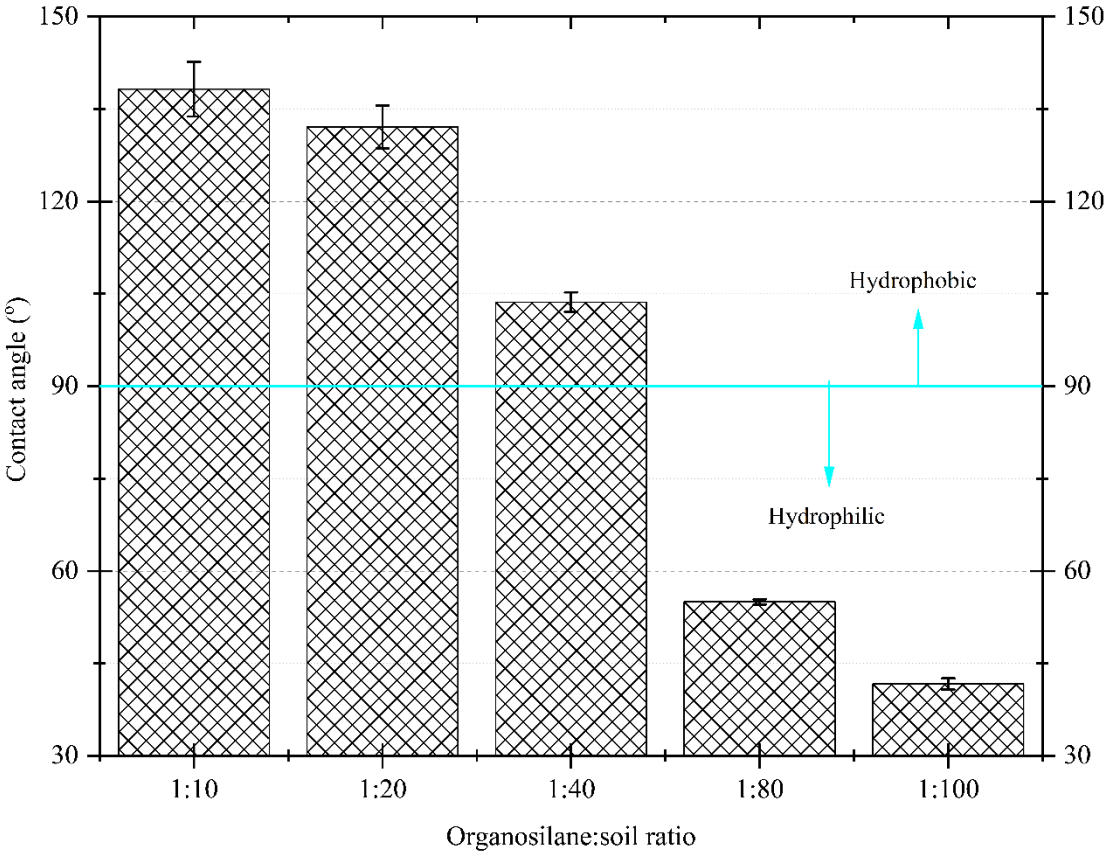

Figure 3.2. Change in contact angle with varying OS concentration.

3.2.1.1 Sample Preparation

The mixing ratio of the investigated hydrophobic soil is presented in Table 3-2. After mixing, each batch was allowed to mellow for 16 hours before compaction in a Harvard mini mold (diameter of 33.02 mm (1.3 inches) and height of 71.12 mm (2.8 inches)) with a 9.1 kg (20-pound) spring-loaded piston according to the compaction method listed in Table 3-3. Harvard mini mold was used because of the limited amount of soil sample available, as the amount of soil needed to run multiple samples was smaller than the alternatives. High compaction energy was utilized for most samples as hydrophobicity is more efficient at high densification (Adeyanju et al., 2024a), as described in Table 3-3. The cylindrical samples were allowed to stand for 1 hour before drying in an oven at 221^{O}F (105^{O}C) for 24 hours, as Adeyanju et al. (2024b) indicate that EWR samples are efficient at about 5% gravimetric moisture content, after which it was cooled for another 24 hours before testing (in a chamber with calcium chloride as a desiccant). For all tests, except the otherwise stated, the dry unit weight of the soil was kept at 13.61 kN/m^3 with a standard deviation of 0.156 kN/m^3.

Table 3-2. Typical Mix design for all samples.

Specimen ID	Soil type	OS: Soil	Soil (g)	OMC (%)	Terrasil (g)	Water (g)	Molding liquid (OS + water) (OMC) (g)
BV (untreated)	IA-BV	0	1000	27.6	0	276	276*
BV10		1:10	1000		100	176	276
BV40		1:40	1000		25	251	
BV80		1:80	1000		12.5	263.5	
BVS10		1:40	1000	10%	25	75	100
BVS15			1000	15%		125	150
BVS20			1000	20%		175	200
BVS28			1000	OMC		251	276
BVS30			1000	30%		275	300

Table 3-3: Compaction energy.

Compaction energy ID	No of layers	No of blows	Mass of soil per layer (g)
High (H)	5	20	27
Medium (M)	3	20	45
Low (L)*	3	15	45

*Compaction is done with light tampering using the same 9.1 kg spring-loaded piston.

3.2.2 Methods

3.2.2.1 Specimen Setup

Each cylindrical sample underwent mass measurement before testing and was positioned within a triaxial cell. In this cell, saturated porous stones and filter papers were carefully placed at the bottom and top of the sample. Each sample was sealed in a 35.56 mm (1.4 inches) diameter latex membrane in the triaxial cell.

Following this setup, the permeameter was filled with water, and the appropriate confining pressure, as displayed in Table 3-4, was applied using a Geocomp FlowTrac II pressure and volume controller (Figure 3.3a. no. 1) (which can maintain the desired pressure within 0.344 kPa (0.05 psi) while monitoring volume change within 0.001 cc (3.381402e-5 oz)). To ensure accurate testing conditions, "flushing" was performed by passing water (from the FlowTrac, Figure 3.3a. no. 2)) through the one bottom-inlet valve opening (Figure 3.3a. no. 4) (which would be used for testing) while flowing out through the second bottom inlet valve (Figure 3.3a. no. 5). Hence, simultaneously, drainage occurred from the other bottom inlet. This careful process was essential to eliminate trapped air throughout the testing system and guarantee thorough saturation of the porous stones (although soaked, porous stones were used).

a

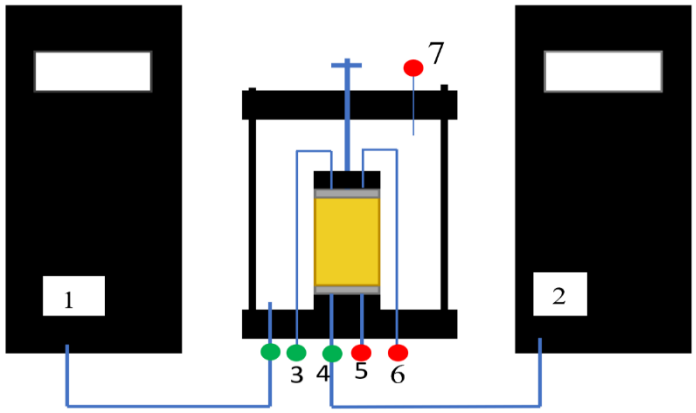

b

Figure 3.3: a) Schematic diagram of the testing setup (1-Cell pressure FlowTrac, 2-Inlet FlowTrac, 3-Top cap for air outlet, 4-Bottom-inlet Cap, 5-Second bottom cap used for flushing (only open during flushing), 6-Second top cap for air outlet - (closed throughout testing), 7- Inlet valve (Open only during initial permeameter filling for confining pressure), and b) actual testing setup.

3.2.2.2 Test Program

BP was measured by determining the breakthrough volume achieved within a specified time frame. This study utilized a modified water ponding method, where the sample was placed in a triaxial cell (Uduebor et al., 2023; Adeyanju et al., 2024a) instead of a conventional permeameter cell (Keatts et al., 2018). In both methods, water pressure is maintained while the changing water head is carefully monitored with high precision, reaching a sensitivity of 0.001 cc in this method. Like traditional water ponding methods, the water pressure incrementally increased until the corresponding BP was reached. Water ponding methods typically indicate the onset of a breakthrough pressure by the inability of a standpipe to maintain a stable height, visual infiltration into the specimen, or both (Jordan et al., 2016; Brooks et al., 2022; Xing et al., 2022).

Table 3-4: Sample designation

Group ID	Sample designation	Sub-testing	MIX design	Confining pressure (kPa)
B1	BV10H, BV10M, BV10L	Density and concentration	BV10	48
	BV40H, BV40M, BV40L		BV40	
	BV80H, BV80M, BV80L		BV80	
B2	BVC4, BVC7, BVC14, BVC20	Confining pressure	BV40	28, 48, 97, 138
B3	BVS10, BVS15, BVS20, BVS27, BVS30	Same compaction with varied molding moisture	BVS10, BVS15, BVS20, BVS27, BVS30	48
B4	BVPF, BV40H, BVRS, BVWRS	Fines Content	BV40	48
B5	BV0.5, BV0.75, BV1	Loading rate	BV40	48
B6	BV7.5, BV15, BV30, BV60	Loading duration	BV40	48
B7	BVCR1, BVCR2, BVCR3, BVCR4	Creep test	BV40	48
B8	BV40R1, BV40R2, BV40R3.	Repetition	BV40	48
B9	BVI1, BVI3, BVI7	Full immersion	BV40	48
B10	BVWD1, BVWD3, BVWD7	Repeat wet and dry	BV40	48

The breakthrough volume at the onset of water ponding pressure was calculated to be 0.0196 cc, corresponding to a 0.1 cm drop in a 5 mm diameter standpipe. Following the approach used in previous BP studies (Brooks et al., 2022; Keatts et al., 2018), the monitoring period was limited to 1 minute. Accordingly, a breakthrough volume of 0.02 cc within a 1-minute timeframe was employed to determine BP. In Figure 3.4, the soil with zero porosity (simulated in this study by fully closing the supply fittings on the FlowTrac system) exhibited minimal water ingress—not into the soil itself, but to pressurize the system. The breakthrough pressure (BP) criterion was not reached in this scenario. However, the BP criterion was reached at just 0.7 kPa for the untreated sample. In contrast, the EWR-treated BV, which contains voids but

remains hydrophobic, had a BP value of 21 kPa. As hydrostatic pressure increases above BP, water infiltration increases exponentially.

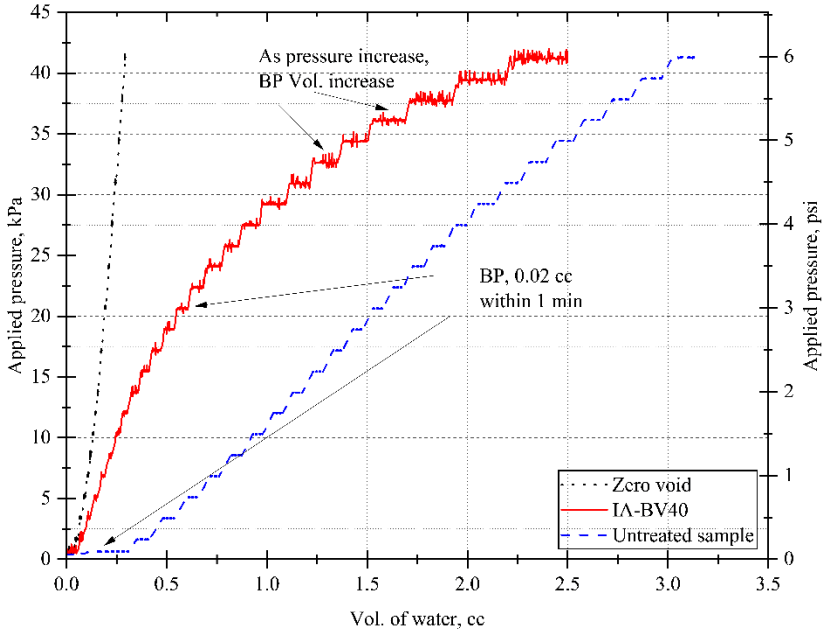

Figure 3.4: Baseline behavior of untreated and treated soil.

3.2.2.3 Test protocol

This study delved into several critical factors influencing BP, such as density, OS concentration, fines content, extended hydrostatic exposure, loading rate, and environmental exposure. The effects of compaction energy (density) and OS concentration were explored by varying compaction energy, the number of layers, and the concentrations, as listed in Table 3-4(B1). The effects of the confining pressure, used to prevent side water leakage, were also investigated at various levels (see B2 in Table 3-4) and explored using the pressure profile displayed in Figure 3.5. These pressures were selected to represent typical subgrade and shallow foundation applications (28 and 48 kPa (AASHTO, 2007)) and retaining wall applications (97 and 138 kPa (Dumenu, 2019)). The molding moisture content was also varied for the soil fabric aspect while maintaining consistent compaction energy (B3 in Table 3-4).

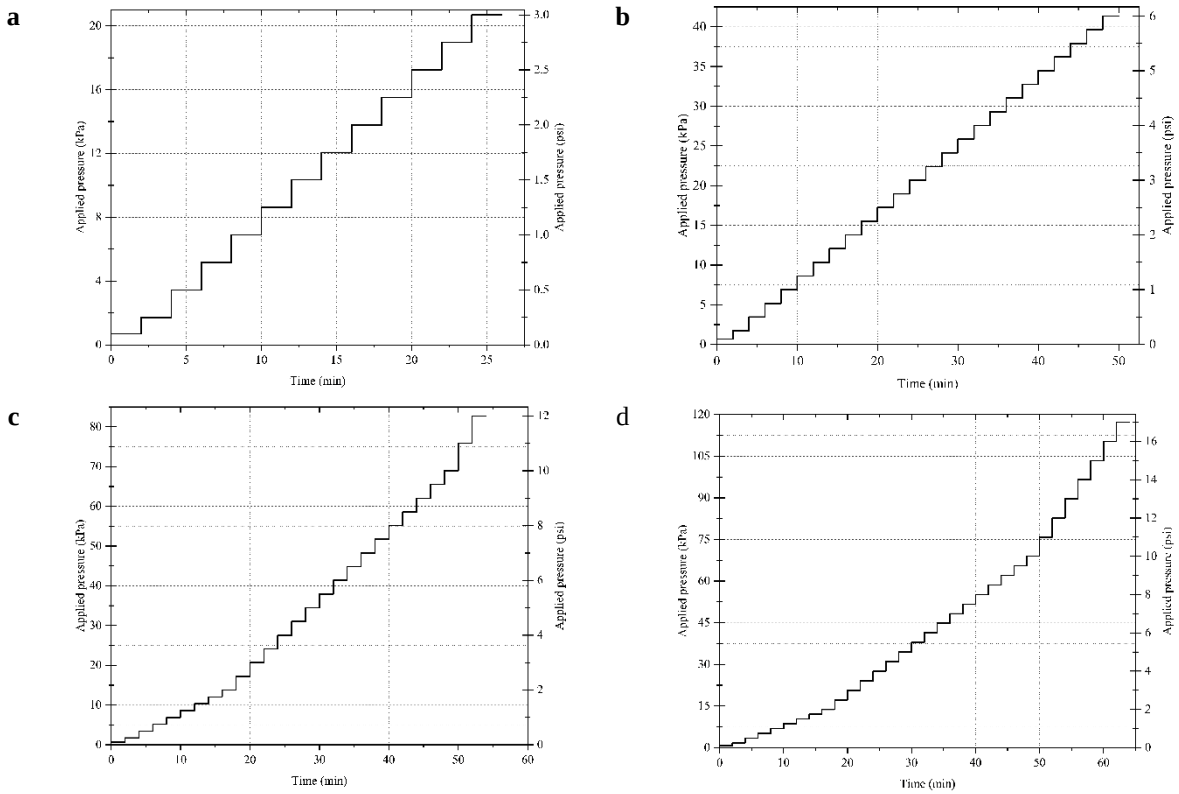

Figure 3.5: Stepwise pressure profile dependent on confining pressure (a- 28 kPa, b- 48 kPa, c-97 kPa, and d-138 kPa).

To assess the influence of fines content (B4 in Table 3-4), IW-BV soil was sieved through a No. 200 sieve, and the fines portion passing through was treated and compacted like BV40, labeled as BVPF. Furthermore, the retained soil particles on the No. 200 sieve were divided into two parts. One part was washed to reduce the fines content further (BVWRS), while the other was used to create reduced fine soil below the natural fines content (BVRS). All variations were treated with soil to OS of 1:40 ratio and compacted at high compaction energy. The grain size distribution for all soil variants with different fines content is presented in Figure 3.6.

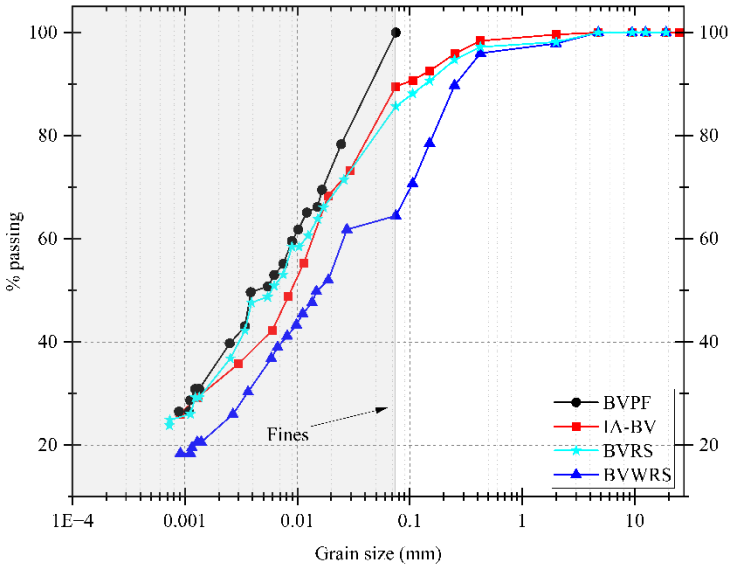

Figure 3.6: Grain size distribution of IA-BV variants with varying fines content.

The loading pressure profile used in this study sustained water pressure for 1 minute to determine whether the BP criteria were met. To investigate the effects of different loading rates (B5 in Table 3-4), the loading pressure varied from 1.7 to 7 kPa, as shown in Figure 3.7a. Additionally, the impact of loading duration (B6), compared to the 2-minute baseline, was examined by extending the loading time to 5, 7.5, 15, 30, and 60 minutes, as displayed in Figure 3.7b. These adjustments helped simulate actual field conditions, where water infiltration and/or hydrostatic pressure occur gradually rather than abruptly.

a

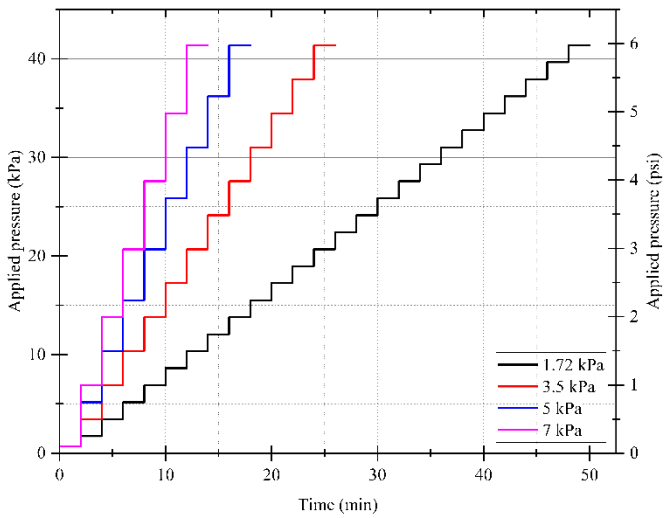

b

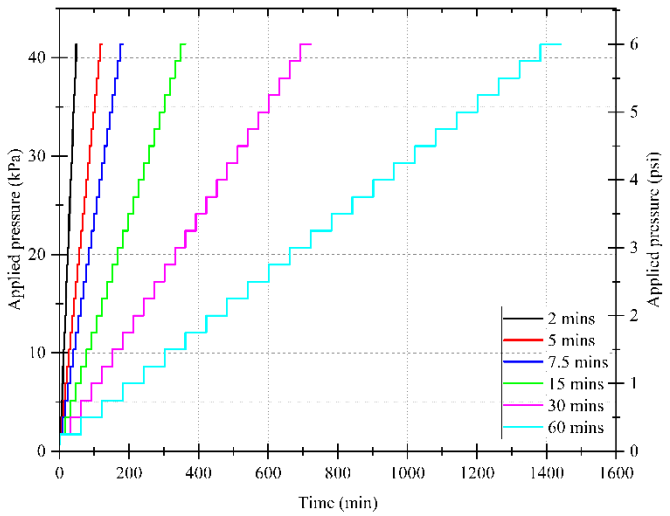

Figure 3.7: Pressure profiles used to simulate a) hydrostatic loading rate and b) duration.

The impact of sustained hydrostatic pressure below the BP was examined (B7). Lee et al. (2015) observed water infiltration before BP after a short time of water ponding. This phenomenon was studied using sustained hydrostatic pressure at 0.7, 7, and 14 kPa for 24 hours. This is called the "creep test," where water resistance failure due to sustained small hydrostatic loading is observed.

The study also examined BP behavior after subjecting hydrophobic soils to durability exposures, including complete immersion, wet-dry cycles, and repetitive hydrostatic pressure. Repetitive hydrostatic pressure was done by testing the triplet samples over and over seven times (B8). After each test, the samples were oven-dried at 71 ± 3°C [160 ± 5°F] for 24 hours and cooled for 6 hours before testing. This test, although aggressive, was used to simulate and explore the reliability of hydrophobicity. Complete immersion involved soaking samples in water for 1, 3, and 7 days with an overhead water height of 30 mm. After the submersion exposure, three samples from each soaking period were oven-dried at 71 ± 3°C [160 ± 5°F] for 24 hours and then tested. At the same time, another set of triplicate samples was tested immediately (B9).

ASTM D559/D559M (2003) and ASTM D870-15 (2015) standards were employed to assess the effects of repeat wet and dry cycles. This entailed submerging the samples in a water bath at room temperature for up to 5 hours, followed by oven-drying at 71 ± 3°C [160 ± 5°F] for 42 hours. After predetermined durability exposure, all samples were oven-dried at 71 ± 3°C [160 ± 5°F] for 42 hours (a

complete cycle process). Different repeated wet-dry cycles (0, 1, 3, and 7) were considered to understand BP behavior after exposure (B10). After each durability exposure, triplicate samples were tested immediately while another set was oven-dried before testing.

3.3 Results and Discussions

3.3.1 Effect of Density and Concentration

Several studies have highlighted the impact of various properties on hydrophobic soil, particularly porosity and concentration (Wang et al., 2000; Hernandez et al., 2005; Lee et al., 2015; Salifu & El Mountassir, 2021; Xing et al., 2022). Figure 3.8a highlights the direct correlation between densification (lower porosity) and BP at different concentrations (surface energy). This relationship aligns with the concept that larger pore sizes correspond to a diminished water repellency "capacity," consistent with findings from Keatts et al. (2018) and Xing et al. (2022). For instance, when considering a 1:40 concentration, the highest BP, 21 kPa, was observed at 14.69 kN/m^3, almost 2 times water resistance at 13.97 kN/m^3. This impact is more pronounced when the density is 13. 2 kN/m^3, where BP is 3 times lower than at 14.69 kN/m^3.

Similarly, at a 1:10 concentration, the highest BP (31 kPa) observed in BV10H at a dense state was roughly four times more than the lowest BP (8 kPa) found in BV10L at a loose state. These results emphasize the substantial influence of porosity and concentration on the water-repellency characteristics of hydrophobic soil. However, it is essential to note that higher concentration does not necessarily lead to higher BP, as an excess of unreactive OS could be a weak link for water infiltration. Furthermore, these findings suggest that in field applications, achieving a compaction level higher than the maximum dry unit weight (MDUW) of untreated soil is essential for improved performance (Hernandez et al., 2005; Lee et al., 2015; Salifu & El Mountassir, 2021). The treatment concentration plays a crucial role in determining the surface energy of a hydrophobic material, as highlighted by Salifu & El Mountassir (2021) and Xing et al. (2022), while density primarily affects pore size.

a

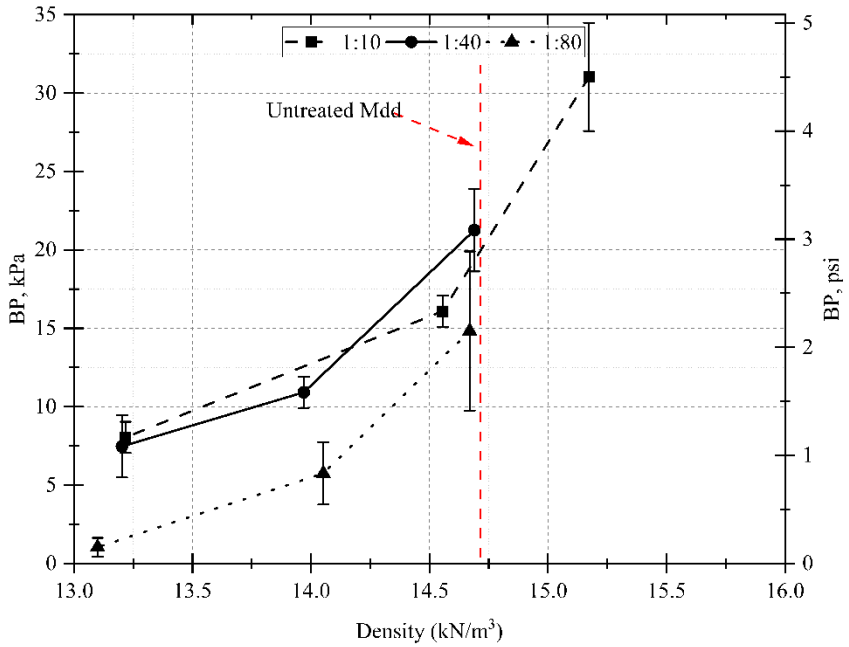

b

Figure 3.8: a) Direct correlation between water entry pressure due to density and b) saturated soil layer, with no preferential flow.

Consequently, compaction can significantly enhance BP for a given surface energy. The study revealed a gradual progression of water infiltration as the pressure increments increased until reaching the predetermined breakthrough criteria, after which the infiltration rate increased even more rapidly. Predictably, the total volume of water required to achieve the stepwise pressure profile increased as

densification decreased. Visual observations also indicated a greater degree of wetting in less dense samples compared to denser ones. Additionally, after testing, a visual examination of the samples indicated no preferential flow paths or finger-like flow patterns. Instead, each soil layer became saturated before progressive infiltration, as shown in Figure 3.8b. Furthermore, the average measured mass change before and after testing reinforced the observation that water inflow was facilitated more easily in loose samples. These findings provide valuable insights into the behavior of hydrophobic soil under various pressure conditions and compaction levels.

Figure 3.9 illustrates the impact of molding moisture on BP, where all samples were compacted with the same energy and treated with a consistent amount of Terasill. BP increases with higher molding moisture content until the MDUW is reached. However, BP sharply declines once the soil becomes almost saturated beyond the MDUW. Importantly, even in this context, the most densely compacted samples consistently exhibit the highest BP values due to their lower porosity. This emphasizes compaction and porosity's critical role in determining BP, regardless of whether the variation arises from differences in compaction energy or molding moisture levels.

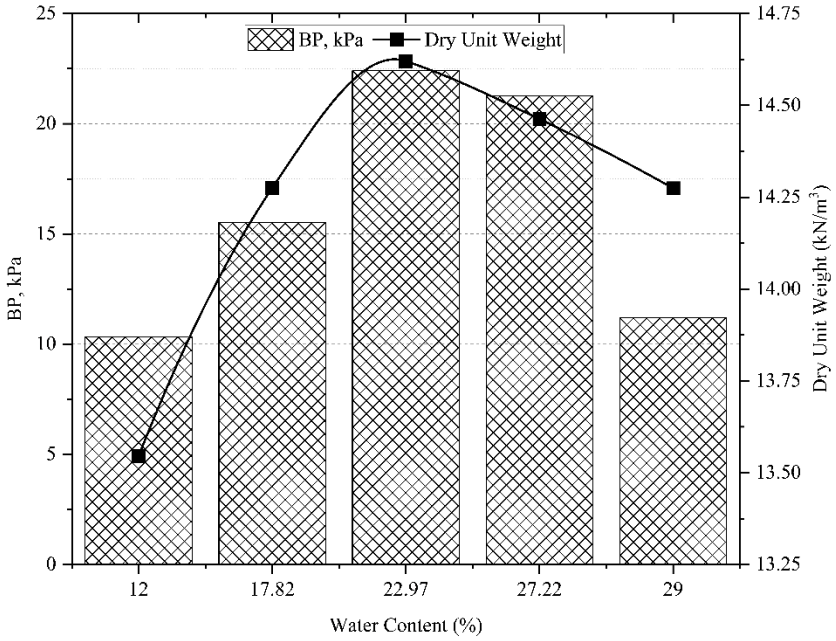

Figure 3.9: Effects of molding moisture on BP (confining pressure of 48 kPa).

3.3.2 Effect of Confining Pressure

Various studies have investigated BP using triaxial methods under different confining pressures. For instance, Dumenu (2019) and Uduebor et al. (2023) used a confining pressure of 138 kPa. However, the specific engineering application must guide the selection of an appropriate confining pressure for BP testing. While 138 kPa may be suitable for embankments or heavily loaded structures, it does not accurately reflect conditions in road applications. The American Association of State Highway and Transportation Officials (AASHTO) recommends a confining pressure of around 48 kPa for triaxial testing (AASHTO, 2007), which aligns more closely with typical roadway applications. Therefore, a confining pressure of around 48 kPa may be more appropriate for road applications, as it balances the impacts of confining pressure without overestimating the BP.

As the confining pressure increases, BP increases, as shown in Figure 3.10. This suggests a strong relationship between confining pressure and soil resistance to water penetration, as higher confining pressures lead to high effective stress and high pore pressure when little moisture infiltrates the soil. Hence, as confining pressure increases, void spaces between particles are compressed, reducing overall porosity and increasing the soil's resistance to water entry. This phenomenon underscores the importance of aligning confining pressure with the intended engineering context, as using too high or too low pressure may lead to inaccurate assessments of soil behavior under actual field conditions.

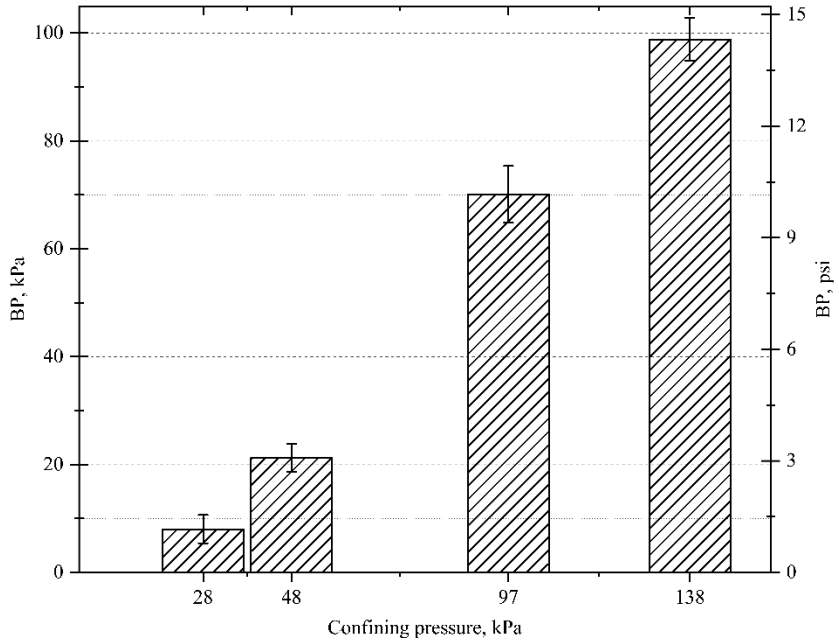

Figure 3.10: Effect of confining pressure on BP (all samples were treated at the same concentration of 1:40).

3.3.3 Effect of Fines

Figure 3.11 highlights a clear inverse relationship between the percentage of fines within soil and BP. Specifically, as the percentage of fines decreases from 100% to 63%, the BP values decline, suggesting that finer particles contribute significantly to the treated soils' BP or hydrophobic behavior. The influence of density and porosity on the hydrophobic behavior of soils is also noticeable in hydrophobized sandy soils or glass beads, where most BP values are reported to be less than 1 meter (approximately 10 kPa), as documented in studies by Jordan et al. (2015) and Xing et al. (2022). In contrast, fly ash, similar to silty soils, has been found to have BP values exceeding 2 meters (around 20 kPa), according to research by Keatts et al. (2018), Jordan et al. (2015), and Feyyisa et al. (2017). This variation in BP values is primarily attributed to pore size (influenced by fines content) and treatment concentration differences.

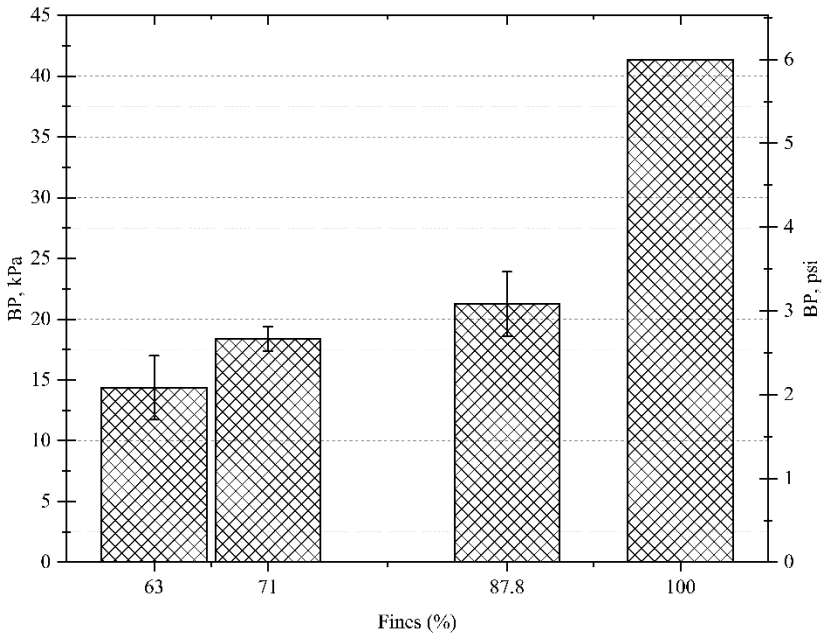

Figure 3.11: Effects of fines on BP.

3.3.4 Effect of Drying and Drying Duration

Figure 3.12 illustrates a clear relationship between curing time, breakthrough pressure (BP), and the corresponding moisture content. The BP test immediately after compaction does not reach a measurable value due to high pore water pressure within the soil. The high moisture content at this stage can break down clay aggregates and eliminate inter-aggregate pores, increasing water infiltration resistance. This condition is expected, as the soil is near its optimum moisture content (OMC) and nearly saturated. As the drying period (air drying) progresses and the sample loses moisture, BP measurement becomes possible and increases significantly. By day 7 (moisture content at 4.2%), the BP reaches its peak value (23 kPa), indicating that as the soil dries and water mass is lost, its ability to resist water flow improves. This change reflects the development of hydrophobic properties in the soil as the moisture content decreases.

The relationship between BP and water loss underscores the critical role of moisture content in determining the soil's hydrophobicity. As the soil dries, its gravimetric moisture content decreases, transitioning the material from a water-saturated state to a hydrophobic state. By day 14 (moisture content at 0.8%), the BP slightly decreased to 22 kPa; the soil remained highly resistant to water infiltration. A significant transformation also occurs in the soil's pore structure as the EWR-treated soil dries. The drying

process leads to a reduction in pore volume due to increased effective stress but leads to an increase in pore connectivity as the soil particles are coated.

More importantly, one of the key factors contributing to the increased water resistance of EWR-treated soil is the change in surface energy. As the soil dries, the contact angle between the water and the soil surface increases, reflecting the growing hydrophobicity. This phenomenon drives the rise in BP, as water encounters greater resistance during infiltration. The hydrophobic state of the soil limits water infiltration by increasing the contact angle, thereby creating a high-energy barrier at the soil-water interface. Even though pore pressure may increase at this interface as water is forced into the soil, the heightened surface energy prevents further penetration, maintaining the elevated BP values observed after several days of curing.

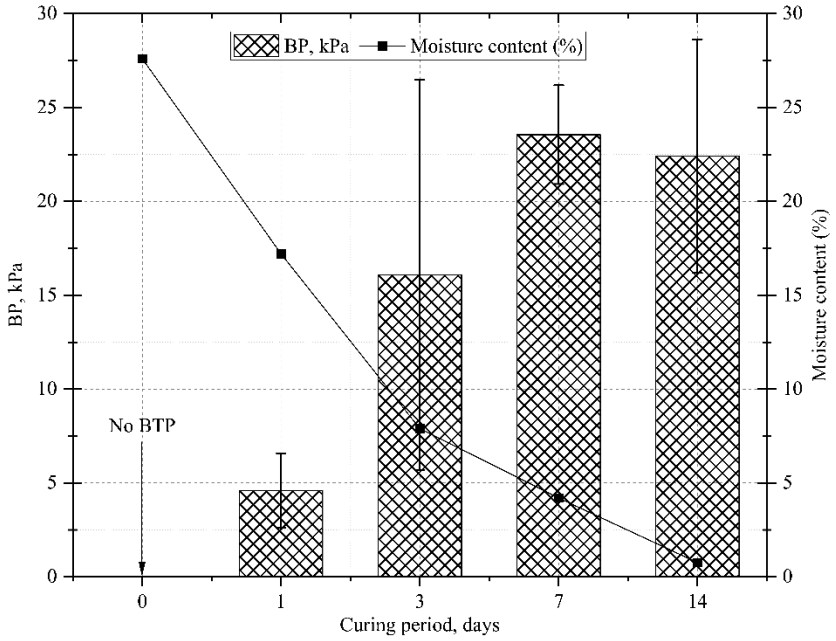

Figure 3.12: Effects of molding moisture on BP and corresponding moisture content (confining pressure of 48 kPa).

3.3.5 Loading Rate

Different studies have employed various loading rates in hydrostatic testing methods, such as water pounding and the tension-pressure infiltrometer method, to assess water infiltration behavior. For instance, Keatts et al. (2018) utilized loading rates of 30 cm/min and 6 cm/min for coal fly ash and sand, while Jordan

et al. (2016) used 1.3 cm/min. Xing et al. (2022) used 6.6 cm/min, while Feyyisa (2017), Feyyisa et al. (2019) and Dumenu (2019) employed a much higher rate of 2100 cm/min. The choice of loading rate in these studies often reflected equipment capability, material type or the need for clear, fast and accurate results within a reasonable timeframe. Theoretically, water infiltration or capillary rise is expected to occur slowly, but due to FlowTrac limitations (in pressure loading programming) and number of tests, 17.57 cm/min (equivalent to 1.7 kPa/min) was used primarily (realistic testing duration). However, to understand the corresponding impact, a range of 17.57 cm/min (1.7 kPa/min) to 70.3 cm/min (7 kPa/min) was tested. In most tests, the typical loading rate utilized was 1.7 kpa, representing an appropriate balance between testing efficiency and clarity of breakthrough pressure (BP) observation.

Figure 3.13a indicates that as the load rate increases, the BP values tend to decrease. BP at 1.7 kPa was 21 kPa, which decreased to 12 kPa at loading rate of 5 kPa, representing a 45.92% reduction in breakthrough pressure. The average BP reduction across the increasing loading rates (1.7 to 5 kPa) was 10 kPa. Therefore, statistical analysis (Pearson correlation of -0.89) shows that there is a negative trend between the loading rate and BP. This means that as the loading rate increases, the BP decreases, confirming the general trend that the soil's ability to resist breakthrough pressure diminishes as the applied pressure rate increases. Although BP decreases as the rate increases, there is a slight anomaly at 7 kPa, where the BP increased. This deviation from the overall trend could be attributed to factors such as soil compaction, which may affect water infiltration behavior.

In addition to varying the loading rate, the interval between each pressure increment was extended to understand its impact on BP. In typical testing protocols, each pressure increment is kept constant for 2 minutes before increasing to the next step in a stepwise profile. However, this experiment extended the waiting time to 7.5, 15, 30, and 60 minutes to observe the effect of longer intervals between each pressure increment. At the 2-minute interval, the BP reached 21 kPa with a standard deviation of 2.6 kPa, reflecting some variability in breakthrough pressure measurements at this interval. When the interval was increased beyond 2 minutes, the standard deviations became zero, indicating consistent measurements. At the 60-minute interval, as illustrated in Figure 3.13b, the soil did not exhibit any breakthrough pressure (BP),

suggesting that extending the time between increments significantly affects the soil's ability to exhibit water breakthrough at any predefined pressure. This could indicate that during longer intervals, the soil had sufficient time to reach equilibrium or adsorb water without reaching the predefined BP. It should be noted that BP is given as the pressure any which visible water (e.g., 0.02 cc, within min) flow continuously in the soil. As this every step of the test, due to the FlowTrac resolution water infiltration is observed, but so significantly small, that the BP is not reached. Hence, a positive trend in BP values as the interval increases beyond 2 minutes. However, the BP slightly dips at 15 minutes, though it remains close to 41 kPa for longer intervals. This might be due to sample preparations.

a

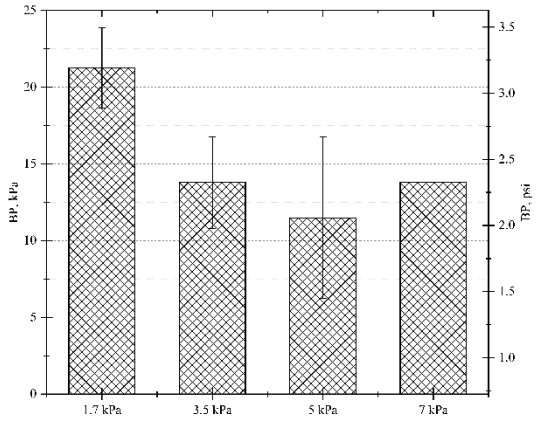

b

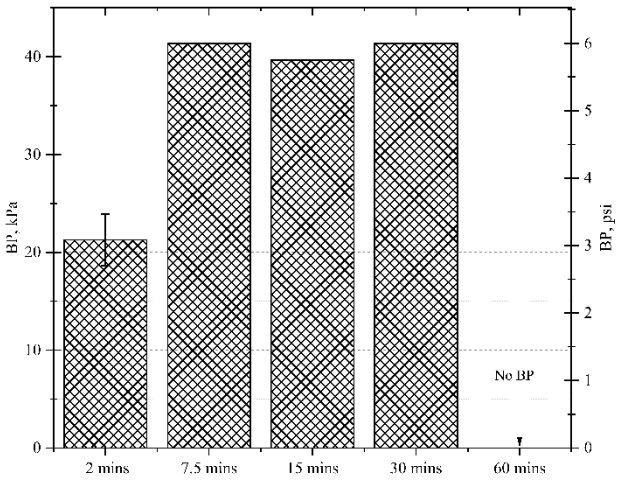

c

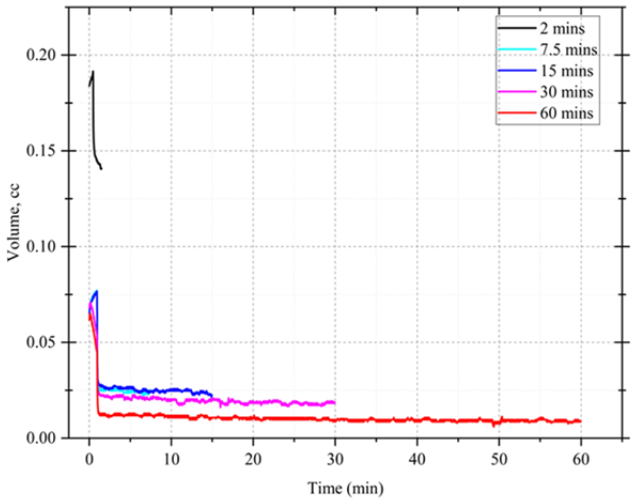

Figure 3.13: Influences of loading a) rate and b) duration, c) prior stepwise effects at 41 kPa loading.

The results clearly demonstrate that increasing the time interval between loading steps significantly impacts the soil's ability to resist water infiltration. As the time interval between pressure increment increases and the pressure increment rate reduces, BP will rise. This adds to the reliability of EWR in the field because pressure buildup due to water infiltration is likely to occur steadily over time rather than in a rapid stepwise manner. In real-world scenarios where hydrostatic pressure is applied gradually and over longer periods, EWR soils may not have BP values. The findings highlight the importance of considering time intervals and loading rates in optimizing EWR on the field. Hence, producing information is crucial for understanding how soils respond under laboratory and field conditions, where dynamic water buildup and pressure application may occur over extended periods.

The interval test also reveals the progressive impact of stepwise pressure loading, as displayed in Figure 3.13c. In the 2-minute test, each successive loading step is heavily influenced by the previous one. Due to the short interval, a significant amount of water remains within the soil matrix, and there is insufficient time for the soil to stabilize between pressure increments. As a result, the next pressure increases compound the preexisting water content and pressure within the soil, leading to faster failures. This rapid water buildup is exacerbated by the confining pressure acting on the soil, further reducing the breakthrough resistance. However, at longer intervals, the soil has time to stabilize between each pressure increment. As a result, there is no cumulative impact from previous steps during the stepwise loading process, allowing

the soil to better resist water infiltration. The ability of the soil to recover and stabilize at longer intervals suggests that water is redistributed or adsorbed within the matrix, preventing the rapid accumulation of water pressure observed in shorter intervals.

3.3.6 Creep

The results of ponding a head of water on the top of treated samples at 1:40 (OS to soil) at different selected pressures are presented in Figure 3.14. Each test was conducted for 24 hours to observe the effect of hydrostatic pressure below the water entry pressure. It is observed that for pressures below the breakthrough pressure, the infiltration into the sample is below 2.5 cc over a 24-hour period. Above the breakthrough pressure, the sample begins to behave like an untreated sample. This indicates that the sample is capable of restricting water flow through it if the pressure is less than BP over a period. This is totally different from the result of the study of Lee et al. (2015), that concluded that water-repellent soils could resist a certain level of hydrostatic pressure for a period and indicates the possibility of creating a temporary hydro-barrier by implementing water repellency in a soil. In that study, hydrostatic pressure, below BP, was sustained for a period of less than 2 hours and the BP criteria was reached. Although, in this study, water permeated into the sample as shown but at a rate far below BP criterion, it did not reach or exceed the breakthrough criteria. It should be noted that the two studies, even though achieved hydrophobicity, utilized different chemicals and utilized different soils.

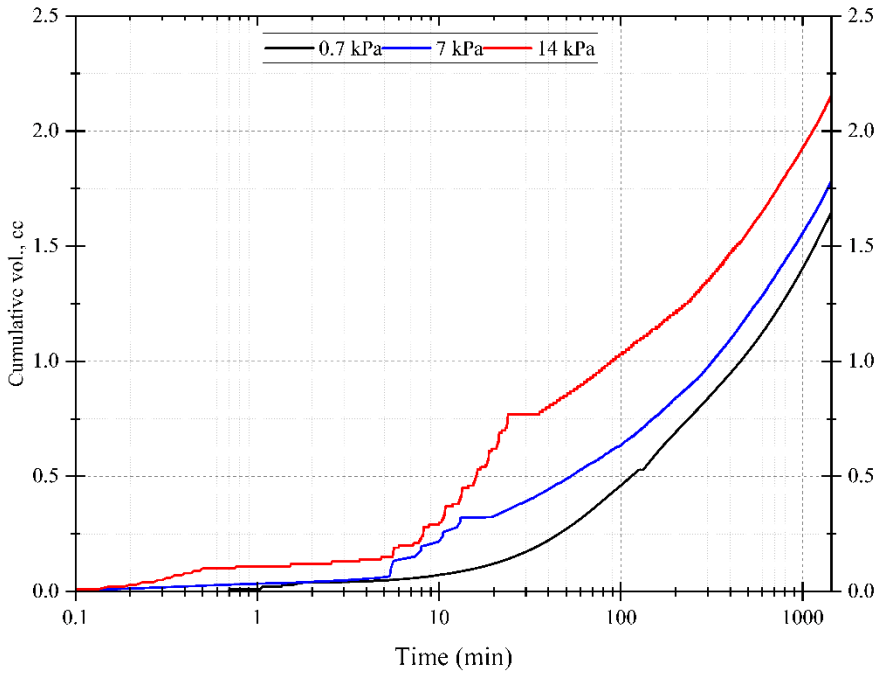

Figure 3.14: Behavior of EWR-treated soil to low hydrostatic pressure.

3.3.7 Durability

Effect of Repeated Testing

Figure 3.15a shows the effects of repeated hydrostatic loading.and drying on EWR samples. EWR-treated soils are designed to be semi-permanent hydrophobic soil and are expected to endure various seasonal conditions, where they face periods of hydrostatic loading followed by drying. This process is especially relevant for frost action mitigation, where the soils are intended to mitigate capillary rise during freezing periods and are exposed to moisture migration during thawing seasons, followed by drying in the summer months. Additionally, capillary rise fluctuation occurs intermittently throughout the year, subjecting EWR-treated soils to constant wetting and drying cycles. In the context of these repeated cycles, Figure 3.15a illustrates how aggressive wet-dry scenarios affect the BP of EWR soils. Initially, the BP value for the first loading cycle starts at 21 kPa, and after the first reloading, it drastically reduces to 10 kPa, representing a 54% reduction. By the seventh cycle, the BP value drops even further to 2.3 kPa, reflecting an 89% reduction in total from the initial BP.

This indicates that EWR soils, intentionally designed for water resistance in environments where they are expected to withstand constant water exposure, experience a significant decrease in water resistance after multiple wetting and drying cycles. However, it should be noted that after each testing cycle, the soil samples were oven-dried at 72°F and allowed to cool before retesting. This process of repeated wetting and drying significantly impacts the soil's porosity and volume stability, as shown in Figure 3.15b, which in turn affects its ability to resist water penetration.

As seen in Figure 3.15a, the BP reduction follows a clear trend, where the resistance capability diminishes progressively with each cycle. This finding is important when considering field applications. In real-world scenarios, the aggressive wet-dry cycles simulated in the lab are not expected to occur with the same intensity or frequency. Hence, the performance of EWR soils in the field should be more stable and longer lasting than observed under these extreme test conditions.

a

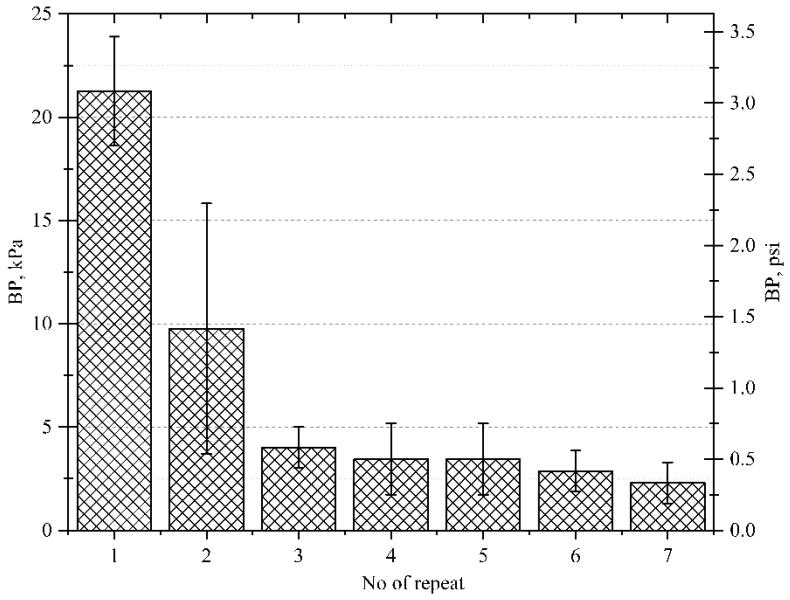

b

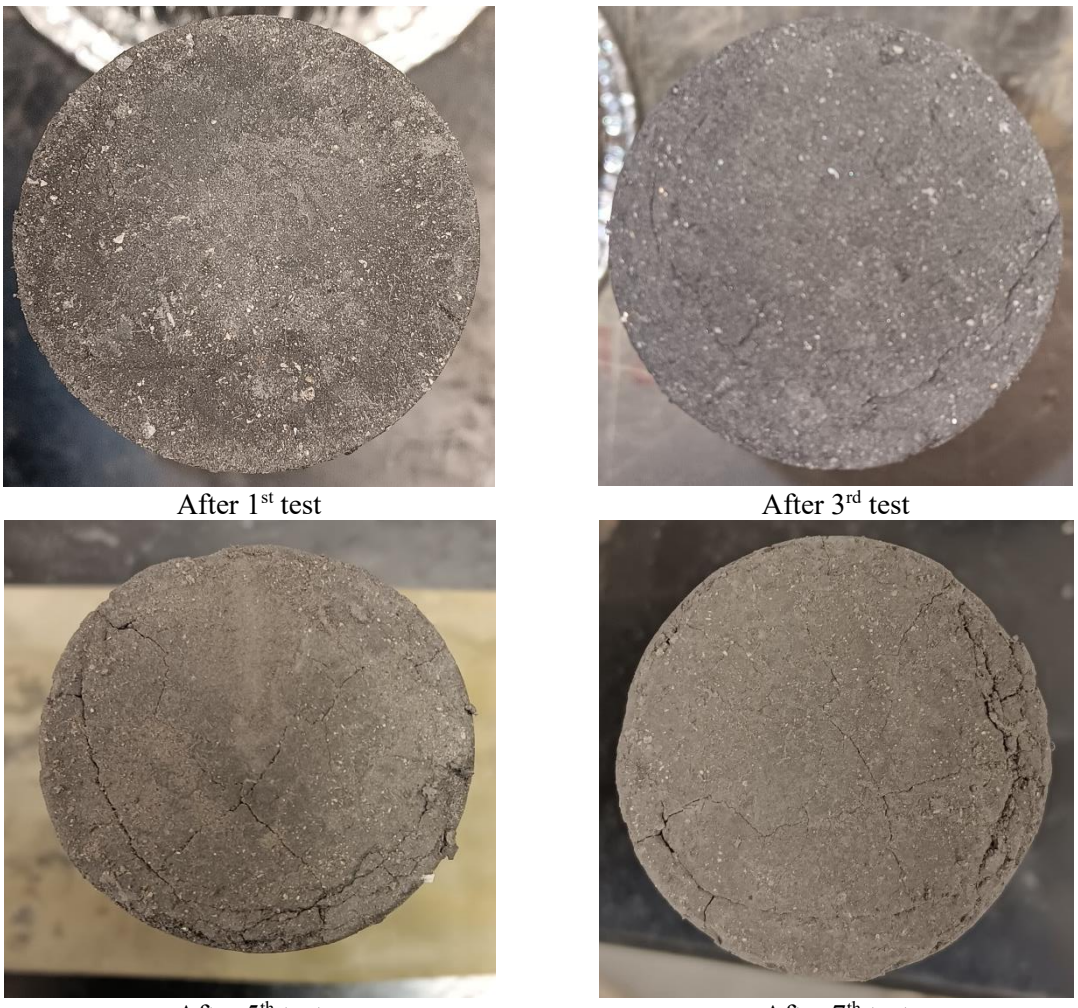

Figure 3.15: Reduction in BP due to a) repetitive testing because of b) changes in sample porosity

3.3.8 Full Immersion

EWR soils are designed to limit water infiltration, such as a capillary rise or the flow of water through soil layers. However, in some cases, these soils may experience flooding or become sandwiched between a high-water table and surface water, leading to submersion scenarios. Figure 3.16a illustrates the response of EWR soils to progressive soaking and their corresponding breakthrough pressure (BP) values over time.

The results show that when EWR soils are exposed to submersion, the BP values exhibit distinct patterns depending on the time submerged and whether the samples were dried after the soaking period. For instance, when the samples were tested immediately after soaking, their BP values were higher than the control, especially after prolonged soaking. At 1 day of soaking, the BP value increased to 30 kPa, compared

to the control value of 21 kPa. By 7 days, the BP rose even further to 38 kPa, indicating that these partially saturated soils retained a higher resistance to water flow.

However, when the samples were oven-dried after soaking to remove any absorbed or infiltrated water, the BP values dropped significantly. After 1 day of soaking and subsequent drying, the BP dropped to 7 kPa representing a 77% decrease compared to the immediate BP value. By 7 days, BP further reduced to 4 kpa, a 90% reduction compared to BP immediately after soaking. This drastic reduction highlights how the removal of absorbed water negatively impacts the hydrophobicity of the soil, decreasing its resistance to water penetration. However, this is the projected water resistance after drying on field in these scenarios.

The reduction in BP is due to volumetric changes as the soaking period extends. These changes, driven by water infiltration through failure planes or weak points created during sample preparation, increase the soil's porosity and reduce its hydrophobic properties. While the immediate BP values after soaking show higher resistance than control, this effect is attributing the effects of water within the soil sample and the compound effect of confining pressure. The oven-dried samples reveal the long-term impact of water absorption on soil stability and hydrophobicity.

a

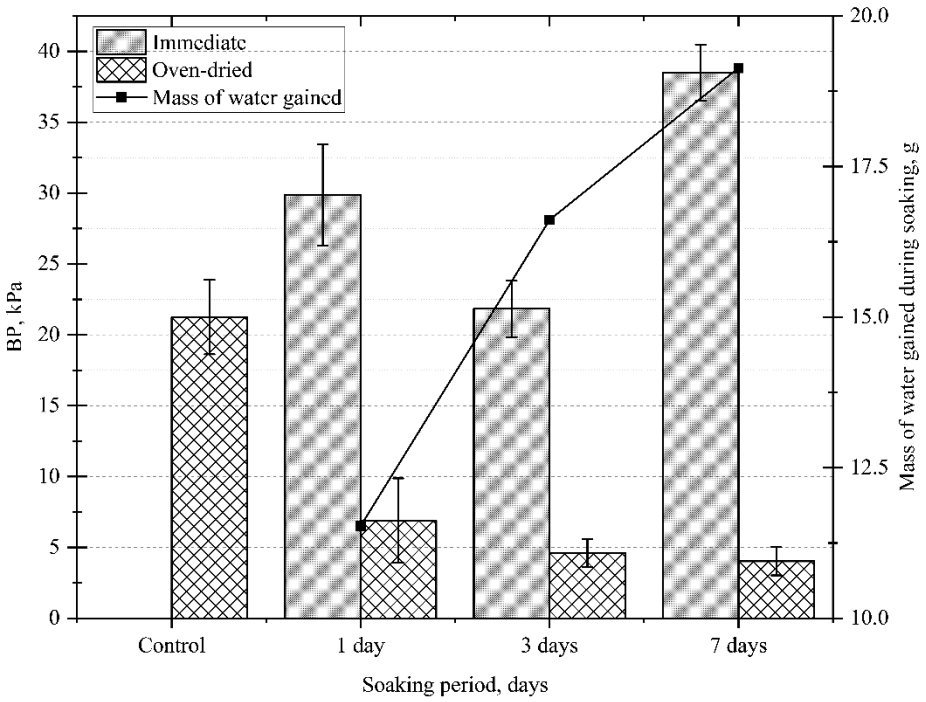

b

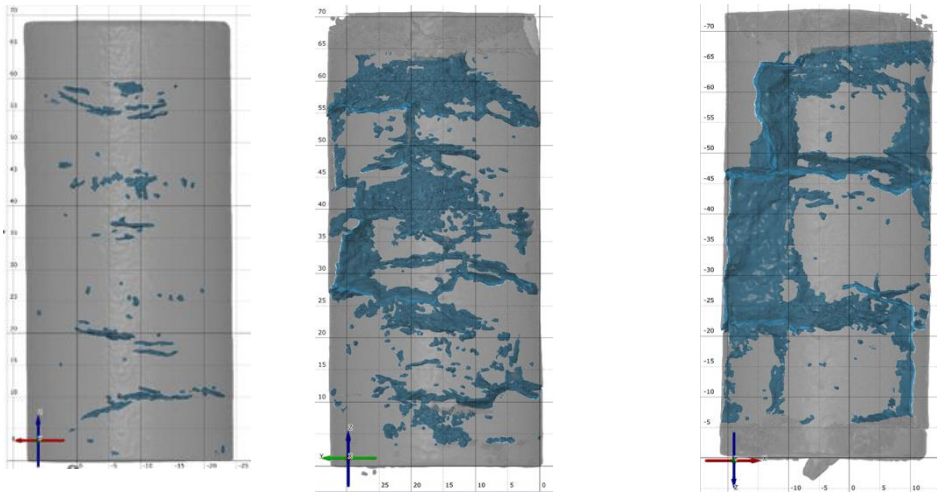

Before testing 1 day 7th days

Figure 3.16: a) Reduction in BP after full immersion due to b) change in the soil microstructure.

3.3.9 Repeat Wet and Dry

Like full immersion, the results of the immediate triplicate testing after wet-dry (W-D cycle end with oven drying for 42 hours) showed reduced water resistance Figure 3.17A. However, the result of soaked samples after W-D (triplicate samples were soaked again for 4 hours after the predetermined w-d cycle was reached and tested immediately after removal to test its water resistance capacity) were higher. While the result is high, this result might be driven by pore pressure within the soil and not due to water resistance. This dynamic of soaking and drying leads to continuous shrinkage and expansion of the soil samples, affecting volumetric stability and reducing resistance. As illustrated in the accompanying Figure 3.17b, these changes in soil structure contribute to a decreased ability to resist water penetration over time. The figures highlight the relationship between the number of cycles and the corresponding BP, emphasizing the fragility of EWR soils under prolonged exposure to water.

a

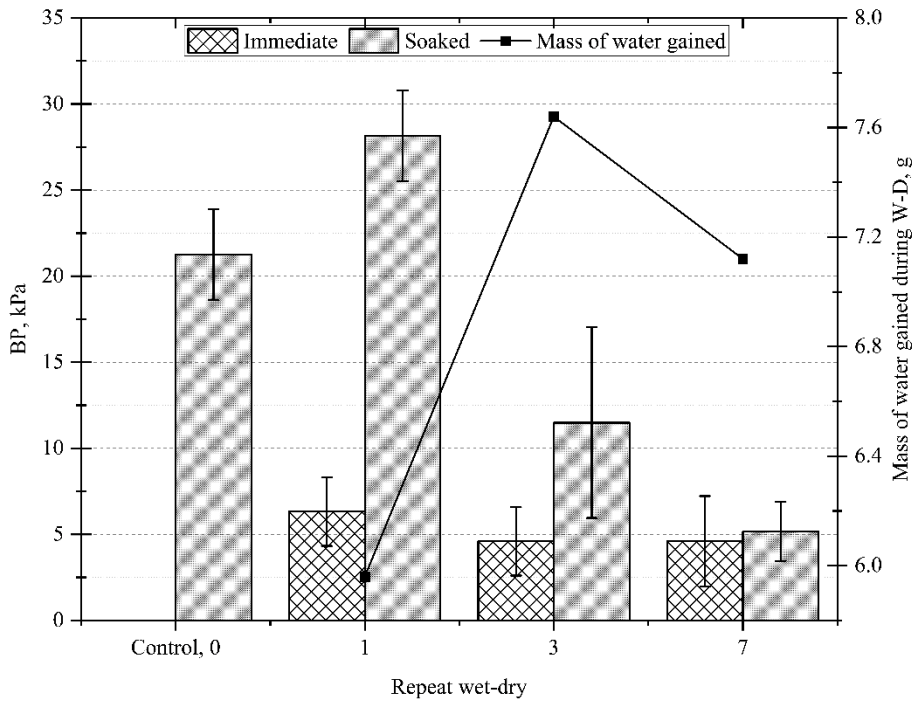

b

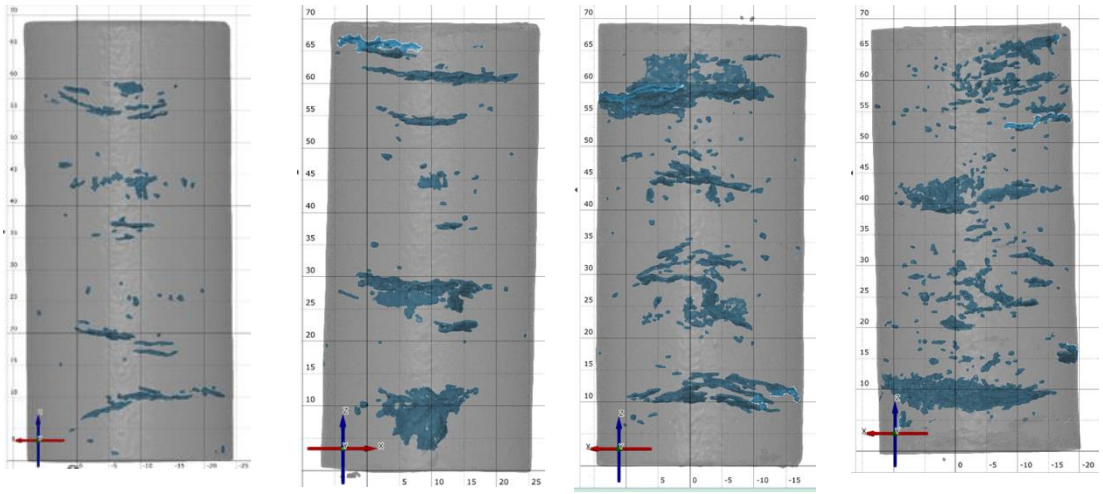

Before testing 1st cycle 3rd cycle 7th cycle

Figure 3.17: The impact of repeat wet-dry a) on BP of EWR soil due to b) microstructural changes.

3.4 Conclusions

Hydrophobic soils are being developed to address various engineering challenges related to moisture, such as frost action, soil moisture fluctuations, seasonal variations in soil stiffness, and leaching prevention. Therefore, it is essential to evaluate the performance of hydrophobic soils, particularly their resistance to hydrostatic pressure, and to understand how they respond to different factors, including

durability and reliability. This study provides a comprehensive assessment. The key findings are summarized below.

- Densification impact on BP: For a given concentration and clay content, densification increases BP by up to three times when comparing dense to loose soil. Densified soils do not exhibit preferential flow, making them ideal for field applications, as water must penetrate through multiple compacted layers. Water infiltration progressively increases once the breakthrough pressure (BP) is reached. Under the same water pressure profile, loose soils absorbed a greater total amount of water compared to denser soils.
- Confining pressure influence: BP is significantly influenced by confining pressure, as it affects soil voids. Higher confining pressures reduce voids and porosity, leading to increased BP. Therefore, selecting the appropriate confining pressure is critical for engineering applications to ensure optimal soil performance.
- Effect of fines content: An increase in clay fines content by 1.5 times leads to at least a threefold increase in BP.
- Soil fabric and moisture: BP increases with higher molding moisture content until the Maximum Dry Density (MDD) is reached. Densely compacted samples consistently show the highest BP values due to their lower porosity. This underscores the critical role of compaction and porosity in determining BP, irrespective of whether the variation arises from differences in compaction energy or moisture content.
- Loading rate and duration: As the loading rate increases, BP decreases, indicating that the soil's ability to resist breakthrough pressure diminishes as the rate of applied pressure increases. In real-world applications, where hydrostatic pressure is applied gradually and over longer periods, EWR soils may not reach BP values. The findings emphasize the importance of considering time intervals and loading rates when optimizing EWR for field applications. In short-duration tests, successive loading steps significantly influence each other due to the short interval, leaving insufficient time

for the soil to stabilize. However, longer intervals allow the soil to stabilize between pressure increments, leading to more accurate readings.

- Creep behavior: The study shows that EWR samples can restrict low hydrostatic pressure below BP over time. Sample exposed to pressures below the BP, has infiltration into the sample, but remains below 2.5cc over a 24-hour period. Hence, while water does permeate into the sample, it remains below the BP threshold, preventing significant infiltration.
- Durability: By the seventh cycle of repetitive testing, the BP decreased by 89% and after seven days of soaking, it also reduced by 81% compared to the control sample. Similarly, by the seventh cycle of W-D exposure, BP value dropped by 76% compared to control sample. This reduction is attributed to the aggressive testing conditions, which are unlikely to occur in the field, but cause microstructural changes in the soil and increase the soil porosity.

In conclusion, this study demonstrates that hydrophobic soils significantly reduce water infiltration, making them ideal for engineering applications where water control and mitigation are crucial. Potential applications range from frost mitigation in roads to landfill and tunnel construction. EWR technology offers a promising, sustainable, and cost-effective solution for mitigating load restrictions imposed by various departments of transportation (DOTs) and reducing the need for constant road repairs due to frost action.

3.5 Acknowledgment

The author gratefully acknowledge-the funding support from the Iowa Highway Research Board (TR-783) and National Science Foundation (Award #1928813 and #1947009) and Zeiss for the X-ray scan and processing.

3.6 Reference

AASHTO, T. (2007). 307–99. Standard Method of Test for Determining the Resilient Modulus of Soils and Aggregate Materials, American Association of State Highway and Transportation Officials, Washington, DC.

Adeyanju, E. D., Uduebor, M. A., Saulick, Y., Daniels, J. L., & Cetin, B. (2024). Influence of Density on Engineered Water Repellent Soil. In *International Conference on Transportation and Development 2024* (pp. 152-161).

Adeyanju, E. D., Saulick, Y., Ogunro, T., Daniels, J. L., & Cetin, B. (2024). Reducing Soil Strength Degradation through Engineering Water Repellency. In *International Conference on Transportation and Development 2024* (pp. 142-151).

Annaka, Takeyuki and Susumu Hanayama. (2005). "Dynamic Water-Entry Pressure for Initially Dry Glass Beads and Sea Sand." Vadose Zone Journal., 4., 127 - 133.

ASTM D422-63. (2007). Standard test method for particle-size analysis of soils, ASTM International.

ASTM, D7928. (2017). Standard test method for particle-size distribution (gradation) of fine-grained soils using the sedimentation (hydrometer) analysis. In ASTM (Vol. 7928, pp. 1–25).

ASTM Committee D854-10 on Soil and Rock. (2006). Standard test methods for specific gravity of soil solids by water pycnometer. ASTM international.

ASTM D 4318-00. (2000). Standard Test Methods for Liquid Limit, Plastic Limit and Plasticity Index of Soils. Annual Book of ASTM Standards, Vol. 04.01, pp. 1–14.

ASTM International. (2012). ASTM D698-12e2 (2012): Standard Test Methods for Laboratory Compaction Characteristics of Soil Using Standard Effort (12 400 ft-lbf/ft3 (600 kN-m/m3)).

ASTM, D. 2487-17 (2017) Standard practice for classification of soils for engineering purposes (unified soil classification system). ASTM D, 2487–17.

ASTM, D. (2016). 2166; Standard Test Method for Unconfined Compressive Strength of Cohesive Soil. West Conshohocken, PA, United States.

ASTM D559, A. (2003). Standard test methods for wetting and drying compacted soil-cement mixtures. Conshohocken, PA (USA).

ASTM D870-15. (2015). Standard Practice for Testing Water Resistance of Coatings Using Water Immersion. ASTM Int.

AASHTO M145-91 (2012). Classification of Soils and Soil-Aggregate Mixtures for Highway Construction Purposes. Washington DC: American Association of State Highway and Transportation Officials.

Bachmann, J., Ellies, A., & Hartge, K. H. (2000). Development and application of a new sessile drop contact angle method to assess soil water repellency. Journal of Hydrology, 231, 66–75. doi:10.1016/s0022-1694(00)00184-0.

Bachmann, J., Deurer, M., & Arye, G. (2007). Modeling water movement in heterogeneous water-repellent soil: 1. Development of a contact angle–dependent water-retention model. Vadose Zone Journal, 6(3), 436-445.

Bauters, T. W. J., Steenhuis, T. S., DiCarlo, D. A., Nieber, J. L., Dekker, L. W., Ritsema, C. J., ... & Haverkamp, R. (2000). Physics of water repellent soils. Journal of Hydrology, 231, 233–243.

Brooks, T.Y., Daniels, J.L., Uduebor, M., Cetin B., N., M.W. (2022). "Engineered Water Repellency for Mitigating Frost Action in Iowa Soils." Geo-Congress 2022: Soil Improvement, Geosynthetics, and Innovative Geomaterials.

Cota, J., Martínez-Lazcano, C., Montoya-Alcaraz, M., García, L., Mungaray-Moctezuma, A., & Sánchez-Atondo, A. (2022). Improvement in Durability and Service of Asphalt Pavements through Regionalization Methods: A Case Study in Baja California, Mexico. Sustainability, 14(9), 5123.

Daniels, J.L., Hourani, M.S. (2009). Soil Improvement with Organo-Silane, Advances in Ground Improvement: Research to Practice in the United States and China. GSP 188.

Daniels. J., Mehta, P., Vaden, M., Sweem, D., Mason, M.D., Zavareh, D.M., Ogunro, V. (2009). "Nano-scale organo-silane applications in geotechnical and geoenvironmental engineering." J. Terraspace Sci. Eng. 1(1), 21–30

Daniels, J.L. (2020). “Engineered Water Repellency for Applications in Environmental Geotechnology.” In: Reddy, K.R., Agnihotri, A.K., Yukselen-Aksoy, Y., Dubey, B.K., Bansal, A. (eds) Sustainable Environmental Geotechnics. Lecture Notes in Civil Engineering, 89. Springer, Cham. https://doi.org/10.1007/978-3-030-51350-4_6

Dekker, L. W., & Ritsema, C. J. (1994). How water moves in a water-repellent sandy soil: 1. Potential and actual water repellency. Water Resources Research, 30(9), 2507-2517.

Deurer, M., & Bachmann, J. (2007). Modeling water movement in heterogeneous water-repellent soil: 2. A conceptual numerical simulation. Vadose Zone Journal, 6(3), 446-457.

Doerr, S. H. (1998). On standardizing the ‘water drop penetration time and the ‘molarity of an ethanol droplet’techniques to classify soil hydrophobicity: a case study using medium textured soils. Earth Surface Processes and Landforms: The Journal of the British Geomorphological Group, 23(7), 663–668. https://doi.org/10.1002/ (SICI)1096-9837(199807)23:73.0.CO;2-6.

Doerr, S. H., Llewellyn, C. T., Douglas, P., Morley, C. P., Mainwaring, K. A., Haskins, C., ... & Diamantis, J. (2005). Extraction of compounds associated with water repellency in sandy soils of different origin. Soil Research, 43(3), 225–237.

Doerr, S. H., Shakesby, R. A., & Walsh, R. (2000). Soil water repellency: its causes, characteristics and hydro-geomorphological significance. Earth-Science Reviews, 51(1-4), 33–65.

Doerr, S. H., & Thomas, A. D. (2000). The role of soil moisture in controlling water repellency: new evidence from forest soils in Portugal. Journal of Hydrology, 231, 134–147.

Dumenu, L. (2019). Water Repellency Effect on Unsaturated Properties of Compacted Coal Combustion Residuals (Doctoral dissertation, The University of North Carolina at Charlotte).

Fallow D.J., Elrick, D.E. (1996). Field measurement of air-entry and water-entry soil water pressure heads.” Soil Sci. Soc. Am. J., 60 (1996), 1036-1039.

Feyyisa, J. L. (2017). *Engineered Water Repellency for Infiltration Control in Coal Fly Ash* (Doctoral dissertation, The University of North Carolina at Charlotte).

Feyyisa, Jenberu L., Daniels, John L., Pando, Miguel A. (2017). “Contact Angle Measurements for Use in Specifying Organosilane-Modified Coal Combustion Fly Ash.” Journal of Materials in Civil Engineering, 29(9), 04017096–. doi:10.1061/(ASCE)MT.1943-5533.0001943

Feyyisa, Jenberu L., Daniels, John L., Pando, Miguel A., Ogunro, Vincent O. (2019). “Relationship between breakthrough pressure and contact angle for organo-silane treated coal fly ash.” Environmental Technology & Innovation, 14, 100332–. doi:10.1016/j.eti.2019.100332

Goebel, M. O., Bachmann, J., Reichstein, M., Janssens, I. A., & Guggenberger, G. (2011). Soil water repellency and its implications for organic matter decomposition–is there a link to extreme climatic events? Global Change Biology, 17(8), 2640-2656. https://doi.org/10.1111/j.1365-2486.2011.02414.x

Granged, A. J., Jordán, A., Zavala, L. M., Muñoz-Rojas, M., & Mataix-Solera, J. (2011). Short-term effects of experimental fire for a soil under eucalyptus forest (SE Australia). Geoderma, 167, 125-134.

Guide for Mechanistic–Empirical Design of New and Rehabilitated Pavement Structures. NCHRP 1-37A Final Report. ARA, Inc., ERES Consultants Division, Champaign, Ill., 2004. http:/www.trb.org/mepdg/guide.htm.

Hardie, M. A., Doyle, R. B., Cotching, W. E., & Lisson, S. (2012). Subsurface lateral flow in texture-contrast (duplex) soils and catchments with shallow bedrock. Applied and Environmental Soil Science, 2012.

Hernandez, J., Vargas, S., Estévez, M., Vázquez, G., Zepeda, A., Rodríguez, R. (2005). “Hydrophobic modification of an expansive soil using polymers and organic compounds: a comparative study with lime.” Géotechnique, 55(8): 613–616. doi:10.1680/geot.2005.55.8.613.

Jiménez-Pinilla, P., Lozano, E., Mataix-Solera, J., Arcenegui, V., Jordán, A., & Zavala, L. M. (2016). Temporal changes in soil water repellency after a forest fire in a Mediterranean calcareous soil: Influence of ash and different vegetation type. Science of the Total Environment, 572, 1252-1260.

Jordan, C.S., Daniels, J.L., & Langley, W. (2015). The effects of temperature and wet-dry cycling on water-repellent soils. Environmental Geotechnics, 4(4): 299–307. doi:10.1680/envgeo.14.00032.

Keatts, M. I., Daniels, J. L., Langley, W. G., Pando, M. A., Ogunro, V. O. (2018). “Apparent Contact Angle and Water Entry Head Measurements for Organo-Silane Modified Sand and Coal Fly Ash.” Journal of Geotechnical and Geoenvironmental Engineering, 144(6), 04018030–. doi:10.1061/(ASCE)GT.1943-5606.0001887

Kim, Byeong-Su., Daoju, Ren., Seong-Wan, Park., Shoji, K. (2021). “Establishing selection criteria of water repellent sandy soils for use in an impervious layer of engineered slope.” Construction and Building Materials, p. 293, 2021, 123551, ISSN 0950-0618, https://doi.org/10.1016/j.conbuildmat.2021.123551.

Lee, C., Yang, H.-J., Yun, Tae S., Choi, Youngmin., Yang, Seongyeong. (2015). “Water-Entry Pressure and Friction Angle in an Artificially Synthesized Water-Repellent Silty Soil.” Vadose Zone Journal, 14(4), doi:10.2136/vzj2014.08.0106

Leelamanie, D. A. L., Karube, J., & Yoshida, A. (2008). Characterizing water repellency indices: Contact angle and water drop penetration time of hydrophobized sand. Soil Science & Plant Nutrition, 54(2), 179-187. https://doi.org/10.1111/j.1747-0765.2007.00232.x.

Lemboye, K., Almajed, A. Experimental Study on the Mechanical Properties and Durability of Sand Using a Semicrystalline Hydrophobic Fluoropolymer. Arab J Sci Eng 48, 13707–13717 (2023). https://doi.org/10.1007/s13369-023-07942-2.

Letey, J., (1969). Measurement of contact angle, water drop penetration time, and critical surface tension. In: LF, DeBano, Letey, J. (Eds.), Water Repellent Soils — Proceedings of the Symposium on Water Repellent Soils. University of California, Riverside, pp. 43–47.

Lin, H., Lourenço, S.D.N., Yao, T., Zhou, Z., Yeung, A.T., Hallett, P.D., Paton, G.I., Shih, K., Hau, J., Cheuk, B.C.H. (2019). “Imparting water repellency in completely decomposed granite with Tung oil.” Journal of Cleaner Production, 230, 1316-1328, ISSN 0959-6526, https://doi.org/10.1016/j.jclepro.2019.05.032.

Mahedi, M., Satvati, S., Cetin, B., & Daniels, J. L. (2020). Chemically induced water repellency and the freeze–thaw durability of soils. Journal of Cold Regions Engineering, 34(3), 04020017.

Malvar, M. C., Prats, S. A., Nunes, J. P., & Keizer, J. J. (2016). Soil water repellency severity and its spatio-temporal variation in burnt eucalypt plantations in North-Central Portugal. Land Degradation & Development, 27(5), 1463-1478.

Martins, M. A., Verheijen, F. G., Malvar, M. C., Serpa, D., González-Pelayo, O., & Keizer, J. J. (2020). Do wildfire and slope aspects affect soil water repellency in eucalypt plantations? –A two-year high resolution temporal dataset. Catena, 189, 104471. https://doi.org/10.1016/j.catena.2020.104471.

Perroux K.M., White, I. (1988). "Designs for disc permeameters." Soil Sci. Soc. Amer. J., 52 (1988), 1205-1215

Roy, J. L., & McGill, W. B. (2002). Assessing soil water repellency using the molarity of ethanol droplet (MED) test. Soil Science, 167(2), 83–97.

Salifu, E., El Mountassir, G. (2021). "Fungal-induced water repellency in sand." Géotechnique, 71: 608–615. doi:10.1680/jgeot.19.P.341.

Smettem, K. R. J., Rye, C., Henry, D. J., Sochacki, S. J., & Harper, R. J. (2021). Soil water repellency and the five spheres of influence: A review of mechanisms, measurement, and ecological implications. Science of the Total Environment, 787, 147429. https://doi.org/10.1016/j.scitotenv.2021.147429.

Terry, J. P., & Shakesby, R. A. (1993). Soil hydrophobicity effects rain splash: simulated rainfall and photographic evidence. Earth Surface Processes and Landforms, 18(6), 519–525.

Uduebor, M., John Daniels, Naqvi, M.W., Cetin B. (2022). "Engineered Water Repellency in Frost Susceptible Soils." Geo-Congress 2022: Soil Improvement, Geosynthetics, and Innovative Geomaterials.

Uduebor, M., Adeyanju, E., Saulick, Y., Daniels, J., Cetin, B. (2022). "A Review of Innovative Frost Heave Mitigation Techniques for Road Pavements." International Conference on Transportation and Development.

M. Uduebor, J. Daniels, D. Adeyanju, Md Fyaz Sadiq & Bora Cetin (2023) Engineered water repellency for resilient and sustainable pavement systems, International Journal of Geotechnical Engineering, 17:5, 530-540, DOI: 10.1080/19386362.2023.2241280

Wang, Z., Wu, L., Wu, Q.U. (2000). “Water-entry value as an alternative indicator of soil water-repellency and wettability.” 231-232, 0–83. doi:10.1016/s0022-1694(00)00185-2.

Wijewardana, N. S., Müller, K., Moldrup, P., Clothier, B., Komatsu, T., Hiradate, S., ... & Kawamoto, K. (2016). Soil-water repellency characteristic curves for soil profiles with organic carbon gradients. Geoderma, 264, 150-159.

Xing, X., Saulick, Y., Lourenço, S.N.D. (2022). “Synergistic effects of density, gradation, particle size, and particle shape on the water entry pressure of hydrophobized sands.” Canadian Geotechnical Journal. 59(11): 1937-1949. https://doi.org/10.1139/cgj-2021-0585

INVESTIGATION OF THE COMPRESSIVE STRENGTH OF ENGINEERED WATER REPELLENCY IN NATURAL SOILS UNDER VARYING ENVIRONMENTAL CONDITIONS.

Abstract

The persistent degradation of soil stiffness and strength due to moisture fluctuations can be mitigated through Engineered Water Repellency (EWR). This technique alters the wettability of soils using organosilane (OS), modifying the soil surface without forming cementitious bonds. This study evaluates the performance of EWR-treated samples under various environmental conditions, including air drying, cyclic wet-dry (W-D) cycles, and prolonged immersion, by assessing the unconfined compressive strength (UCS) of two EWR-treated soils (IA-BV and MnRD). The soils were treated with different OS concentrations and subjected to up to 120 days of immersion and 21 W-D cycles. The UCS of conditioned samples was measured as the hydrophobicity of the EWR soils developed during drying. X-ray scans were used to analyze porosity changes and internal pore structures post-exposure to drastic environmental conditions. The results showed that OS treatment reduced the optimum moisture content (OMC) while having minimal impact on maximum dry density (MDD). However, mechanical strength decreased as OS concentration increased, attributed to the organic moiety of the OS molecule siloxane bond formation, which reduced compressive strength. However, EWR-treated soils maintained structural integrity during extended immersion, with higher OS concentrations offering better resistance to W-D cycles. Over 120 days of soaking, both soils experienced strength reductions of up to 98% due to increased porosity and excess unbound OS. X-ray analysis confirmed volumetric changes correlated with water infiltration and pore expansion. While EWR enhanced moisture resistance, a reduction in mechanical strength was observed. These findings contribute to a deeper understanding of hydrophobic soils, offering valuable insight into EWR and natural soil's mechanical strength and enhancing the feasibility of applying this technology for subgrade modification and other engineering structures.

Keywords: Hydrophobicity, durability, Mechanical strength.

Nomenclature

AASHTO: American Association of Highway and Transportation Officials

EWR: Engineered Water Repellency

MDD: Maximum Dry Density

OMC: Optimum Moisture Content

OS: Organosilane

UCS: Unconfined Compressive Strength

USCS: Unified Soil Classification System

W-D: Wet-Dry

X-ray CT: X-ray computed tomography.

3.7 Introduction

Engineered Water Repellency (EWR) is a significant advancement in pavement engineering, with the practical goal of strengthening subgrade layers against soil submergence and/or soil moisture fluctuations. EWR, achieved by modifying subgrade soil with Organosilane (OS), acts as an in-situ water barrier, crucial for mitigating frost action effects (Uduebor et al., 2023a) and pavement water-related damages. Using EWR aims to enhance durability, sustainability, and resiliency by addressing challenges posed by soil moisture variations, which can significantly impact soil mechanical strength (Adeyanju et al., 2024). Preliminary laboratory investigations (Brooks et al., 2022; Uduebor, 2023) and field trials (Uduebor et al., 2022a; Naqvi et al., 2023) have confirmed the effectiveness of EWR as a water barrier layer. While EWR is not primarily intended as a load-bearing layer, its impact on overall pavement performance is noteworthy. However, there is a lack of comprehensive studies on the compressive strength of hydrophobic soils and the durability of EWR in subgrade soils under extreme environmental conditions characterized by exposure to excessive water and drying conditions. Therefore, there is a pressing need for further research on the mechanical strength and durability of EWR application in subgrade soils.

The singular and combined effects of extreme temperatures, exposure to albedo, including sunlight and snow, and fluctuation in moisture contents (e.g., due to seasonal variations) on the durability of EWR have yet to be fully resolved. To pursue this objective, Lin and Lourenço (2022) used accelerated weathering techniques to investigate the durability of sands; hydrophobicity levels were generally found to degrade at high temperatures and when submerged over long periods. Since the modification of soils to generate hydrophobicity involves coating the surfaces at the micro to nano scales (Saulick *et al*., 2023), the interaction of particles and the subsequent degradation of these coatings was also investigated by Lin and Lourenço (2019), who found out that hydrophobic degradation depends on the hydrophobizing agent, and such mechanisms of hydrophobic degradation depend on the presence/absence of water. With construction materials, e.g., rammed earth, investigating the compressive strength is fundamental to ensuring the integrity of the resulting infrastructure. While several studies, such as Zhou et al. (2021), have focused on and contrasted the shear and compressive characteristics of sands made water-repellent with untreated sands, the investigation of compressive behavior, vital in transportation infrastructure, has been largely unexplored. Although several advances with regard to the adoption of engineered water repellency (EWR) in geotechnical applications have been made, laboratory or in-situ investigations relating to their temporal (both short-term and long-term) viability on natural soils in transportation infrastructure remain largely unexplored. Until now, there have been few investigations performed on the compressive strength and durability of EWR in subgrade soils, in particular, if changes in hydrophobicity and strength occur and are linked under episodic and continuous cycles of wetting-drying.

The current work addresses moisture-related geotechnical concerns present ubiquitously (e.g., in the design of road infrastructure) and targets explicitly the viability of EWR over time. While the current literature (e.g., Lin *et al*. (2024)) demonstrates that the efficacy of EWR is dependent on the depth of implementation (surface or at a depth) and hydrophobizing agent used (e.g., organosilanes or oils consisting predominantly of fatty acids), experimental campaigns have been mostly devoted to clean model sands. To this date, there have been limited investigations regarding the compressive strength of natural soil samples made water-repellent and their subsequent changes, if any, under submerged conditions. This work

specifically addresses this gap by episodically and continuously investigating soils' compressive behavior over a maximum time frame of 120 days. The specific objectives were to: 1. investigate the changes in compressive strength of EWR in soils under different submerged conditions, 2. qualitatively determine changes in the external and internal structure of soils subject to the varying submerged conditions, and 3. elucidate the feasibility of EWR in soils as a novel material in transportation infrastructure based on compressive strength under submerged conditions.

3.8 Materials and Methods

3.8.1 Material

This study used two natural frost susceptible soils from Iowa (IA-BV) and Minnesota (MnRD). Soil characterization, including particle size distribution (ASTM D422-63, 2007; ASTM D7928, 2017), specific gravity (ASTM D854-10, 2006), Atterberg limits (ASTM D 4318-00, 2000), and standard Proctor compaction test (ASTM D698, 2012), was performed and illustrated in Table 3-5 and Figure 3.18.

All soils were classified according to the Unified Soil Classification System [USCS] (ASTM D2487-17, 2017), the American Association of Highway and Transportation Officials [AASHTO] (AASHTO M145-91, 2012), and the Frost Susceptibility Classification of Soils (USACE, 1965).

Table 3-5: Basic Soil properties of selected soils.

Soil properties	Characteristics	Units	Value	
			MnRD	IA-BV
Classification	AASTHO		A-6	A-7-6
	USCS		CL	CH
Physical properties	Specific gravity		2.68	2.73
	Silt	%	42.07	57.24
	Clay	%	17.63	32.28
	Fines	%	59.7	89.52
	Activity		0.7	0.78
Atterberg limits	Liquid limit	%	36.3	57.53
	Plastic limit	%	23.9	32.44
	Plasticity index	%	12.4	25.09
Proctor test	Optimum Moisture Content (OMC)	%	14.1	27.6
	Maximum Dry Density (MDD)	kN/m^3	17.41	13.5

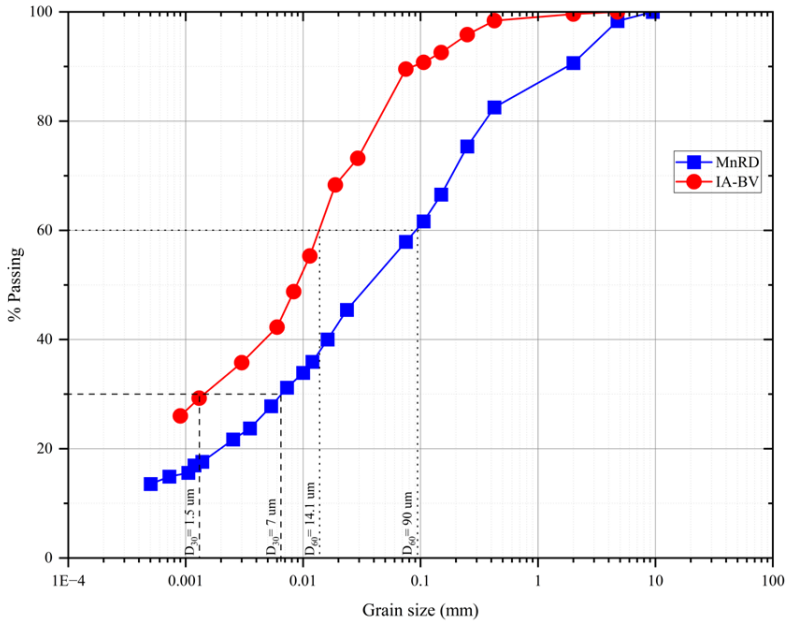

Figure 3.18: Particle size distribution of selected soils.

Terrasil from Zydex Industries, a commercially available organosilane (OS), was used to induce hydrophobicity (see Table 3-6 for properties). Terrasil is a non-leachable, viscous, and water-soluble chemical that modifies the soil surface by coating it without bonding properties (Daniels et al., 2009), as indicated in Figure 3.19a. Several studies have shown that soils treated with varying concentrations of OS become hydrophobic and have a contact angle higher than 90^0 (Uduebor et al., 2022a; Uduebor et al., 2022b; Brooks et al., 2022), indicating it is either hydrophobic or superhydrophobic. Figure 3.19b depicts the variation in the ratio of OS to soil; hence, this study utilized an OS: Soil ratio of 1:40 and 1:20.

Table 3-6: Technical properties of the OS used (Zydex, 2016).

Property	Unit	Terrasil
Color		Pale yellow
Density	g/cm^3	1.01-1.05
Water solubility		Miscible with water
Depth of Penetration	mm	5 - 7
Main component	(%)	Alkoxy-alkysilyl compounds (65-70), Benzyl Alcohol (25-27), Ethylene Glycol (3-5)

3.8.1.1 Sample Preparation

The mixing ratio of all soil samples is presented in Table 3-7. After mixing, each batch was allowed to mellow for 16 hours before compacting in a Harvard mini mold (diameter of 33.02 mm (1.3 inches) and height of 71.12 mm (2.8 inches)) with a 9.1 kg (20-pound) spring-loaded piston using the protocol defined in Saulick *et al*. (2024). Due to the large number of samples and testing, Harvard mold was utilized instead of proctor mold to reduce the soil used. The compaction process for each sample (treated and untreated) involved the application of 20 blows across five layers, with an average soil mass per layer of 27 grams. The cylindrical samples were allowed to stand for 1 hour before drying in an oven at 105 ^{O}C (221 ^{O}F) for 24 hours.

Table 3-7: Mix design for all samples.

Specimen ID	Soil type	OS: Soil	Soil (g)	OS (g)	Water (g)	Molding solution (OS + water) targeting OMC (g)
IA-BV20	IA-BV	1:20	1800	90	406.8	496.8
IA-BV40		1:40		45	451.8	
IA-BV*		-		0	498	
MnRD20	MnRD	1:20	1800	90	163.8	253.8
MnRD40		1:40		45	208.8	
MnRD*		-		0	253.8	

*Control samples (not mixed with OS).

a

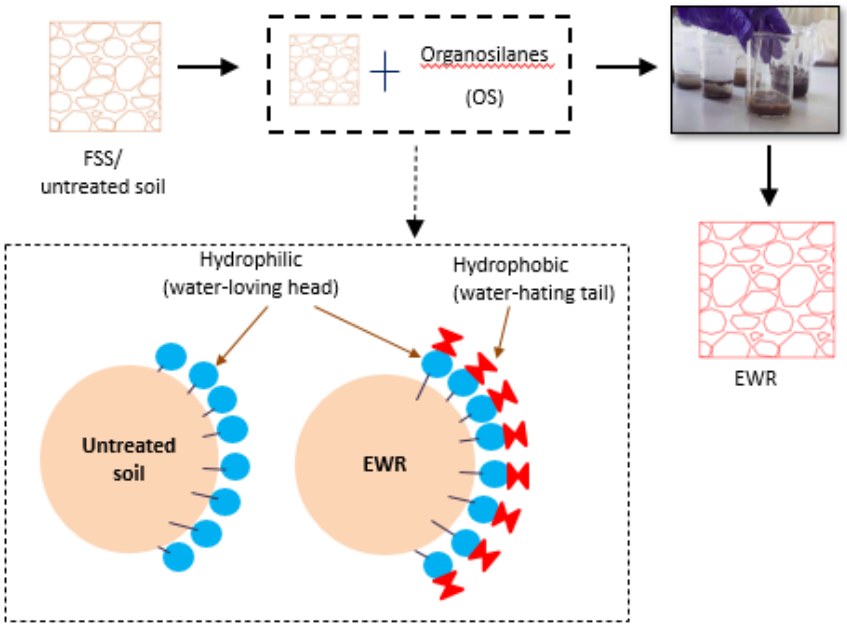

b

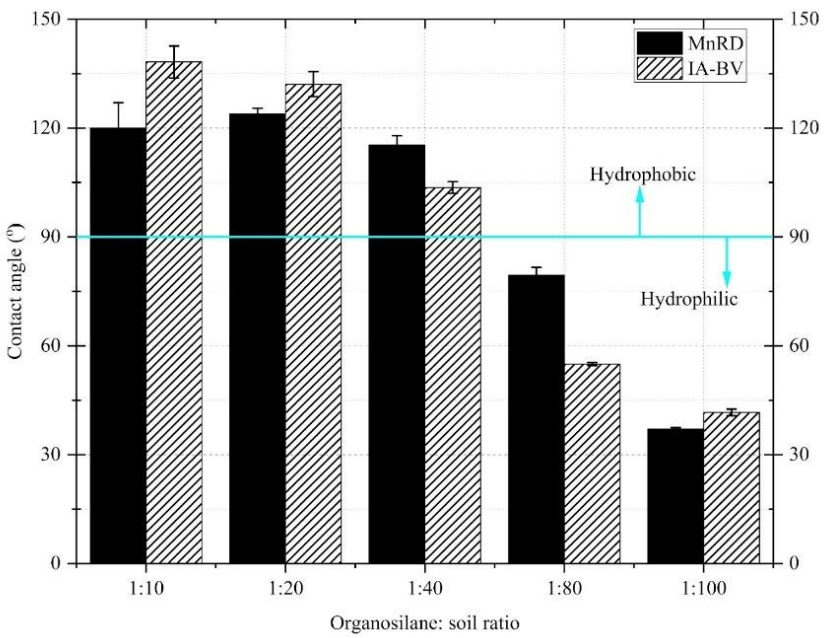

Figure 3.19: a) Hydrophilic modification to hydrophobic soil (red color in EWR to indicate soil coating by OS), and b) Change in contact angle with varying OS concentration.

3.8.1.2 Test Program

Seventeen specimen groups of cylindrical specimens were prepared, conditioned, and mechanically tested, as summarized in Table 3-8. Three testing conditions were investigated, namely drying (using specimen groups D1-D5), repeated wet-dry (using specimen groups D6-D11), and full immersion (D12-D17); these conditions were deemed representative scenarios for investigating any possibility of hydrophobic decay function of fundamental properties such as density, volume change, and pore changes. Quadruplicate samples were prepared for each specimen group. All samples underwent a predetermined durability and drying exposure for each listed condition. Then, three of the four samples were subjected to Unconfined Compressive Strength (UCS) testing following specific durability and drying exposure protocols. The remaining sample was reserved for 3D scanning, enabling the evaluation of pore characteristics, internal structure, and sectional views to compare the control and exposed specimens.

Table 3-8: Mechanical strength durability sample designation.

Group ID	Sample type	Drying	Repeated wet-dry	Full Immersion
D1	Treated and untreated samples.	Immediately after compaction		
D2		1 day		
D3		3 days		
D4		7 days		
D5		60 days		
D6	Treated samples only.		0 cycle	
D7			1 cycle	
D8			3 cycles	
D9			7 cycles	
D10			12 cycles	
D11			21 cycles	
D12				1 day
D13				3 days
D14				7 days
D15				14 days
D16				28 days
D17				120 days

Note: Repeated wet-dry and Full immersion were performed only on the hydrophobic samples, as hydrophilic soil disintegrated within minutes of durability exposure.

3.8.1.2.1 Compaction properties and drying

The compaction properties of soil treated with varying OS-to-soil ratios (i.e., untreated, 1:40, and 1:20) were determined using the previously described preparation method. However, during molding, the total molding solution (OS mass kept constant with water mass varying) was adjusted below and above the OMC. The samples were immediately subjected to Unconfined Compressive Strength (UCS) testing. This procedure was repeated at least eight times to generate the compaction curve.

To investigate compressive strength changes over time, untreated and treated samples were air-dried in the laboratory for predetermined curing periods (0, 1, 3, 7, and 60 days) at an average temperature of 70°F (21°C). This aspect of the study is particularly crucial for the treated (hydrophobic) samples, as the desired water resistance only developed once the moisture content reached approximately 5%. The test assessed the mechanical strength development as the treated samples dried out and became hydrophobic, with direct comparisons to the untreated counterparts.

3.8.1.2.2 Repeated wetting-drying

The recurring nature of moisture variation was modeled after seasonal fluctuations because of rainfall infiltration and drying (e.g., due to evaporation). Based on ASTM D559/D559M (2003) and ASTM D870-15 (2015), the number of repeated wetting-drying periods were 1, 3, 7, 12 and 24. For each cycle, the sample was submerged in a water bath of 101.6 mm height at room temperature for 5 hours and then oven-dried at 71 ± 3 °C [160 ± 5 ºF] for 42 hours. Changes in soil mass and water absorbed were recorded after each cycle.

3.8.1.2.3 Total immersion

Full immersion tests were carried out to simulate conditions representative of relatively higher moisture contents because of continuous water supply via capillary action from regions of high moisture potential and ice thawing (Taber, 1916; Christopher et al., 2006). The compacted samples were fully immersed in deionized water (water depth of 101.6 mm) at room temperature for the following periods (days): 1, 3, 7, 14, 28, 90, and 120, the latter representative of an aggressive worst-case scenario.

3.8.1.2.4 UCS testing

The UCS strength test followed ASTM D2166/D2166M-16 (2016) at a 1 %/min strain rate. All UCS testing was carried out using GeoTac's GeoJac Sigma-1 UC-SI equipment, which has a load capacity of 907 kg and a 38.1-mm stroke. Each sample was positioned within the load frame, ensuring central alignment and contact with the top load cell button. Specimen groups D6-D17 were air-dried at room temperature (21 ºC) for 1 hour before UCS testing.

3.8.1.2.5 X-ray Scans

A micro-focus X-ray Computed tomography (X-ray CT) device (Zeiss METROTOM 1) was used to scan the durability specimens. All the specimens were scanned in a continual rotation mode at a voltage of 160 kV, current of 250 μA, and exposure time of 500 ms. The specimen was rotated 360° in about 20 min to capture all its 3D details, as shown in Figure 3.20. The 3D data was processed using GOM Volume Inspect to visualize and inspect CT data.

One of the goals of this study was to evaluate the durability of treated samples, MN and BV, under varying conditions, such as full soaking and repeated wet-dry, using micro-focus X-ray CT imaging and volumetric data. The percentage change in volume served as the key indicator of durability across the different exposure conditions (equation 1).

Porosity, % = Pore volume (Vp)/Total volume (Vt)×100 Equation 1

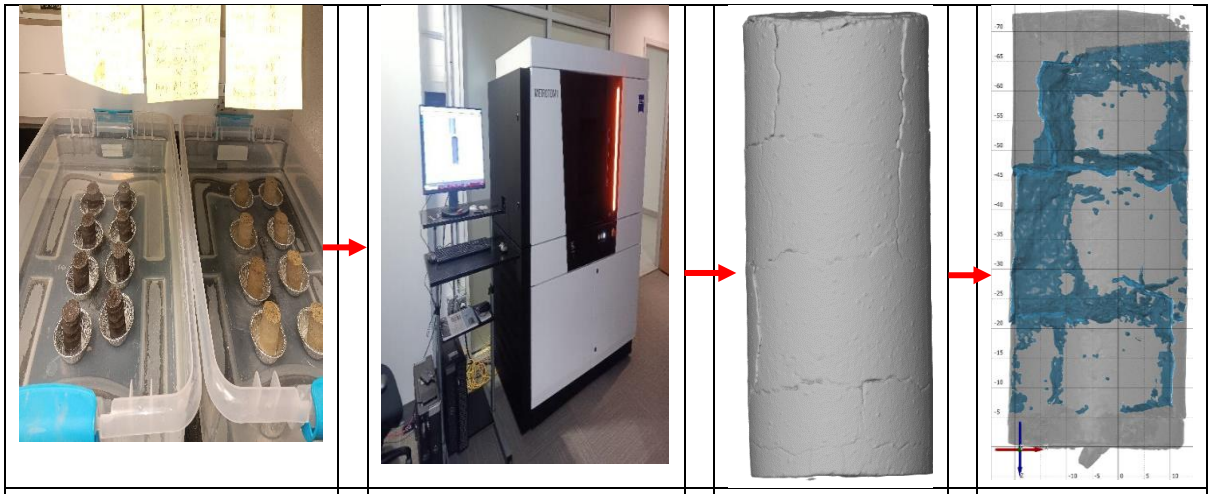

a b c d

Figure 3.20: X-ray Methodology: a) Samples were subjected to predefined environmental conditions and air-dried before scanning. b) Scanning was performed using the Metrotom 1 system. c) A 3D scan was generated for each sample. d) GOM Volume Inspect software was used used to process the 3D scans, creating a mesh representation and an internal pore network analysis.

3.9 Results and Discussion

3.9.1 Compaction Properties of Hydrophilic and Hydrophobic soils.

Figure 3.21 presents the results of Harvard mini-compaction tests carried out on the various samples (treated and untreated) and their corresponding UCS tests. The optimum moisture content (OMC) of all treated samples (MnRD20, MnRD40, IA-BV20, and IA-BV40) experienced a decrease, a trend consistent with the findings of other studies (Saulick et al., 2024; Uduebor et al., 2022a; Uduebor et al., 2023a; Jerez et al., 2018). Samples treated at a concentration of 1:20, i.e., IA-BV20 and MnRD20, had the highest OMC variation due to their high-water replacement (50% and 18%, respectively). A reduction in OMC from 28 to 22.56% for IA-BV20 and 12.3 to 10% for MnRD20 was observed. Similarly, for 1A-BV40 and MnRD40, OMC decreased from 28 to 24.92% and 12.3 to 12%, respectively, as OS replaced water by 25% and 9%

in each case. This reduced OMC is advantageous due to the reduced quantity of water required to obtain the maximum dry unit weight.

Regarding maximum dry unit weight (MDUW), treated MnRD samples had higher MDUW than the untreated samples, while IA-BV treated samples experienced reduced MDUW values. Different studies have indicated an increase (Uduebor et al., 2022a; Uduebor et al., 2023a) and a decrease (Jerez et al., 2018) in MDUW. This test demonstrates that when OS partially replaces water in the molding solution of clay with low moisture content, there is still effective lubrication, resulting in densely packed soil. However, when the OMC value is high, as in the case of IA-BV, at about 27.9 %, the effects of the molding moisture are less. The MDUW of IA-BV, both treated and untreated, had a difference of less than 0.3 %, making OS impact significantly marginal; a similar conclusion was observed by (Saulick et al., 2024). Change in MDUW is generally about 2 % of the untreated sample, far less than the 5% variation accepted in many fields' applications (Christopher et al., 2006).

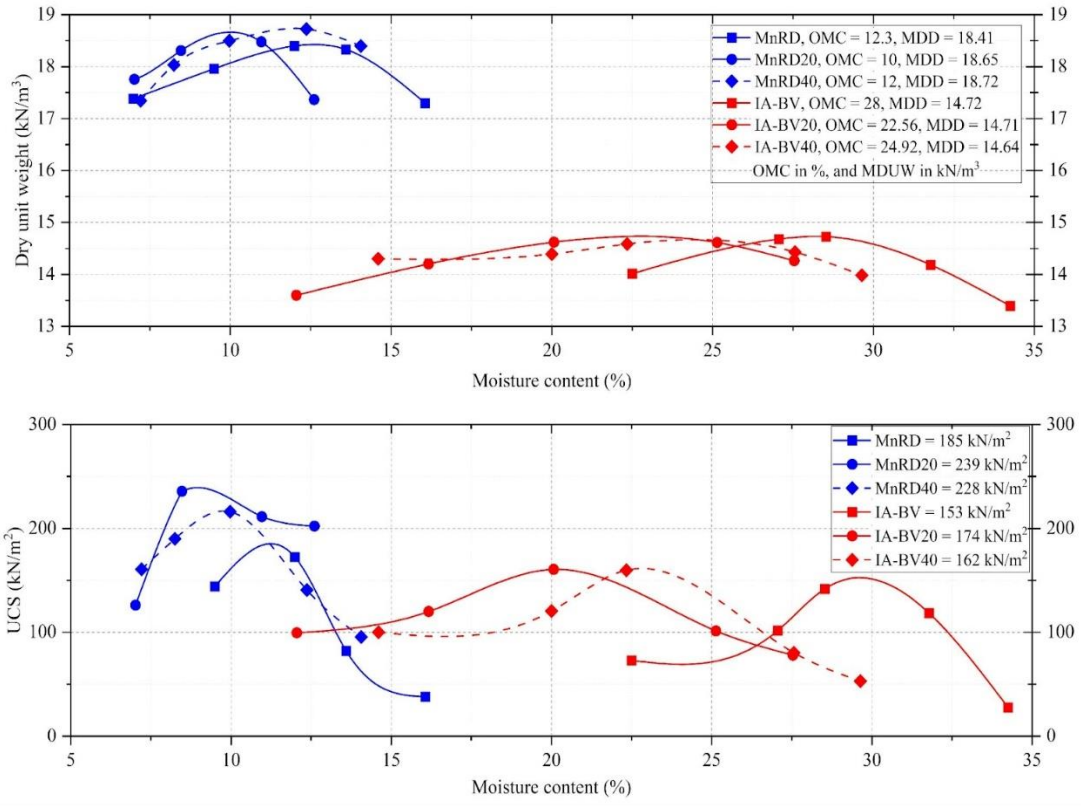

Figure 3.21: Variation of dry unit weight and unconfined compressive strength of tested samples with moisture content

Furthermore, Figure 3.21 summarizes the unconfined compressive strength (UCS) variation between the control sample (untreated MnRD and IA-BV) and treated samples (IA-BV20, IA-BV40, MnRD20, and MnRD40). It can be noted that both soil types reacted differently, with all treated IA-BV samples (174 kN/m^2 and 162 kN/m^{2,} for IA-BV20 and IA-BV40, respectively) experiencing slightly higher mechanical strength than the control sample (153 kN/m^{2,}). Meanwhile, the MnRD samples experienced significantly increased compressive strength (239.4 kN/m^2 and 228 kN/m^{2,} for MnRD20 and MnRD40, respectively) compared to the control samples, 184.7 kN/m^2. These results show that mechanical strength increased by 5% to 29%. Hence, the mechanical strength of EWR does not drastically reduce soil mechanical strength immediately after compaction. However, EWR is only effective when its gravimetric moisture content is about 5% (Adeyanju et al., 2024) after achieving an appropriate level of drying or losing sufficient moisture content, a condition typically associated with the curing phase. Hence, there is a need to understand the evolution of UCS as EWR samples dry out.

3.9.2 Drying Effects.

Figure 3.22 presents the moisture content of all soil samples during the curing process, a key parameter in activating water resistance properties for field application. The trends in Figure 3.22 demonstrate that the rate of mass loss is not constant but rapid between day one and three, reaching a plateau by day seven (where the gravimetric moisture content of all samples was around 5%). It also shows a hierarchical sequence in mass loss, with untreated samples leading the trend, followed by IA-BV40 and MnRD40. This hierarchy significantly indicates the initial moisture content rather than the effectiveness of each treatment method in allowing water to escape. While this data shows that drying can be achieved on the field within seven days, a prolonged exposure curing period is impractical (Naqvi et al., 2023). Furthermore, the impact of subsequent layer placement on the drying rate of EWR soil is still being investigated, especially in scenarios where additional layers are applied before the initial layer has attained the appropriate level of drying.

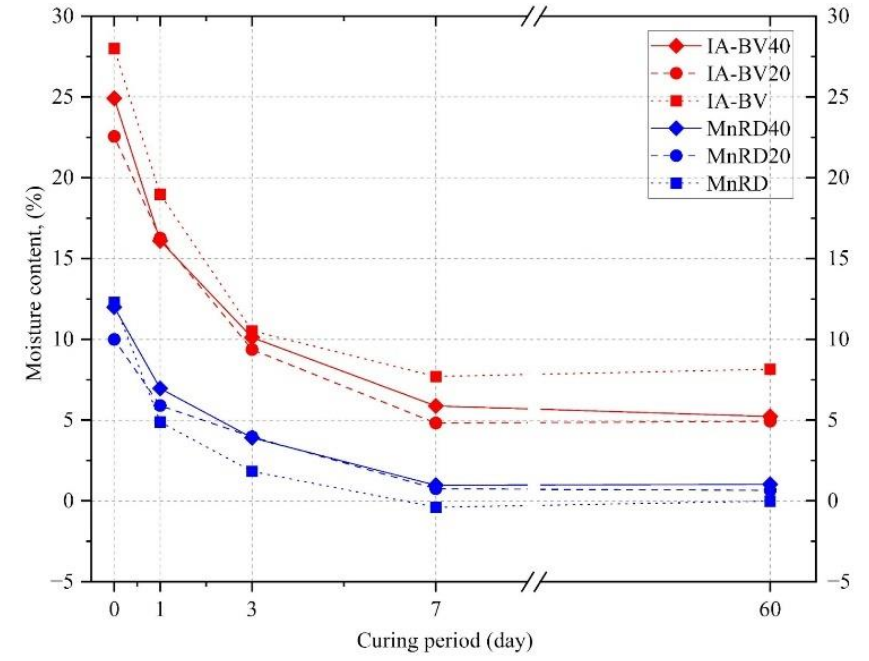

Figure 3.22: Moisture content during curing.

Figure 3.23 presents a corresponding mechanical strength in relation to the mass loss of soil samples subjected to different OS treatments over a drying period of 60 days. The untreated soil exhibits the highest mechanical strength immediately after a 1-day curing period. Several studies, such as Barbieri

et al., 2020 and Uduebor et al. 2023a, have shown that OS-modified soils tend to exhibit a decrease in frictional angles, leading to lower mechanical strength. During OS modification, the OS molecule bonds covalently with silica-based soils through the formation of siloxane bonds (=Si-O-Si=).

The observed reduction is attributed to the organic moiety of the OS molecule, which may reduce interparticle friction. The trends in Figure 3.23 reveal a clear correlation between the amount of OS and the mechanical strength of the soil, where increased OS content is associated with a decrease in mechanical strength. For instance, IA-BV40 exhibits a 41% reduction in mechanical strength relative to IA-BV, the control sample, whereas IA-BV20 shows a more substantial 61% reduction after 60 days of drying. This pattern is also observed in the MnRD samples, where MnRD40 showed a 51% reduction in strength (relative to the 60-day mechanical strength of MnRD) compared to a 66% reduction in MnRD20 over the same period. Although this indicates a significant reduction, the primary consideration is the targeted design strength, as these reductions may not pose a substantial issue in relation to the intended design performance.

These findings support the EWR design philosophy, which is not to augment mechanical strength but rather to mitigate the adverse effects of moisture variations on soil stability. The reduced mechanical strength in OS-modified soils could be a trade-off for enhanced moisture resistance and elimination of mechanical strength variation. Landfills, subgrades, and tunnels are examples for applications where moisture control is more critical than strength (Uduebor et al., 2023b). However, the trade-off between mechanical strength and water repellency must be carefully balanced, particularly in field applications where strength cannot be compromised.

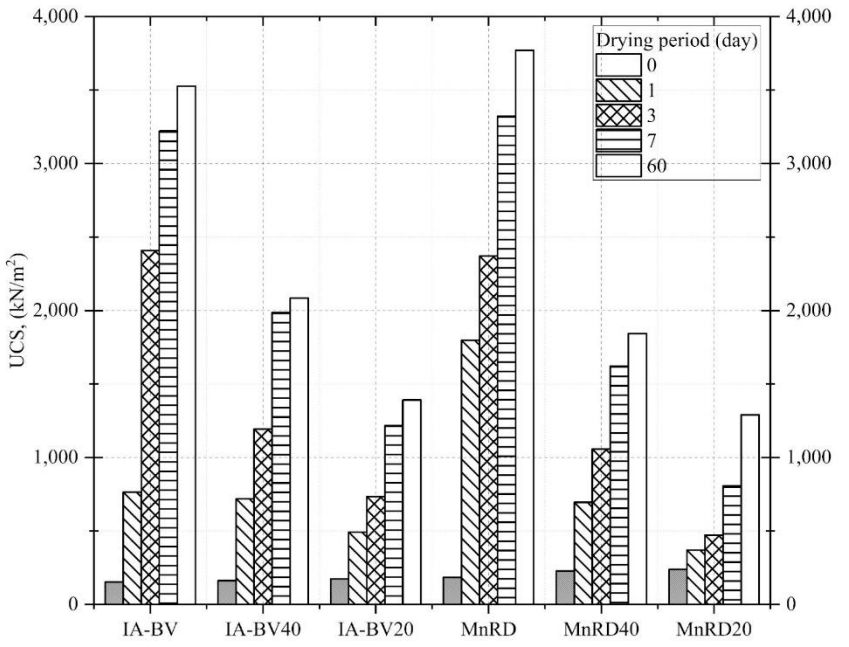

Figure 3.23: Evolution of mechanical strength during curing/drying.

3.9.3 Durability.

3.9.3.1 Wet dry cycle

Figure 3.24a illustrates the impact of repeated wet-dry (W-D) cycles on the mechanical strength of various Engineered Water Repellency (EWR) samples, demonstrating a clear pattern of decline in mechanical strength with an increasing number of cycles. The figure also indicates that increasing W-D cycles and other factors, such as density, affect continuous mechanical strength degradation as certain cycles performed slightly better than the general trends. Figure 3.24b shows that infiltration was not caused by a reduction in hydrophobicity, as indicated by the contact angle measurements. In fact, hydrophobicity either remained the same or increased with the number of repeated wet-dry cycles

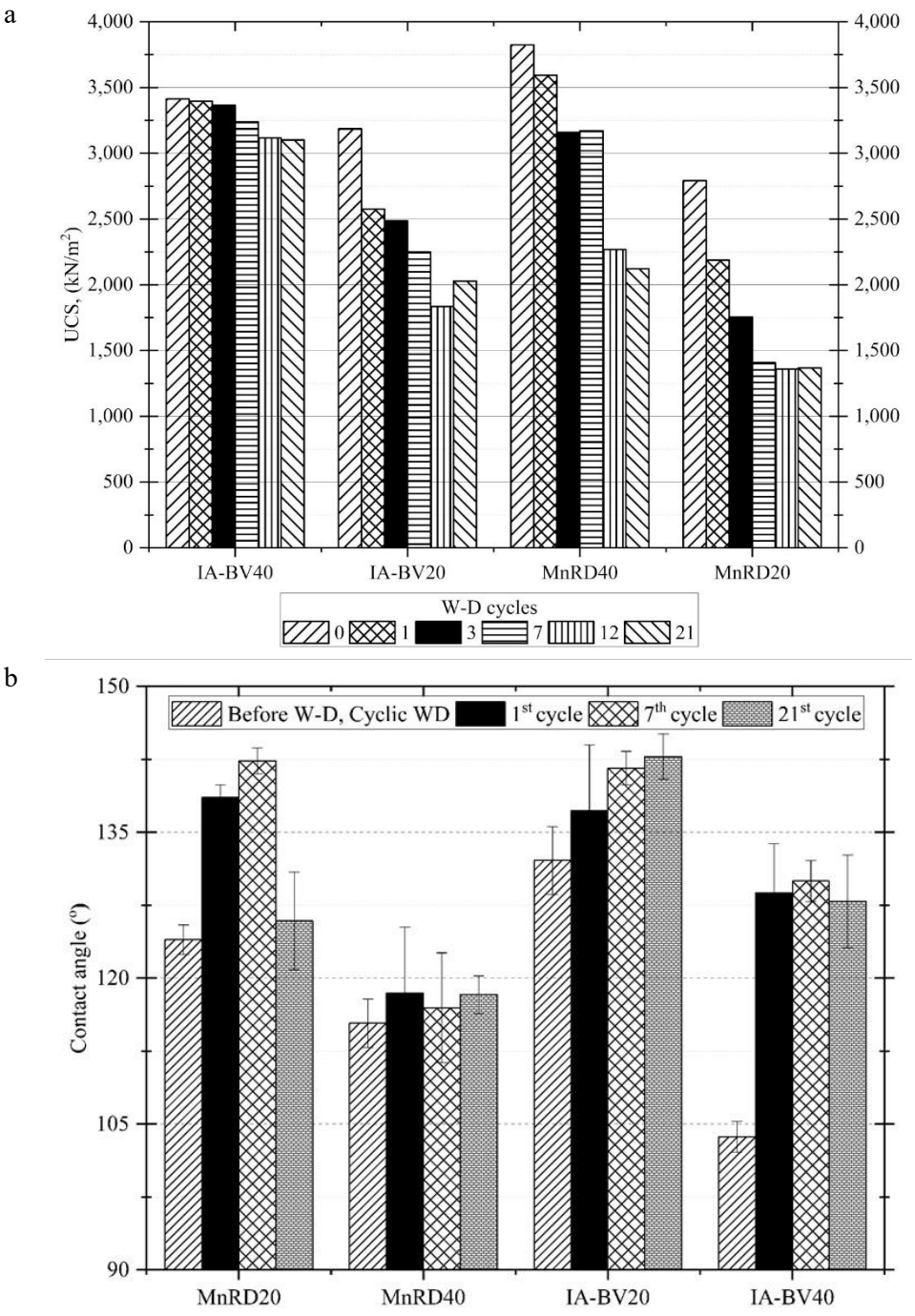

Figure 3.24: a) The UCS of IA-BV and MnRD after cyclic wet-dry (all samples tested were oven-dried) b) contact angle test before and after wet-dry indicate no loss of hydrophobicity.

Specifically, IA-BV40 displayed a resilience with a decrease in mechanical strength from 3412.9 to 3101.5 kN/m² after 21 cycles, a reduction of approximately 9.12%, while IA-BV20 showed a more pronounced vulnerability, with its strength dropping by 36.32%. MnRD40's strength fell dramatically by 44.48%, though MnRD20 endured the most severe decline of 50.99%. These findings reveal that IA-BV40

and MnRD40 are comparatively more robust against the effects of W-D cycling. Conversely, IA-BV20 and MnRD20, which contain higher amounts of OS, are more susceptible to deterioration under these conditions—notably, the increased OS content results in reduced mechanical strength. Therefore, the mechanical strength declines observed in both IA-BV20 and MnRD20 are significantly influenced by the presence of OS first, then by the water absorption in these samples.

Throughout the W-D cycles, IA-BV samples, which contain more fines, absorb more water than MnRD samples, as they have more surface area. The water absorption is related to the sample's porosity, surface tension (hydrophobicity induced by OS addition), and interconnected pores and capillaries (Hoy et al., 2023). Hence, as the sample absorbs water (wetting) and is oven-dried (drying), it undergoes volumetric changes, leading to changes in the pore structure. The constant expansion and contraction lead to more cracks and increase the overall porosity, resulting in increased water absorption. Also, repeated wetting and drying leads to external crack formation, as water infiltrates the samples. Furthermore, the cracks propagate inward, through the crack, the path of least resistance, and erode the surface tension on the soil particles. The major failure planes are the soil surface cracks and the interface between two compacting layers.

Specifically, the MnRD20, with a higher OS content, shows a greater propensity for water uptake compared to MnRD40. MnRD40-21 started with an initial water absorption of 4g, indicating an increasing trend, which reached 5 g by the 21st cycle. Also, MnRD20-21 begins with 4.3 g and exhibits a general upward trend in water absorption, culminating at 4 g. This upward trajectory suggests that the sample's capacity to absorb water increases with each cycle, potentially due to progressive degradation or changes in its microstructure that enhance its porosity or water retention capability.

The reduced hydrophobicity observed is more aligned with microstructural changes within the samples (Figure 3.25) and not due to a reduction in the degree of hydrophobicity. Figure 3.25 shows progressive pore formation within the samples as the W-D increases, allowing more water infiltration. The increase in porosity is linked to the leaching of the unbound OS compounds occupying spaces in the specimens. Once leached out of the specimens, the volumes artificially occupied by the OS compounds

become voids in the samples. The increase is not as pronounced as with MnRD40-21, which could suggest that while there is an increase in water absorption capacity, it does so at a slower rate. The absence of a baseline measurement, primarily due to the instantaneous dissolution of natural soils in water, makes it impossible to observe their water absorption, which would have provided a critical reference point for quantifying the effectiveness of EWR samples in withstanding the rigors of wet-dry cycles.

a)

b)

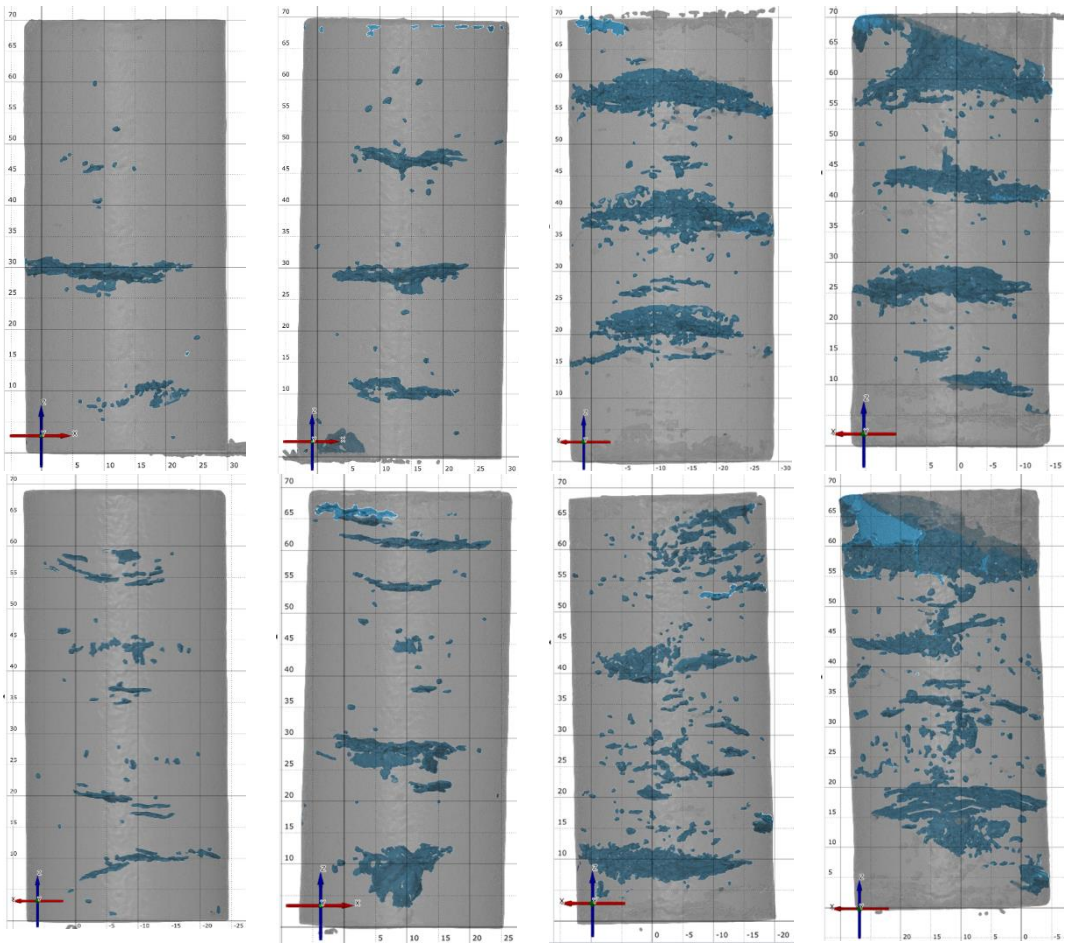

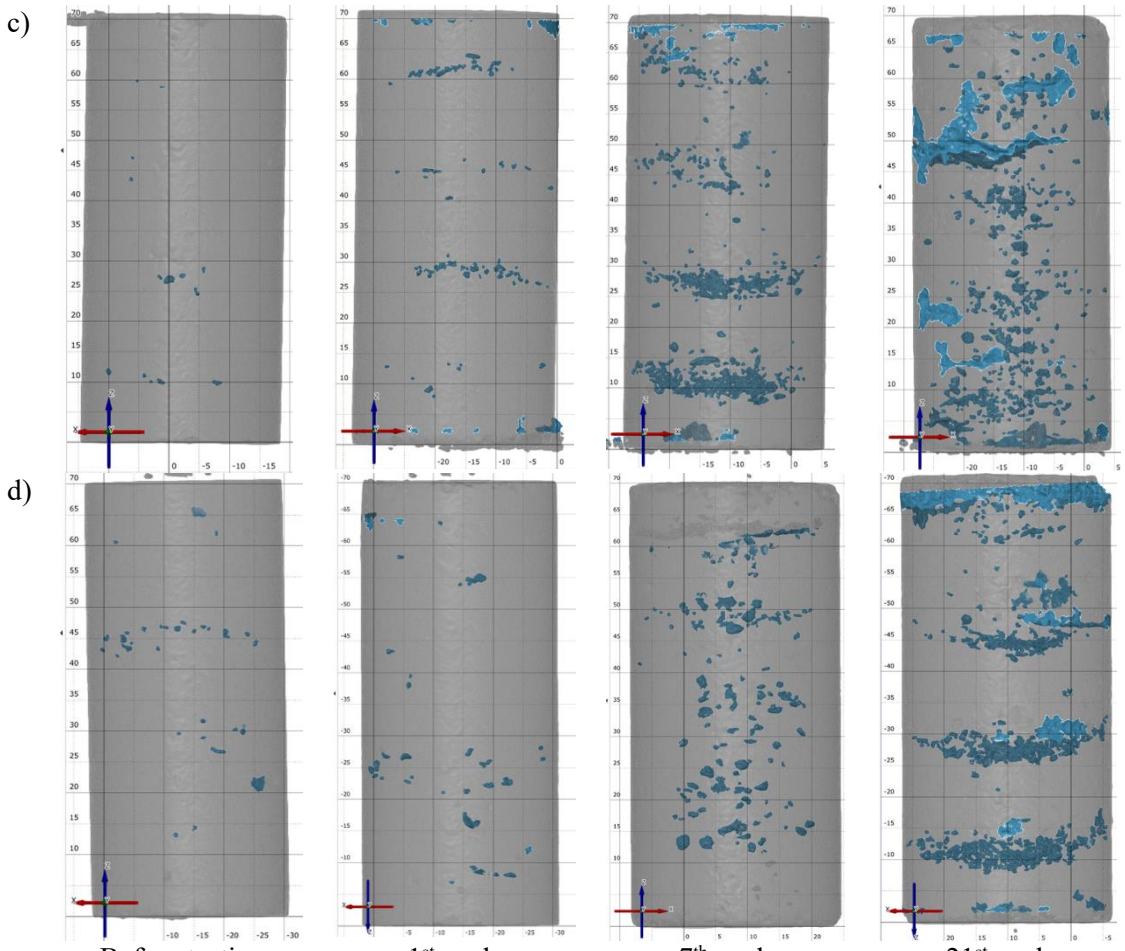

Figure 3.25: Microstructural changes as cyclic wet dry increase a) IA-BV20, b) IA-BV40, c) MnRD20, and d) MnRD40 (Note: the scanned samples are not the same from 1st cycle to 21st cycle).

3.9.3.2 Immersion.

Figure 3.26a shows the effect of full immersion on EWR for prolonged periods (1 to 120 days) and control samples. The result showed a reduction in the strength of the soaked samples compared to the control specimen. All samples experienced a sharp reduction (on an average of 67.5%) in compressive strength after the first 24 hours. Another major reduction (on an average of 82%) in compressive strength is between 24 to 72 hours of soaking. Therefore, all samples experienced a decline of about 98% within 120 days of soaking. While there is a significant reduction as the soaking period continues, it should be noted that natural or hydrophilic soil could not withstand being soaked in water for 2 hours, as seen in the time-stamped images in Figure 3.27. A study by Dhakal et al. (2024), which used Calcium Sulfo-Aluminate Cement (CSAC) to stabilize clayey, observed sample disintegration during submergence in water during

the wetting phase, a phenomenon not experienced in any treated sample but in untreated samples. Hydrophobic soil maintains its physical appearance and volume even after several days (120 days as observed in this study) of immersion.

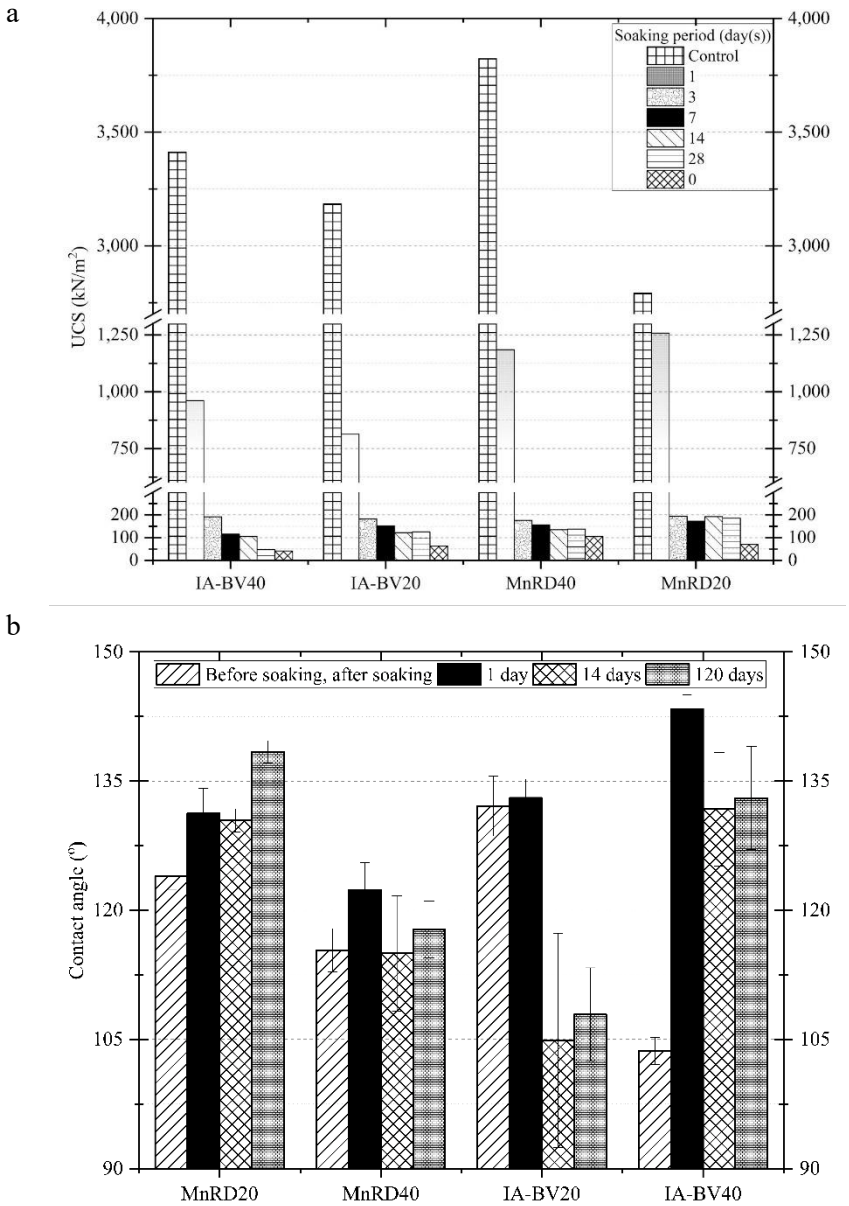

Figure 3.26: a) The UCS of IA-BV and MnRD after 120 days of soaking, and b) contact angle test before and after soaking indicates no loss of hydrophobicity.

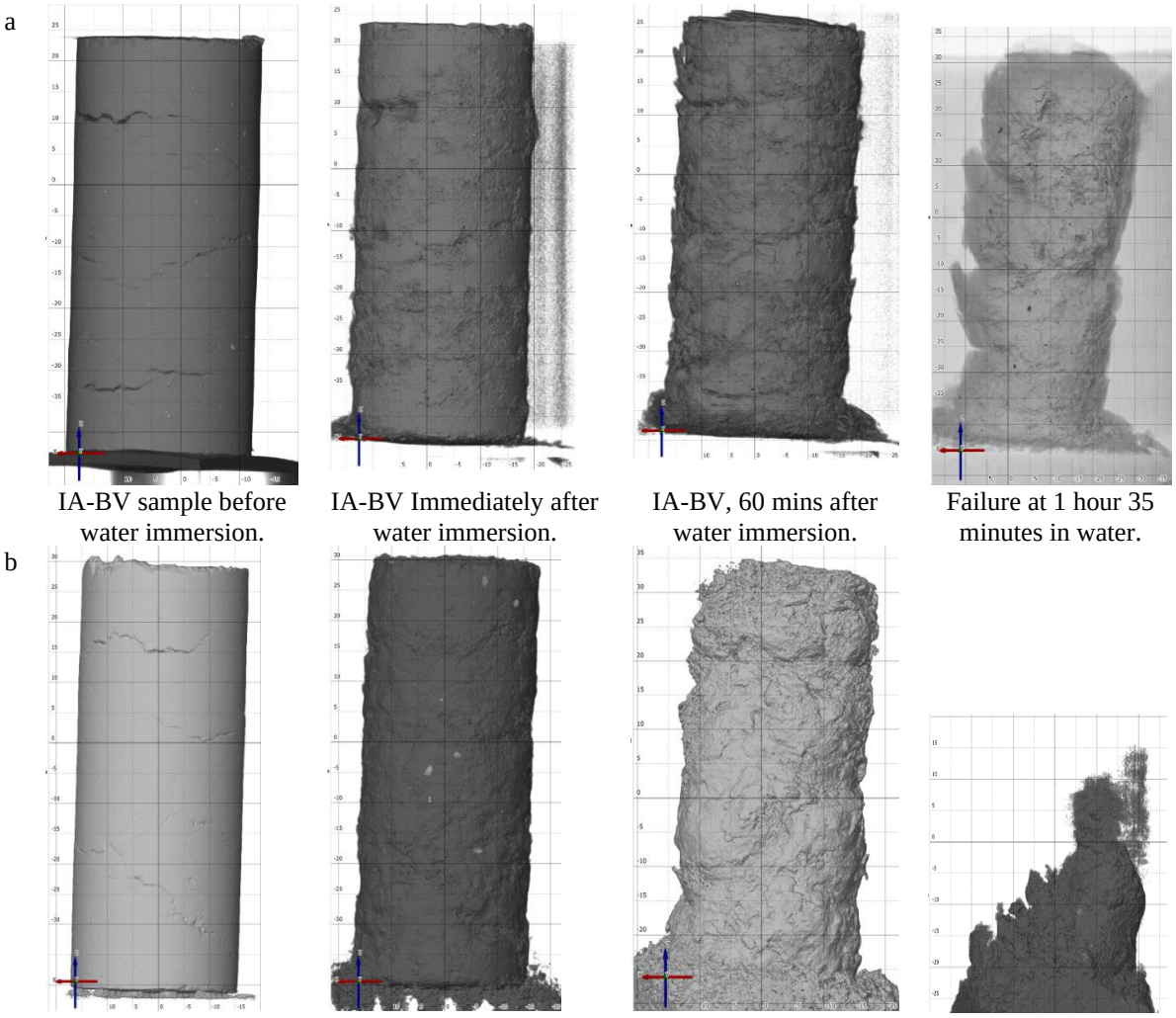

IA-BV sample before water immersion. | IA-BV Immediately after water immersion. | IA-BV, 60 mins after water immersion. | Failure at 1 hour 35 minutes in water.

MnRD sample before water immersion. | MnRD Immediately after water immersion. | MnRD, 30 mins after water immersion. | Failure at 45 minutes in water.

Figure 3.27: Hydrophilic soil reaction to Submersion

Figure 3-28 offer insights into the corresponding reason behind the reduction in mechanical strength due to water infiltration as observed through water absorption characteristics and degree of saturation. The premise of hydrophobic soil treatment is to minimize water infiltration, thus preserving compressive strength by maintaining unsaturated conditions. However, these figures show that prolonged water exposure increases saturation by creating extra voids from leaching of the unbound OS, changes in porosity, and/or crack formation. Figure 3.26b indicates that the infiltration was not triggered by reduce hydrophobicity but by other mechanisms, such as porosity changes due to unused OS leaching especially though the main failure points of the sample.

a

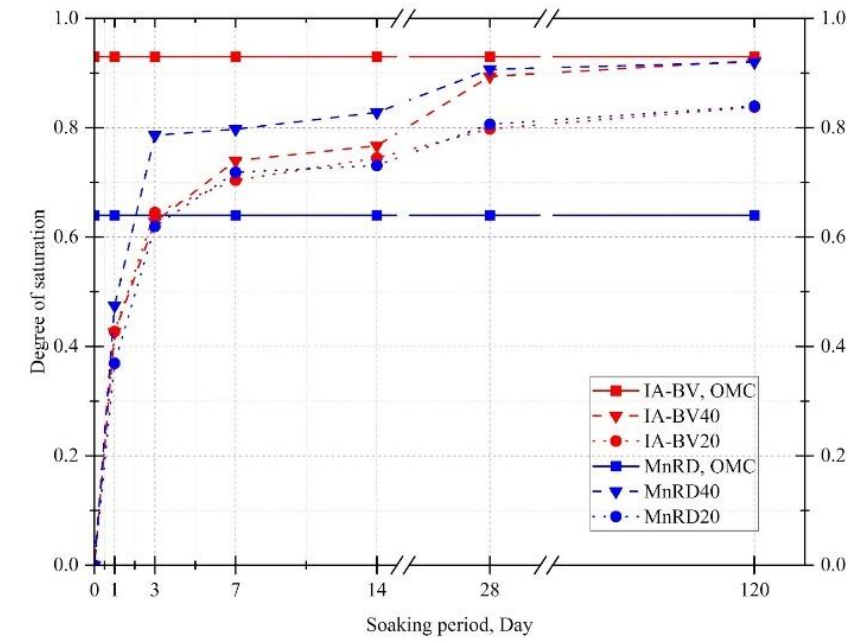

b

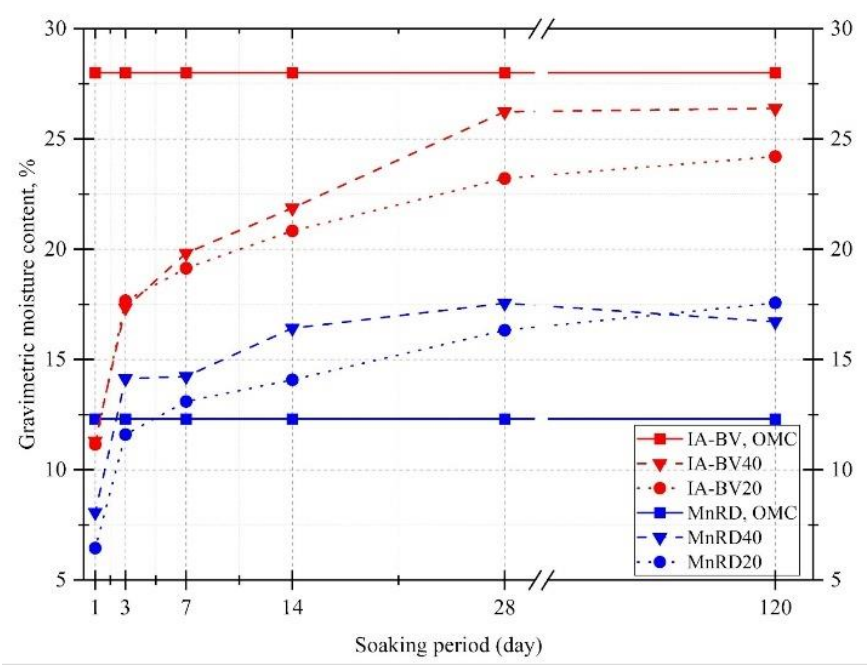

Figure 3.28: a) Calculated degree of saturation during full immersion and b) Gravimetric moisture content during soaking.

Similarly, Figure 3-28a illustrates the corresponding calculated degree of saturation; all samples initially showed a trend of rapid water absorption, which then levels off after about 14 days. The degree of saturation reaches as high as 63% for IA-BV40 and 79% for MnRD40 between days one and three. Figure 3-28b shows that the samples absorb a significant mass of water, especially in the early days of soaking.

Figure 3-29 further substantiates this, as pore formation progressively increases with longer duration. The X-ray CT scans also showed that the failure points were the interfaces of layer compaction during sample preparations. As mentioned previously, high water resistance through hydrophobicity is governed by porosity. Hence, the observed penetration points were from layer interfaces. Different studies have observed that soils that were initially hydrophobic eventually reduced or allowed water infiltration (Lee et al., 2015), as observed from the water entry pressure test and water penetration test (Uduebor et al., 2022b; Uduebor et al., 2023b). This study observed hydrophobic decay given by porosity and not chemical or binding decline. Studies of the use of organo-silane in concrete suggest that water repellency can last for decades (Christodoulou et al., 2013; Ley and Moradllo, 2015; Sudbrink et al., 2017).

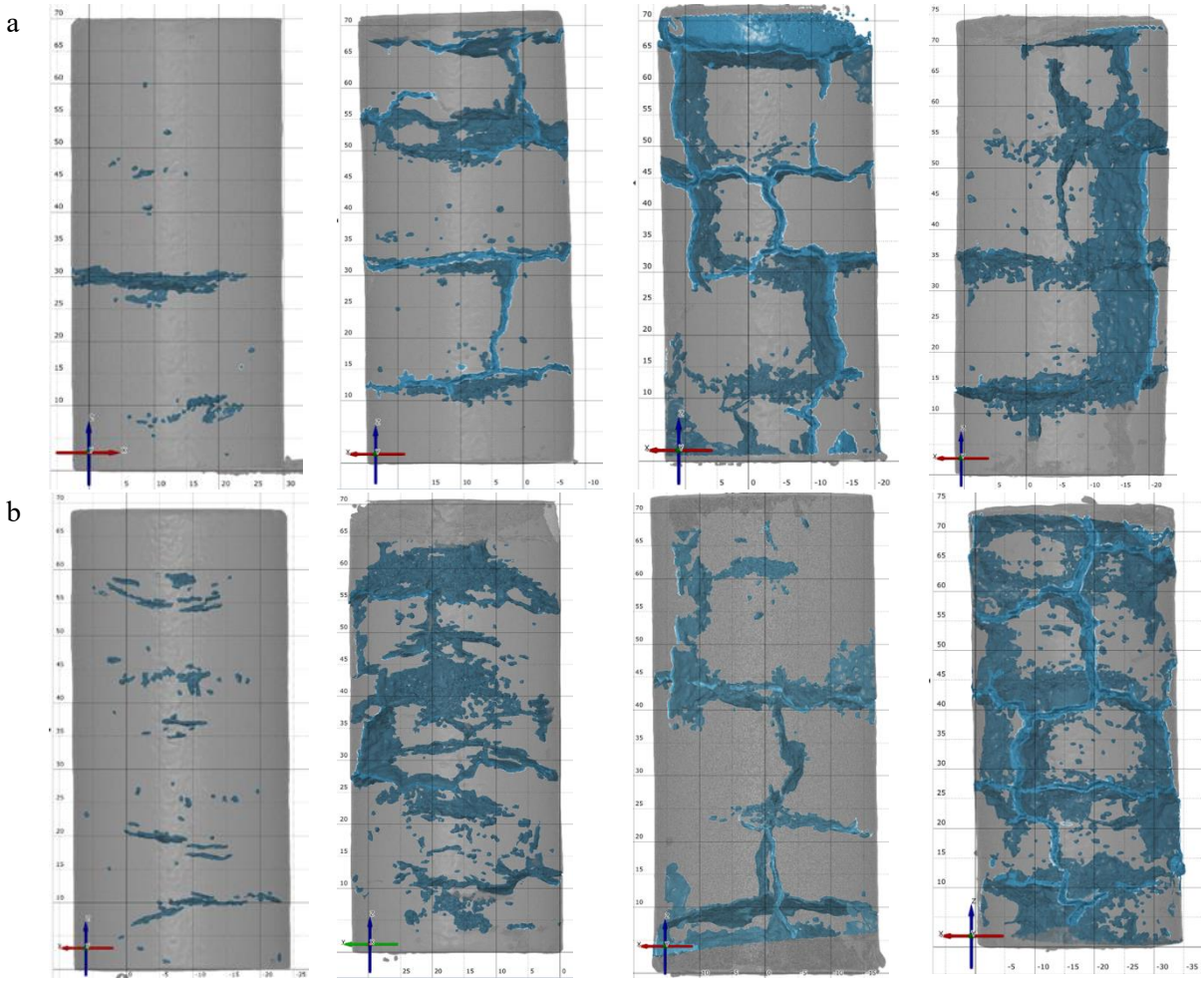

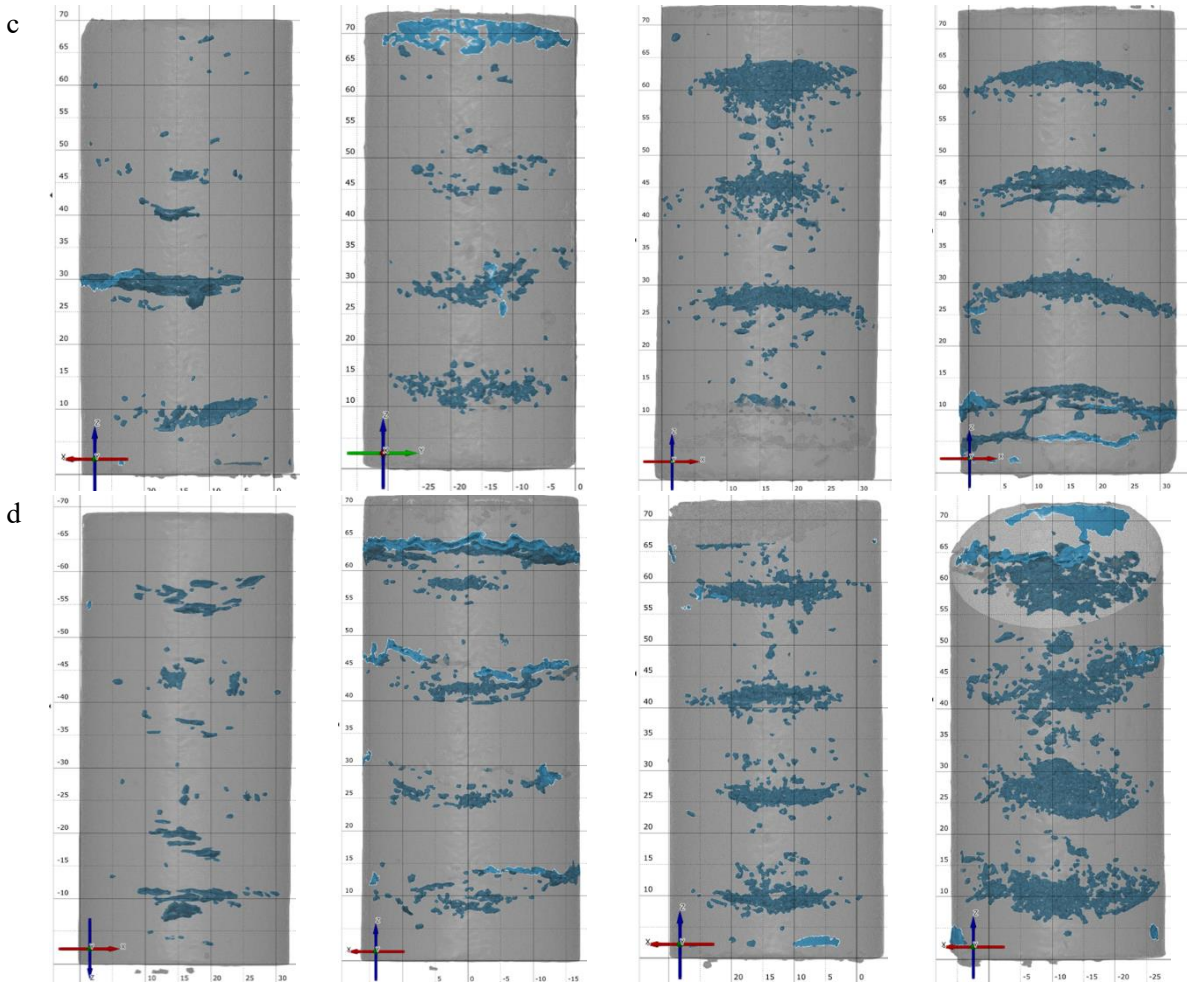

Figure 3.29: Microstructural changes during immersion a) IA-BV20, b) IA-BV40, c) MnRD20, and d) MnRD40 (Note: the scanned samples are not the same but are replicates).

3.9.4 X-ray scans

3.9.4.1 Changes in MnRD Samples

For the MnRD samples, porosity calculated from the X-ray CT scans post-treatment revealed notable trends. After full soaking for 120 days, the MnRD samples exhibited a porosity change of 7961.39 and 8382.86% (MnRD20 and MnRD40) compared to untreated MnRD soil. However, the samples subjected to wet-dry cycles demonstrated much less change, with a maximum porosity change of 1602.3 and 1624.29% (MnRD20 and MnRD40, respectively) after 21 cycles, as shown in Figure 3.30. This relatively smaller volume change indicates that while the repeating cycle between wetting and drying imposed stress on the material, the alteration allowed the samples to retain more of their volumetric integrity

compared to continuous soaking. The relative minimal change after wet-dry cycles suggests that the treatment carried out on MnRD samples resists significant volume fluctuations, making it suitable for environments with varying moisture levels.

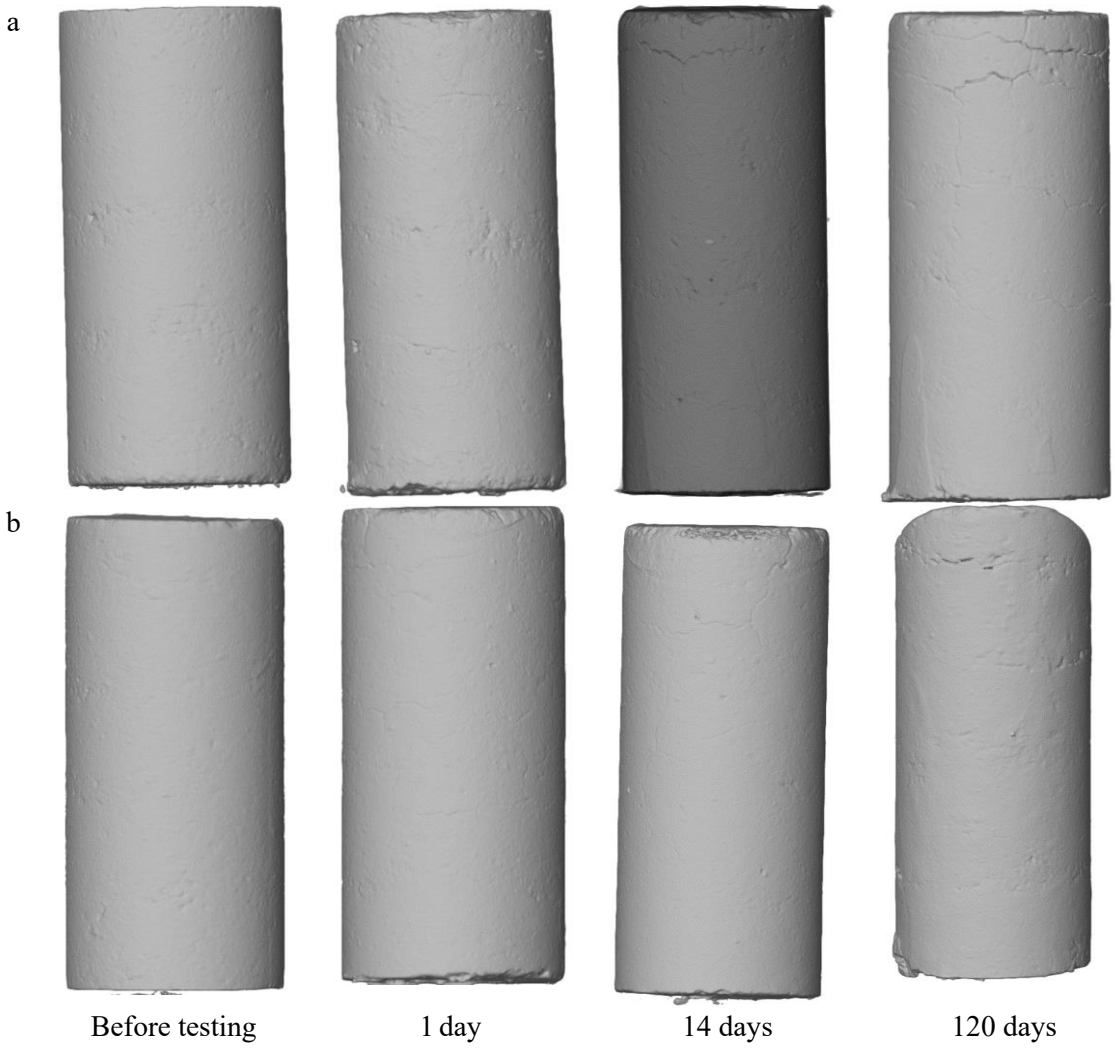

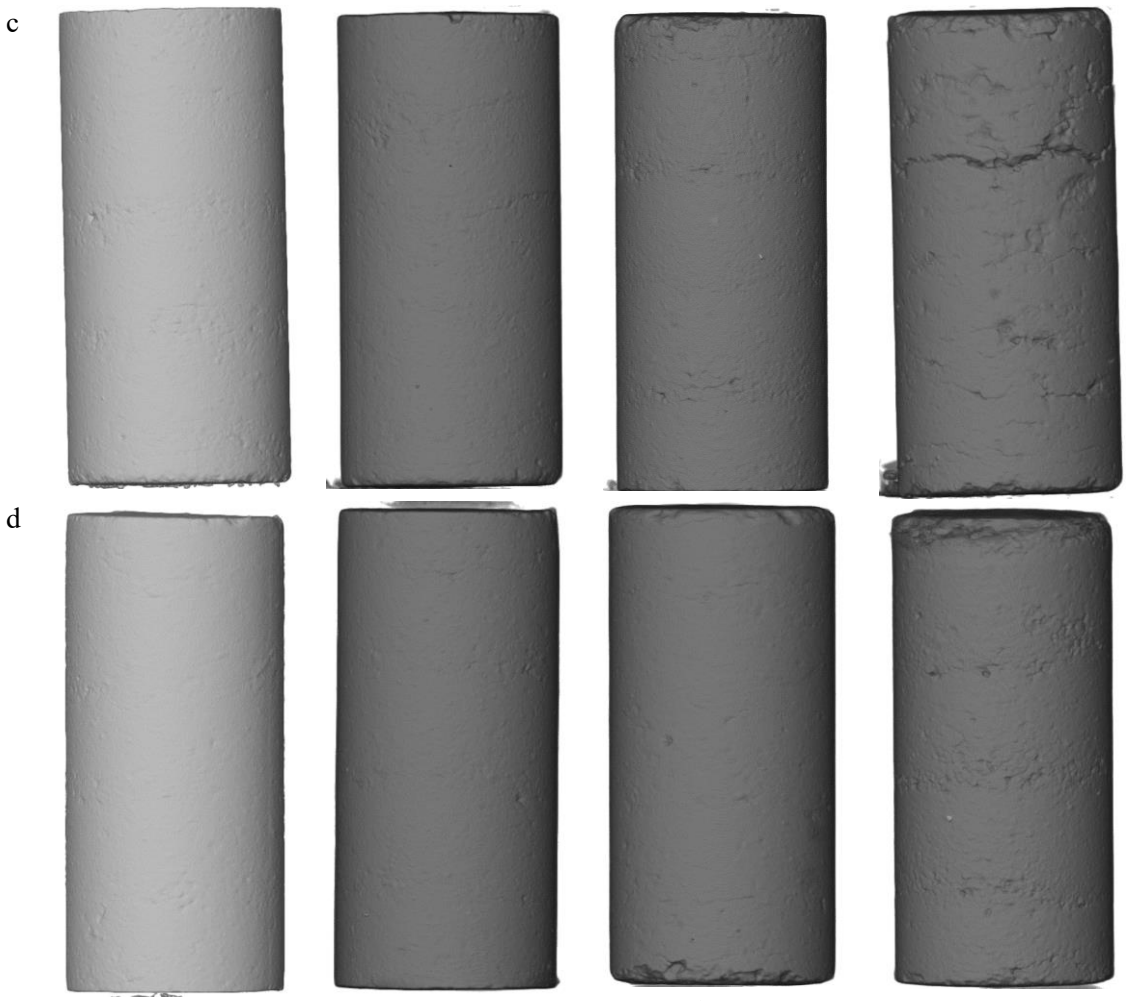

Figure 3.30: Longitudinal Views of MnRD during immersion a) MnRD20, b) MnRD40, and after cyclic wet dry c) MnRD20, and d) MnRD40 (Note: the scanned samples are not the same but are replicates).

3.9.4.2 Changes in IA-BV Samples

The IA-BV samples followed similar trends but showed more pronounced changes. The largest void change observed under full soaking reached 250% compared to the untreated sample (significantly higher than MnRD samples because IA-BV generally had higher void volume than MnRD in both concentrations). This larger change suggests that the IA-BV samples are more affected by water ingress during prolonged soaking, potentially due to their material properties. The volume changes were smaller for shorter soaking durations, 50% after 28 days and 250% after 120 days. This reduction in void volume change with shorter soaking times demonstrates that while IA-BV samples are affected by full soaking, the extent of volume change decreases over shorter exposures, as depicted in Figure 3.31. For wet-dry cycling,

the IA-BV samples showed a maximum change of 200%, slightly larger than that observed for MnRD samples under similar conditions. This suggests that the IA-BV material is more susceptible to changes under repetitive moisture fluctuations, though less so than under full soaking.

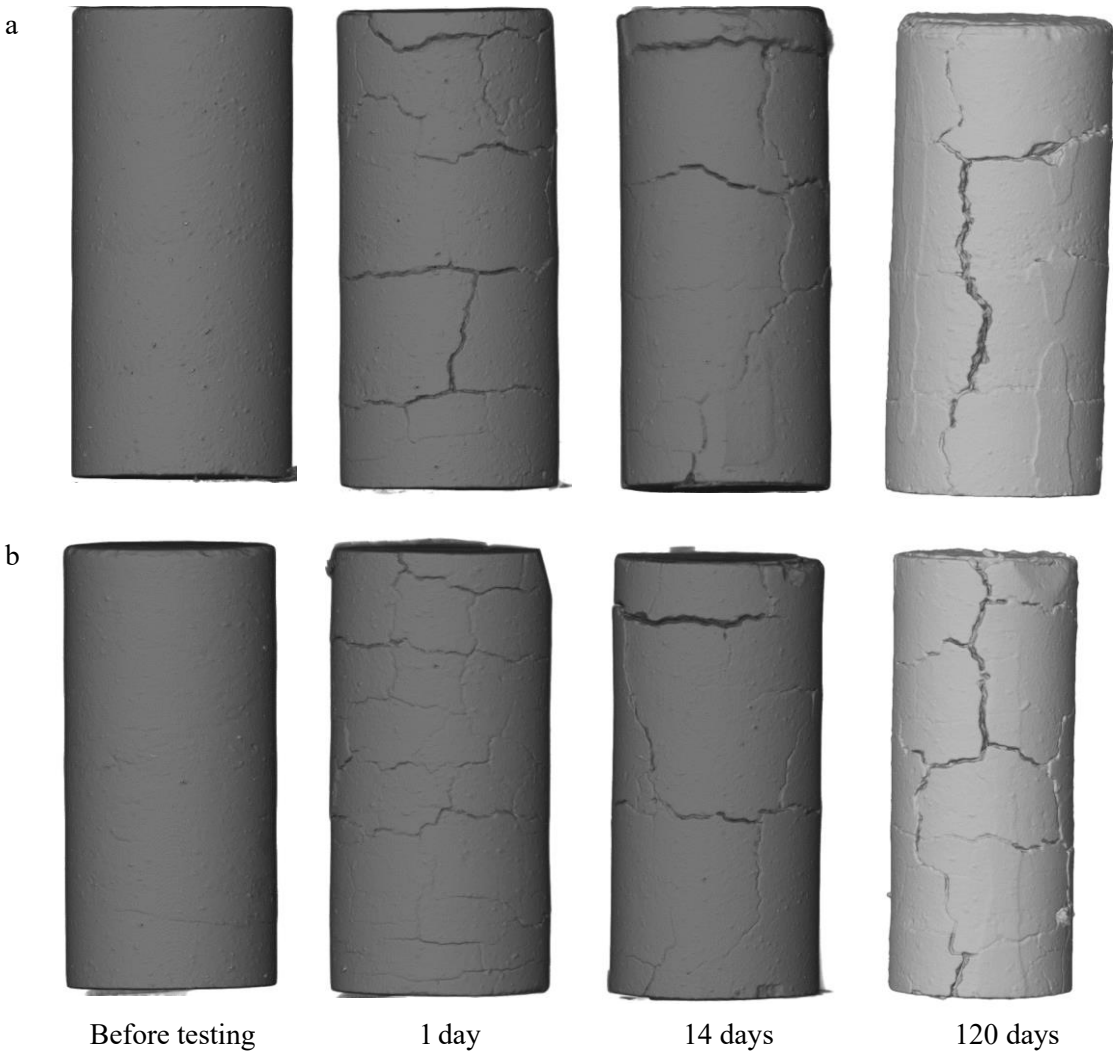

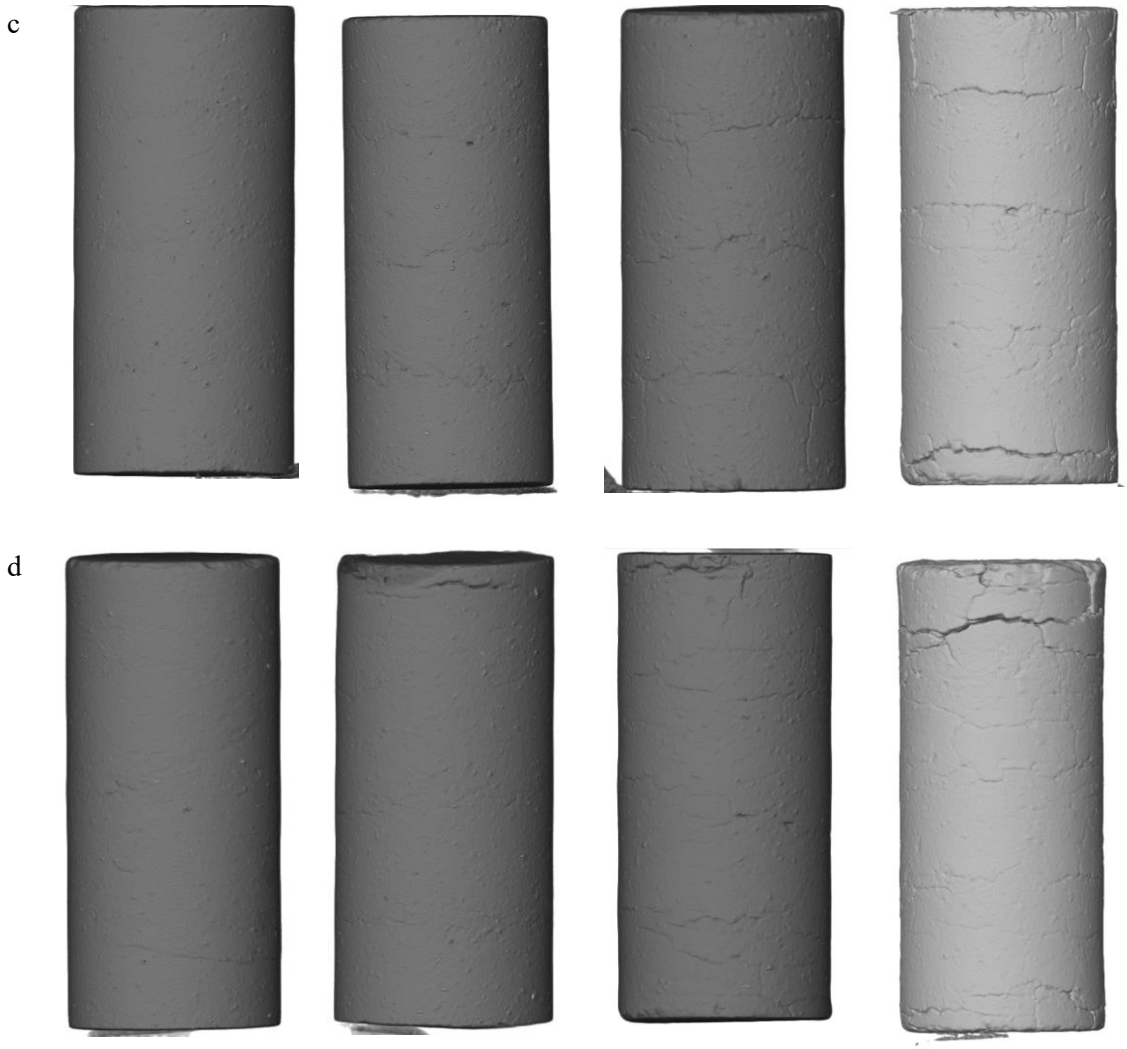

Figure 3.31: Longitudinal Views of IA-BV during immersion a) IA-BV20, b) IA-BV40, and after cyclic wet dry c) IA-BV20, and d) IA-BV40 (Note: the scanned samples are not the same but are replicates).

3.9.4.3 Comparative Analysis

MnRD and IA-BV samples exhibited greater stability under wet-dry cycles compared to full soaking, possibly indicating that repeated moisture exposure followed by drying induces less cumulative stress than continuous soaking. However, BV samples (average control void volume of 6.55 cc) were more prone to void volume changes in both conditions compared to MN samples (average control void volume of 0.197 cc), demonstrating that the MnRD-treated samples possess better durability, especially in resisting volumetric changes. The micro-focus X-ray CT data further supports these findings by capturing 3D structural changes (Figure 3.25, Figure 3.30, Figure 3.30, and Figure 3.31).

The larger volume changes in BV samples under full soaking reflect more significant water ingress, while the relatively smaller changes in MN samples confirm its relatively better performance in maintaining its volume. MN samples show better resistance to volume changes, particularly under repeated wet-dry conditions, making them a more reliable choice for applications requiring long-term durability.

Some volume changes that have been defined in this study, particularly in the BV samples, may have been influenced by disturbances during sample handling. Future studies should focus on improving handling techniques and incorporating more precise methods for volume change quantification. Extending the range of wet-dry cycles and soaking durations would provide further insight into the longer-term durability of treated soils. In summary, the use of X-ray CT scanning provided novel insights into the durability behavior of treated MN and BV soils under challenging environmental conditions.

3.10 Conclusions

The study highlights the effectiveness and limitations of engineered water-repellent (EWR) soil in improving moisture resistance and durability in various soil conditions.

- Hydrophobicity and water resistance: EWR soils demonstrate significant hydrophobicity, with contact angles exceeding 90 degrees, effectively resisting water infiltration in the short term. EWR-treated samples similarly maintain structural integrity for extended periods, delaying water penetration. However, prolonged water exposure (120 days) under 30 mm head ultimately enables water to infiltrate into the samples through increased porosity and crack networks.
- Compaction and mechanical strength: The OS-treated soils exhibit favorable compaction properties, with reduced Optimum Moisture Content (OMC) and minimal changes in Maximum Dry Density (MDD). However, EWR treatments reduce mechanical strength, particularly at higher concentrations of OS. This is attributed to the presence of the organic moiety of the OS molecule that lowers shear resistance. While moisture resistance is improved, the reduction in mechanical strength may limit the application of these treatments in conditions requiring high compressive strength.

- Resistance to wet-dry cycles and prolonged water immersion: EWR samples, especially at higher concentrations, demonstrate better resilience to wet-dry cycles, with less degradation over time than untreated soils. Similarly, EWR-treated samples show better stability under wet-dry cycles than continuous soaking, with minimal volumetric changes observed in MnROAD samples. However, under prolonged water immersion, EWR-treated soils experience significant strength reductions of up to 98% at 120 days and increased water absorption, compromising their long-term durability.
- Water absorption and porosity: Both studies show that water absorption and porosity increase under prolonged exposure to water or repeated wet-dry cycles. This leads to cracks and diminished resistance to water infiltration over time, indicating that while hydrophobic soils initially resist water inflow, their effectiveness diminishes due to structural changes in the soil matrix.
- Field application considerations: The primary benefit of EWR treatment is moisture control rather than mechanical strength enhancement. OS-treated soils are suitable for applications where moisture resistance is critical, such as landfills, subgrades, and tunnels. EWR-treated soils show promise for similar applications, especially in environments subject to wet-dry cycles. However, the reduction in mechanical strength and eventual penetration of water with crack propagation and prolonged water exposure necessitates careful consideration when these treatments are used in field applications requiring water resistance and compressive strength.

Overall, EWR significantly enhances moisture resistance, particularly in the early stages of exposure and in conditions of repeated wet and dry, but exhibits limitations under prolonged and sustained water contact. These findings underscore the need to balance hydrophobicity and mechanical strength for specific field conditions and highlight the importance of further research to improve the long-term durability of these treatments.

3.11 Acknowledgment

The author gratefully acknowledge the funding support from Iowa Highway Research Board (TR-783) and National Science Foundation (Award #1928813 and #1947009) and Zeiss for the X-ray scan and processing.

3.12 Reference

Adeyanju, E. D., Uduebor, M. A., Saulick, Y., Daniels, J. L., & Cetin, B. (2024). Influence of Density on Engineered Water Repellent Soil. In International Conference on Transportation and Development 2024 (pp. 152-161).

ASTM D4318-00 (2000), "Standard Test Methods for Liquid Limit, Plastic Limit, and Plasticity Index of Soils.," ASTM International, West Conshohocken, PA., 2017.

ASTM International, " ASTM D7928-17: Standard Test Method for Particle-Size Distribution (Gradation) of Fine-Grained Soils Using the Sedimentation (Hydrometer) Analysis," ASTM International, 2017.

ASTM D698, (2012). Standard Test Methods for Laboratory Compaction Characteristics of Soil Using Standard Effort. ASTM International, West Conshohocken, PA.

ASTM D854-10 (2006), "Standard Test Methods for Specific Gravity of Soil Solids by Water Pycnometer.," ASTM International, West Conshohocken, PA., 2014.

ASTM D2166, "Standard Test Methods for Laboratory Compaction Characteristics of Soil Using Standard Effort.," ASTM International, West Conshohocken, PA., 2012.

ASTM D559 (American Society for Testing and Materials). (2003). Standard test methods for wetting and drying compacted soil-cement mixtures. Conshohocken, PA.

ASTM D870-15 (American Society for Testing and Materials). (2015). Standard Practice for Testing Water Resistance of Coatings Using Water Immersion.

AASHTO, "Standard Specification for Classification of Soils and Soil-Aggregate Mixtures for Highway Construction Purposes.," American Association of State and Highway Transportation Officials: Washington, DC, USA., 2017.

ASTM D2487-17 (2017), "Standard Practice for Classification of Soils for Engineering Purposes (Unified Soil Classification System)," ASTM International.

Barbieri, D. M., Hoff, I., & Mørk, M. B. E. (2020). Organosilane and lignosulfonate as innovative stabilization techniques for crushed rocks used in road unbound layers. *Transportation Geotechnics*, *22*, 100308.

Brooks, T., Daniels, J. L., Uduebor, M., Cetin, B., & Wasif Naqvi, M. (2022). Engineered Water Repellency for Mitigating Frost Action in Iowa Soils. In *Geo-Congress 2022* (pp. 448-456).

Christodoulou, C., Goodier, C. I., Austin, S. A., Webb, J., & Glass, G. K. (2013). Long-term performance of surface impregnation of reinforced concrete structures with silane. *Construction and Building Materials*, *48*, 708-716.

Christopher, B. R., Schwartz, C. W., Boudreaux, R., & Berg, R. R. (2006). *Geotechnical aspects of pavements* (No. FHWA-NHI-05-037). United States. Federal Highway Administration.

Daniels, J. L., Mehta, P., Vaden, M., Sweem, D., Mason, M. D., Zavareh, M., & Ogunro, V. (2009). Nano-scale organo-silane applications in geotechnical and geoenvironmental engineering. *Journal of Terraspace Science and Engineering*, *1*(1), 21-30.

Dhakal, S., Kolay, P., & Puri, V. (2024). The durability of clayey soil stabilized with calcium sulfoaluminate cement and polypropylene fiber under extreme environments. *Transportation Geotechnics*, *44*, 101164.

Jerez, L. D., Gómez, O. E., & Murillo, C. A. (2018). Stabilization of Colombian lateritic soil with a hydrophobic compound (organosilane). *International Journal of Pavement Research and Technology*, *11*(6), 639-646.

Hoy, M., Tran, N. Q., Suddeepong, A., Horpibulsuk, S., Buritatum, A., Yaowarat, T., & Arulrajah, A. (2023). Wetting-drying durability performance of cement-stabilized recycled materials and lateritic soil using natural rubber latex. *Construction and Building Materials*, *403*, 133108.

Lee, C., Yang, H. J., Yun, T. S., Choi, Y., & Yang, S. (2015). Water-Entry Pressure and Friction Angle in an Artificially Synthesized Water-Repellent Silty Soil. *Vadose Zone Journal*, *14*(4), 1-9.

Ley, T., & Moradllo, M. K. (2015). Expected Life of Silane Water Repellent Treatments on Bridge Decks, Phase 2. *Research & Development Division Oklahoma Department of Transportation. No. FHWA-OK-15-05/ODOT-2229*.

Lin, H., & Lourenço, S. D. (2019). Durability assessment of engineered hydrophobic soils. In *Proceedings of the XVII European Conference on Soil Mechanics and Geotechnical Engineering (ECSMGE-2019)*. Icelandic Geotechnical Society.

Lin, H., Huang, G., Lourenço, S.D., Beckett, C.T., Xing, X. and Liu, J., 2024. An exploration on the degradation of hydrophobized sands as a subgrade impervious barrier during one-year outdoor weathering. *Acta Geotechnica*, pp.1-15.

Lin, H. and Lourenço, S.D., 2022. Accelerated weathering of hydrophobized sands. *Acta Geotechnica*, *17*(2), pp.377-390.

Naqvi, M. W., Sadiq, M. F., Cetin, B., Adeyanju, E., & Daniels, J. (2023). Development, Construction, and Instrumentation of Pilot Freeze–Thaw Resistant Granular Roadways Test Cells. In *13th International Conference on Low-Volume Roads* (p. 3).

Saulick, Y., Malisher, M. L., Familusi, A., & Daniels, J. L. (2024). Compaction Characteristics of Organo-silane Treated Soils. *Geotechnical Testing Journal*, *47*(2).

Saulick, Y., Yang, H.W. and Lourenço, S.D., 2023. Temporal variations of surface roughness and thickness of polymer-coated quartz sand. Journal of Coatings Technology and Research, 20(5), pp.1795-1800.

Sudbrink, B., Moradllo, M. K., Hu, Q., Ley, M. T., Davis, J. M., Materer, N., & Apblett, A. (2017). Imaging the presence of silane coatings in concrete with micro X-ray fluorescence. *Cement and Concrete Research*, *92*, 121-127.

Taber, S. (1916). The growth of crystals under external pressure. American Journal of Science, 4(246), 532–556.

Uduebor, M., Daniels, J., Naqvi, M. W., & Cetin, B. (2022b). Engineered Water Repellency in Frost Susceptible Soils. In *Geo-Congress 2022* (pp. 457-466).

Uduebor, M., Adeyanju, E., Saulick, Y., Daniels, J., & Cetin, B. (2022a). A review of innovative frost heave mitigation techniques for road pavements. In *International Conference on Transportation and Development 2022* (pp. 95-106).

Uduebor, M., Adeyanju, E., Saulick, Y., Daniels, J., & Cetin, B. (2023a). Engineered Water Repellency for Moisture Control in Airport Pavement Soils. In *Airfield and Highway Pavements 2023* (pp. 92-102).

Uduebor, M. (2023b). *Engineered Water Repellency for Frost Heave Mitigation: Decoupling the Relative Influence of Matric and Osmotic Suction* (Doctoral dissertation, The University of North Carolina at Charlotte).

Uduebor, M., Daniels, J., Saulick, Y., Naqvi, W., & Cetin, B. (2023c). Optimization of water repellency in soils for geotechnical applications. *International Journal of Geotechnical Engineering*, 1-11.

U.S. Army, "Soils and geology: Pavement design for frost conditions.," US Army Corps of Engineers, Washington, DC., 1965.

Zhou, Z., Leung, A.K., Zhu, W.J. and Li, Y.Y., 2021. Hydromechanical behavior of unsaturated artificially–hydrophobized sand: Compression, shearing, and dilatancy. *Engineering Geology*, *291*, p.106223.

CHAPTER 4: FIELD EVALUATION OF ENGINEERED WATER REPELLENCY.

TRANSLATING LABORATORY WATER REPELLENCY TESTS TO FIELD DESIGN: DEVELOPING A CAPILLARY BREAK SYSTEM FOR FROST ACTION MITIGATION IN PAVEMENT FOUNDATIONS AT MNROAD.

Abstract

This study investigates optimizing organosilane (OS) applications for field conditions by evaluating contact angle (CA) and breakthrough tests across different sample preparation methods. The aim is to bridge the gap between laboratory testing and real-world field applications and to utilize the laboratory results in field design involving spraying or compacting OS-treated soils. Six different soil types were analyzed using various approaches, including typical batch procedure, mixing at optimum moisture content (OMC) for compacted Engineered Water Repellency (EWR), simulated field spraying (at 0.55, 0.33, and 0.22 OS liters/m² on untreated soils)), and different liquid-to-soil ratios. A breakthrough test was done simulating both the compaction and spray methods. Then, the breakthrough result was used to design a capillary barrier system. Results showed that CA values decreased with lower OS concentrations but remained above 90° (hydrophobic) for most soils at a 1:40 ratio. However, the relationship between OS concentration and CA was not linear, especially for soils mixed at OMC. From the sprayed contact angle test, penetration depth was generally limited to less than 2 mm for soils at OMC but increased to 4.2 mm for air-dried and 4.7 mm for oven-dried samples, indicating that drier conditions enhance OS penetration. Lower OS concentrations had improved CA values with depth. Breakthrough pressure (BP) testing, simulating field water pressures, indicated that higher OS concentrations (0.55 OS liters/m²) provided the best water resistance. However, limitations in penetration depth and the volume of molding solution applied pose challenges for field applications. The study concludes that while laboratory tests provide insights into OS application efficiency, real-world conditions necessitate adjustments in OS concentration and application methods to achieve optimal hydrophobic performance.

Keywords: Hydrophobicity, water entry pressure, Contact angle.

Nomenclature

BP: Breakthrough pressure

CA: Contact angle

HDPE: High-Density Polyethylene

OS: Organosilane

OMC: Optimum moisture content

WDPT: Water droplet penetration time

WEP: Water-entry pressure

4.1 Introduction

The infiltration of water into soil can present significant geotechnical and geoenvironmental challenges, including reduced soil strength, increased leachate generation, and slope stability issues. Traditional approaches to managing water infiltration often involve physical barriers, such as clay liners or geomembranes. However, an innovative approach involves the chemical modification of soil surfaces using organosilane (OS), which render the soil hydrophobic and impede water entry (Keatts et al., 2018; Uduebor et al., 2023). Laboratory testing of hydrophobic soils often involves methods such as water droplet penetration time (WDPT) (Doerr, 1998; Wang et al., 2000; Leelamanie et al., 2008), contact angle (CA) measurements (Feyyisa et al., 2017; Saulick et al., 2017; Feyyisa et al., 2019), and breakthrough pressure (BP, also, known as water-entry pressure (WEP)) (Lee et al., 2015; Adeyanju et a., 2024) assessments. These techniques help to characterize the degree of soil water repellency, which impacts water infiltration behavior. The contact angle is a fundamental measure of a material's hydrophobic or hydrophilic nature. It quantifies the angle formed between a liquid droplet and the solid surface upon which it rests. The material is considered hydrophilic when the contact angle is less than 90°, as the water droplet spreads across the surface (Yuan and Lee, 2013). Conversely, when the contact angle exceeds 90°, the surface is hydrophobic,

meaning the droplet tends to bead up rather than spread, indicating a resistance to water infiltration (McHale et al., 2005; Saulick, 2018).

BP is defined as the pressure required to initiate water infiltration into a porous medium (Wang et al., 2000; Zhou et al., 2021). In the case of hydrophilic soils, water entry occurs readily, often at negative pressure values, because water is the wetting fluid (Wang et al., 2000; Lourenço et al., 2021). For OS-modified soils, however, BP becomes positive, indicating the need for external pressure to overcome the soil's resistance to water penetration (Uduebor et al., 2023). A nonlinear trend characterizes the relationship between contact angle and BP. As the contact angle increases beyond 90°, BP rises sharply, meaning that higher hydrophobicity levels correlate with greater water infiltration resistance (Feyyisa et al., 2019). This behavior is because as the contact angle increases, the adhesive forces between the water droplet and the soil surface diminish relative to the cohesive forces within the water. Consequently, greater pressure is required to force the water into the soil pores.

At high levels of contact angle, typically above 110°, even small increases in hydrophobicity can lead to substantial gains in BP. This trend suggests that achieving a high contact angle through OS treatment is crucial for practical applications where the objective is to minimize water infiltration. Several factors impact the relationship between contact angle and water entry pressure in OS-modified soils, including organo-silane dosage, material characteristics, dry density, and pore size distribution (Lee et al. 2015; Keatts et al. 2018). The findings on the relationship between contact angle and water entry pressure have important implications for the design of infiltration control systems using OS-treated soils. In engineering applications, the goal is to maximize BP to prevent unwanted water infiltration. This can be achieved by optimizing OS dosage, selecting materials with appropriate characteristics, and considering the effects of compaction and pore size.

The relationship between the contact angle and BP in OS-treated soils forms the scientific basis for hydrophobic modification to control water infiltration. As contact angles increase, water entry pressure also rises, indicating greater resistance to water infiltration (Uduebor et al., 2023). This relationship is nonlinear

and becomes more pronounced with higher levels of hydrophobicity. Notably, the contact angle observed within the pore spaces of soil, called the pore contact angle, differs from the contact angle measured on a flat surface, known as the apparent contact angle (Li et al., 2014). This difference between the two values grows with increasing applied pressure, especially beyond a certain threshold. When water is forced into the pore space under pressure, the liquid deforms, resulting in a reduced radius of curvature at the contact surface. Thus, water entry is mainly governed by the pore size and the surface energy of the treated soil (Lee et al., 2015). Other factors influencing the relationship between contact angle (OS dosage) and BP include soil mineralogy, dry density, and pore size distribution. As OS technology advances, it shows significant potential for geotechnical and geoenvironmental applications where controlling infiltration is crucial. The primary design parameter for practical field applications that reduce infiltration should be the water entry pressure rather than the contact angle alone.

In laboratory settings, contact angle testing is often conducted using the sessile drop method, which employs a batching approach with a 1:1 liquid-to-soil ratio. This method ensures that the molding moisture matches the soil mass, but it presents practical limitations for field applications due to cost, strength, and workability constraints. Furthermore, field applications increasingly utilize spray applications for OS treatments, a practice not typically simulated in laboratory settings where the OS and soil are mixed rather than applied as a spray. Daniels et al. (2009) proposed that in field conditions, OS solutions could be added to mold moisture during compaction to enhance mixing efficiency. This approach opens various practical applications, as OS treatment can transform a wide range of soils or byproducts into functional barriers for use such as covers, liners, or similar containment structures.

This study aims to compare laboratory testing methods with field practices in evaluating hydrophobic properties, specifically focusing on contact angle and BP. The research aims to identify any significant differences between the two methodologies. Additionally, since most field applications involving EWR are conducted through spraying or compaction, the study examines the laboratory and field testing results to assess their consistency and implications for practical use. This refined understanding

provides insights into optimizing OS applications for real-world conditions and informs best practices for hydrophobic soil treatment in various engineering contexts. Lastly, the result of BP will be used to design test sites at the MnROAD facility

4.2 Materials and Methods

Six natural frost susceptible soils (FSS) from Iowa (IA-BV, IA-CC, and IA-PC), Minnesota (MnROAD), North Carolina (NC-AS), and New Hampshire (NH-HS), where frost action has been a major historical problem, are utilized in this study. These soils were selected as they have varied particle size distribution profiles, as shown in Figure 4.1. Basic geotechnical testing, including particle size distribution (ASTM D422-63, 2007; ASTM D7928, 2017), specific gravity (ASTM D854-10, 2006), Atterberg limit (i.e., liquid and plastic limit) (ASTM D 4318-00, 2000), and Standard Proctor compaction test (ASTM D698, 2012), are summarized in Table 4-1. All soils were classified according to the Unified Soil Classification System [USCS] (ASTM D2487-17, 2017), the American Association of Highway and Transportation Officials [AASHTO] (AASHTO M145-91, 2012), and the Frost Susceptibility Classification of Soils (NCHRP 1-37A, 2004).

Terrasil from Zydex Industries, India, a reactive soil modifier that permanently modifies the soil surface, making it hydrophobic by converting water-absorbing hydroxyl groups to water-resistant alkyl groups, was used to induce hydrophobicity. Terrasil treated soil is nano modification, which keeps the pores open to allow vapor to escape while preventing water from entering (Daniels et al., 2009a; Daniels et al., 2009b). Uduebor et al. 2022a, Uduebor et al. 2022b, and Brooks et al. (2022) have shown that soil treated with varying concentrations of OS displayed hydrophobicity and a contact angle higher than 90^0, indicating it is either hydrophobic or superhydrophobic.

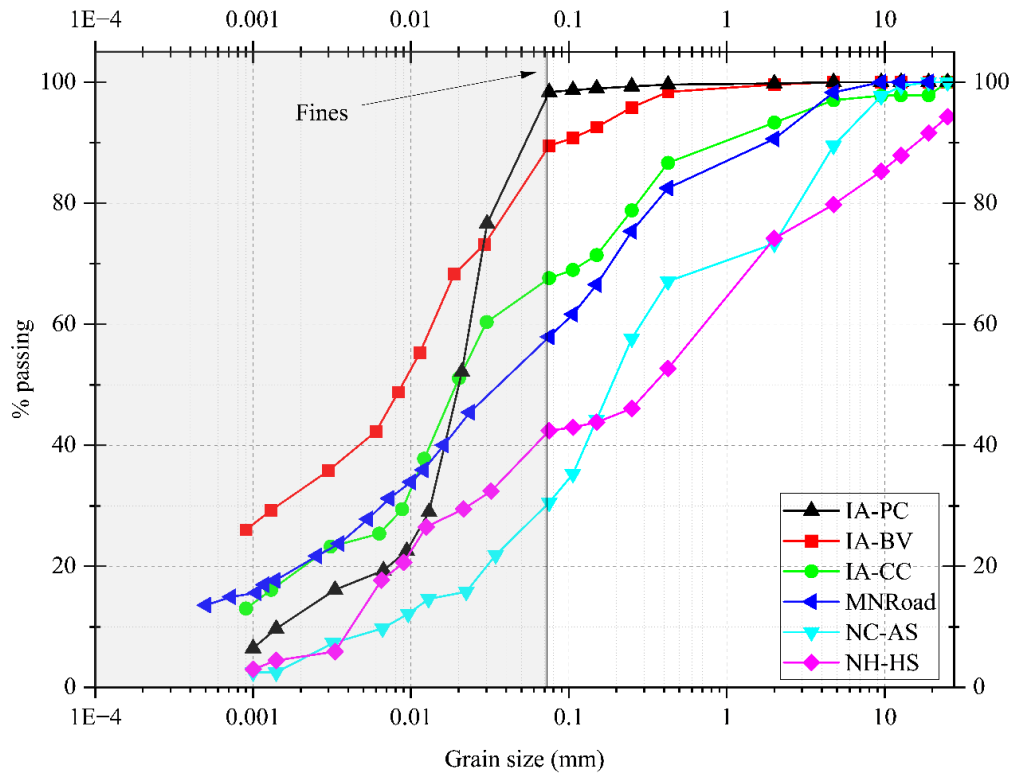

Figure 4.1. Particle size distribution of selected soils.

Table 4-1: Basic Soil properties of selected soils.

Soil properties	Characteristics	Units	NC-AS	IA-CC	Mn ROAD	NH-HS	IA-PC	IA-BV
Classification	AASTHO		A-4	A-7-6	A-6	A-2-5	A-6	A-7-6
	USCS		SM/SC	CH	CL	ML	CL	CH
	D_{60}		0.294	0.030	0.092	0.961	0.024	0.014
	D_{30}		0.073	0.009	0.007	0.023	0.013	0.001
Fines	Total	%	30.52	67.60	59.70	20.19	98.36	87.80
	Silt	%	26.47	48.74	39.70	17.90	86.67	72.80
	Clay	%	4.05	18.86	20.00	2.30	11.69	15.00
Physical properties	Specific gravity		2.65	2.64	2.68	2.63	2.74	2.69
Atterberg limits	Liquid limit	%	38.44	47.20	36.30	41.80	33.73	66.54
	Plastic limit	%	NP	22.88	23.90	NP	23.03	26
	Plasticity index	%	NP	24.32	12.4	NP	10.7	40.54
Proctor test	Optimum Moisture Content (OMC)	%	18.50	19.00	14.10	10.70	17.50	27.60
	Maximum Dry Density (MDD)	kN/m^3	15.02	16.00	19.46	19.40	16.30	13.50

4.2.1 CA testing

To optimize OS application for field conditions, contact angle (CA) testing was conducted as the initial step. This study evaluated various sample preparation methods across six different soils, including the standard laboratory method, mixing at optimum moisture content (OMC) for compacted EWR lifts, simulated field spraying conditions, and different liquid-to-soil ratios. These variations were explored to bridge the gap between traditional laboratory testing and real-world field conditions, which involve either spraying or compacting the OS-treated soil. Additionally, the study aimed to understand how the amount of liquid used in sample preparation affects the results, providing insights into optimizing treatment strategies for different field applications.

The typical laboratory procedure for testing CA involves a batching approach with a liquid-to-soil ratio of 1:1 (Feyyisa et al., 2017). In this procedure, the OS product (Terasill) is mixed with soil and deionized water to achieve the desired ratio using Table 4-2. For instance, in a 1:10 dosage contact angle test, 10 grams of OS is diluted with 90 grams of deionized water, resulting in a total of 100 grams of liquid. This mixture is then added to 100 grams of oven-dried soil. The combined mixture is tumbled for 24 hours using a laboratory tumbler to ensure thorough mixing. Following this, the mixture is oven-dried at 60°C for another 24 hours in an electric oven (Humboldt H-30135 Lab Bench Oven). After drying, the sample is allowed to cool for an additional 24 hours before testing.

Table 4-2: Typical CA preparation mix ratio (per 50g of dry soils)

Soil ID	All soil (IA-BV, IA-CC, IA-PC, NC-AS, NH-HS, and MnROAD)	
Concentration	OS mass (g)	Water mass (g)
1:10	5	45
1:20	2.5	47.5
1:40	1.25	48.75
1:80	0.625	49.375
1:100	0.5	49.5
1:250	0.2	49.8

However, on the field, the molding moisture (OS + water mixture) must be less than the soil OMC because of density and workability constraints. To understand the possible contact angle in this scenario, the molding solution was prepared according to Table 4-3.

Table 4-3: CA preparation mix ratio using OMC (per 50g of dry soils).

Soil ID		IA-BV	IA-CC	IA-PC	NC-AS	NH-HS	MnROAD
OMC (%)		27.60	19.00	17.50	18.50	10.70	14.10
Concentration	OS mass (g)	Amount of water (g)					
1:10	5	8.80	4.50	3.75	4.25	0.35	2.50
1:20	2.5	11.30	7.00	6.25	6.75	2.85	4.55
1:40	1.25	12.55	8.25	7.50	8.00	4.10	5.8
1:80	0.625	13.18	8.88	8.13	8.63	4.73	6.425
1:100	0.5	13.30	9.00	8.25	8.75	4.85	6.55
1:250	0.2	13.60	9.30	8.55	9.05	5.15	6.85

The second field method simulated spraying conditions by applying OS, diluted with water, onto the surface of untreated, compacted soil. The untreated soil compaction was done according to standard Proctor compaction (ASTM D698-12). This approach is aimed at replicating potential field concentrations and dilution ratios. Three different OS application rates were tested; 0.55, 0.33, and 0.22 liters/m^2—selected based on cost considerations and the need to limit additional moisture beyond the existing soil moisture content, as outlined in Table 4-4. Three different field conditions with varying moisture content were explored, which include immediate Spray at OMC, air, and oven-dried samples.

OS was sprayed on samples prepared at the optimum moisture content (OMC) to replicate conditions immediately after compaction. Also, samples were air-dried for 2 days to simulate natural drying conditions in the field, allowing moisture levels to decrease gradually. Then, to achieve extremely dry conditions, samples were oven-dried at 60°C for 24 hours, mimicking an environment with minimal residual moisture. These varying conditions allowed for assessing OS application effectiveness under different moisture scenarios, reflecting realistic field situations.

For spraying, a 473 cc (16 oz) Natural High-Density Polyethylene (HDPE) plastic spray bottle was used. After spraying, the treated samples were oven-dried at 60°C for 24 hours in an electric oven. After drying, the samples were carefully sectioned into various thicknesses (surface (0), 2, 4, 6, and 8 mm). Each section was then collected, oven-dried once more, and allowed to cool for 24 hours before undergoing contact angle testing using the previously described procedure. To handle values that could not be directly

measured, a contact angle of 20° was assigned for interpolation purposes. This approach ensured the data could be consistently analyzed across different sample thicknesses and OS concentrations.

Table 4-4: Sprayed OS mix ratio.

	Spray concentration (OS liters/m^2)		
	0.55	0.33	0.22
Water (g)	64.24	82.60	91.77
OS (g)	48.12	28.87	19.25

The liquid-to-soil ratio varied from 2:1, 0.5:1, and 0.25:1 (above and below the usual 1:1 typically used) using a batching approach described previously but with a mix ratio outlined in Table 4-5 to further explore the impact of the amount of water used in sample preparation. This was also done to understand if there is an appropriate ratio for the mixture to optimize OS applications. Attention was paid to just 1:10, 1:40, and 1:80, based on their performance from the Liquid to soil ratio of the 1:1 test, which indicated that both 1:10 and 1:40 were above 90^o, but 1:80 was marginally around 90^o.

Table 4-5: Mix ratio for varied Liquid impact on CA (per 50g of dry soils).

Soil ID	IA-BV, IA-CC, IA-PC, MnROAD, NH-HS, NC-AS			
Concentration	Liquid-to-soil ratio	2	0.5	0.25
1:10	OS(g)	5	5	5
	Water (g)	95	20	7.5
1:40	OS (g)	1.25	1.25	1.25
	Water (g)	98.75	23.75	11.25
1:80	OS (g)	0.63	0.63	0.63
	Water (g)	99.38	24.38	11.88

The soil mass used for each test was 50g.

After each sample preparation, CA test was done using the sessile drop technique (Bachmann et al. 2000) in which a drop of water was applied (using Geocomp FlowTrac II) to the soil surface and the angle formed at the intersection of the soil and water surfaces was measured. The reported apparent contact angle is an average value derived from at least three measurements (on both the left and right side of each sessile drop) using a goniometer (Ramehart Instruments, 260-U1) after Uduebor et al. (2023).

4.2.2 BP

BP was measured by determining the breakthrough volume achieved within a specified time frame. This study utilized a modified water ponding method following the studies of (Uduebor et al., 2023; Adeyanju et al., 2024a). Also, the breakthrough volume at the onset of water ponding pressure was calculated to be 0.0196 cc. Following the approach used in previous BP studies (Brooks et al., 2022; Keatts et al., 2018), the monitoring period was limited to 1 minute. Accordingly, a breakthrough volume of 0.02 cc within a 1-minute timeframe was employed as the reference point for BP measurement.

Two different sample preparations similar to possible field applications were observed. The first method involves using the molding solution (combined OS and water) at the soil OMC (as presented in Table 4-6) to compact the soil samples, simulating a compaction lift. After mixing, each batch was allowed to mellow for 16 hours before compaction in a Harvard mini mold (diameter of 33.02 mm and height of 71.12 mm) with a 9.1 kg (20-pound) spring-loaded piston. Each sample was compacted at five layers with 20 blows. High compaction energy was utilized for most samples as hydrophobicity is more efficient at high densification (Adeyanju et al., 2024a). The cylinder samples were allowed to stand for 1 hour before drying in an oven at 221^{O}F (105^{O}C) for 24 hours, as Adeyanju et al. (2024b) indicate that EWR samples are efficient at about 5% gravimetric moisture content, after which it was cooled for another 24 hours (in a chamber with calcium chloride as a desiccant) before testing.

Table 4-6: Mix design for all samples

Method	Sample designation	OMC (%)	Soil mass (g)	Water (g)	OS (g)	Molding moisture (OS + Water), g
Compacted lift	IA-PC10	17.50	100.00	7.50	10.00	17.50
	IA-PC40	17.50	100.00	15.00	2.50	17.50
	IA-PC80	17.50	100.00	16.25	1.25	17.50
	NC-AS10	18.50	100.00	8.50	10.00	18.50
	NC-AS40	18.50	100.00	16.00	2.50	18.50
	NC-AS80	18.50	100.00	17.25	1.25	18.50
	NH-HS10	10.70	100.00	0.70	10.00	10.70
	NH-HS40	10.70	100.00	8.20	2.50	10.70
	NH-HS80	10.70	100.00	9.45	1.25	10.70
	IA-CC10	19.00	100.00	9.00	10.00	19.00

	IA-CC40	19.00	100.00	16.50	2.50	19.00
	IA-CC80	19.00	100.00	17.75	1.25	19.00
	MnROAD10	14.10	100.00	4.10	10.00	14.10
	MnROAD40	14.10	100.00	11.6	2.50	14.10
	MnROAD80	14.10	100.00	12.85	1.25	14.10
	IA-BV10	27.60	100.00	17.60	10.00	27.60
	IA-BV40	27.60	100.00	25.10	2.50	27.60
	IA-BV80	27.60	100.00	26.35	1.25	27.60
Sprayed	IA-PC*	17.50	100.00	17.50	0.00	17.50
	NC-AS*	18.50	100.00	18.50	0.00	18.50
	NH-HS*	10.70	100.00	10.70	0.00	10.70
	IA-CC*	19.00	100.00	19.00	0.00	19.00
	MnROAD*	11.00	100.00	11.00	0.00	11.00
	IA-BV*	27.60	100.00	27.60	0.00	27.60

*Untreated soil

Untreated samples (no OS was added to the molding moisture) were prepared following Table 4-6 for the sprayed method. Compacted untreated samples were prepared and then oven-dried to optimize penetration depth. Then, each triplicate samples were sprayed with the spray concentration provided in table Table 4-4 (see Figure 4.2) using an HDPE plastic spray bottle and dried in an electric oven at 60^{o}C for 24 hours before testing.

a

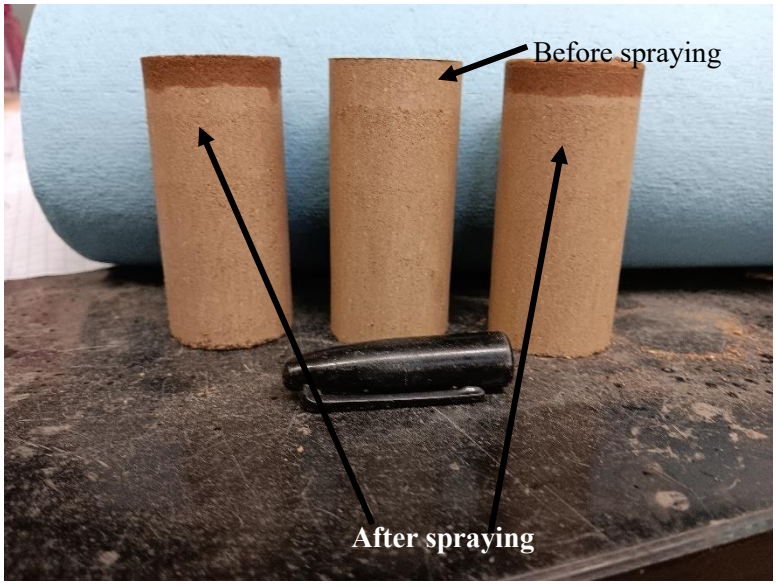

b

c

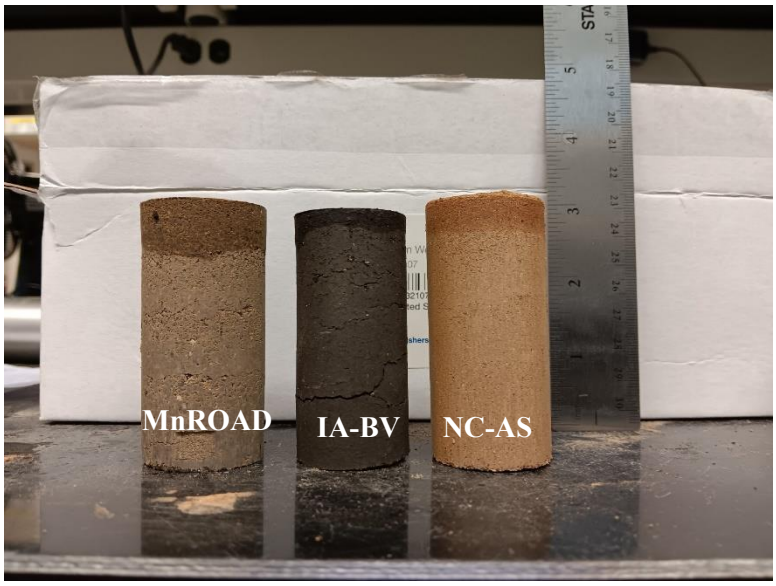

Figure 4.2: a) NC-AS during spraying showing penetration depth, b) after spraying, and c) MnROAD, IA-BV, and NC-AS after spraying.

4.3 Results and Discussions

4.3.1 Contact Angle

Figure 4.3a and Figure 4.3b illustrate the variation in contact angles (CA) resulting from liquid-to-soil ratios (1:1) and samples prepared at the optimum moisture content (OMC) of the soils. The contact angle gradually decreases as the OS concentration decreases, aligning with previous studies' findings (Lee et al., 2015; Uduebor et al., 2023). All soils, except MnROAD, exhibited contact angles above 90°, indicating hydrophobic behavior at an OS concentration of 1:40 or higher. Soils such as IA-PC and NC-AS

remained hydrophobic even at a 1:250 concentration. Although these two soils have different fines content (see Table 4-1), their high contact angles can be attributed to their mineralogical composition, rich in silica and aluminum oxide (Uduebor et al., 2023).

For all tested soils, there was a consistent and gradual reduction in CA as the amount of OS was reduced. However, no direct relationship between the amount of OS and CA was observed when the soil samples were prepared based on their respective OMC. Interestingly, half of the soils (NC-AS, NH-HS, and MnROAD) showed a slight initial increase in CA. In this subset, NC-AS had the highest OMC at 18.50%, while the other soils had OMC values equal to or below 14%. For instance, NH-HS, with an OMC of 10.7%, had only 0.35 grams of water available for mixing with 5 grams of OS, potentially leading to excess unbound OS within the soil from lack of sufficient water to achieve hydrolysis of the OS chemicals. This excess could slightly diminish the soil's hydrophobicity or indicate that lower concentrations are more effective in developing hydrophobic properties.

Regarding field applications, CA values for soils prepared at OMC tended to be consistent, with only minor differences across samples. Therefore, the results suggest that the CA will fall within a similar range, regardless of the sample preparation method used. Figure 4.4a-c shows minimal differences in CA values when comparing the liquid-to-soil ratio 1:1 with those prepared at OMC. A detailed analysis of OS-to-soil ratios of 1:10, 1:40, and 1:80 revealed that, regardless of the liquid-to-soil ratio, the resulting CA values were relatively similar.

A related study (Uduebor et al., 2023) examined the effects of different drying methods (air-drying and oven-drying) on three of the soils tested in this research (IA-PC, NC-AS, and NH-HS). It reported an STD of 14.5, 6.8, and 8.8, respectively. While this study used a concentration of 1:10 and a single liquid-to-soil ratio of 1:1, it helped determine whether the observed variability in results across concentrations fell within an acceptable range, considering other factors that could affect CA values. The standard deviation (STD) of the mean results in Figure 4.4d fell within an acceptable range (compared to), except for MnROAD at ratios of 1:40 and 1:80. Although there is no standardized range for STD, significant

deviations are commonly encountered in similar studies. For example, Saulick et al. (2017) reported STD values ranging from ±6 (Leelamanie and Karube, 2012; Koc and Bulut) to ±25 (Lourenço et al., 2015), even when different materials and methodologies were used.

Overall, the findings underscore those variations in OS concentration, preparation method, and soil type influence CA measurements, with certain trends emerging consistently across different conditions.

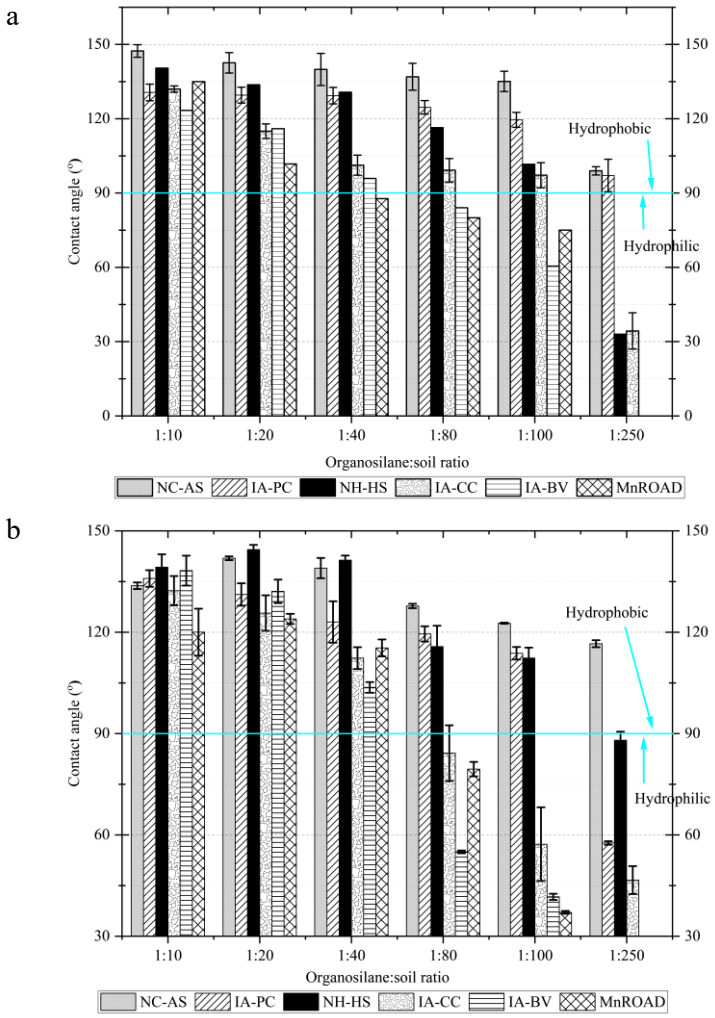

Figure 4.3: Hydrophilic modification to hydrophobic soil due to varying OS concentration done at a) liquid to soil (1:1) and b) OMC.

a

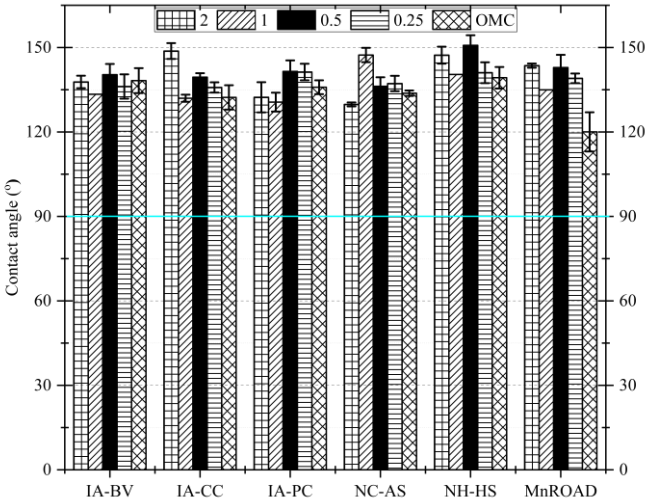
2
1
0.5
0.25
OMC
Contact angle (°)
0
30
60
90
120
150
IA-BV
IA-CC
IA-PC
NC-AS
NH-HS
MnROAD

b

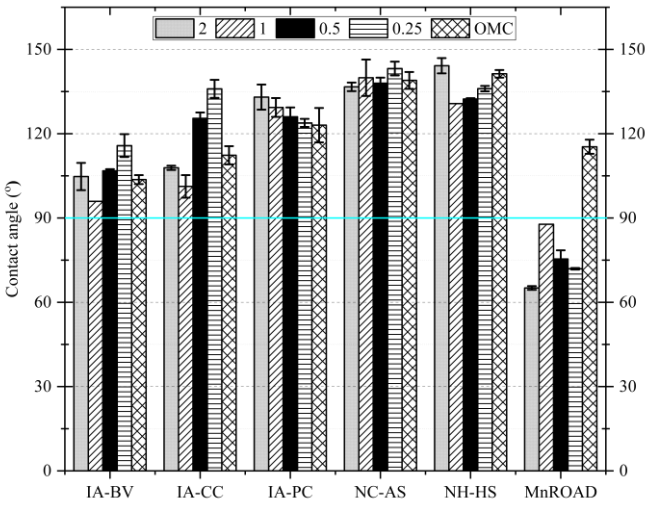
2
1
0.5
0.25
OMC
Contact angle (°)
0
30
60
90
120
150
IA-BV
IA-CC
IA-PC
NC-AS
NH-HS
MnROAD

c

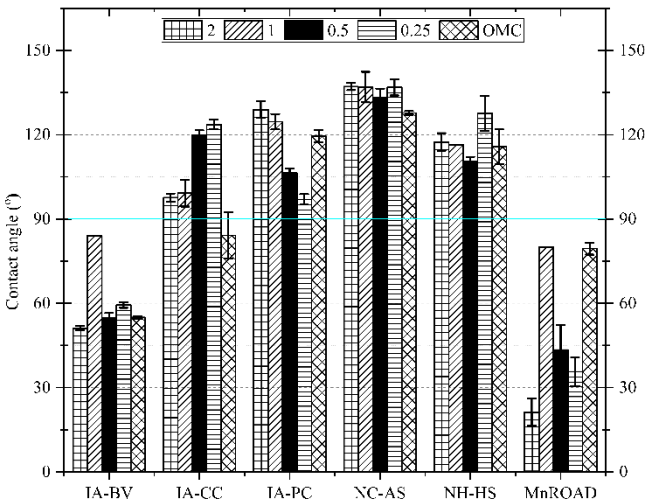
2
1
0.5
0.25
OMC
Contact angle (°)
0
30
60
90
120
150
IA-BV
IA-CC
IA-PC
NC-AS
NH-HS
MnROAD

d

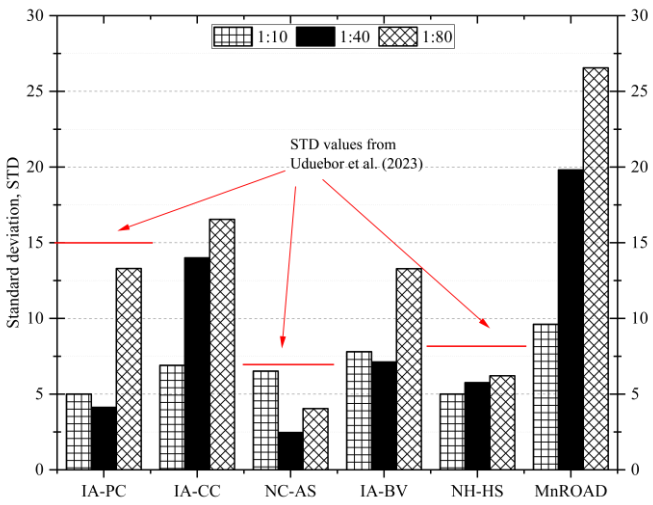

Figure 4.4: Change in contact angle with varying OS concentration and liquid ratio at concentration a) 1:10, b) 1:40, and c) 1:80, and d) showing the deviation of CA tests done at the different liquid-to-soil ratios.

Figure 4.5 illustrates the effects of varying OS concentrations (0.55, 0.33, and 0.22 OS liters/m²) and initial soil conditions (prepared at OMC, air-dried, and oven-dried) on contact angle and penetration depth. The results indicate that all sprayed surfaces exhibited hydrophobic characteristics, with contact angles ranging from 146° (NC-AS at 0.22 OS liters/m²) to 117° (MnRoad at 0.55 OS liters/m²). Soils with higher contact angles at a liquid-to-soil ratio of 1:1 (e.g., IA-PC, NH-HS, and NC-AS from Figure 4.3a) showed the best hydrophobicity at the surface. Although the OS solution visibly penetrated all soil types, the extent of penetration depended on the initial soil condition and inherent soil properties, such as fines content. For soils prepared at OMC, the penetration depth for all concentrations was typically less than 2 mm, except for NC-AS across all concentrations (average depth of 3 mm). NH-HS sprayed with 0.55 OS liters/m², and MnRoad at 0.22 OS liters/m² reached an average depth of 3 mm, as shown in Figure 4.6. This scenario is unlikely in actual field conditions, as spraying would not typically occur after the soil reaches OMC due to workability constraints and the need to maintain density and modulus.

The findings suggest that the drier the soil, the better the penetration of the OS treatment. When air-dried and oven-dried conditions were used, the average penetration depth increased to 4.2 mm and 4.7 mm, respectively, compared to 1.6 mm for soils at OMC. Among the soils tested, MnRoad, NH-HS, and NC-AS showed the greatest penetration depth, reaching 7 mm, 7 mm, and 8.5 mm, respectively. The overall

average penetration depth was 3.5 mm, with a standard deviation of 2.1 mm, indicating that the first 3.5 mm exhibited hydrophobic behavior for most samples. Regarding the effect of OS concentration, lower concentrations (0.22 OS liters/m²) resulted in better contact angle values with depth, likely due to increased water dilution and ease to coat soil particles as the liquid penetrates the soil samples. The penetration depths for the three concentrations were as follows: 3.1 mm for 0.55 OS liters/m², 3.69 mm for 0.33 OS liters/m², and 3.66 mm for 0.22 OS liters/m², with standard deviations of 1.6, 2.5, and 2.1 mm, respectively. This study assumes that deeper depth of hydrophobic layer within the soil improves the resistance to water infiltration.

Based on these findings, an assumed target penetration depth of 3.5 mm and the selected OS application rates of 0.55, 0.33, and 0.22 OS liters/m², the equivalent OS to soil mix (in the Laboratory using liquid to soil ratio of 1, Figure 4.3a) was linearly interpolated and listed in Table 4-7. The linear interpolation was performed to determine the equivalent liquid-to-soil ratio achieved through spraying, enabling a clearer understanding of the relationship between field and laboratory conditions.

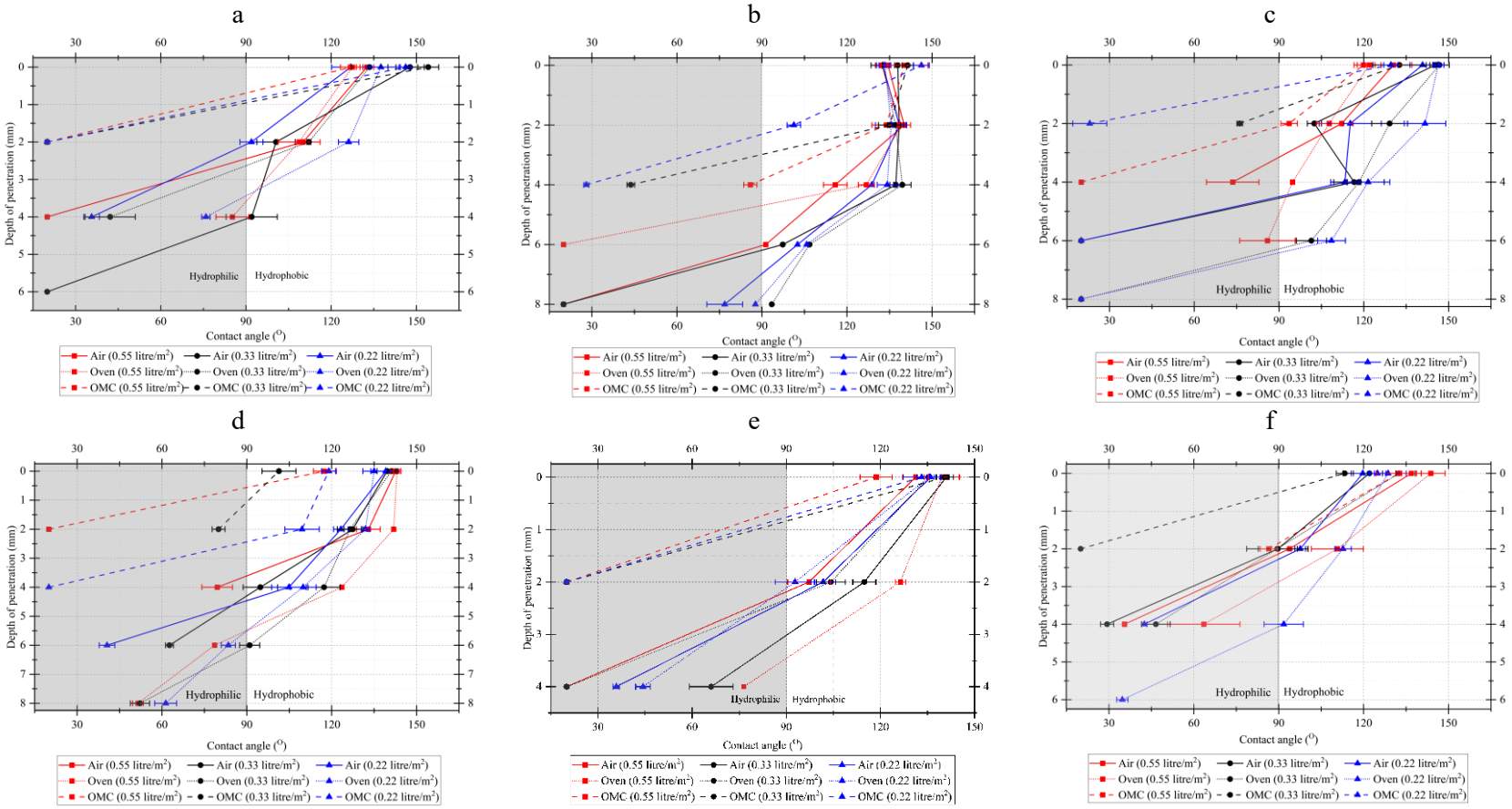

Figure 4.5: Change in contact angle with depth a) IA-PC, b) NC-AS, c) NH-HS, d) MnROAD, e) IA-BV, and f) IA-CC.

Table 4-7: OS to soil equivalence to contact angle (liquid to soil ratio, 1:1) at a depth of 3.5 mm.

Concentration	Soil ID	NC-AS	IA-BV	IA-CC	MnROAD	NH-HS	IA-PC
0.55 OS liter/m^2	Actual CA	129.90	88.97	75.31	128.17	98.03	91.06
	Equivalent OS to soil	121.46	63.41	152.22	12.04	107.89	290.24
0.33 OS liter/m^2	Actual CA	138.91	61.00	57.29	119.62	121.00	59.66
	Equivalent OS to soil	53.36	99.59	195.22	14.62	67.15	499.97
0.22 OS liter/m$^{2`}$	Actual CA	134.50	56.40	96.99	115.41	126.56	88.45
	Equivalent OS to soil	102.36	110.21	100.49	15.89	51.62	307.68

These contact angle values were obtained from linear interpolating Figure 4.5 and correlated with Figure 4.3A to obtain the liquid-to-soil ratio.

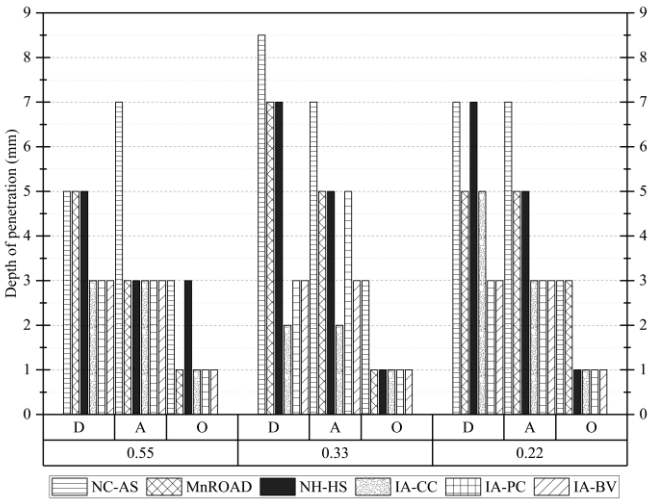

Figure 4.6: Average penetration depth across all soil at different conditions (where d=Oven dried, A= air dried, and O= at OMC).

While contact angle indicates hydrophobicity, it does not state or indicate the field performance of hydrophobicity. CA is one of the factors alongside soil texture, fines content, moisture content, and soil porosity. A BP test is carried out to understand the water resistance and simulate the two field scenarios.

4.3.2 BP

Figure 4.7 presents BP values for various soil types compacted in lifts, ranging from silty and clayey sands to fat clays, tested at different organosilane (OS) concentrations. While all samples were compacted using the same compaction energy, each soil exhibited distinct characteristics in terms of maximum dry density (MDD), optimum moisture content (OMC), fines content, and mineralogy, which significantly influenced their BP performance. The results demonstrate considerable variability among the soils.

Regarding OS concentration, the molding moisture was adjusted based on the OMC of each soil, with OS accounting for a specific percentage of the total molding moisture. For example, in NH-HS-10, OS comprised 93% of the molding moisture, corresponding to a contact angle of 138° and a BP of 14 kPa. However, NH-HS-40 achieved a higher BP (20 kPa) despite OS only accounting for 23% of the molding moisture, as listed in Table 4-8. This suggests that while higher OS concentrations improve water repellency, there is no simple linear correlation to OS concentration and BP. Furthermore, NH-HS-80, with only 11.68% OS, still exhibited a higher BP of 18 kPa than NH-HS-10, indicating that a critical balance between OS concentration and soil characteristics (such as pore structure and compaction) is key in determining water repellency.

The relationship between contact angle (CA) and BP is complex. While both are indicators of water repellency, their relationship is not necessarily linear (Feyyisa et al., 2019). The contact angle measures surface energy, but BP reflects actual resistance to water penetration through the soil's pore structure (Lee et al., 2015). For instance, the pressure exerted during infiltration can affect the fluid's curvature, thus altering the CA in ways that are difficult to measure directly. The CA measured on a flat surface may not fully represent the conditions within the soil matrix under pressure. This makes BP a more comprehensive metric for evaluating the water resistance of compacted soils.

Regarding MDD, NH-HS-10 had the highest MDD at 19.40 kN/m³, while IA-BV-10 had the lowest at 13.50 kN/m³. Generally, higher MDD values correspond to fewer voids and better compaction, improving the soil's resistance to water infiltration. This was evident in the NH-HS samples, which performed well across various OS concentrations. Despite having higher sand content, NH-HS maintained good surface energy and achieved high BP values, even at lower OS concentrations. This highlights the importance of fine-tuning the soil's pore structure to enhance water resistance. Conversely, IA-BV, despite having the lowest MDD, exhibited strong BP performance due to its high fines content, which likely resulted in tighter particle packing within the soil matrix. This packing provided better resistance to water flow, even though

OS only accounted for 36.23% of the molding moisture. IA-BV also had the highest OMC, offering better lubrication during compaction, which may have contributed to its performance at a 1:10 concentration.

The effect of fines content on BP is not uniform across all samples. For example, IA-CC-40 underperformed, achieving a BP of just 3.4 kPa with a contact angle of 112°, despite its high fines content (67.60%) and moderate MDD (16 kN/m³). The lower-than-expected performance may be due to reduced density and efficient pore connectivity in this sample. Conversely, IA-CC-10 performed better at a higher OS concentration, with a contact angle of 132°, likely due to a more compacted structure that reduced pore connectivity and enhanced water resistance. Interestingly, IA-PC and IA-BV, both with high fines content, exhibited lower BP values in specific scenarios, suggesting that other factors, such as soil mineralogy and pore structure, play significant roles in determining water resistance.

The analysis indicates no significant improvement in BP when OS concentration is increased from 1:80 to 1:10, except in specific cases. For instance, NH-HS maintained high BP values even at lower OS concentrations, underscoring the importance of adequate compaction and less pore networks. Soils with higher untreated MDD, such as NH-HS, generally exhibited higher BP due to their reduced void ratios. However, the relationship between BP and factors like fines content, soil mineralogy, and OS concentration (untreated organosilane) is multifaceted. Therefore, BP is influenced by a combination of factors, including surface energy (indicated by contact angle), soil porosity, compaction characteristics (molding moisture and void distribution), and soil mineralogy. While the contact angle provides insights into surface repellency, BP offers a more comprehensive understanding of how soils behave under real-world wetting conditions. The results suggest that optimizing soil structure/fabrics (to hinder flow) and targeted OS concentration are crucial for enhancing water repellency.

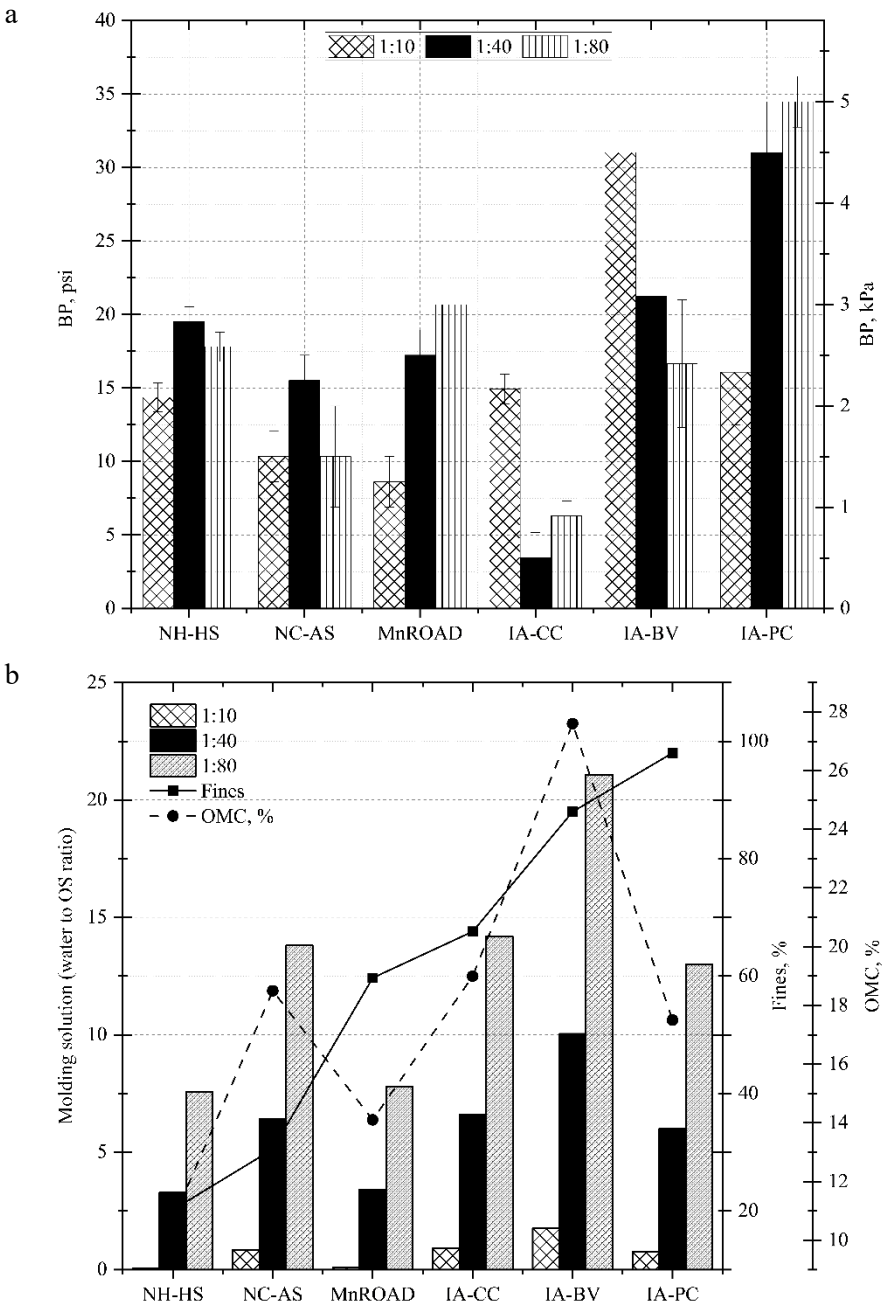

Figure 4.7: a) BP values of different soils ranging from Silty, clayey sand to Fat clay. (same compaction energy). b) relation of different properties such fines, molding solution affecting the BP result.

Table 4-8: Relationship between soil, water, and OS.

Sample Name	Contact angle	Treatment					
	Mean	OS mass (g)	OS to Soil ratio	Water to chemical ratio	OS percent in molding Solution (%)	Water to Soil Ratio	Total solution mass(g)
NC-AS-10	133.76	9	0.1	0.85	54.05	0.085	16.65
IA-CC-10	132.28	9	0.1	0.9	52.63	0.09	17.1
MnROAD-10	120.03	9	0.1	0.41	70.92	0.01	9.9
NH-HS-10	139.26	9	0.1	0.07	93.46	0.007	9.63
IA-PC-10	135.9	9	0.1	0.75	57.14	0.075	15.75
IA-BV-10	138.24	9	0.1	1.76	36.23	0.176	24.84
NC-AS-40	138.98	2.25	0.025	6.4	13.51	0.16	16.65
IA-CC-40	112.34	2.25	0.025	6.6	13.16	0.165	17.1
MnROAD-40	115.36	2.25	0.025	4.64	17.73	0.085	9.9
NH-HS-40	141.32	2.25	0.025	3.28	23.36	0.082	9.63
IA-PC-40	123.04	2.25	0.025	6	14.29	0.15	15.75
IA-BV-40	103.66	2.25	0.025	10.04	9.06	0.251	24.84
NC-AS-80	127.76	1.13	0.0125	13.8	6.76	0.1725	16.65
IA-CC-80	84.2	1.13	0.0125	14.2	6.58	0.1775	17.1
MnROAD-80	79.47	1.13	0.0125	10.28	8.87	0.0975	9.9
NH-HS-80	115.75	1.13	0.0125	7.56	11.68	0.0945	9.63
IA-PC-80	119.49	1.13	0.0125	13	7.14	0.1625	15.75
IA-BV-80	54.98	1.13	0.0125	21.08	4.53	0.2635	24.84

Figure 4.8a presents the BP results for different OS concentrations applied through spraying. The findings indicate that the highest sprayed concentration, 0.55 OS liters/m², with an average penetration depth of 4 mm, provided the best water resistance for MnROAD and NC-AS. This was followed by the 0.33 OS liters/m² concentration, which showed effective water resistance but slightly less. In contrast, the low BP values observed for IA-BV were attributed to the soil's properties, which caused significant volume shrinkage and cracking. This behavior increased pore sizes, reducing the soil's ability to resist water infiltration. As depicted in Figure 4.8b, these structural changes in the soil underscore the limitations associated with specific soil types.

The spray method does have two significant drawbacks. First, only a limited molding solution (OS + water) can be applied at a time, or the soil must be dried out before spraying can continue. For example, during field trials at the MnROAD facility, the application was limited to 227 liters of molding solution for a test section measuring 7.5 m by 23 m. This limitation restricts the amount of OS that can be used effectively. Second, the average depth of OS penetration with the spray method was about 3.5 mm (with a standard deviation of 2.1 mm). Compared to compacted samples, which typically have greater depths of water-resistant layers (approximately 70 mm), the sprayed layers are much thinner and the OS solution may not be effectively distributed across the surface.

As shown in Figure 4.8c, the average water inflow through the BP testing for sprayed samples was 6.65, 16.74, and 6.67 cc for MnROAD, NC-AS, and IA-BV, respectively. In compacted samples, water infiltration is impeded at multiple levels throughout the thicker hydrophobic layer, whereas sprayed applications provide a relatively shallow barrier, as shown in Figure 4.8d. The compacted section had lower water infiltration. This difference in penetration depth and layer thickness results in compacted samples generally exhibiting superior water resistance. Overall, while the spray method effectively creates a hydrophobic layer, its solution volume and penetration depth limitations must be considered when selecting treatment approaches for field applications.

a

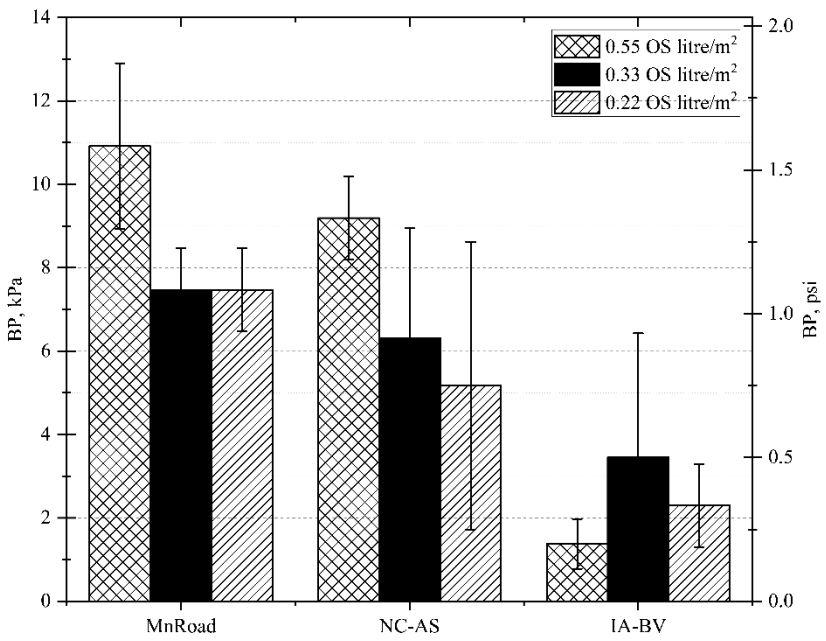

b

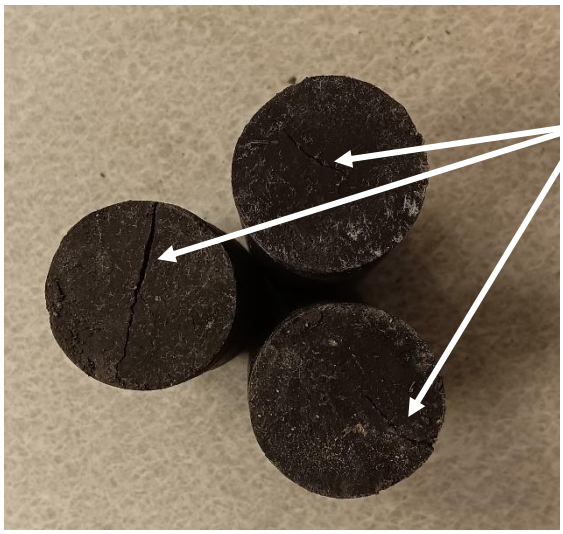

Cracks formed after oven drying untreated IA-BV samples.

c

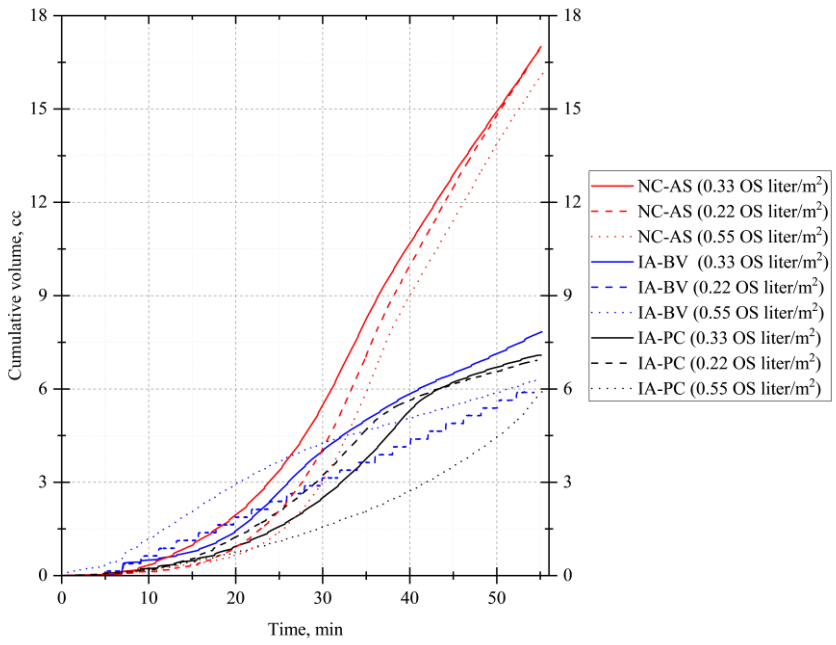

d

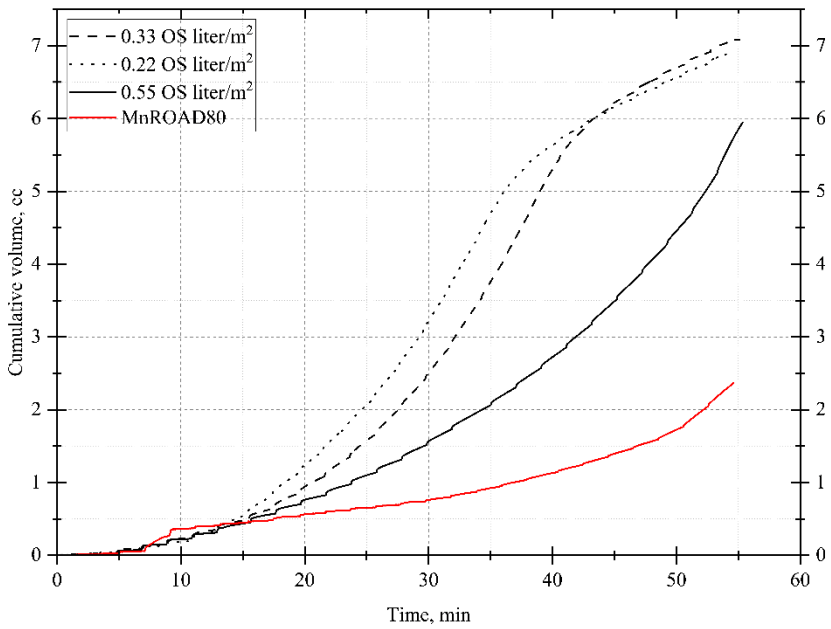

Figure 4.8: The BP result from the simulated sprayed application of OS, b) large cracks on IA-BV, after oven drying c) the cumulative water intake during BP of OS sprayed soils, and d) the cumulative water intake of sprayed and compacted EWR soil.

4.3.3 Field Application

BP is currently the most effective method for assessing hydrophobicity because it simulates the water pressures expected in field conditions. For example, at the MnROAD facility, where the EWR technique is applied (Figure 4.9a), the high-water table depth is 1.87 m as illustrated in Figure 4.9b. A physics-based model was used to determine the optimal placement depth for the EWR, 1.2 m from the road surface. In this scenario, the EWR layer must resist water pressure equivalent to 1.15 m to account for worst-case conditions (Figure 4.9c). Figure 4.8a shows that the MnROAD sample treated with 0.55 OS liters/m² has a water resistance corresponding to BP values of 11 to 13 kPa, translating to a water pressure resistance of approximately 1.12 to 1.33 m. This makes the 0.55 OS liter/m^2 treatment suitable for the site requirements. Additionally, EWR placements at depths of 1.1 m and 0.9 m provide a safety factor, ensuring that the barrier can withstand variations in water table levels. Thus, BP testing measures the hydrophobicity of treated soils and provides valuable insights into the suitability and placement depth of hydrophobic treatments in the field, enhancing the reliability and effectiveness of water infiltration control strategies.

a

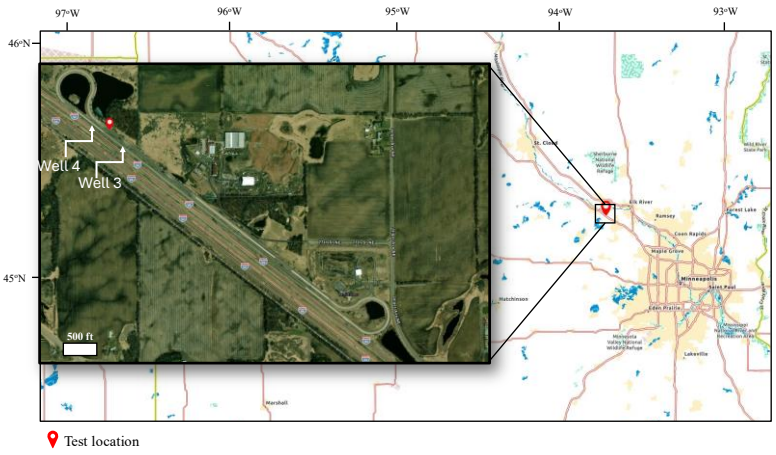

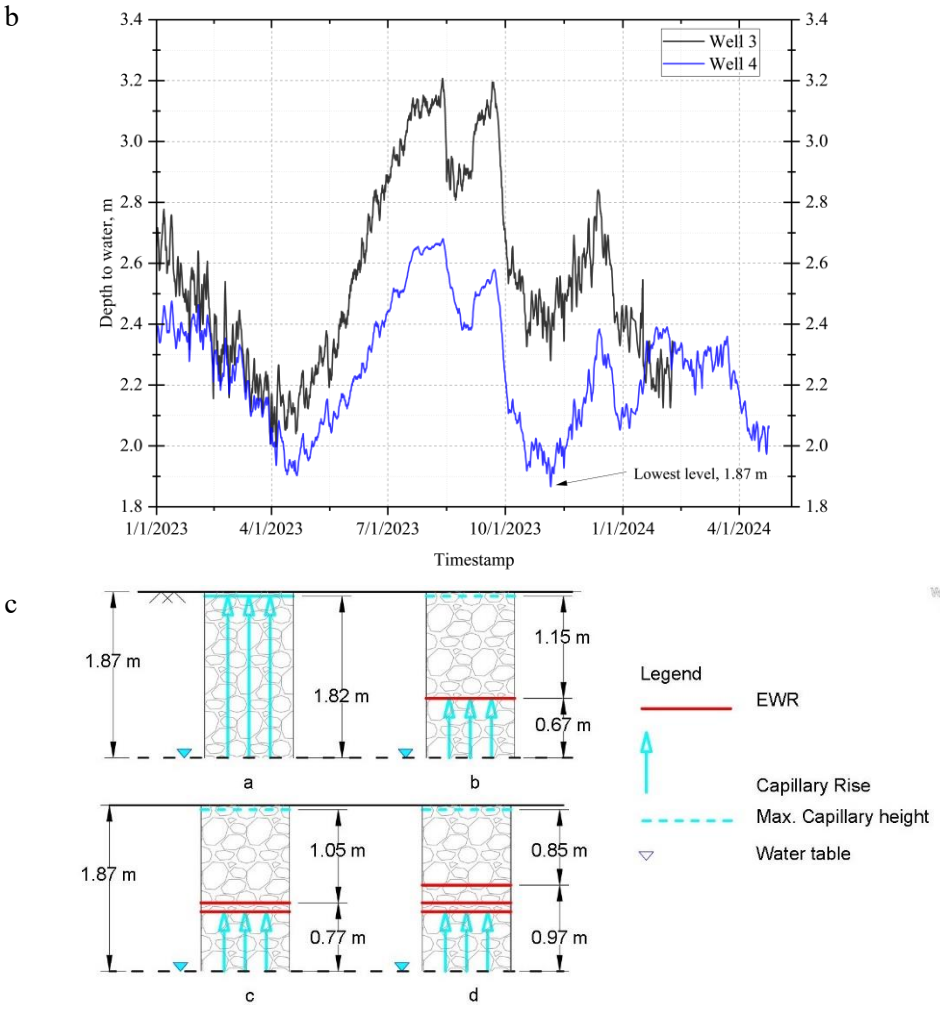

Figure 4.9: a) Test site location at MnROAD, b) The water table level at MnROAD at wells 3 and 4, near the test site, and c) the field application of BP result.

4.4 Conclusion

This study provides insights into optimizing organosilane (OS) applications for hydrophobic soil treatment under various field conditions. Contact angle (CA) and breakthrough testing across different OS concentrations, soil types, and preparation methods revealed significant findings:

- Contact angle and hydrophobicity: The results indicated that most soils achieved hydrophobicity (CA > 90°) at OS concentrations of 1:40 and higher. For example, IA-PC and NC-AS maintained CA values above 90° even at a 1:250 concentration due to their mineralogical composition, including high silica and aluminum oxide content. The highest CA observed was 146° for NC-AS

at 0.22 OS liters/m², while MnRoad showed a lower CA of 117° at 0.55 OS liters/m², reflecting variations in hydrophobicity based on soil properties.

- Penetration depth: The OS treatment's penetration depth varied with the soil's initial moisture condition. Soils prepared at optimum moisture content (OMC) showed limited penetration, with depths generally less than 2 mm. In contrast, air-dried and oven-dried samples exhibited increased penetration depths, averaging 4.2 mm and 4.7 mm, respectively. The maximum penetration depth recorded was 8.5 mm for NC-AS under oven-dried conditions. The average penetration depth across all conditions was 3.5 mm, with a standard deviation of 2.1 mm.
- BP: BP testing demonstrated that higher OS concentrations (0.55 liters/m²) provided superior water resistance. For MnROAD and NC-AS, the BP values ranged from 11 to 13 kPa, equivalent to water pressure resistance of 1.12 to 1.33 meters. In contrast, IA-BV exhibited lower BP values due to significant soil shrinkage and cracking, leading to increased pore sizes and reduced resistance to water infiltration.
- Limitations of spraying methods: The average penetration depth for sprayed applications was limited to approximately 3.5 mm, compared to 70 mm for compacted samples. Additionally, the maximum volume of OS solution applied during field trials was restricted to 227 liters for a 7.5 m by 23 m test section, limiting the achievable depth of hydrophobicity.

The study concludes that achieving optimal hydrophobic performance in field applications requires careful consideration of OS concentration, soil moisture content, and application method. While laboratory tests offer a baseline understanding, real-world conditions necessitate adjustments to enhance OS penetration and water resistance.

4.5 Acknowledgment

The author gratefully acknowledge the funding support from Iowa Highway Research Board (TR-783) and National Science Foundation (Award #1928813 and #1947009).

4.6 Reference

Adeyanju, E. D., Uduebor, M. A., Saulick, Y., Daniels, J. L., & Cetin, B. (2024). Influence of Density on Engineered Water Repellent Soil. In *International Conference on Transportation and Development 2024* (pp. 152-161).

ASTM D4318-00 (2000), "Standard Test Methods for Liquid Limit, Plastic Limit, and Plasticity Index of Soils.," ASTM International, West Conshohocken, PA., 2017.

ASTM International, " ASTM D7928-17: Standard Test Method for Particle-Size Distribution (Gradation) of Fine-Grained Soils Using the Sedimentation (Hydrometer) Analysis," ASTM International, 2017.

ASTM D698, (2012). Standard Test Methods for Laboratory Compaction Characteristics of Soil Using Standard Effort. ASTM International, West Conshohocken, PA.

ASTM D854-10 (2006), "Standard Test Methods for Specific Gravity of Soil Solids by Water Pycnometer.," ASTM International, West Conshohocken, PA., 2014.

ASTM D2166, "Standard Test Methods for Laboratory Compaction Characteristics of Soil Using Standard Effort.," ASTM International, West Conshohocken, PA., 2012.

ASTM D559 (American Society for Testing and Materials). (2003). Standard test methods for wetting and drying compacted soil-cement mixtures. Conshohocken, PA.

ASTM D870-15 (American Society for Testing and Materials). (2015). Standard Practice for Testing Water Resistance of Coatings Using Water Immersion.

ASTM D2487-17 (2017), "Standard Practice for Classification of Soils for Engineering Purposes (Unified Soil Classification System)," ASTM International.

Bachmann, J., Ellies, A., & Hartge, K. H. (2000). Development and application of a new sessile drop contact angle method to assess soil water repellency. Journal of Hydrology, 231, 66–75. doi:10.1016/s0022-1694(00)00184-0.

Brooks, T.Y., Daniels, J.L., Uduebor, M., Cetin B., N., M.W. (2022). “Engineered Water Repellency for Mitigating Frost Action in Iowa Soils.” Geo-Congress 2022: Soil Improvement, Geosynthetics, and Innovative Geomaterials.

Daniels, J. L., Hourani, M. S., & Harper, L. S. (2009, May). Organo-silane chemistry: A water repellent technology for coal ash and soils. In *Proceedings* (pp. 4-7). Lexington, KY, USA: 2009 World of Coal Ash (WOCA) Conference.

Daniels. J., Mehta, P., Vaden, M., Sweem, D., Mason, M.D., Zavareh, D.M., Ogunro, V. (2009). “Nano-scale organo-silane applications in geotechnical and geoenvironmental engineering.” J. Terraspace Sci. Eng. 1(1), 21–30

Doerr, S. H. (1998). On standardizing the ‘water drop penetration time’ and the ‘molarity of an ethanol droplet’techniques to classify soil hydrophobicity: a case study using medium textured soils. Earth Surface Processes and Landforms: The Journal of the British Geomorphological Group, 23(7), 663–668. https://doi.org/10.1002/ (SICI)1096-9837(199807)23:73.0.CO;2-6.

Feyyisa, J. L., Daniels, J. L., & Pando, M. A. (2017). Contact angle measurements for use in specifying organosilane-modified coal combustion fly ash. *Journal of materials in civil engineering*, *29*(9), 04017096.

Feyyisa, J. L., Daniels, J. L., Pando, M. A., & Ogunro, V. O. (2019). Relationship between breakthrough pressure and contact angle for organo-silane treated coal fly ash. *Environmental technology & innovation*, *14*, 100332.

Keatts, M. I., Daniels, J. L., Langley, W. G., Pando, M. A., & Ogunro, V. O. (2018). Apparent contact angle and water entry head measurements for organo-silane modified sand and coal fly ash. *Journal of Geotechnical and Geoenvironmental Engineering*, *144*(6), 04018030.

Koc, M., and R. Bulut. 2014. Assessment of a sessile drop device and a new testing approach measuring contact angles on aggregates and asphalt binders. J. Mater. Civ. Eng. 26:391–398. doi:10.1061/(ASCE)MT.1943- 5533.0000852

Lee, C., Yang, H.-J., Yun, T. S., Choi, Y., and Yang, S. (2015). “Water-Entry Pressure andFriction Angle in an Artificially Synthesized Water-Repellent Silty Soil.” Vadose ZoneJournal, 14(4).

Li, X., Fan, X., & Brandani, S. (2014). Difference in pore contact angle and the contact angle measured on a flat surface and in an open space. *Chemical engineering science*, *117*, 137-145.

Leelamanie, D.A.L., and J. Karube. 2012. Drop size dependence of soil-water contact angle in relation to the droplet geometry and line tension. Soil Sci. Plant Nutr. 58:675–683. doi:10.1080/00380768.2012.745798

Leelamanie, D. A. L., Karube, J., & Yoshida, A. (2008). Characterizing water repellency indices: Contact angle and water drop penetration time of hydrophobized sand. Soil Science & Plant Nutrition, 54(2), 179-187. https://doi.org/10.1111/j.1747-0765.2007.00232.x.

Lourenço, S. D., Saulick, Y., Shuang, Z., Xing, X., Hongjie, L., Hongwei, Y., ... & Rui, Q. (2021). Hydrophobized Granular Materials for Ground Infrastructure. Materials with Extreme Wetting Properties: Methods and Emerging Industrial Applications, 153-177.

Lourenço, S., S. Woche, J. Bachmann, and Y. Saulick. 2015b. Wettability of crushed air-dried minerals. Géotech. Letters 5:173–177. doi:10.1680/ jgele.15.00075

McHale, G., Newton, M. I., & Shirtcliffe, N. J. (2005). Water-repellent soil and its relationship to granularity, surface roughness, and hydrophobicity: a materials science view. European Journal of Soil Science, 56(4), 445–452. https://doi.org/10.1111/j.1365-2389.2004.00683.x

Saulick, Y., Lourenço, S. D. N., & Baudet, B. A. (2017). A semi-automated technique for repeatable and reproducible contact angle measurements in granular materials using the sessile drop method. *Soil Science Society of America Journal*, *81*(2), 241-249.

Saulick, Y. (2018). Synthesized water-repellent granular solids. HKU Theses Online (HKUTO).

Uduebor, M., Daniels, J., Naqvi, M. W., & Cetin, B. (2022b). Engineered Water Repellency in Frost Susceptible Soils. In *Geo-Congress 2022* (pp. 457-466).

Uduebor, M., Adeyanju, E., Saulick, Y., Daniels, J., & Cetin, B. (2022a). A review of innovative frost heave mitigation techniques for road pavements. In *International Conference on Transportation and Development 2022* (pp. 95-106).

Uduebor, M., Daniels, J., Saulick, Y., Naqvi, W., & Cetin, B. (2023). Optimization of water repellency in soils for geotechnical applications. *International Journal of Geotechnical Engineering*, 1-11.

Wang, Z., Wu, L., & Wu, Q. J. (2000). Water-entry value as an alternative indicator of soil water-repellency and wettability. *Journal of Hydrology*, *231*, 76-83.

Yuan, Y., & Lee, T. R. (2013). Contact angle and wetting properties. In *Surface science techniques* (pp. 3-34). Berlin, Heidelberg: Springer Berlin Heidelberg.

Zhou, Z., Kwan Leung, A., Akbar Karimzadeh, A., Hei Lau, C., and Li, K.W. 2021. Infiltration through an artificially hydrophobized silica sand barrier. Journal of Geotechnical and Geoenvironmental Engineering, 147(6): 06021006. doi:10.1061/(ASCE)GT.1943-5606.0002543.

DESIGN AND CONSTRUCTION OF ENGINEERED WATER REPELLENCY (EWR) AT MNROAD

Abstract

This study highlights mitigating frost action through Engineered Water Repellency (EWR) in which large deformations are reduced in frost susceptible soils by preventing water migration toward a growing ice lens in response to matric and osmotic potentials generated within them. Using a framework, a physics-based model was utilized to explore the sensitivity and determine the EWR placement depth (between the frost depth and water table) for the treatment. Contact Angle (CA) tests were carried out to determine the optimal dosage required for the soil. Two field test sections were constructed and instrumented at the low-volume MnROAD facility, Otsego MN, where a commercially available organosilane was sprayed at three different depths at predetermined rates. These test cells were instrumented to monitor various parameters, including volumetric water content, temperature, matric suction, frost heave-thaw settlement, and pavement quality. The preliminary result indicates that the soil lift between the two spray treatments had a relatively constant volumetric water content, indicating restricted moisture migration. Measurable heave was observed in the control section, while the treated section experienced settlement. Moisture sensors in the control section indicated full saturation, while there were variations in the results from the treated section. The study presents a methodology for EWR utilization as an engineering solution in moisture migration mitigation within pavement alongside relevant field performance assessment.

Keywords: Engineered Water Repellency (EWR), Hydrophobicity, Frost action.

4.7 Introduction

Results from the American Association of State Highway Official (AASHO) road test indicate that 60 % of pavement failure occurs during the spring season (White & Coree, 1990). This failure results from large deformations occurring in frost susceptible soils under subfreezing temperatures with the presence of a continuous water source (Oman et al., 2018). This damage is exacerbated due to alternating cycles of frost heaving and the subsequent thawing, which results in continuous seasonal variation of subgrade and base course modulus (Richter, 2006; Papuc, 2021). A study by St-Laurent and M. Roy (1995) noticed that the "loss of stiffness relative to summer modulus is equal to 36, 30, and 54 percent for the granular base, subbase, and subgrade soil, respectively" and "takes over approximately three months for the base, four months for the subbase and nearly five months for the clay subgrade" to recover to their original (summer) value.

Frost action is a significant problem because it is rarely uniform, leading to uneven deformation across a given section. Differential frost heaving is attributable to causes such as instability of the one-dimensional freezing process, variability in the frost susceptibility of the soil and temperature, moisture availability, and surface topography (Dore & Zubeck, 2009; Peterson & Krantz, 2003). To extend pavement life and reduce maintenance costs, different counties and Department of Transportation (DOTs) utilize spring load restrictions of up to 50 %, among other mitigation methods, which extend the useful life of asphalt roads up to 95 % (Isotalo, 1993; Ovik et al., 2000; Kestler et al., 2007) but impose significant economic costs on road users. Sixteen states in the US and eight provinces in Canada utilize varying degrees of load restrictions, as displayed in Figure 4.10.

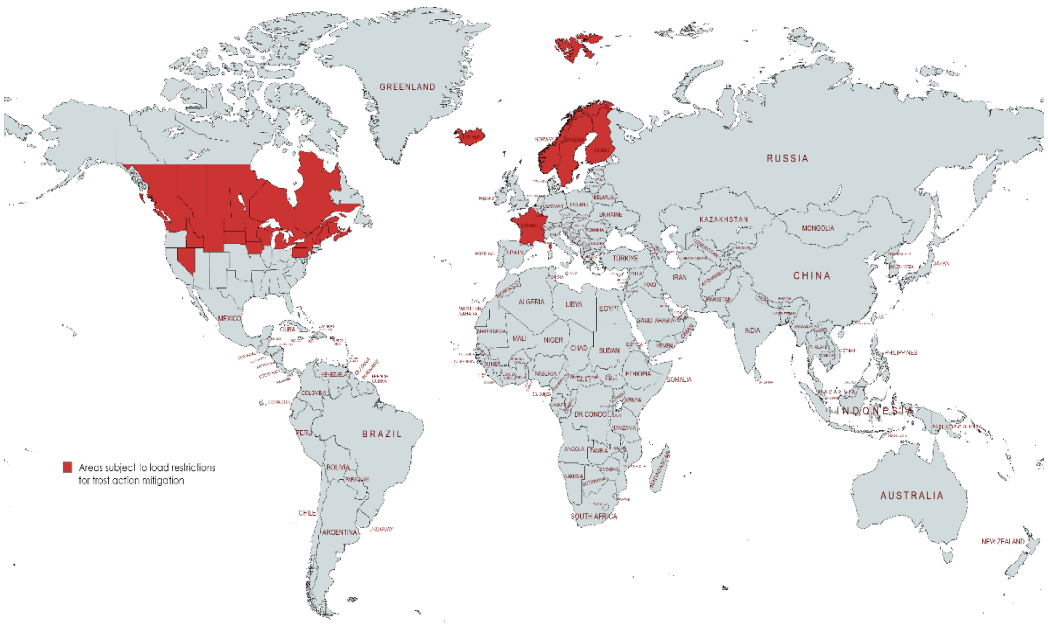

Figure 4.10: Areas subject to load restrictions for frost action mitigation.

Some frost action mitigation approaches utilize non-frost-susceptible materials (e.g., via "cut and replace") within or up to the expected frost depth, combined with a high-strength, open-graded granular layer that can withstand thaw-weakened periods and traffic loading (Christopher *et al., 2006; Uduebor et al., 2022*). The U.S. Army Corps of Engineers (USACE) recommends non-frost-susceptible materials for flexible pavements in the top 50% of the granular unbound base. In contrast, frost susceptible soil (FSS) should be replaced with non-FSS equal to the slab thickness in rigid pavement (*USACE, 1973*). The American Association of State Highway and Transportation Officials (AASHTO) 1993 guide recommends replacing FSS with one-half or more of the frost depth. These methods involve substantial quantities of non-FSS material, usually sandy or granular, leading to energy-intensive processes, heavy machinery, construction time, labor, and emissions.

An alternative approach explored in this study involves making the subgrade or subbase materials unaffected by moisture variation through Engineered Water Repellency (EWR). EWR involves making the existing hydrophilic in-situ FSS become hydrophobic using organosilanes (OS). This silica-based organic coupling agent permanently modifies the soil surface without any bonding properties (Daniels & Hourani, 2009; Daniel, 2020). Hydrophobic soil cannot absorb water or allow water to flow through it without

applying a high positive hydrostatic head, in part because the hydroxyl (-OH) surface groups are otherwise readily available in the soil (i.e., to absorb water) are replaced by Alkyl Siloxane (Meeravali et al., 2020). EWR provides resistance to moisture absorption or movement (Mahedi et al., 2020; Uduebor et al., 2022) to mitigate ice lens growth as water supply is hindered.

Part of moving a given geotechnical engineering innovation up the technology readiness pathway involves field-scale testing. This study describes the design, construction, and instrumentation of pilot test cells using water-repellent treatments on subgrade soils of a flexible pavement at MnROAD. The focus of the intervention was to evaluate the extent to which EWR treatment in mitigating freeze-thaw-related damages. Distinct concentrations of OS at varying placement depths were employed to investigate their effects on cost-effectiveness, long-term durability, and performance. These test cells underwent extensive instrumentation to monitor volumetric water content, electrical conductivity, matric potential, temperature, settlement or heaving, groundwater fluctuations, various weather parameters, and comprehensive pre- and post-construction mechanical strength field tests.

However, the practical implementation of EWR is subject to construction constraints and economic limitations. As such, a resource-conscious approach is required to ensure that the advantages of EWR are maximized while considering financial considerations. EWR presents a promising approach for frost action mitigation, but it is crucial to develop an optimal place depth approach to fully harness its benefits and strike a balance with limited resources and constructability. The ideal depth for EWR application typically falls within two key zones: either at the frost depth or within the zone between the frost depth and the water table or capillary zone. These depths are strategically designed to address frost-related issues effectively by curtailing water flow to regions where it can feed ice lenes. A physics-based model was employed to determine the optimum EWR placement depth to simulate various scenarios.

The overall objective of this study is to evaluate the extent to which EWR can prevent water from migrating upward from groundwater toward a freezing front impinging the pavement system from above. Comparably warmer water from below is attracted to ice lenses, which flow in frost susceptible soils

through a matric and osmotic suction. Specifically, this paper outlines the in-situ soil characteristics, construction, instrumentation, and initial field performance assessment. This study also compares laboratory data with statistical analysis and a physics-based model to evaluate the significance of EWR placement depth. To understand factors influencing the test site, an analysis of the capillary fringe in relation to the underlying water table, the soil water characteristic curve (SWCC), and the linearly interpolated frost line were used to gain insights into how various sources of soil moisture affect frost heave. Lastly, results from the field trial are discussed.

4.8 Methodology

Figure 4.11 shows the research methodology for this study. Initially, the EWR placement depth is optimized through a combination of historical data analysis (primarily soil temperature and historical frost penetration depths) and a physics-based model to predict the depth with the least expected heave alongside minimal required soil excavation. Laboratory testing was conducted to optimize OS dosage with in-situ soil. Based on both OS optimization and optimized placement depth, field trial sections are constructed. Continuous on-site monitoring of the different sections (treated and untreated) is performed to validate EWR performance. Each of the steps in the flowchart presented in Figure 4.11 is explained in subsequent sections.

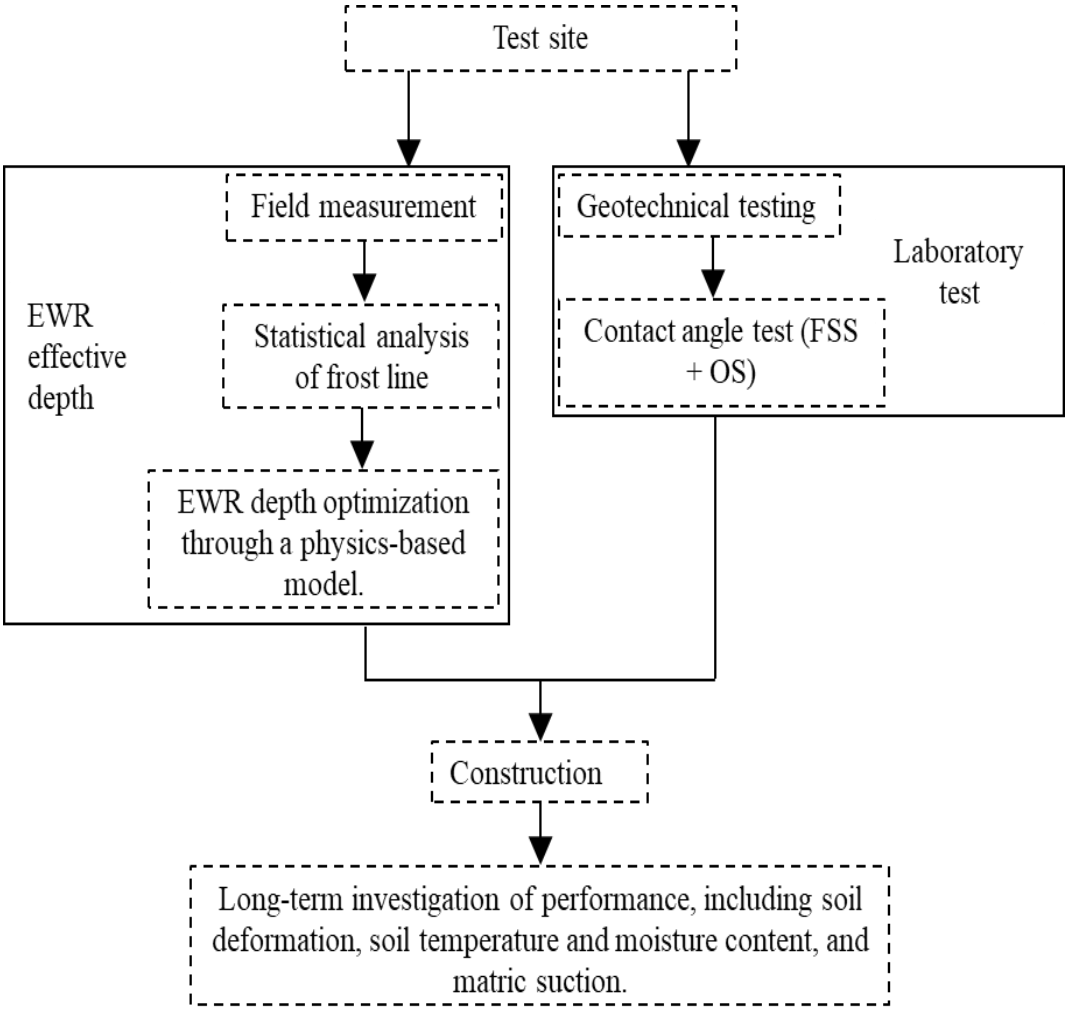

Figure 4.11: The research flow of this study.

The test section was constructed at the MnROAD facility in Monticello, MN, in upper Midwest USA (Figure 4.12). The selection of the site was motivated by its significant frost hazard potential due to high water levels, reaching 1.5 meters, and the presence of frost-susceptible soil in the frost zone (Christopher et al., 2006). The test site has two lanes, 7.3 m wide and 45.7 m long. The asphaltic pavement sections were constructed in a low-volume traffic test loop (design speed of 64.4 km/hr.), which experiences about 6,000 Equivalent single axle loads (ESALs) per year. One section was treated with EWR, while the other was used as the control section.

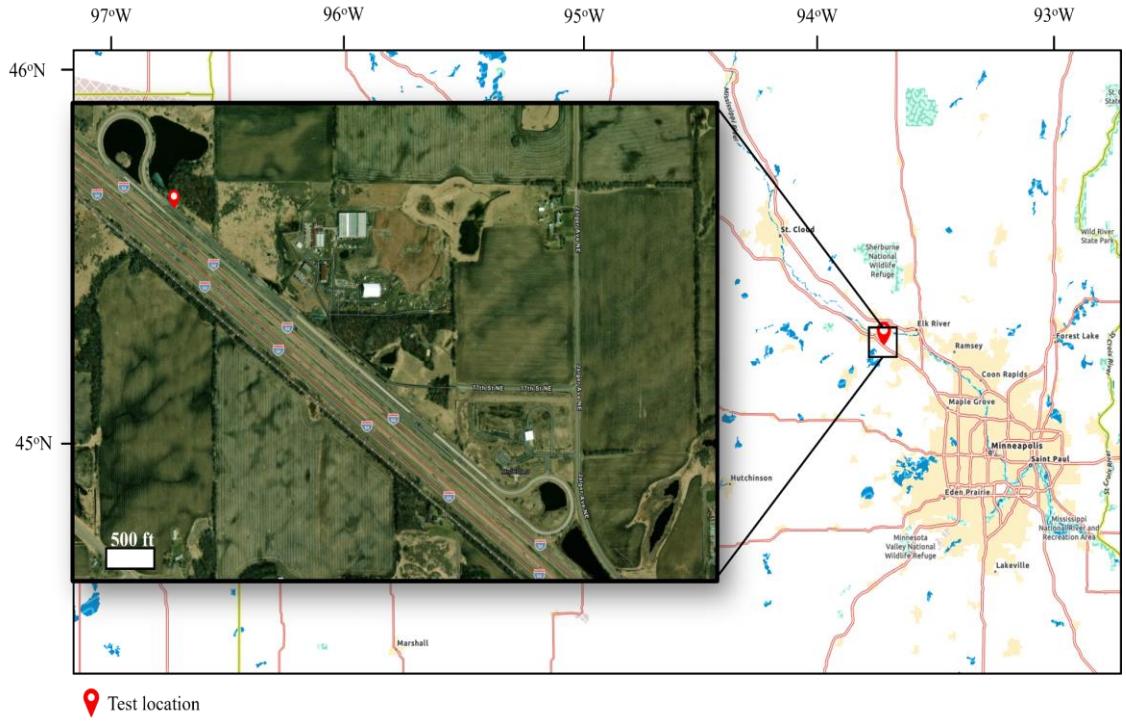

Figure 4.12: Inset map: Location of the study area within MnROAD facility, MN. Main map: Map of main cities around MnROAD, Minnesota.

4.9 Laboratory Test

4.9.1 Geotechnical Test.

General geotechnical site conditions (stratigraphy, soil properties) at the MnROAD facility have been well documented (Cetin et al., 2021). Additional data were collected closer to the actual test cells in this study, including six boreholes to substantiate local conditions (pavement thickness and soil strata) (see Figure 4.13). Disturbed samples were collected for subsequent laboratory material characterization during the site investigation. Atterberg limits (ASTM D 4318-00), particle size distribution (ASTM D7928), specific gravity (ASTM D854-10), saturated hydraulic conductivity (ASTM D2434), Soil Water Characteristic Curve (SWCC) (ASTM D6836), Contact Angle, and Unconfined Compressive Strength (UCS) (ASTM D2166) were performed. The soil's in-situ grain size distribution is depicted in Figure 4.14, with additional geotechnical characteristics listed in Table 4-9.

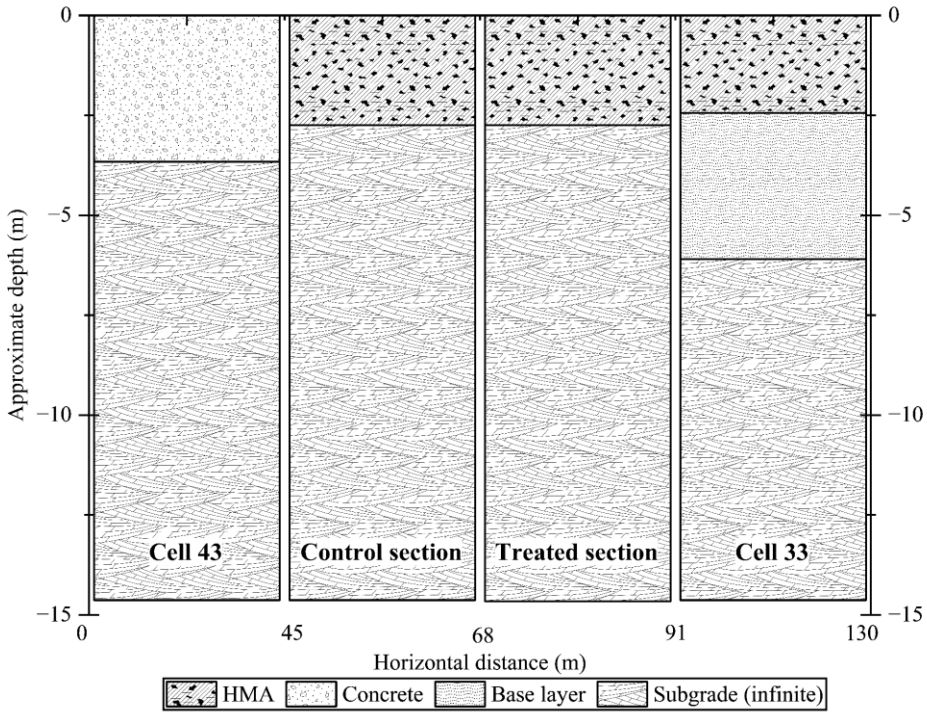

Figure 4.13: Soil strata of the site (Cell 2305/2306 [where control and treated section was constructed] borders cell 43 to the west, while cell 33 is to the east [as of 2022]).

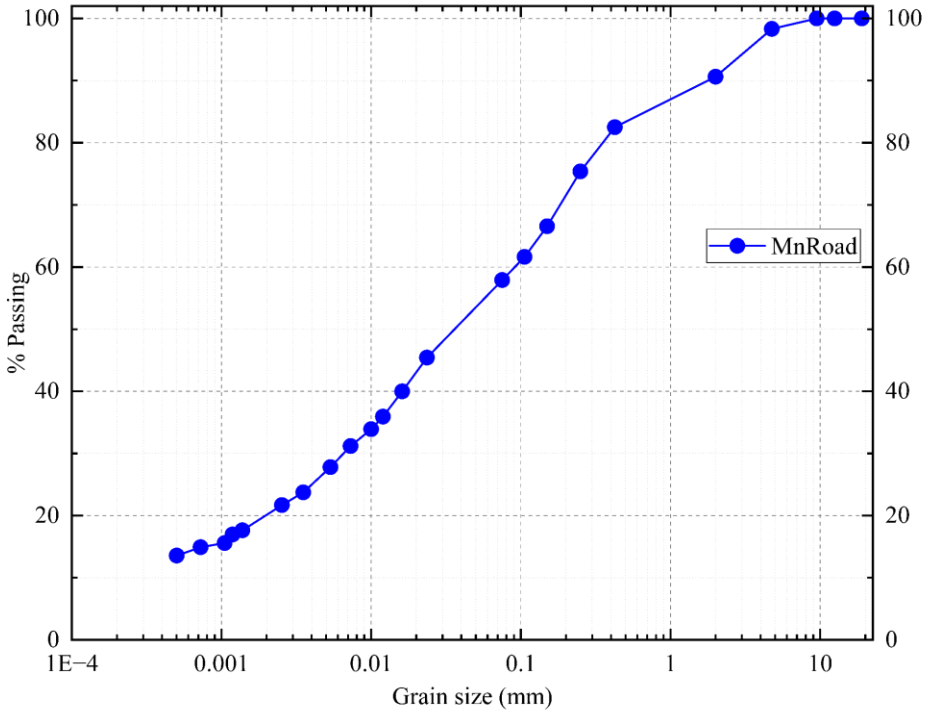

Figure 4.14: Particle size distribution of in-situ subgrade.

Table 4-9: Basic Subgrade properties.

Soil properties	Characteristics	Units	
Classification	AASTHO		A-6
	USCS		CL
	Frost Susceptibility		F4
Physical properties	Specific gravity		2.68
Atterberg limits	Liquid limit	%	36.3
	Plastic limit	%	23.9
	Plasticity index	%	12.4
	Hydraulic conductivity	cm/s	$1.19e^{-7}$
Proctor test	Optimum Moisture Content (OMC)	%	10
(Modified)	Maximum Dry Density (MDD)	kN/m^3	19.5
(Standard)	Optimum Moisture Content (OMC)	%	14.1
	Maximum Dry Density (MDD)	kN/m^3	17.41

USCS = Unified Soil Classification System; AASHTO = American Association of State Highway and Transportation Officials; CL = low plasticity clay; F4-Very high frost susceptibility

4.9.2 SWCC

SWCC was performed using Hyprop (accuracy of 0.15 kPa with a resolution of 0.001 kPa) and WP4 (±0.05 MPa from 0 to -5 MPa, 1% from -5 to -300 MPa), both from the Meter group. The Van Genuchten fitting is utilized in this study and shown in Figure 4.15. From the SWCC, capillary height was calculated using equation 1 based on (Kumar & Malik, 1990).

$$h_c = h_a + 134.84 - 5.16\,(SQTR(r)) \quad (1)\ (28)$$

Where h_a is the air entry head (L; cm or kPa) and r is the equivalent pore radius (L; cm or m). The unit of r is μm, so it has little influence on the result of the calculation.

The maximum capillary height was calculated to be 2.43 m; however, a more conservative capillary height of 1.82 meters (0.75 of maximum capillary height) was used as (Fredlund et al., 2013) and (Fetter & Kreamer, 2022), observed that Maximum capillary is rarely reached. Water table data from the MnROAD database was combined with the capillary height to understand the water table's influence on the test section and the EWR placement details, as shown in Figure 4.16. In theory, EWR efficacy is maximized when placed between the estimated capillary height and the prevailing phreatic surface (water table). However, beyond the construction challenges of treating wet soil, the deeper the EWR layer is placed, the higher the construction cost and associated greenhouse gas emissions. As such, it is desirable to estimate a more practical design depth for EWR. For example, between the frost line and capillary height.

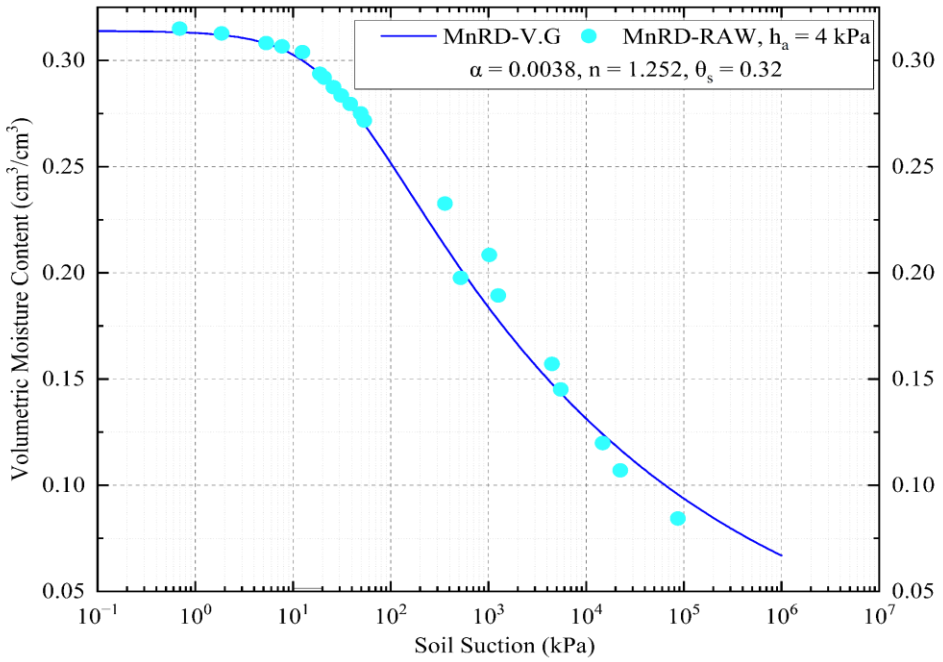

Figure 4.15: SWCC of MnROAD subgrade (USCS Classification: CL).

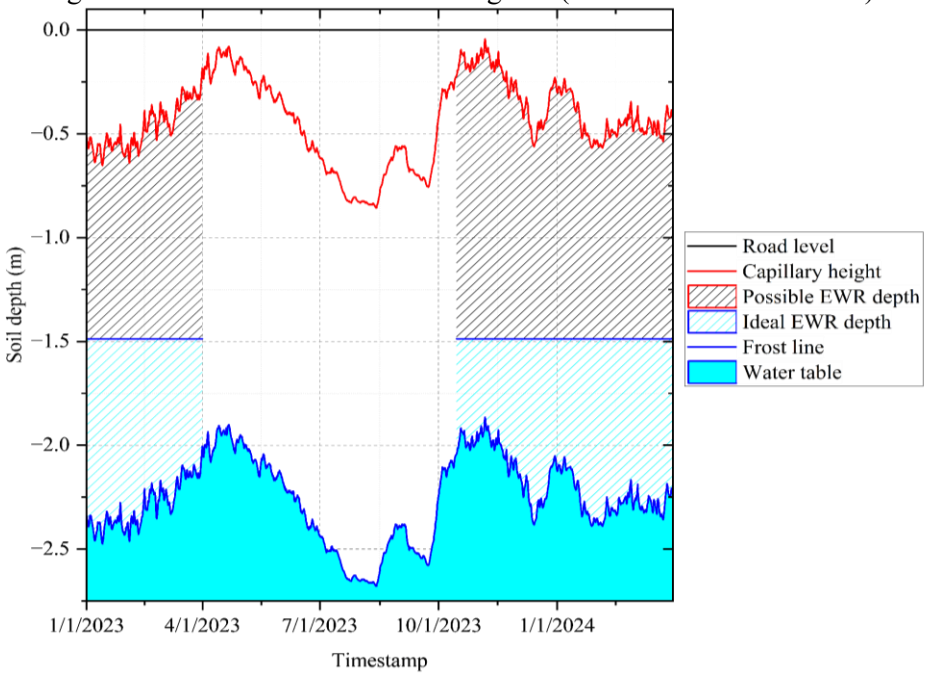

Figure 4.16: Water table, capillary height and, (maximum measured frost depth was utilized in this plot, frost line drops to zero after winter (April) until late fall (November)).

4.9.3 Contact Angle Test.

A commercially available OS (Terrasil from Zydex Industries) was used to induce hydrophobicity in the subgrade soils. Terrasil, which is miscible with water, consists of Alkoxy-alkysilyl compounds (65-70%), Benzyl Alcohol (25-27%), and Ethylene Glycol (3-5%) (Zydex, 2016). These types of OS additives

tend to react with silica in the soil to form covalent siloxane bonds. These reactions change the surface chemistry of soil particles from hydrophilic to hydrophobic without cementing or bridging individual particles together, as documented by Daniels and Hourani (*2009*). Prior research by Brooks et al. (2022) and Uduebor et al. (*2023*) has demonstrated that subgrade soils treated with varying concentrations of OS exhibit hydrophobicity, reflected by contact angles exceeding 90^{o}.

To evaluate OS application for field application, contact angle measurements were made with two different procedures. The first involved typical laboratory methodology (Feyyisa et al., 2017), which involves the OS product mixed with the soil and deionized water to achieve a liquid-to-solid ratio of 1:1. For instance, for the 1:10 dosage contact angle test, 10 g of OS was diluted with 40 g of deionized water (50 g of liquid in total), then added to 50 g of soil. The resulting mixture was tumbled for 24 hours using a laboratory tumbler, after which it was oven-dried at 60^{O}C for 24 hours using an electric oven (Humboldt H-30135 Lab Bench Oven). Afterward, it was allowed to cool for 24 hours. before testing using a goniometer (Ramehart Instruments, 260-U1) and Geocomp FlowTrac II after (Uduebor et al., 2023). The variation in the OS-to-soil ratio and resulting contact angles are presented in Figure 4.17**a**. Based on the results and an assumed penetration depth of 5 mm, the selected application rates were 0.57, 0.34, and 0.23 OS liters/m^{2}, as it corresponds to 112.8^{o}, 97.5^{o}, and 90^{o}, respectively. Also, above the depth of penetration, the contact angle values will be higher. These varying concentrations were chosen based on the hypothesis that deeper EWR spray would need to resist higher water pressure than the other top sprays. Furthermore, considering that the optimum moisture content (OMC) of the soil is approximately 10%, to prevent diluted water runoff during spraying and to ensure workability, the total diluted OS was limited to 227 liters.

a

b

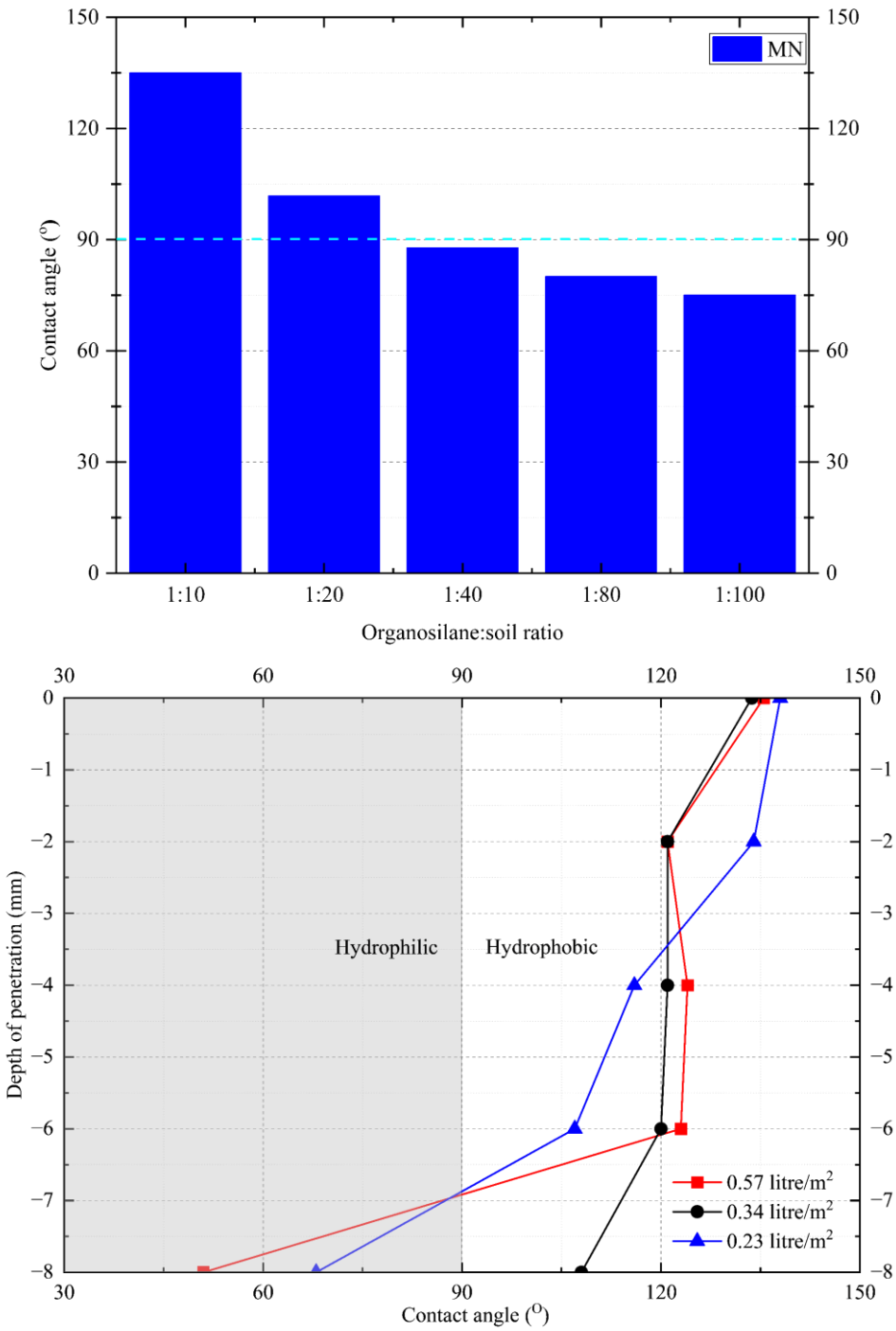

Figure 4.17: Change in contact angle with varying OS concentration.

The second method simulated field conditions where the OS, diluted with water, is sprayed on the untreated compacted soil surface (simulating potential field concentration and dilution ratio). After spraying using a 16 oz natural high-density polyethylene (HDPE) plastic spray bottle, it was oven-dried in an electric oven at 60ºC for 24 hours. Afterward, the samples are carefully divided into different thicknesses

(at the surface, 2, 4, and 6 mm) with samples collected, oven-dried, and then allowed to cool for 24 hours before contact angle testing using the same testing procedure described above. Figure 4.17**b**. illustrates the effects of change in contact angle with depth. Hence, for this study, an OS:Soil ratio varied from less than 10 to 100 between the surface and a depth of 8 mm, with a contact angle ranging from 138^{o} (at the surface) to 51^{o} (at 6mm depth). This test showed that irrespective of the chemical applied, a similar contact angle (above 90^{o}) is achieved with an effective penetration of about 7 mm for all concentrations. A similar contact angle of about 135^{o} for all concentrations shows high OS concentration at the surface. The lower concentration with more water dilution had better contact angle values with depth.

4.10 EWR Effective Depth.

For the application of EWR treatment in the field, optimization of the placement depth is critical as it ensures that EWR is cost-effective and constructively feasible. Ideally, this depth should either coincide with the frost depth or fall between the frost depth and the water table or capillary fringe. EWR placement at this maximum frost depth would be expensive and labor-intensive. Hence, EWR depth must be balanced between constructability, cost, and effectiveness. This involves several steps, encompassing field soil measurements, frost line interpolation, statistical analysis, and physics-based modeling, as depicted in Figure 4.18.

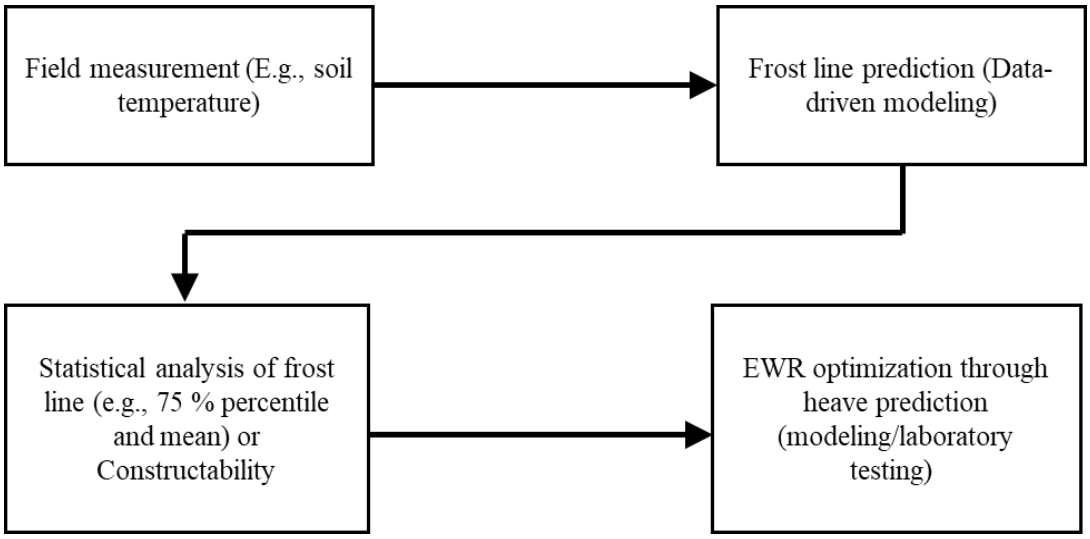

Figure 4.18: Schematic framework of treatment design approach.

4.10.1 Field Measurement

At the MnROAD research facility, soil temperature data was collected from various depths using a thermocouple tree (a linear array of thermocouples measuring temperatures at defined intervals from the pavement surface to eight feet below the surface) from 2017 to 2021. This dataset was then employed to establish a site-specific frost line utilizing a linear interpolation technique, as shown in Figure 4.19. Various statistical analyses (normal distribution analysis, standard deviation, measures of central tendency, minimum and maximum) were conducted on the frost depth data from soil temperature measurements. For instance, utilizing soil property measurements previously collected at MnROAD (cell 127) and the interpolated frost line data for different winter seasons, as illustrated in Figure 4.20, a normal distribution analysis was performed. This analysis revealed that the third quartile of all the frost depths amounts to 1.18 m and accounts for most frozen periods, as depicted in Figure 4.20. Consequently, this value can be utilized as the placement depth for EWR for MnROAD. Yet, little is known about the potential effects of placing EWR at any depth, even at 1.18 m.

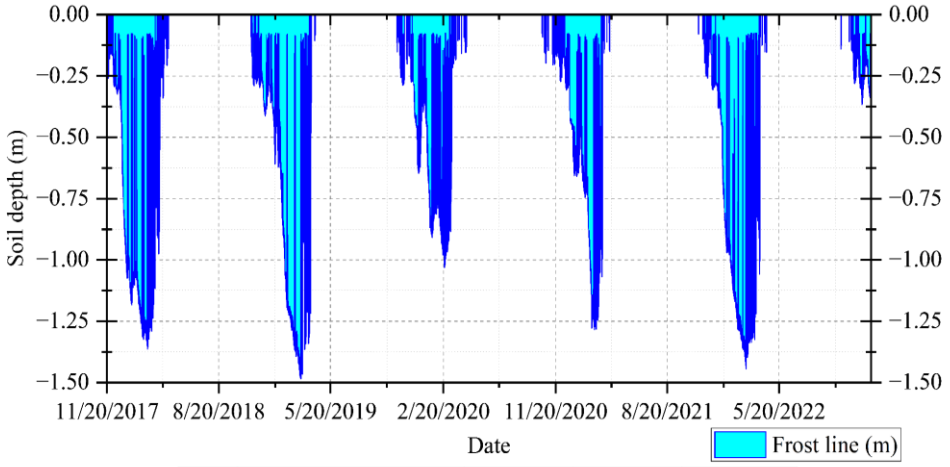

	2017-2018	2018-2019	2019-2020	2020-2021	2021-2022
Mean	0.91	0.69	0.52	0.57	0.77
std	0.37	0.44	0.27	0.34	0.42
min	0.08	0.08	0.08	0.08	0.08
0.25	0.72	0.29	0.27	0.27	0.34
0.5	1.05	0.49	0.48	0.55	0.83
0.75	1.18	1.18	0.78	0.73	1.12
Max	1.36	1.48	1.03	1.28	1.44

Figure 4.19: Frost depth (linear interpolation) from MnROAD soil temperature data (Cell 127) from 2017 to 2022.

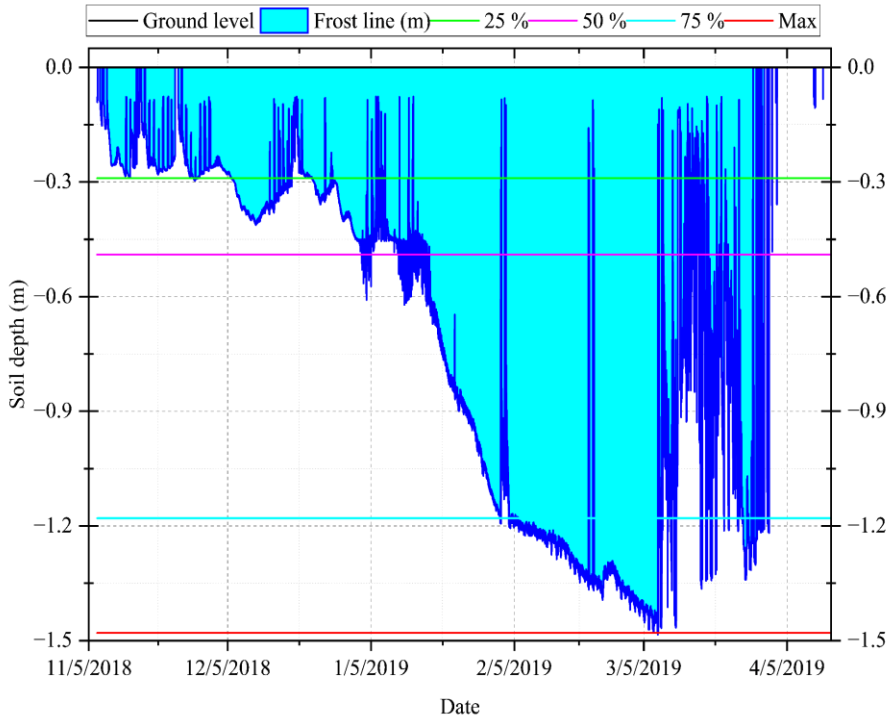

Figure 4.20: Frost depth (linear interpolation) from MnROAD soil temperature data (Cell 127) for 2018/2019.

4.10.2 Physics-based model

A physics-based model coupling thermal, hydraulic, and mechanical fields under saturated conditions was used to predict ice lenses' spatial and temporal distributions and subsequent heaving within samples. The mathematical model enabled simulated processes such as phase change, moisture migration via matric and osmotic suction, heat transfer (through conduction and convection), and ice lens growth. Like the studies of Zhou and Li (2012) and Huang and Rudolph (*2021*), the void ratio was used as a dependent variable to indicate the formation of ice lenses. Water migration within the samples was carried out via Darcy's law, relating water flux and head of water. Hydraulic conductivity was defined empirically as a function of temperature (Gilpin, R. 1980; Nixon, 1991) to describe the movement of unfrozen water to the growing ice lenses (**Equation 2**)

$$k = \{k_o[1-(T-T_0)]^{\beta} \;\; T \leq T_0 \;\; k_o[1-(T-T_0)]^{\beta} \;\; T > T_0 \qquad (2)$$

Where k is the hydraulic conductivity (m/s), K_0 is the saturated hydraulic conductivity (m/s), T_0 is the freezing point (deg C), and β is the empirical parameter.

The two primary governing equations (**Equations 3 and 4**) used for simulating the coupled thermo hydro mechanical analysis are non-linear and require adequate initial and boundary conditions. The system of equations was numerically solved using the finite element method in COMSOL Multiphysics v. 6.1 with a time-dependent solver.

$$\frac{\rho_i S_i + \rho_w(1-S_i)}{\rho_w(1+e)} \frac{\partial e}{\partial t} + \frac{e(\rho_i-\rho_w)}{\rho_w(1+e)} \frac{\partial S_i}{\partial T} \frac{\partial T}{\partial t} = \frac{\partial}{\partial x}\left(k \frac{\partial \psi}{\partial x}\right) \qquad (3)$$

$$\left(C - \frac{L\rho_i e}{1+e} \frac{\partial S_i}{\partial T}\right) \frac{\partial T}{\partial t} - \frac{L\rho_i S_i}{1+e} \frac{\partial e}{\partial t} = \frac{\partial}{\partial x}\left(\lambda \frac{\partial T}{\partial x}\right) + C_w k \frac{\partial \psi}{\partial x} \frac{\partial T}{\partial x} \qquad (4)$$

Where Si is the degree of ice saturation, ρ_i the density of ice (kg/m^3), ρ_w is the density of water (kg/m^3), e is the void ratio, T is Temperature (K), t is time, x is the length of domain (m), Psi is the water head (m), k is the hydraulic conductivity (m/s), C is the volumetric heat capacity of soil, L is the Latent heat of fusion, Lambda is the coefficient of heat conductivity of soil, C_w is the volumetric heat capacity of water.

4.10.3 EWR Placement Depth Optimization

Using the physics-based model, different case scenarios were explored to determine the optimum EWR placement depth, which balances frost heave mitigation and constructability. Not placing the EWR at the maximum frost depth results in the creation of a distinct boundary condition between the EWR-protected layer and the maximum frost depth, as depicted in Figure 4.21. Hence, there is an unprotected depth, i.e., the difference between the maximum frost depth and the depth of the EWR. Therefore, the unprotected depth could give rise to frost-related effects, as shown in Figure 4.21**b**. This approach is based on the hypothesis that continuous ice lens growth will not occur above the EWR layer. However, ice lens formation is possible beneath the treated layer, which might lead to frost heaving. In essence, this strategy aims to balance frost mitigation and the practicality of construction, acknowledging that some frost action might persist below the EWR-protected layer, as indicated in Figure 4.21**c**.

Various scenarios, encompassing -4.9°C at the surface (obtained from MnROAD thermocouple data) and to the maximum frost depth as control and varied EWR placement, were simulated (see Figure 4.22), as outlined in Table 4-10. The initial temperature of the domain was set as 1°C, and the boundary condition at the bottom of the sample was set as 0°C. For each of the different cases defined, the domain size as well as the overburden pressure were adjusted accordingly, and the simulations ran for a period of 20 days. The most challenging scenario occurred at -4.9°C with no EWR application, giving a resulting heave of 4.76 cm. Heaving decreased as the EWR was placed at deeper levels. The model consistently demonstrated reduced heaving with EWR placement. Furthermore, it reinforced the initial hypothesis that the closer the EWR is positioned to the frost depth, the better its performance in mitigating frost heave as shown by case 1 in Table 4-10. The simulation also shows that a 50% reduction is achieved at a placement depth of 1.2 meters. Beyond this, the reduction drastically fails. Hence, for field construction, the deepest EWR layer was placed at 1.2 meters.

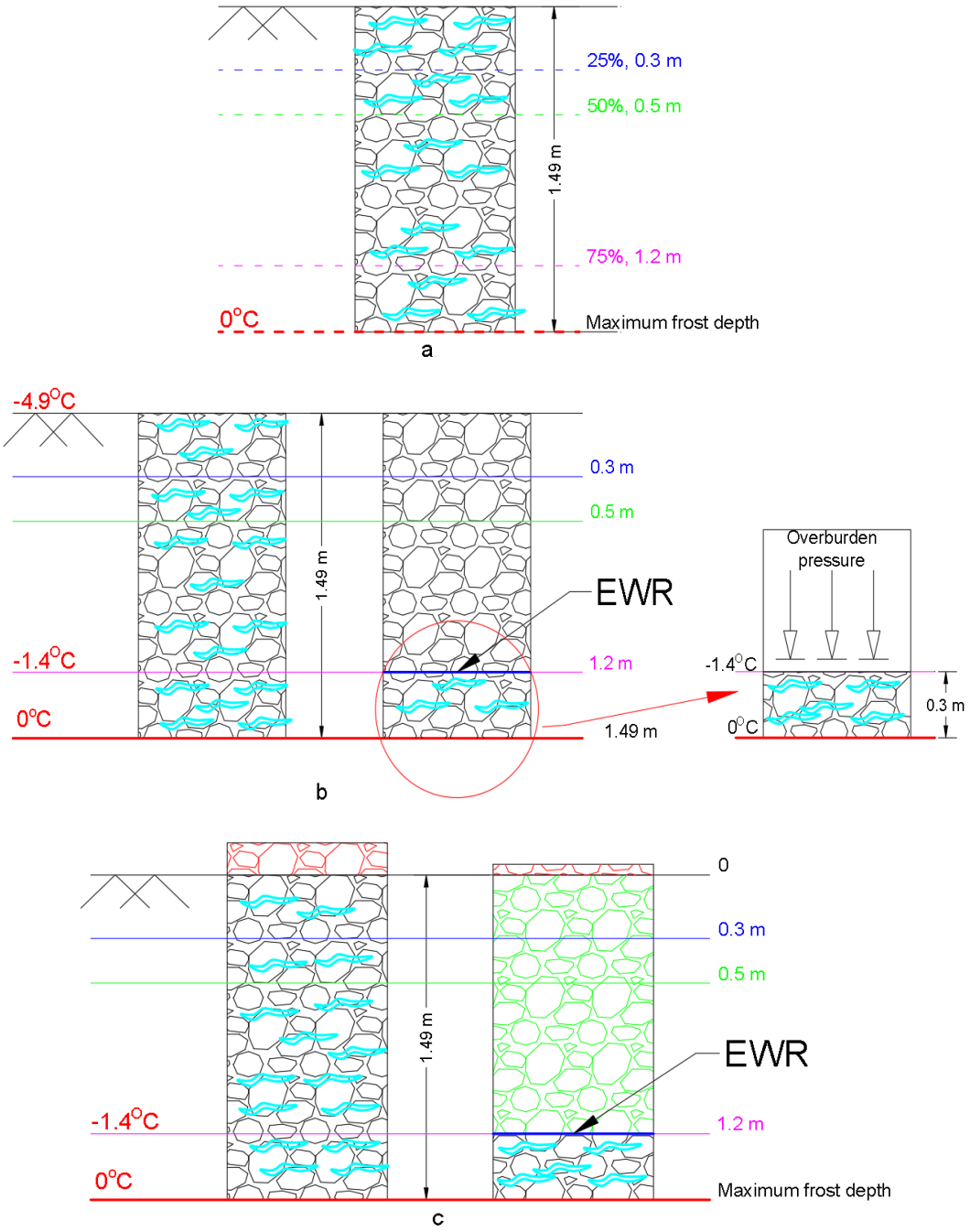

Figure 4.21: Effective EWR on boundary condition (a - initial boundary condition, b - typical EWR boundary condition, and c - expectations from the EWR application.

Table 4-10: Effect of EWR placement on Frost heave.

Scenarios	Top boundary temp (^{0}C)	Placement Depth (m)	Depth from maximum frost depth/Domain length, x (m)	Overburden pressure (kN/m^2)	Max Heave (cm)
Case 1	-0.625	1.3	0.2	26.0	0.95
Case 2	-1.15	1.2	0.3	23.7	2.25
Case 3	-2.9	0.6	0.9	11.2	3.78
Case 4	-3.8	0.4	1.1	8.2	3.87
Case 5	-4.9	0	1.49	0	4.76

*Depth placement at 1.2 meters is equivalent to the 75% percentile of front depth obtained in 2018/2019 (the last major severe frost event).

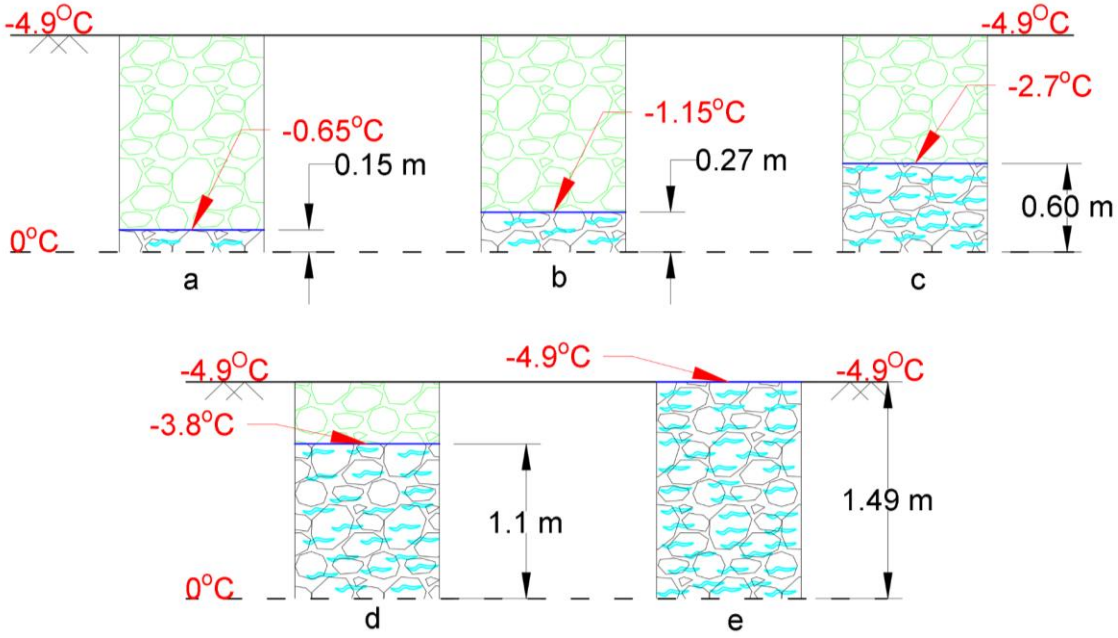

Figure 4.22: Effective EWR on boundary condition (a) case 1, (b) case 2, (c) case 3, (d) case 4 and (e) case 5

4.11 Construction

Adopting a comprehensive methodology that integrated diverse laboratory tests and effective placement depth, two test sections were constructed at MnROAD. These experimental field test sections were devised to closely monitor the performance of water-repellent treatments when applied to subgrade soils, with the primary objective of mitigating the detrimental impact of recurrent freeze-thaw cycles on low-volume roads. The major source of water supply for ice lens growth is from the water table through capillary. Two 23-meter-long sections were built at the low-volume track at the MnROAD facility, with one section treated with a commercially available organo-silane and the other utilized as the control section, as

shown in Figure 4.23. The treated section comprises of three sprayed layers at a depth of 1.2, 1.1, and 0.9 meters (based on Table 4-11 results) sprayed with OS concentrations of 0.57, 0.34, and 0.23 liters per square meter (based on Figure 4.17b), respectively.

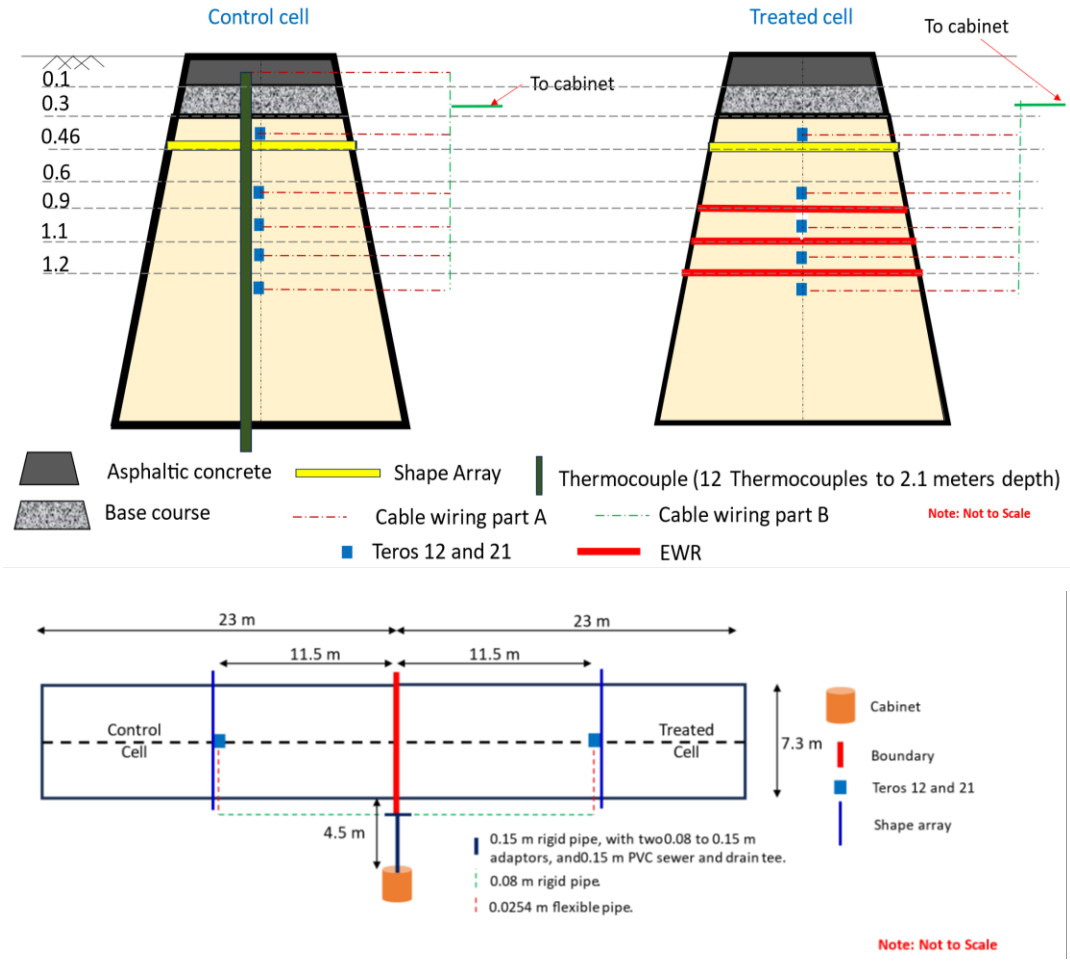

Figure 4.23: The schematic diagram of the test cells with the location of treated layers and sensors

Table 4-11: Resource utilization at MnROAD and OS application in the treated section

	Unit	Control section	Treated section
Milled HMA	Metric tons	72.5	72.5
Soil excavated/backfilled	Metric tons	325.76	325.76
Base layer (Class 5Q)	m^3	52.47	52.47
HMA (4")	Metric tons	45	45
Water	liters	0	492
OS	liters	0	189
	OS application (liter/m^2)	OS (liters)	Water (liters)
Spray1 (1.2 m)	0.57	95	132
Spray 2 (1.1 m)	0.34	57	170
Spray 3 (0.9 m)	0.23	38	189

The construction process started with milling away the existing Hot Mix Asphalt (HMA) of 0.1 to 0.25 m thickness. Then, subgrade excavation to a depth of 1.2 m was performed with two Kubota SVL75-3 skid steer loaders as displayed in Figure 4.24. After subgrade excavation, the deepest sensors (Teros 12 and 21) were installed at 1.34 m to measure parameters such as soil temperature, electrical conductivity, matric suction, and volumetric water content below the EWR sprayed layer. In the treated section (cell 2306), OS was first sprayed at a rate of 0.57 liters/m² using a Country Way 227-liter sprayer at 8.32 liters per minute, attached to a New Holland L190 skid steer. After spraying, the soil was pulled back and compacted using a CAT CC34B utility compactor and Hamm HD 12 (or 13) VV roller to a depth of 1.04 m. Further applications of OS were conducted at depths of 1.1 and 0.91 m, followed by additional sensor installations at 1.09, 0.98, and 0.85 m. Sensors were later installed at similar depths in the control section (cell 2305) after sequential backfilling and compaction. In both sections, shape arrays were installed horizontally and with additional sensors at 0.5 m before the soil was brought back and compacted to a depth of 0.3 m.

In the control section, 2.1-meter drilling for a thermocouple tree sensor was conducted using a McMillen Auger Driver X1975d attached to a New Holland L190 skid steer. The construction was finished

with a 0.15 m subbase layer (class 5Q) and a 0.1 m HMA surfacing (2 lift of PG 58S-28) placed using a Weiler P385B paver. Light Weight Deflectometer (LWD) tests were performed after each lift compaction to ensure adequate compaction of 20 MN/m^2 (elastic modulus of soil) based on MnROAD construction requirements. Similarly, LWD tests were performed on the base as shown in Figure 4.25. Immediately after construction, Falling Weight Deflectometer (FWD) tests were performed as an initial reference point for future FWD tests.

f 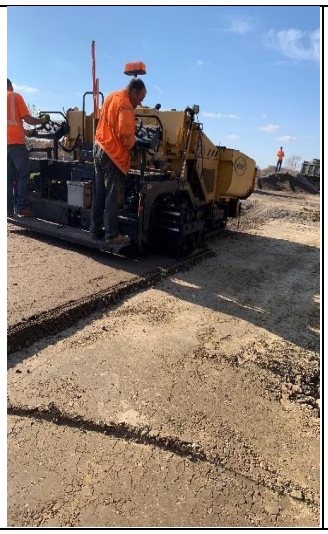 g  h 

Figure 4.24: Construction images: (a) soil excavation, (b) diluted OS spraying, (c) sensor installation, (d), compaction quality assurance, (e) measurand shape array installation, (f) base layer construction, (g) enclosure for data acquisition system, (h) completed construction

Extensive instrumentation was installed within all test cells to monitor various parameters, as indicated in Figure 4.23. Volumetric water content, electrical conductivity, and soil temperature at different depths were monitored using ten Metergroup Teros 12 sensors (ranges: 0.00–0.70 m^3/m^3, −40 to +60 °C, 0–20,000 µS/cm (bulk), and resolution of 0.0010 m^3/m^3 , 0.10 °C, 1 µS/cm), while 10 Metergroup Teros 21 sensors (Range: 0 to −100,000 kPa and accuracy of ±(10% of reading + 2 kPa) from −100 to −5 kPa) were used to measure matric potential and soil temperature. Additionally, a T-type thermocouple tree (Multipair Thermocouple Extension Cable - 12TX20PP) was strategically placed at regular intervals up to a depth of 1.92 meters to measure soil temperature far beyond the frost penetration depth. The frostline was determined using linear interpolation, as shown in Figure 4.26. To assess potential heaving and settlement, Shape Array Accelerometer (SAA) sensors from Measurand (with a resolution of ± 1.5 mm (0.06 inch) for 32 meters (105 ft) array) were installed at a depth of 0.2 meters from the road surface (i.e., below the base layer).

To facilitate data acquisition and management, an enclosure (McCain 334 Controller Cabinet) was set up, housing a CR1000X data logger, an AM16/32B multiplexer, two SAA 232 interfaces for connecting shape arrays to the data logger, a BP 24 battery (12V Sealed rechargeable battery, 24 Ah), and a CH 150

charging regulator to link the solar panel and battery. The enclosure was equipped with a 20-watt solar panel to meet power requirements. Furthermore, one Cell 205 modem from Campbell Scientific was installed in the enclosures to facilitate remote data collection. Meteorological and groundwater data were collected from the MnROAD Oracle database.

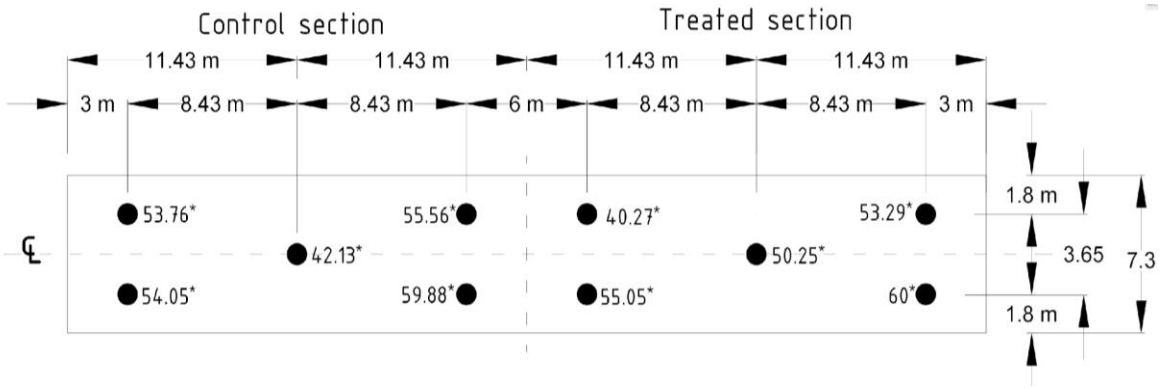

Figure 4.25: LWD test on the Base layer (* in MN/m2). Note: average Sm is 0.5816, and s/v is 3.2259)

4.12 Preliminary Evaluation

The typical frost depth for Minnesota is about 1.5 meters, however, in 2023/2024, the maximum frost depth was observed to be 0.76 meters (*MnDOT, 2024*), as shown in Figure 4.26, due to El Niño and climate change (MnDNR, 2024). Hence, the heaving observed at the test sections was marginal (0.15 cm). Still, there was a significant difference between the control and treated sections in terms of soil displacement. The maximum heave observed at the control was 0.15 cm. However, the treated section experienced settlement of 0.32 cm instead, as shown in Figure 4.27. Heaving in the control section is because of continuous ice lens growth as it coincides with soil subfreezing temperatures as shown in Figure 4.26. The hypothesis for settlement in the treated section is that due to compression of the protected layer. Consolidation/shrinkage of the second treated zone during the winter period when the pavement section undergoes freezing results in settlement. The presence of a water repellent treated layer prevents the migration of water to the top freezing zones from the groundwater beneath under potentials, resulting in the suction of the moisture within the zone directly above it causing settlement. This is observed in the decrease in the moisture content values for the sensor placed at 1.01m (Figure 4.28). This settlement/shrinkage is recovered as soon as the layer above thaws out and water is transported back creating a moisture equilibrium

within the zone. For the untreated section there is no decrease in the moisture content at similar depth because there is a continuous supply of water to the freezing zone at the top via capillary action.

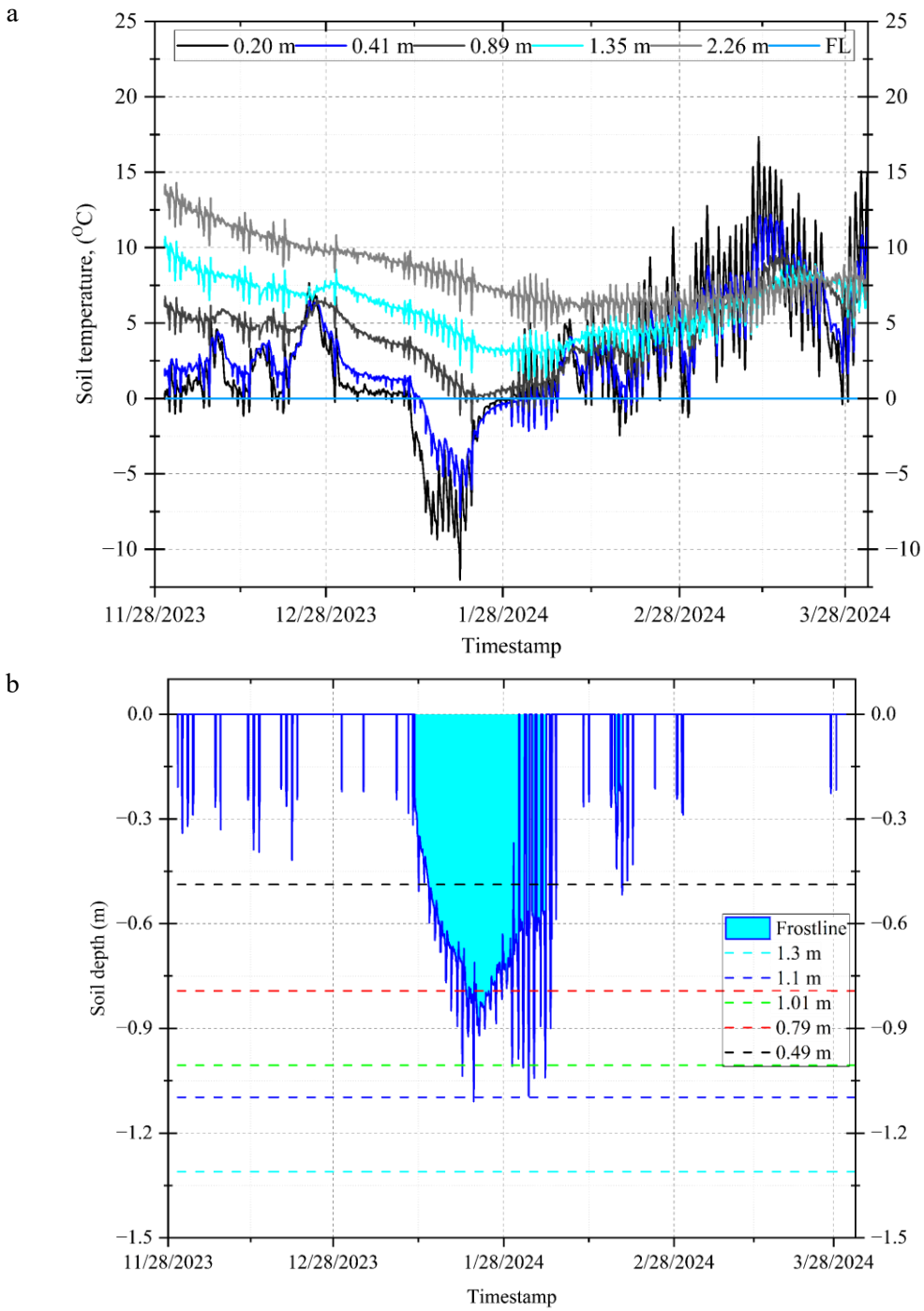

Figure 4.26: Data from installed thermocouple tree a) Soil temperature and b) frostline at the treated section.

The expectation from the EWR-protected soil layer is that the moisture content will be constant or that the moisture content will gradually decrease continuously, as observed by (Uduebor et al., *2022*). This study and Uduebor et al. (*2022*) have not shown a significant reduction in the moisture content of the protected layer or molded EWR after construction. The EWR was designed as a vapor-permitting membrane which should allow the vapor to escape, hence, subsequent drying of the layer. However, the depth of placement exceeds 0.5 m, except in the case of Uduebor et al. (*2022*), which prevents drying from occurring. In the case of Uduebor et al. (*2022*), frequent rainfall hindered the continuous drying of the compacted EWR layer. Hence, for further field application, drying of the sprayed layer must be done before subsequent placement of upper layers.

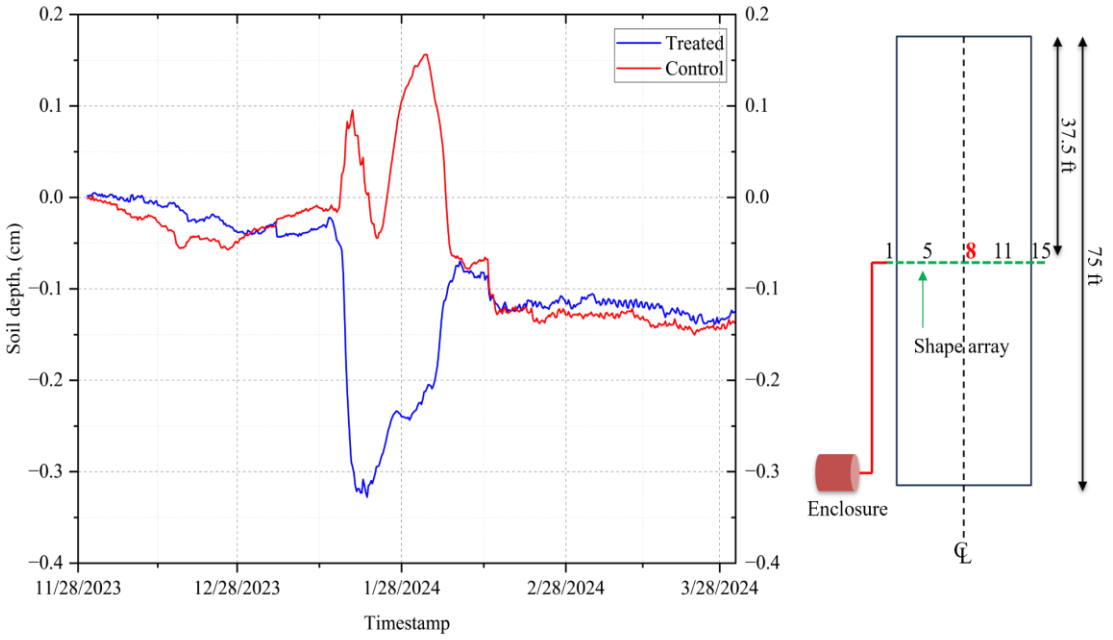

Figure 4.27: Soil deformation at the center of the test sections

While the deeper protected layer was gradually drying, significant variation in moisture content was observed in the upper protected layer. The current test indicates that the OS treatment varied from 0.34 to 0.57 liters per m^2. In the upper treated layer, the cause of moisture ingress appears to have been from localized water leakage through the flexible conduit (used to protect the sensors' wiring). Other hypotheses include failure of the EWR sprayed layer (due to lower OS concentrations) or lateral infiltration from

ponding and infiltration. It should be noted that the entire protected layer was not sprayed on the sides, only the top and bottom. These hypotheses are subject to longer-term monitoring and analysis.

The volumetric moisture reading indicated full saturation in the control section, as shown in Figure 4.28. This is backed up by capillary height juxtaposed with the water table reading, as illustrated in Figure 4.26, which shows that capillary water rises almost to the asphaltic layer. However, in the treated section, full saturation across all depths is hindered, which indicates that capillary action might not contribute to my ice lens growth. However, side leakage is a significant source of water above the treated layer, which can still lead to ice lens growth. The main objective of the EWR is to prevent capillary rise within the subgrade to hinder ice growth. Preliminary data obtained have shown that with an increased water table and perched aquifer (due to clay soil presence), side infiltration of water still occurs above the protected soil layer.

a

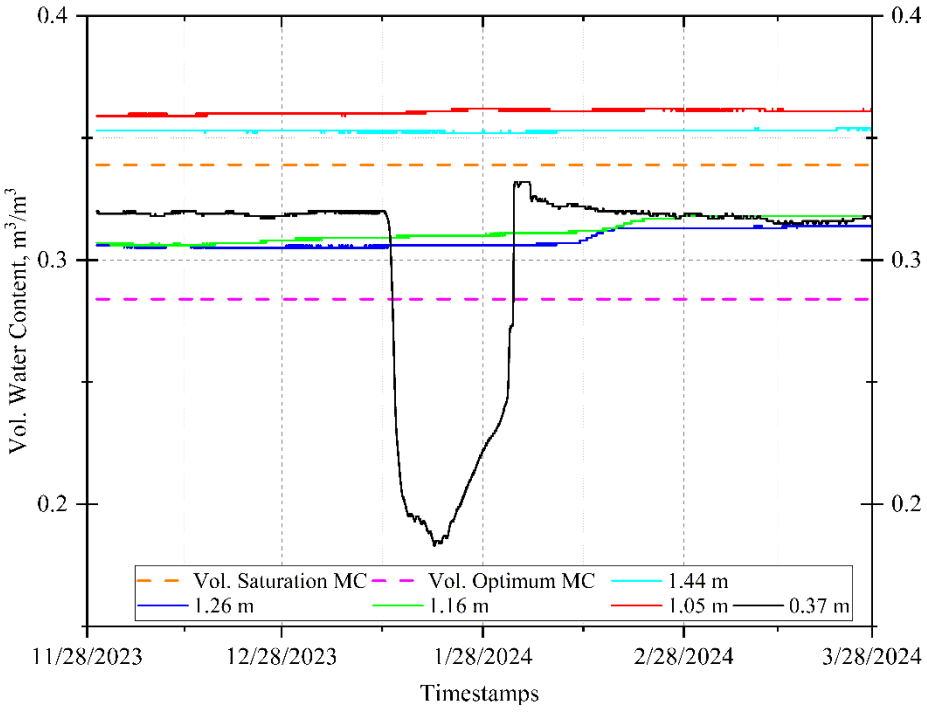

b

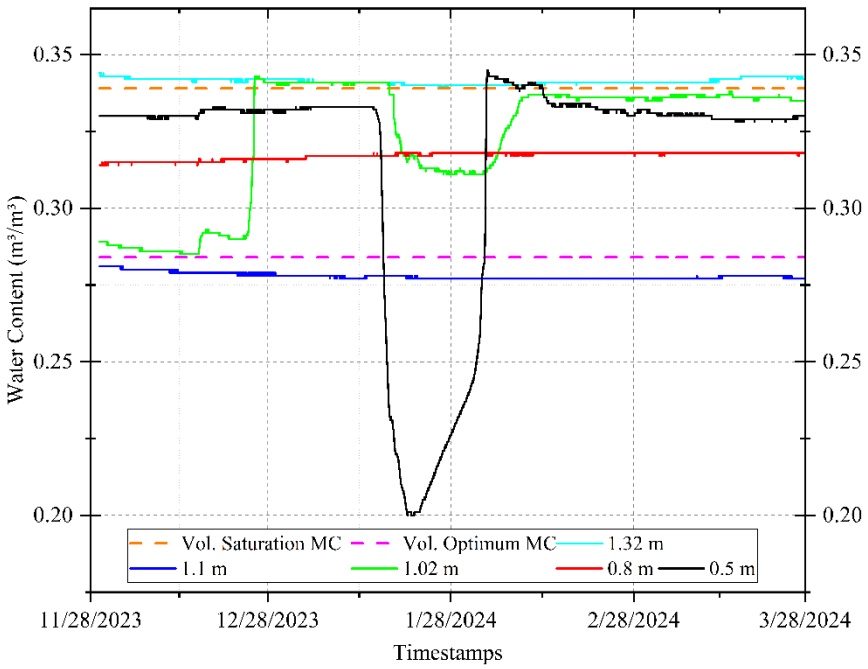

Figure 4.28: Volumetric moisture readings from a) control and b) treated sections

4.13 Conclusions

This study explores the field test construction of frost mitigation through Engineered Water Repellency (EWR). EWR involves converting hydrophilic soil into hydrophobic soil using organosilanes, which modify the soil particle surface. The study includes the design, construction, and preliminary results of test cells (control and treated) and aims to evaluate the potential of EWR in mitigating frost action. The current results show that EWR can impede capillary rise but might not reduce water supply to ice lenses, since lateral moisture transport is possible. Laboratory, modeling, and field results indicate that EWR can prevent moisture migration and limit frost heave. The results of this analysis can be summarized as follows:

- Irrespective of the chemical used in this study, a similar contact angle (above 90°, indicating hydrophobicity) is achieved with an effective penetration of about 7 mm for all concentrations.
- The closer the EWR is positioned to the frost depth, the more effectively it mitigates frost heave. Hence, for field construction, the deepest EWR layer should be placed at 75% percentile of frost depth to reduce frost heaving by 50%.

- The current results show that EWR can impede capillary rise but might not reduce the water supply to the ice lens, especially when side infiltration is highly possible.
- Initial data from the moisture sensors indicate full saturation in the control section, whereas the results from the treated section showed moisture variations due to treated layers impeding the transport of water across the soil matrix.

Although EWR can effectively reduce water migration to ice lens formation via capillary action, substantial water infiltration from side leakage can still occur, diminishing EWR's effectiveness. Therefore, it is essential to implement proper subdrainage and daylighting systems. This study expands the knowledge base on frost mitigation through EWR by evaluating its application on flexible pavement in frost areas.

4.14 Acknowledgement

This research is sponsored by the National Science Foundation (Award #1928813 and Award #1947009) with counterpart funding from the National Road Research Alliance (MnDOT Contract #: 1036336 WO13). Authors also acknowledge the contributions of various Engineers and technical staff of MnDOT and the MnRoad Facility, as well as Dr. Wasif Naqvi and Fyaz Sadiq.

4.15 Reference

ASTM (American Society for Testing and Materials), "Standard Test Methods for Liquid Limit, Plastic Limit, and Plasticity Index of Soils.," ASTM International, West Conshohocken, PA., 2017.

ASTM International, " ASTM D7928-17: Standard Test Method for Particle-Size Distribution (Gradation) of Fine-Grained Soils Using the Sedimentation (Hydrometer) Analysis," ASTM International, 2017.

ASTM, "Standard Test Methods for Specific Gravity of Soil Solids by Water Pycnometer.," ASTM International, West Conshohocken, PA., 2014.

ASTM D2434-22., "Standard Test Method for Measurement of Hydraulic Conductivity of Coarse-Grained Soils.," 2022.

ASTM D6836, "Standard test methods for determination of the soil water characteristic curve for desorption using a hanging column, pressure extractor, chilled mirror hygrometer, and/or centrifuge.," West Conshohocken, PA, 2016.

ASTM D2166, "Standard Test Methods for Laboratory Compaction Characteristics of Soil Using Standard Effort.," ASTM International, West Conshohocken, PA., 2012.

ASTM Committee D-18 on Soil and Rock, "Standard Practice for Classification of Soils for Engineering Purposes (Unified Soil Classification System)," ASTM International., 2017.

AASHTO, "Standard Specification for Classification of Soils and Soil-Aggregate Mixtures for Highway Construction Purposes.," American Association of State and Highway Transportation Officials: Washington, DC, USA., 2017.

Brooks, T. Y., Daniels, J. L., Uduebor, M., Cetin, B., & Wasif Naqvi, M. (2022). Engineered Water Repellency for Mitigating Frost Action in Iowa Soils. In *Geo-Congress 2022* (pp. 448-456).

Cetin, B., Coban, H. S., Edil, T. B., Ceylan, H., Likos, W. J., Zheng, J., & Buss, A. (2021). *Determining Pavement Design Criteria for Recycled Aggregate Base and Large Stone Subbase* (No. NRRA202103). Minnesota. Dept. of Transportation. Office of Policy Analysis, Research & Innovation.

Christopher, B. R., Schwartz, C. W., Boudreaux, R., & Berg, R. R. (2006). *Geotechnical aspects of pavements* (No. FHWA-NHI-05-037). United States. Federal Highway Administration.

Coastal Engineering Research Center (US). (1973). *Shore protection manual* (Vol. 1). US Army Coastal Engineering Research Center.

Daniels, J. L. (2020). Engineered water repellency for applications in environmental geotechnology. *Sustainable Environmental Geotechnics: Proceedings of EGRWSE 2019*, 39-46.

Daniels, J. L., & Hourani, M. S. (2009). Soil improvement with organo-silane. In *Advances in ground improvement: research to practice in the United States and China* (pp. 217-224).

Dore, G., and Zubeck, H. K. (2009). Cold Regions Pavement Engineering, American Society of Civil Engineers, 1801 Alexander Bell Drive, Reston, VA, United States, 20191-4400, p. 416.

Fetter. C. W., and Kreamer, D. (2022). Applied Hydrogeology, 5 ed., Waveland Press, INC.

Feyyisa, J. L., Daniels, J. L., & Pando, M. A. (2017). Contact angle measurements for use in specifying organosilane-modified coal combustion fly ash. *Journal of materials in civil engineering*, *29*(9), 04017096.

Fredlund, D. G., Rahardjo, H., & Fredlund, M. D. (2013). Unsaturated soil mechanics in engineering practice. *Wiley-Interscience,* vol. 61, no. 5, p. 101, 2013.

Gilpin, R. (1980). A model for the prediction of ice lensing and frost heave in soils. *Water Resources Research*, *16*(5), 918-930.

Huang, X., & Rudolph, D. L. (2021). Coupled model for water, vapour, heat, stress and strain fields in variably saturated freezing soils. *Advances in Water Resources*, *154*, 103945.

Isotalo, J. (1993). Seasonal truck-load restrictions and road maintenance in countries with cold climate. *Infrastructure Notes: Transportation, Water and Urban Development Department*.

Kestler, M. A., Berg, R. L., Steinert, B. C., Hanek, G. L., Truebe, M. A., & Humphrey, D. N. (2007). Determining when to place and remove spring load restrictions on low-volume roads: Three low-cost techniques. *Transportation research record*, *1989*(1), 219-229.

Kumar, S., & Malik, R. S. (1990). Verification of quick capillary rise approach for determining pore geometrical characteristics in soils of varying texture. *Soil Science*, *150*(6), 883-888.

Mahedi, M., Satvati, S., Cetin, B., & Daniels, J. L. (2020). Chemically induced water repellency and the freeze–thaw durability of soils. *Journal of cold regions engineering*, *34*(3), 04020017.

Meeravali, K., Ruben, N., & Rangaswamy, K. (2020). Stabilization of soft-clay using nanomaterial: Terrasil. *Materials Today: Proceedings*, *27*, 1030-1037.

MnDOT, "Wright County frozen soil profile," 2024.

MnDNR, ""El Niño" is Coming. What Might That Mean for Minnesota's Weather?," Minnesota Department of Natural Resources, 21 February 2024. [Online]. Available: https://www.dnr.state.mn.us/climate/journal/el-nino-oct-2023.html. [Accessed 2 July 2024].

Nixon, J. F. (1991). Discrete ice lens theory for frost heave in soils. *Canadian geotechnical journal*, *28*(6), 843-859.

Oman, M. S., Lund, N. G., & Intertec, B. (2018). *Designing base and subbase to resist environmental effects on pavements* (No. MN/RC 2018-06). Minnesota. Dept. of Transportation. Research Services & Library.

Ovik, J. M., Siekmeier, J. A., & Van Deusen, D. A. (2000). Improved spring load restriction guidelines using mechanistic analysis.

Papuc, D. (2021). *Laboratory and full-scale pavement sections testing for evaluating frost action in cold regions*. Rowan University.

Peterson, R. A., & Krantz, W. B. (2003). A mechanism for differential frost heave and its implications for patterned-ground formation. *Journal of Glaciology*, *49*(164), 69-80.

Richter, C. A. (2006). *Seasonal variations in the moduli of unbound pavement layers* (No. FHWA-HRT-04-079). United States. Federal Highway Administration.

St-Laurent, D., & Roy, M. (1995). *Evaluation structurale de chaussees souples dans un contexte climatique nordique*. Universite Laval.

Uduebor, M., Adeyanju, E., Saulick, Y., Daniels, J., & Cetin, B. (2022). A review of innovative frost heave mitigation techniques for road pavements. In *International Conference on Transportation and Development 2022* (pp. 95-106).

Uduebor, M., Daniels, J., Saulick, Y., Naqvi, W., & Cetin, B. (2023). Optimization of water repellency in soils for geotechnical applications. *International Journal of Geotechnical Engineering*, 1-11.

U.S. Army, "Soils and geology: Pavement design for frost conditions.," US Army Corps of Engineers, Washington, DC., 1965.

White, T. D., & Coree, B. J. (1990). Threshold pavement thickness to survive spring thaw. Third international conference on bearing capacity of roads and airfields. Proceedings, Norwegian Institute Of Technology, Trondheim, Norway, July 3-5 1990. VOLUMES 1-2. *Publication of: Tapir Publishers*.

Zhou, J., & Li, D. (2012). Numerical analysis of coupled water, heat and stress in saturated freezing soil. *Cold Regions Science and Technology*, *72*, 43-49.

Zydex. (2016). Safety data sheets: Terrasil. https://asmg.com/wp-content/uploads/2020/10/Terrasil_SDS.pdf

CHAPTER 5: LIFE CYCLE ASSESSMENT (LCA) AND LIFE CYCLE COST ANALYSIS (LCCA) OF EWR APPLICATIONS

COMPARATIVE LIFE CYCLE ASSESSMENT AND COST ANALYSIS OF FROST-RESISTANT GRAVEL ROAD TREATMENTS IN RURAL IOWA

Abstract

Gravel roads are vital to rural transportation, supporting industrial, agricultural, and residential activities. In Keokuk County, Iowa, 78% of the roads are gravel and require frequent maintenance due to their non-frost-resistant nature. This study evaluates typical gravel roads (2-lane, 1-mile) and four frost-resistant alternatives using Life Cycle Assessment (LCA) and Life Cycle Cost Analysis (LCCA). The scenarios include standard gravel (regrade), gravel with a macadam base, chemically stabilized roadstone, and two EWR treatments (spray and compacted). Primary data were collected from the County Engineering Office, with LCA modeling performed using the FHWA LCA PAVE tool and economic impact assessed via Net Present Value (NPV) following ISO 15686-5. A spend-based approach integrated financial and environmental costs. Gravel roads with chemicals emerged as the most sustainable and cost-effective, with regrade being 45% more expensive and generating 47% more emissions. The primary emission source was material transportation, comprising 52-67% of total emissions, with the 4-inch roadstone being the major contributor. Raw material costs accounted for 67-80% of NPV, while transportation represented 15-26%. The LCA contributed less than 8% to the total integrated cost, highlighting the dominance of LCCA in decision-making. The study recommends low-cost performance evaluations, such as the International Roughness Index (IRI), to enhance maintenance and repair strategies.

Keywords: Gravel Roads, Life Cycle Assessment (LCA), Life Cycle Cost Analysis (LCCA), Frost Resistance

5.1 Introduction

Gravel roads are a critical component of the national transportation network, facilitating industrial, agricultural, and residential activities. Generally, gravel roads provide the lowest level of service to the traveling public, making paving them economically unfeasible. In some counties, economic constraints mean gravel roads are the primary type of road that can be provided (FHWA, 2015). The U.S. Department of Transportation's Bureau of Statistics (BTS) reports that, as of 2020, 1.317 million miles of roads, or 32% of all roads in the United States, remain unpaved (BTS, 2021). These unpaved low-volume roads are mainly gravel roads, with an average daily traffic (ADT) of about 150 vehicles per day. In Iowa, 60% of its entire road network (IowaDOT, 2022) and 74% of its rural roads (IowaDOT, 2024) are gravel roads. The pavement section analyzed for this paper is in Keokuk County in Iowa, where 78% of roads maintained by county engineers are gravel roads (IowaDOT, 2021).

Gravel roads typically consist of a gravel surface layer on top of a subgrade layer and require constant maintenance and dust control. When properly maintained, these roads can serve light, low-volume traffic. When exposed to heavy traffic, gravel roads with weak subgrade and marginal gravel depth can fail for rutting and gravel displacements. Due to these failure mechanisms, gravel roads require routine maintenance through blading or reshaping, regardless of the traffic volume experienced. In 2020, it was estimated that Iowa's county road departments spent over $35 million on maintenance for blading and $110 million on resurfacing (Ceylan & Kim, 2021). Figure 5.1 shows the cost of two Class A gravel roads, RD2201 and RD1201, which are compared in terms of material, equipment, and labor for 2019 and 2020 (collected from the Keokuk County Engineering Department). These gravel roads have little resistance to frost action, necessitating significant repair costs after severe frost boils in 2019 and mild weather in 2020. Based on Figure 5.1, severe frost action leads to 1.7 to 2.3 times more immediate maintenance costs for RD 2201 and RD 1201 for 2019 and 2020, respectively.

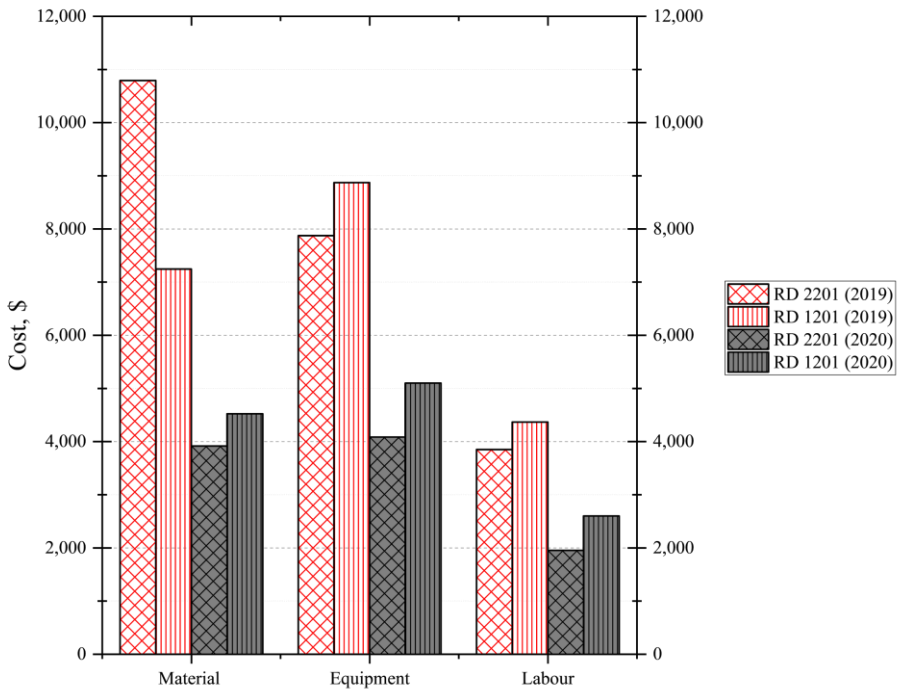

Figure 5.1: The maintenance cost of two Class A gravel roads in Iowa

County engineers are constantly exploring different methodological alternatives to improve road conditions in search of more economical yet equally or better-performing gravel roads with lower maintenance requirements, especially after severe frost action. To date, such methods include modifying the typical gravel road layers, which involves adding a macadam base, stabilizing the surface gravel layer, or modifying the subgrade to increase pavement depth, improve subgrade stiffness, or minimizing water infiltration and seepage.

While the performance of the gravel roads is the primary concern to the public due to its impact on safety, both performance and cost are of significant concern to county engineers. Using macadam and hydrophobic and stabilizing chemicals such as Organosilane (OS) or Base One for stabilization or modification leads to consuming virgin materials and emissions from stabilizer production, but they provide a more durable road. However, they also add to the initial economic burden.

5.2 Objectives

While there is a call from the Federal Highway Administration (FHWA) to embrace road sustainability at the Federal level (FHWA, 2014; FHWA, 2024), few studies focus on gravel roads despite the significant number of miles of unpaved roads across the country. Independent studies focus on either Life Cycle Assessment (LCA) or Life Cycle Cost Analysis (LCCA) without merging them in a comprehensive evaluation. Therefore, from a holistic perspective, combining the economic and environmental impacts of different alternatives is necessary.

This study reports the results of cradle-to-gate life cycle assessment and life cycle cost analysis of five different pavement alternatives for gravel roads. These five gravel roads were designed and constructed due to the necessity of Keokuk County engineers to evaluate more efficient ways to reduce maintenance costs and activities due to damage from frost boils. The constructed gravel pavements located in Keokuk County are illustrated in Figure 5.2. Figure 5.2a shows the regrade gravel road. This is the typical no-frost-resistant gravel road with two layers of subgrade and roadstone, predominantly used in Iowa. Figure 5.2b shows the second pavement (GRWMB), which includes an additional 6 inches of Macadam base layer between the subgrade and gravel roadstone. Figure 5.2c presents the third pavement (GRWCT), with two layers, similar to the typical gravel road, but the roadstone is stabilized with Base 1 chemical to a depth of 4.5 inches. Figure 5.2d presents the Engineered Water Repellency (EWR) spray treatment (EWRST). Figure 5.2e presents the EWR compacted treatment (EWRCT). The subgrades were modified with an EWR treatment to prevent frost action by limiting water migration. The EWRST was applied by spraying the subgrade with OS, and the EWRCT was applied by mixing a 6-inch lift of subgrade with OS and recompacting it. The constructed roads represent typical Iowa rural low-volume roads with an overall width of 29 ft.

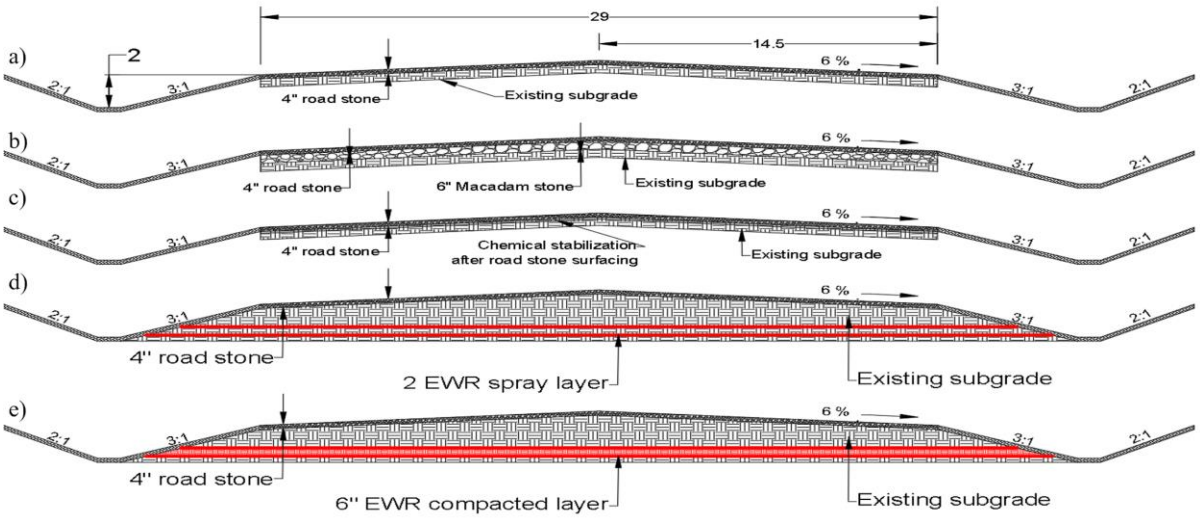

Figure 5.2: Pavement structures evaluated, a) Regrade, b) Gravel road with macadam base (GRWMB), c) Gravel road with chemical treatment (GRWCT), d) EWRST, and e) EWRCT

5.3 Materials and Methods

Table 5-1 presents the measured subgrade and specifications limits for aggregate gradations for all gravel roads studied. The in-situ subgrade is classified as low-plasticity clay (CL) according to the Unified Soil Classification System (USCS) (ASTM D2487, 2017) and A-6 based on the American Association of State Highway and Transportation Officials (AASHTO) (AASHTO 2021). Based on the soil classification, it is considered an F4 based on the frost susceptibility index (USACE, 1965). Roadstone and macadam meet Iowa DOT specifications under sections 4120.04 and 4122.02, respectively (IowaDOT, 2024).

Table 5-1: Subgrade, Macadam, and Roadstone gradation

	% Passing		
Standard sieve no.	Measured	Specs. Limits	
	Subgrade	Macadam stone	Roadstone
1 in	100	100	100
3/4 in	100	16-6	100-95
1/2 in	100	-	90-70
3/8 in	100	-	-
No.4	100	-	55-30
No. 8	100	-	40-15
No.10	94	-	-
No.40	93	-	-
No.60	93	-	-
No.100	92	-	-
No.140	92	-	-
No.200	92	-	16-6

Terrasil from Zydex Industries, a commercially available Organosilane (OS), was utilized to induce hydrophobicity in the EWRST and EWRCT subgrade soils. For the EWRST and EWRCT, 2.69 and 8.07 tons of OS were used, respectively. For GRWCT, the 4 inches of roadstone and 0.5 inches of subgrade were stabilized with Base One. Base One is a base and aggregate surface stabilizer sprayed and hogged at 0.005 gal/sy/following Keokuk country specifications.

Figure 5.3 illustrates the methodological framework adopted in this study. Primary data inputs for the LCA and LCCA modeling were gathered from the Keokuk County Engineering office. The life cycle assessment was modeled using the FHWA LCA PAVE tool. The LCCA was calculated based on the Keokuk country labor rate, equipment and transportation, and manufacturer material costs.

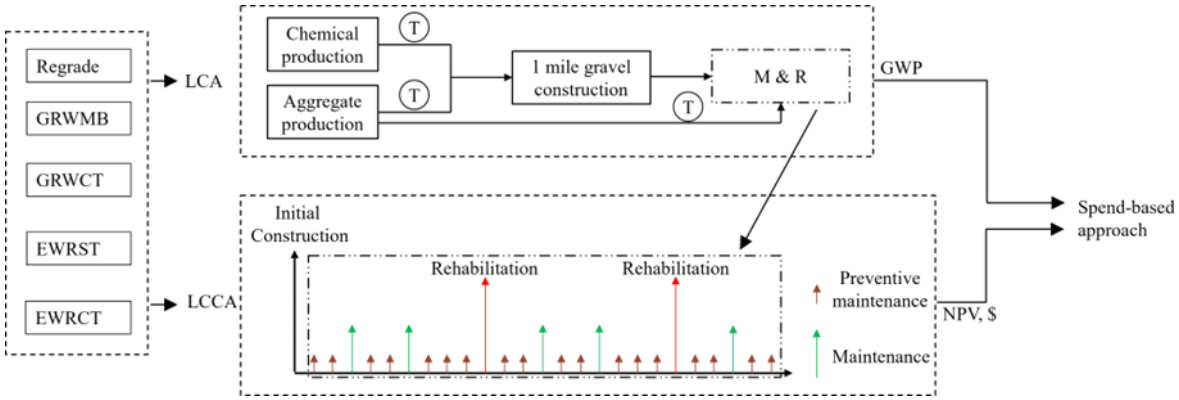

Figure 5.3: Methodological framework of the study

5.4 Life Cycle Assessment (LCA)

5.4.1 Goal and Scope

The main objective of this study is to evaluate the life cycle of different gravel road alternatives that are typically constructed in rural areas in terms of cost and environmental impacts. LCA addresses the environmental aspects and potential environmental impacts throughout a pavement's life cycle, from raw material acquisition through production, use, transportation, construction maintenance, preservation, and rehabilitation. To achieve this goal, the LCA was conducted following the ISO14040 and ISO 14044 to normalize the total environmental impacts into an environmental pollution index using site-specific primary data, paying particular attention to transportation-related and chemical impacts (Qiao et al., 2022).

This study evaluated five constructed gravel roads in Iowa using different frost mitigation approaches with expected similar performance. The defined functional unit is a 2-lane, 1-mile-long, 14.5-ft-wide low-volume gravel road with an average daily traffic (ADT) of 80 vehicles (15% truck). A localized sensitivity analysis was also performed to determine the effect of hydrophobic and stabilizing chemicals and haulage distance on the overall GWP values.

5.4.2 System Boundaries

The system boundary is presented in Figure 5.4. Five life cycle stages are considered: (1) raw materials production, (2) materials transportation, (3) construction, (4) maintenance, and (5) rehabilitation. The end-of-life stage is not included, as the gravel road at the end of the analysis period forms the foundation for reconstruction. The analysis period is defined as twenty-five years because GRWMB and GRWCT had rehabilitation at twenty years. The raw material production entails extraction and process used in all other stages (i.e., construction, maintenance, and rehabilitation). Likewise, material transportation encompasses all construction material transportation for initial construction, maintenance, and rehabilitation.

The construction entails all equipment operation during initial construction. The maintenance stage considers the routine reblading and reblading with 300 tons of roadstone, while the rehabilitation phase involves reconstruction where blading, compaction, and four inches of roadstone were done except for the GRWCT, where Base One stabilizing chemical was utilized again on the surface layer. Blading for snow removal was excluded as it has no direct correlation with pavement type or performance. Supporting facilities such as streetlights, signs, drains, and structures are excluded, as the same configuration is expected in all pavement types.

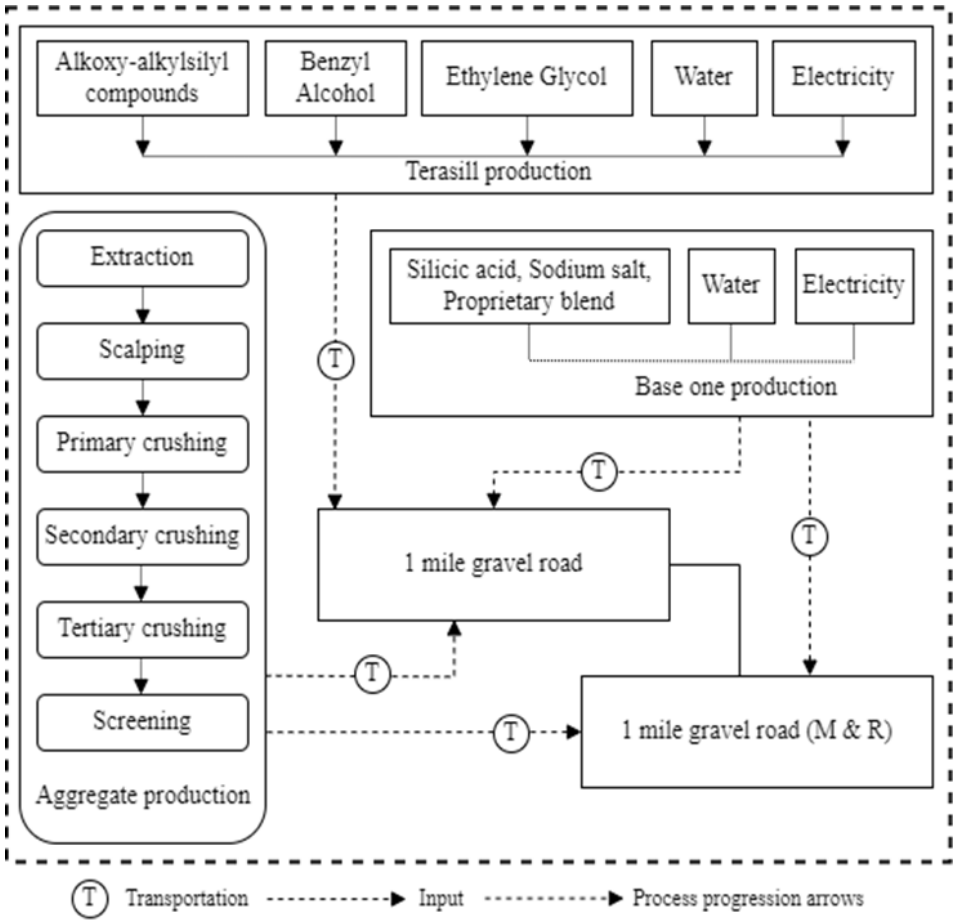

Figure 5.4: LCA system boundaries

5.5 Impact Assessment Methodology

The analysis presented in this study relied on the IPCC 2013 100a impact assessment methodology, which utilizes global warming potential (GWP) as the primary indicator to determine the environmental impacts over the 25-year analysis period. The GWP, expressed in kg CO_2 eq, measures how much a specific gaseous emission contributes to global warming relative to the carbon dioxide.

5.5.1 Pavement Sections and Life Cycle Assessment Inventory

The LCI data utilized to model the foreground system were collected from the Keokuk Country Engineering Office, Iowa, and FHWA LCA PAVE. For each gravel road, the quantities of the materials, which include aggregates and hydrophobic (OS) and stabilizing (Base One) chemicals, were calculated according to the Iowa DOT information and summarized in Table 5-2.

Table 5-2: Quantification of material used for each section (1-mile).

	Density (pcf)	Regrade	GRWMB	GRWCT	EWRST	EWRCT
6" Macadam (ton)	130.0	0	4,976	0	0	0
4" roadstone (ton)	140.0	12,218	8,346	8,3460	9,246	8,346
OS (ton)	69.3	0	0	0	2.69	8.07
Base One (ton)	87.9	0	0	2.33	0	0
Water (ton)	62.4	0	0	45.68	46	65.46

The LCI phase includes collecting, describing, and verifying all crucial information, such as materials and equipment operating time. Additionally, the data sources depend on several models chosen to simulate the analyzed processes in the subsystems that comprise the entire system. Two major sources of information were used in this study. Primary data was obtained from Keokuk County, which includes construction schedules, equipment operating hours, and site-specific information. Secondary data, which refers to material or equipment emission or unit energy demand, was obtained from the FHWA LCA Pave tool.

Raw material production phase

The main materials utilized throughout the analysis are virgin aggregates (roadstones and Macadam), Base One chemical, and Organosalines (Terrasil). The virgin aggregates were modeled as base and subbase materials using the FHWA LCA Pave tool, while both Base One and Terrasil were initially modeled by assigning a fixed value of GWP equal to 392 kg CO_2 eq. This hypothesis was necessary since no official EPD exists for either chemical. However, the authors realize that the impact of these assumptions must be evaluated. Hence, an analysis of the sensitivity of GWP results to the environmental impacts of these chemicals is later provided in the document.

Transportation phase

This phase assesses the transportation of various raw (virgin aggregate and chemicals) to the construction site. All aggregates in this study came from a River Products Company quarry, 6.4 miles from the site. The county utilizes a 20-ton Mack GR84F (425 horsepower); hence, an off-highway truck, nonroad (300 < hp <= 600), was used. The Base One and OS chemicals were obtained from the manufacturer's

warehouse located in the US and transported using a combination truck (diesel) to model the environmental burdens. Their warehouses were 1,000 and 2,000 miles from the site, respectively. All equipment used in construction came from the Keokuk County Office and Maintenance Facility, located 12.8 miles from the test site. A haulage distance sensitivity analysis was conducted to observe the effect of virgin aggregate transportation to the site.

Construction phase

The fuel consumption of various construction machines, such as motor graders, trucks, rollers, and wheel loaders, cause environmental burdens during the construction phase. All equipment utilized in this study is diesel-powered. Table 5-3 summarizes all emissions related to the performance of each construction machine. These were determined by combining LCI data from the FHWA LCA PAVE database.

Table 5-3: Construction equipment specification used

Type	Model	Horsepower (hp)	FHWA LCA Pave equivalent
Excavator	Caterpillar 320 GC	146	Guillotine, Nonroad Diesel Fuel, 175 < hp <= 300
Grader	Caterpillar 150	200	Tractors/Loaders/Backhoes, Nonroad Diesel Fuel, 175 < hp <= 300
Water tank	Mack GR84F	425	Paving Equipment, Nonroad Diesel Fuel, 300 < hp <= 600
Sheep roller	Pull behind John Deere tractor 7220	110	Rollers, Nonroad Diesel Fuel, 100 < hp <= 175
Truck	Mack GR84F	425	Off-highway Trucks, Nonroad Diesel Fuel, 300 < hp <= 600
Front-end loader with road hog	Caterpillar 938M	188	Guillotine, Nonroad Diesel Fuel, 175 < hp <= 300

Maintenance and rehabilitation (M&R) phases

Table 5-4 presents a summary of the expected maintenance schedule. Preventive maintenance (P), maintenance (M), and rehabilitation (R) routines were selected based on standard practices utilized by Keokuk County, Iowa. According to Keokuk County's typical maintenance plan, every gravel road would be rebladed annually at least twice as preventive maintenance (P). At determined regular intervals, 300 tons of roadstone are added per 1-mile section to fill potholes or rutted areas. Based on the information provided, the maintenance schedule below will provide sections with similar performance.

Limitations of the LCA framework

The analysis period for this study spans 25 years, a timeframe long enough to encompass significant technological and societal advancements in areas such as construction material, equipment and methodologies, energy sources and efficiencies, carbon capture technologies, and discount rates (Qiao et al., 2022). With the rapid progress of new energy sources, the phase-out of diesel-powered vehicles is expected, impacting GWP. Also, the rehabilitation stage had no subgrade modification with only 4 inches of roadstone "overlay." This study does not consider the impact of heavy farm equipment causing rutting, leading to higher maintenance costs, and carries out specific local sensitivity analysis for chemical use and haulage.

Table 5-4: Maintenance and rehabilitation plan based on local county schedule.

No of years	Regrade	GRWMB	GRWCT	EWRST	EWRCT
1	#	#	#	#	#
2	#	#	#	#	#
3	# + 300 tons	#	#	# + 300 tons	#
4	#	#	#	#	#
5	#	# + 300 tons	# + 300 tons	#	# + 300 tons
6	# + 300 tons	#	#	# + 300 tons	#
7	#	#	#	#	#

8	#	#	#	#	#
9	#	#	#	# + 300 tons	#
10	**	# + 300 tons	# + 300 tons	#	# + 300 tons
11	#	#	#	#	#
12	#	#	#	# + 300 tons	#
13	# + 300 tons	#	#	#	#
14	#	#	#	#	#
15	#	# + 300 tons	# + 300 tons	***	***
16	# + 300 tons	#	#	#	#
17	#	#	#	#	#
18	#	#	#	# + 300 tons	#
19	#	#	#	#	#
20	***	***	***	#	# + 300 tons
21	#	#	#	# + 300 tons	#
22	#	#	#	#	#
23	# + 300 tons	#	#	#	#
24	#	#	#	# + 300 tons	#
25	#	# + 300 tons	# + 300 tons	#	# + 300 tons

= blade twice, # = blade twice plus add 300 tons of roadstone. Rehabilitation (***) for all cases revolves blade twice and 4” roadstone.

5.5.2 Life Cycle Cost Analysis (LCCA)

LCCA was carried out following ISO 15686-5 framework and FHWA LCCA guide, summing the life cycle costs of pavements using Net Present Value (NPV). LCCA is defined as a process to evaluate the total economic worth of a usable project segment by analyzing initial costs and discounted future costs, such as maintenance, user, reconstruction, rehabilitation, restoring, and resurfacing costs, over the life of a project segment (Walls, 1998; Airfield Asphalt Pavement Technology Program [AAPTP], 2011).

Conversely, the life cycle cost assessment was conducted following the ISO 15686-5 framework and FHWA LCCA guide, summarizing the pavements' life cycle costs using Net Present Value (NPV). The

pavement cost was evaluated using the same analysis periods of 25 years of the LCA analysis. All inputs such as raw materials, construction schedule and methodology, and maintenance and rehabilitation plan used for LCA were utilized for LCCA. The net present value (NPV) was utilized as the economic indicator to evaluate the economic impact using Equation 1. NPV was selected because it utilizes a single value to specify the total cost throughout the analysis period while considering the time value of money (Azadgoleh et al., 2024). In this study, a discount rate of 1% was considered. It is worth noting that a low discount rate is a safe choice as it represents a pessimistic scenario.

$$NPV = \sum_{n=0}^{T} \left(\frac{(C_C + M_C + R_C) - Salvage\ value}{(1+d)^t} \right) \quad \text{(Equation 1)}$$

Where:

NPV = net present value of the pavement life cycle costs ($);

T = Analysis period (25 years).

t = Years after construction (year).

C_C = Construction costs in year t ($).

M_C = Maintenance cost in year t ($).

R_C = Rehabilitation Cost in year t ($).

d = Discount rate (1%).

When a road pavement reaches its service life, it will remain in place; hence, the salvage value is given by the remaining service life value (Equation 2) (Yan et al., 2023; Azadgoleh et al., 2024).

$$Salvage\ value = C_{Last\ Activity} \times \frac{N_{RL}}{N_{SL}} \quad \text{(Equation 2)}$$

Where, $C_{Last\ Activity}$= Cost of the last rehabilitation activity, N_{RL}= Unused service life, in years, of the last activity at the end of the Analysis Period, and N_{SL}= Service life of the last activity in years.

5.5.3 Spend-Based Normalization of Environmental Impacts

A spend-based approach was utilized to integrate the LCCA and LCA calculations. This method was selected as appropriate because both LCCA and LCA employed the same data and assumptions for their respective analyses. Specifically, the GWP emissions were normalized into monetary costs by

converting the GWP, in kg CO_2 eq values, to tons CO_2 eq and then assigning a price per ton of CO_2 as shown in Equation 3. A conversion rate of $185 per ton of CO_2 was used based on a study by Rennert et al. (2022).

This monetary conversion enabled the integration of environmental impacts into the economic analysis. The resulting cost from the GWP emissions was then added to the calculated LCCA cost, allowing for a comprehensive assessment that incorporates both financial and environmental considerations.

The calculation for the spend-based cost is as follows:

$$Spend - based\ cost = \frac{GWP, kg\ CO_2\ eq}{1000} * \$185 \qquad \text{(Equation 3)}$$

By integrating the GWP cost into the LCCA, the analysis provided a more holistic view of the project's overall impact, encompassing economic and environmental dimensions. This approach ensures that decision-making processes consider the direct financial costs and the broader environmental consequences, promoting sustainable development practices.

5.6 Results and Discussion

5.6.1 Life Cycle Assessment

The results of the LCA are presented in Figure 5.5. The representation with primary and secondary vertical axes provides the overall GWP magnitude of the sections evaluated, as well as the GWP values normalized based on the regrade, i.e., expressed in percentage of the typical gravel road pavement in Iowa. The GRWMB had the highest contribution by +11% more than the regrade option. Impacts below the regrade option were observed for both EWRCT and EWRST, at -11%, and -18% for GRWCT.

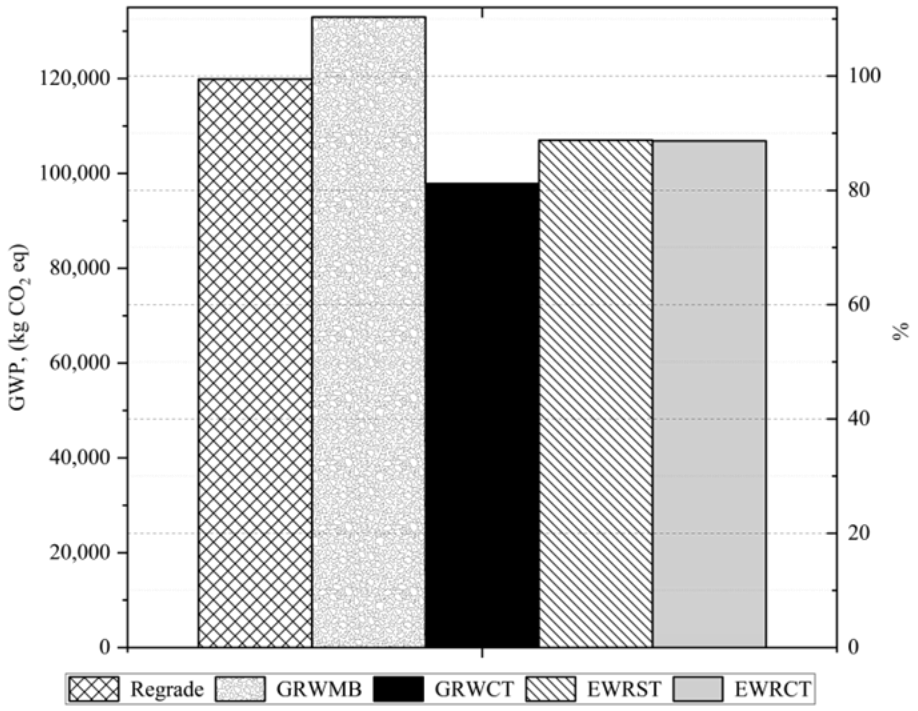

Figure 5.5: Comparison of normalized impact indicator values for each alternative.

The higher value of GWP calculated for the GRWMB is primarily due to the 6 inches of macadam used throughout its life cycle. The lower impact observed in the GRWCT that using stabilized roadstone without additional virgin aggregates can significantly reduce GHG emissions with equal performance. The EWR-treated gravel roads show a lower impact than regrade because only one rehabilitation is required to maintain the road. It is worth noticing that the benefit estimated for the chemically treated gravel road is highly dependent on the specific stabilizer used. For instance, cement-stabilized roadstone (assuming its

adequate performance) would increase the GWP to over 120,000 kg CO_2 eq, negating its low emission advantage.

Figure 5.6 shows the GWP breakdown by cycle of the pavement service life. Material production and transportation (used for construction, maintenance, and rehabilitation) account for between 74,000 to 114,500 kg CO_2 eq (71% and 88%) of all GHG emissions across all cases, with material production contributing an average of 22,430 kg CO_2 eq (21%). Furthermore, construction (equipment transportation and operation) accounts for 2,965 to 20,188 kg CO_2 eq (2.5% to 19% of the total emission). The impact of construction on regrade, GRWMB, and GRWCT is less than 9,000 kg CO_2 eq, but it ranges between 15,000 and 21,000 kg CO_2 eq in EWRST and EWRCT. Figure 5.6 shows the contribution of equipment transportation and operation during the maintenance (M) and rehabilitation (R) stages (excluding associated material production and material transport). The equipment emissions in both M&R stages range from 5,981 to 6,241 kg CO_2 eq and 4,409 to 8,816 kg CO_2 eq, respectively. Including M and R's associated material production and transport (initially embedded in material production and transportation) increases its contribution to 16,541 to 24,268 kg CO_2 eq and 35,122 to 67,356 kg CO_2 eq. This impact of maintenance and rehabilitation (including material production and transportation) is more pronounced in regrade, accounting for 86,213 kg CO_2 eq (72%) of its total emission. However, GRWMB had the least impact from M&R, primarily due to huge macadam usage during initial construction.

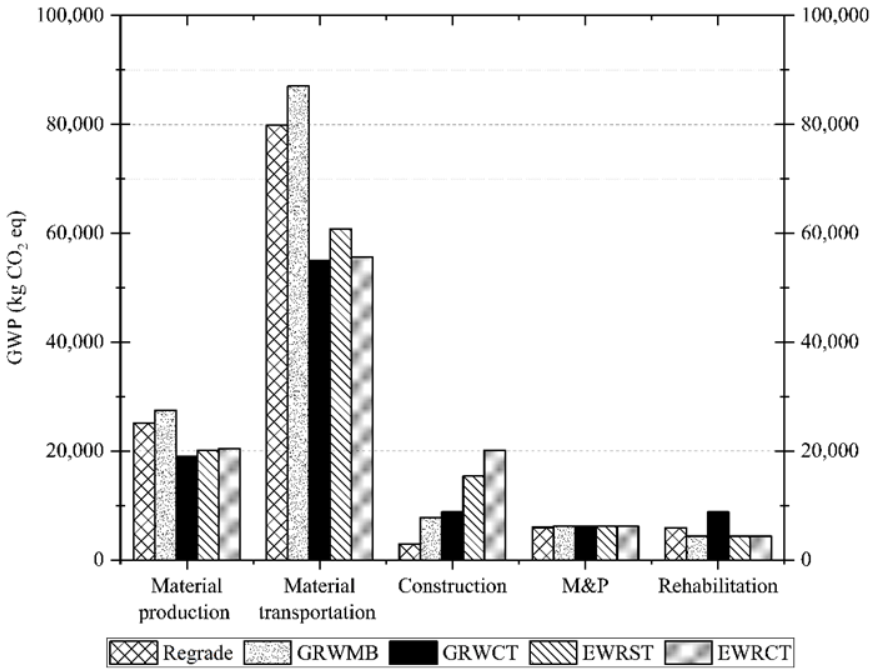

Figure 5.6: Breakdown of different activities leading to GWP (kg CO_2 eq) by life cycle

Figure 5.7 shows the GWP breakdown by process type (material, equipment, and transportation). Material and equipment transportation is the main driver of GWP, contributing between 60,314 and 91,620 kg CO_2 eq. Within the transportation category, material transport accounts for more than 92% of this category's emissions, ranging from 54,934 to 87,030 kg CO_2 eq. Material is the second driver for regrade and GRWCT accounting for 25,161 and 27,434 kg CO_2 eq, respectively. However, for GRWCT, EWRST, and EWRCT, equipment operation is the second main emission source at 19,281 to 26.168 kg CO_2 eq. The activities related to 4-inch roadstone contributed 92,139 kg CO_2 eq (76%) in regrade and 61,426 kg CO_2 eq, which represents 46%, 63%, 57%, and 58% of total GHG emissions in GRWMB, GRWCT, EWRST, and EWRCT, respectively. A single 4-inch roadstone consists of 7,357 kg CO_2 eq from material production and 23,356 kg CO_2 eq from material transportation. The diminished impact of 4 inches of roadstone in the GRWMB is attributed to the impact of macadam, which contributed 10,248 kg CO_2 eq from material production and 32,490 kg CO_2 eq from transportation. In other options, chemical stabilization in GRWCT and OS-related activities in EWRCT and EWRST (OS application and soil excavation and backfill) accounted for 11,076 kg CO_2 eq (11%) and 13,9846 to 21,527 kg CO_2 eq (13 to 20%) respectively.

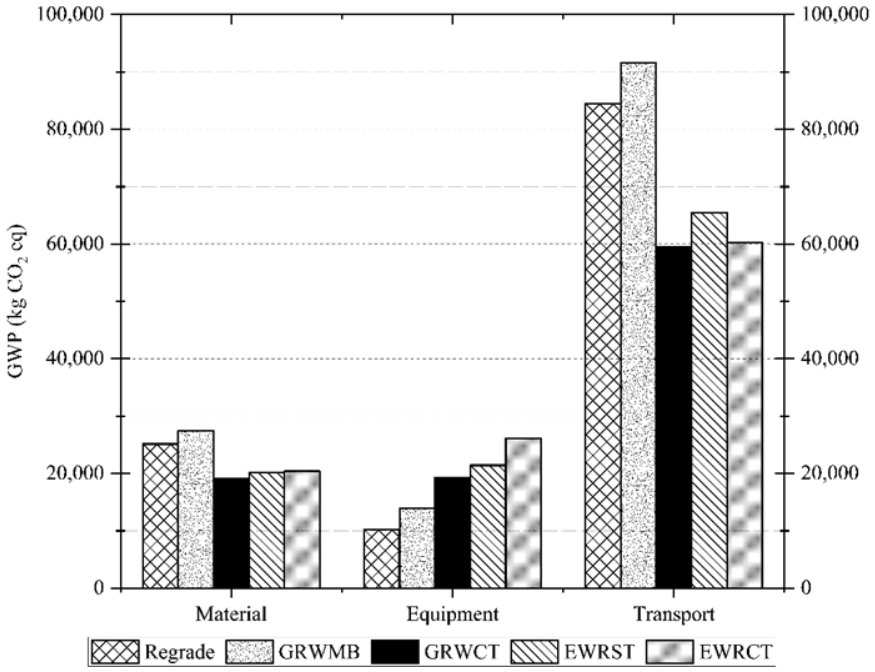

Figure 5.7: Breakdown of different activities leading to GWP (kg CO2 eq) by process type

The breakdown of the various activities leading to GWP is illustrated in Figure 5.8. It is evident that regardless of the pavement option, the primary source of emissions is associated with the use of a 4-inch roadstone, occurring three times in regrade and twice in other scenarios. A deeper dive into the 4-inch roadstone placement reveals that transporting the roadstone to the site accounts for 23,356 out of the 29,428 kg CO_2 eq, 76% of the emissions, assuming a quarry distance of 6.3 miles. Notably, the impact of transportation scales significantly with distance, resulting in emissions of 26,418 kg CO_2 eq (78%) at 10 miles, 32,245 kg CO_2 eq (81%) at 15 miles, 45,065 kg CO_2 eq (85%) at 30 miles, and 62,158 kg CO_2 eq (89%) at 50 miles. It is important to note that while transportation emissions escalate with distance, production emissions remain constant, as illustrated in Figure 5.9.

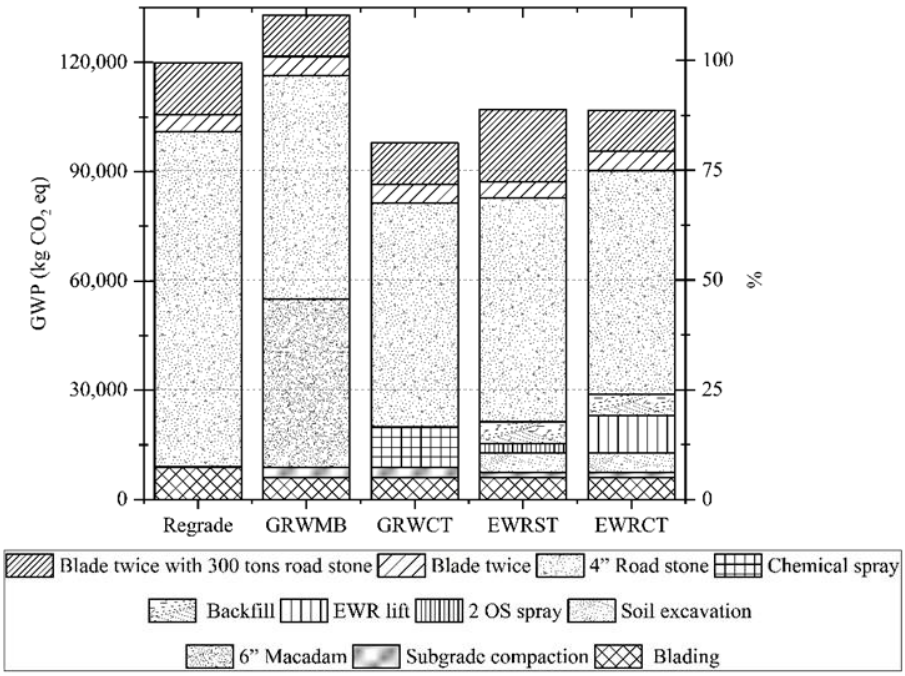

Figure 5.8: Breakdown of different activities leading to GWP (kg CO_2 eq)

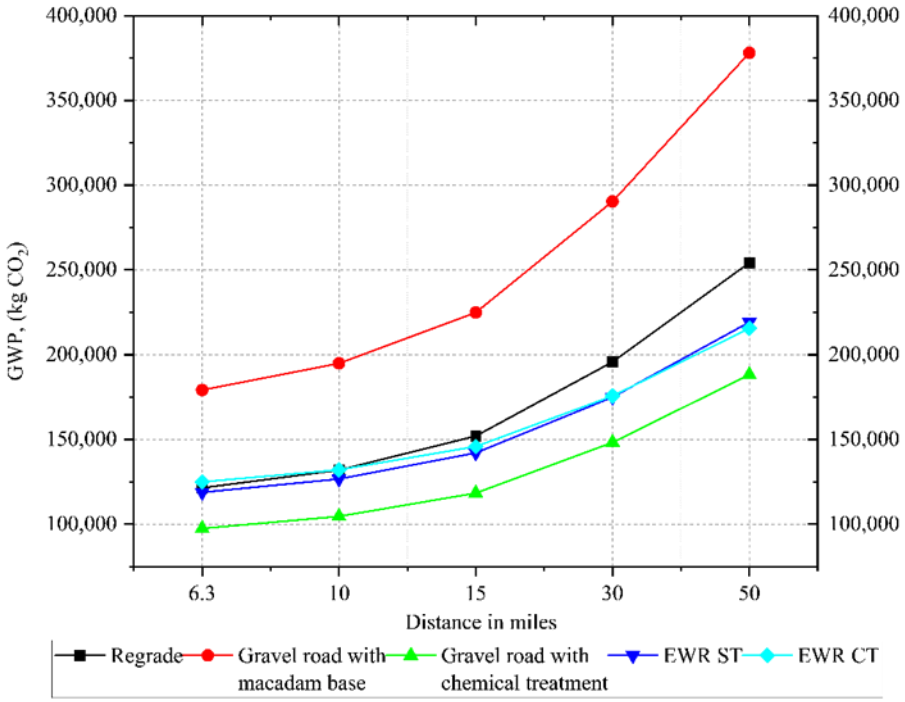

Figure 5.9: Effect of haulage distance on Total GWP.

Figure 5.10 shows the effect of global warming impact indicator of chemicals on Total GWP. As no EPDs exist for the chemicals used, 392 kg CO_2 eq was assumed for 1 short ton of chemical used. Based on this assumption, the GWP of EWRCT, EWRST, and GRWCT are between 11 and 18% compared to

regrade, where no chemicals were used. Additionally, reducing the assumed global warming impact indicator (GWII) from 392 kg CO_2 eq to 150 kg CO_2 eq and 15 kg CO_2 eq resulted in a 1-2% reduction compared to the regrade option. The maximum reduction below the regrade option for both EWRCT and EWRST were 13% and 12%, respectively, and 20% for the GRWCT. As expected, an increase in GWII of the chemicals will erode the sustainability of these alternatives. For 1500 kg CO_2 eq simulation, all alternatives were still below the level of the regrade, with EWRCT and EWRST at 3 and 8%, respectively, and 14% for the GRWCT. From a much higher GWII, only EWRCT exceeds regrade by 7 %, moving its emission from 106,868 kg CO_2 eq to 127,915 kg CO_2 eq. Other alternatives, such as EWRST and GRWCT, still had emissions below regrade at 5 and 8%, respectively. The significant impact of higher GWII is due primarily to the amount of chemical use. The significant impact of the higher global warming impact indicator primarily stems from the amount of chemical use. This is evident as an additional 21,000 kg CO_2 eq was added when the GWII was changed from 392 to 3000 kg CO_2 eq. However, in EWRST and the GRWCT, only 7000 and 12,000 kg CO_2 eq were added in the exact scenarios. However, in EWRST and GRWCT, only 7,000 and 12,000 kg CO_2 eq were added in the exact scenarios.

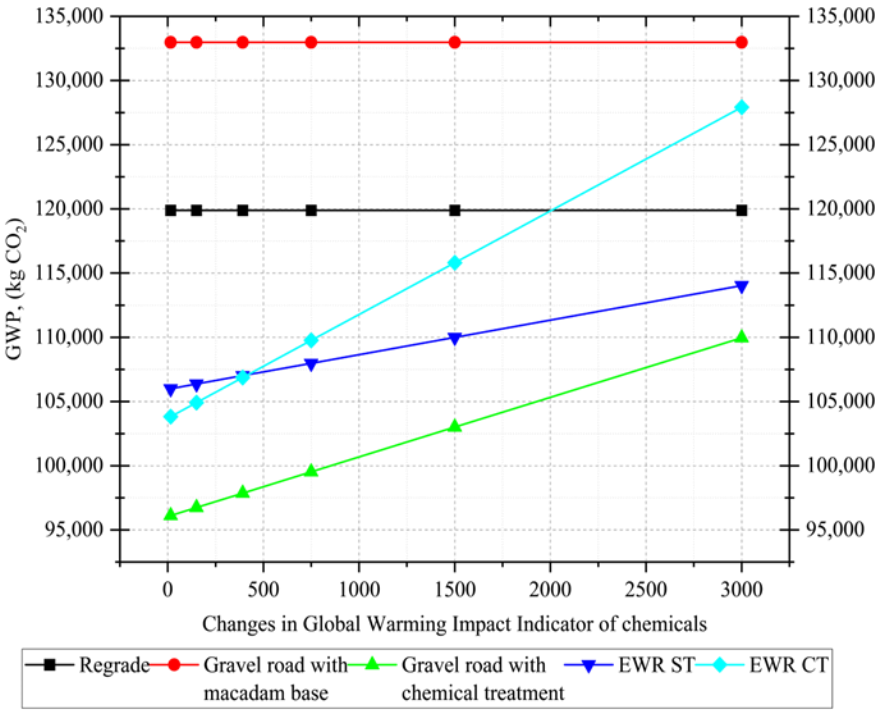

Figure 5.10: Effect of GWII of chemicals on Total GWP.

5.6.2 Life Cycle Cost Analysis

The results of the LCCA analysis are presented in Figure 5.11. The analysis indicates that the GRWCT had the lowest net present value (NPV). When breaking down the cost components considered in calculating the NPV of each pavement structure, it was found that the cost of raw materials and the transportation of these materials to the site constitute the most significant portion of the final NPV. Specifically, the raw material cost accounts for $182,608 (70%), $206,689 (76%), $141,295 (80%), $167,068 (63%), and $207,536 (67%) of the NPV for regrade, GRWMB, GRWCT, EWRST, and EWRCT, respectively. Similarly, the transportation of materials represents $48,103 (19%), $71,842 (26%), $45,138.52 (26%), $50,594 (19%), and $45,966 (15%) of the NPV for these same structures. This highlights that most of the life cycle cost is dominated by the procurement and transportation of raw materials, underscoring the importance of optimizing these components to achieve cost-effective pavement solutions. Initial construction costs account for 67 to 80% ($118,816 to $246,000) of the total cost in all alternatives, except for regrade, which accounts for only 37% ($94,693).

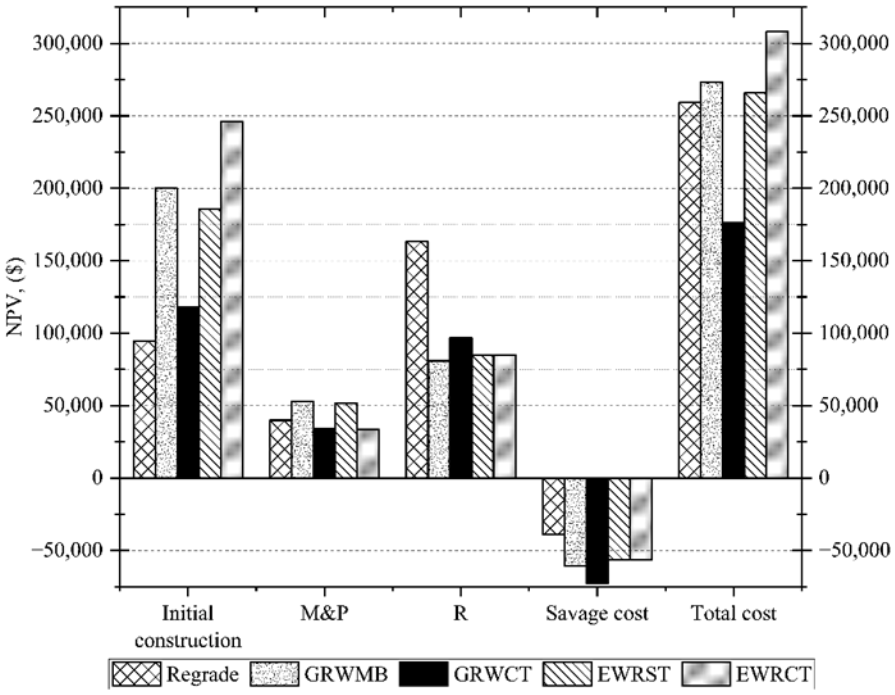

Figure 5.11: LCCA Net Present Values (NPVs) results

Among all the alternatives, regrade is the cheapest to build initially, while EWRCT is the most expensive at $246,000. However, when rehabilitation is considered, regrade becomes the most expensive, based on the cost of reconstruction per decade, while EWRCT is the cheapest. Regarding maintenance, GRWMB are the most expensive to maintain at $52,995, while EWRCT is the cheapest at $33,794. The breakdown of the various activities leading to NPV is illustrated in Figure 5.12. The cost of 4 inches of roadstone-associated activities is the predominant driver of costs across all sections. This impact is particularly significant in the regrade option, accounting for 84% of the total cost due to the utilization of a total of 12 inches of gravel throughout the analysis period. Conversely, in the GRWMB, roadstone accounts for only 53% of the total cost, with the macadam base itself contributing 44%. In other options, chemical stabilization and OS-related activities have substantial impacts. Specifically, in the GRWCT, chemical stabilization accounts for $35,171, representing 20% of the total cost. In the EWRST and EWRCT options, OS-related activities, including OS application, soil excavation, and backfill, account for $91,122 to $151,307, representing 34% to 49% of the total cost, respectively. Overall, blading and subgrade

compaction are relatively minor across all treatment options. The high salvage cost savings of $60,668 were observed in GRWMB, while regrade had the lowest salvage cost savings at $38,802.

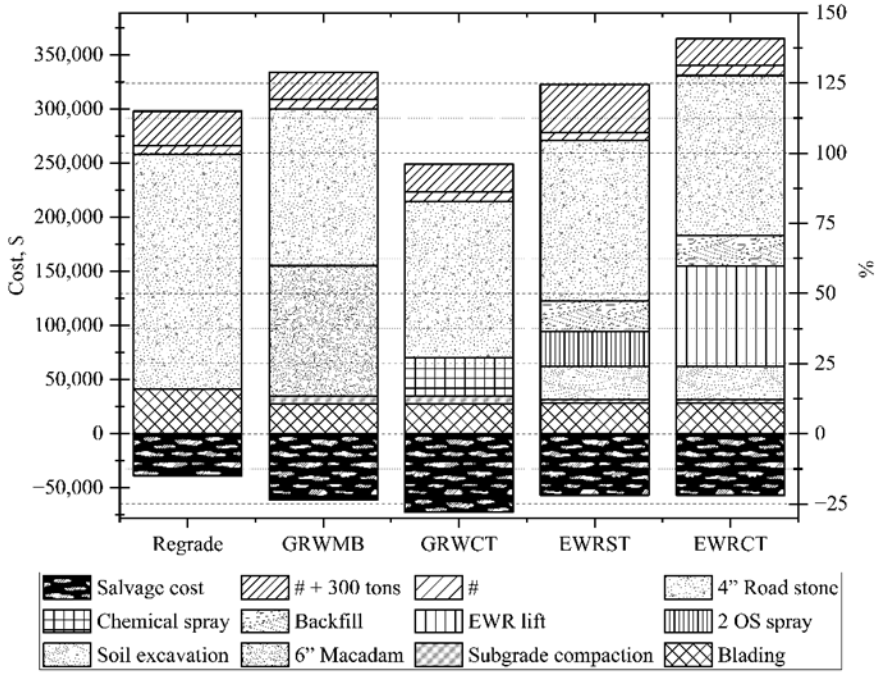

Figure 5.12: Breakdown of different activities leading to cost ($).
= Blade twice, # + 300 tons = blade twice plus add 300 tons of roadstone

5.6.3 Spend-Based Normalization of Environmental Impacts

This study explores a spend-based approach, where GWP emissions are converted to carbon tax and added to the present net value. This approach could be a standardized approach easily applicable to governmental agencies' policies. From the above analysis, the best alternative from an environmental perspective is the GRWCT with 97,862 kg CO_2 eq. Using a 185 US$/t CO_2 eq, its financial cost is about $15,364. This corresponding NPV cost is $176,309. Hence, the cost of the spend-based approach is $191,674, and the environmental impacts account for 9% of the total life cycle cost (Table 5-5).

Regrade is the typical gravel pavement method used in Iowa, but in terms of environmental impact and cost-effectiveness, this technique is outperformed by GRWCT only. However, the perception is that other methods, such as engineered water-repellent treatments and GRWMB, might be better for field applications, disregarding the results obtained in this analysis. In fact, these methods require less frequent maintenance and offer improved road conditions, which engineers and road users prefer.

Table 5-5: Integration of LCA and LCCA through the spend-based approach.

	Option	1st alternative	2nd alternative	3rd alternative	Worst option
LCA	GRWCT	EWRCT	EWRST	Regrade	GRWMB
GWP, (kg CO_2 eq)	97,862	106,869	107,014	119,891	132,975
157 US$/ton CO_2 eq ($)	18,104	19,771	19,798	22,180	24,600
% increase of best option	0%	9%	9%	23%	36%
LCCA	GRWCT	Regrade	EWRST	GRWMB	EWRCT
Cost, ($)	$176,309.85	$259,134.51	$265,909.11	$273,275.44	$308,134.48
% increase	0%	47%	51%	55%	75%
Spend-based approach ($)	GRWCT	Regrade	EWRST	GRWMB	EWRCT
	194,414	281,314	285,707	297,876	327,905
Spend-based approach ($)	0%	45%	47%	53%	69%

5.7 Conclusions

This study aims to provide a thorough LCA and LCCA evaluation of different frost-resistant gravel road technologies typically used in Iowa. Additionally, this study explores the monetary normalization of environmental impacts, GWP, to create a more holistic cost with LCCA. The results of this analysis can be summarized as follows:

- GRWCT is the most sustainable and cost-effective. The traditional method, referred to as regrade, is about 45% more expensive and produces 47% more emissions than gravel roads with chemicals. GRWMB had the highest emissions, but EWRCT had the highest NPV.
- The major emission source is material transportation, which accounts for 52 to 67% of the total emissions. Due to low machinery use, material production was more critical than construction in simple gravel options like regrade and GRWCT. M&R (without associated material production and transportation) accounts for 8 to 15% of total emissions.
- Regardless of the pavement option, the primary source of emissions is associated with the 4-inch roadstone. Specifically, the 6 inches of Macadam in GRWMB accounts for 35% of emissions. In other options, chemical stabilization in GRWCT and OS-related activities in EWRCT and EWRST (OS application and soil excavation and backfill) accounted for 11% and 13% to 20%, respectively.
- The cost of raw materials and transportation constitute the most significant portion of the final NPV. Specifically, the raw material cost accounts for 67 to 80% of the NPV. Similarly, the transportation of materials represents 15 to 26% of the NPV for these same structures.
- The spend-based approach proved to be an easy technique to be implemented for linking LCA and LCCA results. However, the valuation of the environmental impacts through this methodology did not significantly affect the overall cost of the technologies evaluated in this paper. Hence GRWCT was selected as the best option, with the lowest LCCA values, and for which the LCA accounts for less than 9% of the spend-based approach.

The practical and policy implications of the findings of this paper are significant. Local governments and transportation departments should consider integrating LCA and LCCA into their decision-making processes to support sustainable infrastructure development. Moreover, low-cost performance evaluations, like the International Roughness Index (IRI), should be conducted to enhance maintenance and repair strategy selection and prediction.

In conclusion, while GRWCT offer the best balance of cost and environmental impact, ongoing research and policy adaptation are essential to advancing sustainable road construction practices.

The environmental benefits of chemical treatments extend beyond cost-effectiveness. They also contribute to reduced maintenance frequency and potentially longer road life, further lowering overall environmental impacts. Strategies such as sourcing materials locally or optimizing logistics should be considered to mitigate the significant emissions from material transportation.

While this study primarily focused on GHG emissions, future research should include a broader range of environmental indicators, such as water use, air quality impacts, and ecosystem effects, to provide a more comprehensive environmental assessment. Additionally, addressing the study's limitations, such as the potential impact of heavy farm equipment and technological advancements, could further refine the findings.

5.8 Acknowledgments

This research is sponsored by the National Science Foundation (Award #1928813 and Award #1947009) with counterpart funding from Iowa Highway Research Board. Authors also acknowledge the contributions of various Engineers and technical staff of Keokuk County Engineer.

5.9 References

AASHTO M145 (American Association of State and Highway Transportation Officials), 2021. AASHTO Soil Classification System, Washington, D.C. https://dlvn.vn/uploads/files/AASHTO%20M%20145-91%20(2021).pdf (accessed 10 July 2024).

Airfield Asphalt Pavement Technology Program (AAPTP), 2011. Life cycle cost analysis for airport pavements. AAPTP 06-06, Applied Research Associates, Inc. 100 Trade Centre Drive, Suite 200 Champaign, IL 61820. efaidnbmnnnibpcajpcglclefindmkaj/https://eng.auburn.edu/research/centers/ncat/files/aaptp/Report.Final.06-06.pdf

ASTM D2487-17 (American Society for Testing and Materials), 2017. Standard practice for classification of soils for engineering purposes (unified soil classification system), ASTM International, West Conshohocken, PA, 2017.

Azadgoleh, M. A., Mohammadi, M. M., AzariJafari, H., Santos, J., Ahmadi, A., Alavi, M. Z., & Ayar, P. 2024. A comparative life cycle assessment (LCA), life cycle cost analysis (LCCA), mechanical and long-term leaching evaluation of road pavement structures containing multiple secondary materials. Journal of Cleaner Production, 458, 142484.

BTS, 2021. National Transportation Statistics 2021 50th Anniversary Edition, Bureau of Transportation Statistics and Volpe National Transportation Systems Center, 2021, pp. 1-587. https://www.bts.gov/sites/bts.dot.gov/files/2021-12/NTS-50th-complete-11-30-2021.pdf (accessed 12 July 2024).

Ceylan, H., Kim, S,. 2021. Iowa Granular Road Structural Design Tool. Iowa Highway Research Board (IHRB). https://intrans.iastate.edu/research/in-progress/iowa-granular-road-structural-design-tool/#:~:text=Considering%20the%20lack%20of%20granular%20road%20structural%20design (accessed 13 July 2024)

FHWA, 2014. FHWA Order 5520 - Transportation System Preparedness and Resilience to Climate Change and Extreme Weather Events. https://www.fhwa.dot.gov/legsregs/directives/orders/5520.cfm. (accessed 10 July 2024).

FHWA, 2015. Gravel roads: Construction & maintenance guide. US Department of Transportation, Federal Highway Administration, United States. FHWA-OTS-15-002 https://www.fhwa.dot.gov/construction/pubs/ots15002.pdf (accessed 12 July 2024).

FHWA, 2024. FHWA Highlights Efforts to Reduce Pollution, Combat Climate Change, and Improve Resiliency in Communities Nationwide. https://highways.dot.gov/newsroom/fhwa-highlights-efforts-reduce-pollution-combat-climate-change-and-improve-resiliency. (accessed 10 July 2024).

IowaDOT, 2021. Roads, Streets, And Bridges. https://iowadot.gov/about/roads. (accessed 10 July 2024).

IowaDOT, 2022. Iowa miles of rural secondary roads as of January 1, 2022 (2023rd ed., p. 105). The Iowa Department of Transportation's Office of Analytics Bureau. https://iowadot.gov/analytics/pdf/Secondary-Road-Report-2024.Pdf#:~:text=management-system/secondary-road-miles%20.%20The%20Iowa%20Department%20of%20Transportation%E2%80%99s%20(Iowa (accessed 13 July 2024).

IowaDOT, 2024. General supplemental highway and bridge construction specifications, GS-23002, Iowa Department of Transportation, Ames, Iowa., 2024. https://iowadot.gov/specifications/General-Supplemental-Specifications-GS/2023 (accessed 9 September 2024)

Qiao, Y., Wang, Z., Meng, F., Parry, T., Cullen, J., & Liu, S. 2022. Evaluating the economic and environmental impacts of road pavement using an integrated local sensitivity model. Journal of Cleaner Production, 371, 133615.

Rennert, K., Errickson, F., Prest, B. C., Rennels, L., Newell, R. G., Pizer, W., ... & Anthoff, D., 2022. Comprehensive evidence implies a higher social cost of CO2. Nature, 610(7933), 687-692. https://doi.org/10.1038/s41586-022-05224-9

US Army Corps of Engineers [USACE], 1965. Soils and geology: Pavement design for frost conditions. Washington, DC.

Walls, J., Smith, M., 1998. Life-cycle cost analysis in pavement design: in search of better investment decisions. US Department of Transportation, Federal Highway Administration. FHWA-SA-98-079.

Yan, T., Marasteanu, M., Turos, M., Barman, M., Manikavasagan, V., & Chakraborty, M. 2023. Cost Estimate of B vs. C Grade Asphalt Binders (No. MN 2023-19). Minnesota. Department of Transportation. Local Road Research Board.

ENVIRONMENTAL AND ECONOMIC ASSESSMENT OF ENGINEERED WATER REPELLENCY FOR FROST MITIGATION IN LOW-VOLUME FLEXIBLE PAVEMENTS IN MINNESOTA

Abstract

Engineered Water Repellency (EWR) using organosilanes provides a promising approach for mitigating frost heave by preventing ice lens formation. This study evaluates the environmental and economic impacts of typical flexible pavement structures used in Minnesota, as well as three EWR-treated variants. Primary data for the Life Cycle Assessment were collected from MnDOT and MnROAD and analyzed with the FHWA LCA PAVE tool. The LCCA was performed with the MnDOT tool to calculate the Net Present Value (NPV) per the ISO 15686-5 standard. The MnDOT Soil Replacement Method (SRM) with EWR emerged as the most sustainable and cost-effective, showing a 23% reduction in global warming potential (GWP) compared to the traditional SRM. The primary sources of emissions and expenses were Hot Mix Asphalt (HMA) activities, accounting for 58-71% of the total. The LCA contributed less than 8% to the overall integrated cost, underscoring the predominance of LCCA in decision-making. Further field evaluations are recommended to confirm the long-term performance of EWR technologies and optimize their integration into pavement design.

Keywords: Engineered Water Repellency, Frost Mitigation, Life Cycle Assessment, Life Cycle Cost Analysis (LCCA), Flexible Pavements

5.10 Introduction

Frost action presents a significant challenge due to its non-uniform nature, resulting in patchy damage. This differential frost heaving can be attributed to various factors, including the instability of the freezing process, variability in the Frost Susceptibility Soil (FSS), moisture availability, thermal regime fluctuations, and surface topography (Peterson & Krantz, 2003; Dore & Zubeck, 2009). It affects all types of pavements, even those subjected to low traffic loads, which are common in cold regions and typically consist of traditional hot-mix asphalt, cold mixes, surface treatments, and gravel surfaces (Dore & Zubeck, 2009; Salour & Erlingsson, 2012). Various testing methods, such as California Bearing Ratio (CBR) tests (Janoo, 2002), back-calculated modulus (Ovik et al., 2000, Saarelainen & H. Gustavsson, 2001), and Falling Weight Deflectometer (FWD) tests (Saarelainen & H. Gustavsson, 2001), have been used to assess capacity losses, which have shown losses ranging from 20% to 60%, depending on soil properties and other factors (pavement structures, temperature, subsurface drainage). This leads to significant load-induced damage, often 1.5 to 3 times the average annual damage, with more deterioration during thawing (Janoo & Berg, 1990; White & Coree, 1990). Also, various researchers have noted that 90% of fatigue damage (Dore & Savard, 1998) and 60 to 75% of permanent deformation (Zhang & Macdonald, 1999) occurs during thaw periods. An AASHO road test revealed that 60% of pavement failures happen during the spring (White & Coree, 1990). Another study found that the "loss of stiffness relative to summer modulus" was substantial for granular base, subbase, and subgrade soil (St-Laurent & M. Roy, 1995).

Research has shown that frost action is the most severe environmental factor affecting pavement performance, leading to changes in the International Roughness Index (IRI) over time compared to non-frost-affected pavements (Oman et al., 2018). Current design standards include inherent measures to mitigate such environmental impact through subsurface drainage, granular material depths beyond structural design requirements, and subgrade preparation or excavation and replacement with select grading materials (AASHTO, 1993; USACE, 1984). Hence, in 1994, MnDOT began considering frost treatment and the use of “frost-free” material (FFM), and by 1995, MnDOT had established minimum FFM depths

of 30 and 36 inches for Hot Mix Asphalt (HMA) pavements, depending on traffic volume, which is still in effect today (Oman et al., 2018; MnDOT, 2019).

Some design approaches utilize non-frost-susceptible materials within or up to the expected frost depth, combined with high-strength and durable materials that can withstand thaw-weakened periods and traffic loading (Oman et al., 2018; Christopher et al., 2006). The U.S. Army Corps of Engineers recommends non-frost-susceptible materials for flexible pavements in the top 50% of the granular unbound base. In contrast, rigid pavements should replace FSS with non-FSS equal to the slab thickness (USACE, 1984). The AASHTO 1993 guide recommends replacing FSS with one-half or more of the frost depth (AASHTO, 1993). Other studies suggest 50 to 70% of non-FSS material within the frost depth (Newcomb et al., 2010). These methods involve substantial quantities of non-FSS material, usually sandy or granular, leading to energy-intensive processes, heavy machinery, construction time, labor, and emissions. Also, the FSS removal method leads to substantial construction costs, which are feasible for high-traffic roads but uneconomical for low-volume roads. Hence, alternatives such as geosynthetics (especially wicking fabrics and geotextile) and engineered water repellency (EWR) are being developed.

This research evaluates the environmental and economic impacts of various low-volume traffic flexible pavements constructed in frost-prone areas. The pavement types evaluated include a 10-inch design meeting traffic and environmental loading requirements, labeled as CPD (Control Pavement Design). There is also a 30-inch pavement recommended by MnDOT, labeled as SRM (Soil Replacement Method), although it is excessive for traffic needs. Additionally, there is a 10-inch pavement on an EWR-modified subgrade, designed as a low-cost method to minimize frost action, referred to as EWR variants.

5.11 Test Sections and Materials

This study was modeled after test sections in Cell 2305 and 2306 at the 2.5-mile low-volume road (LVR) full-scale pavement test track of the MnROAD facility in Otsego, MN (Figure 5.13). The test site has two lanes, with only one of them subjected to traffic. The full-scale pavement test track receives approximately 32 and 36 in. of rain and snow per year, respectively, with mid-depth pavement temperatures ranging from 20°F to 90°F (Barman et al., 2013). The test loop has a design speed of 64.4 km/h (40 miles/h) and experiences about 6,000 Equivalent Single-Axle Loads (ESALs) yearly.

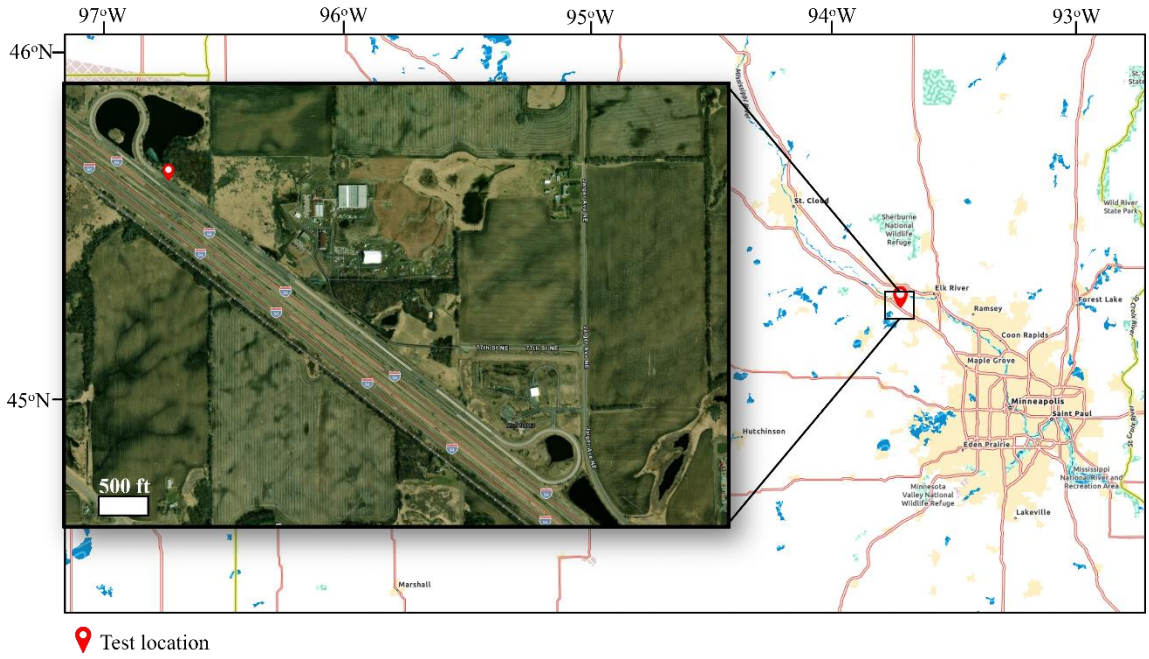

Figure 5.13: MnROAD and Cell Location Map

Figure 5.14 shows the pavement cross-section of Cell 2305, denominated Control Pavement Design or CPD. It consists of 4" of HMA and 6" of Class 6 base material sitting on the natural subgrade. The in-situ subgrade (Table 5-6) is classified as low-plasticity clay (CL) according to the Unified Soil Classification System (USCS) (ASTM D2487-17) and A-6 based on the American Association of State Highway and Transportation Officials (AASHTO) (ASTM, D3282; AASHTO M145). Based on the soil classification, it is considered an F4 based on the frost susceptibility index (USACE, 1965).

Class 6 base (Table 5-6) follows the MnDOT materials specification 3138 (MnDOT 2020). It was sourced from either Martin Marietta—Elk River South Pit or Hassan Sand & Gravel, Inc., located 15 and 9.1 miles from the test site, respectively. Hence, 12 miles were utilized for haulage distance.

The binder used in the asphalt mixture is classified as PG 58S-28. It was obtained from the Pine blend refinery, 59.2 miles from the test section. The HMA produced with such a binder contains 20% recycled asphalt pavement (RAP). Table 5-7 lists the volumetric properties of the HMA. Potholes and uneven bumps are expected in this pavement, and the maintenance and rehabilitation plan for "CDP" sections developed by the MnDOT Pavement Design Office is typically followed during its service life.

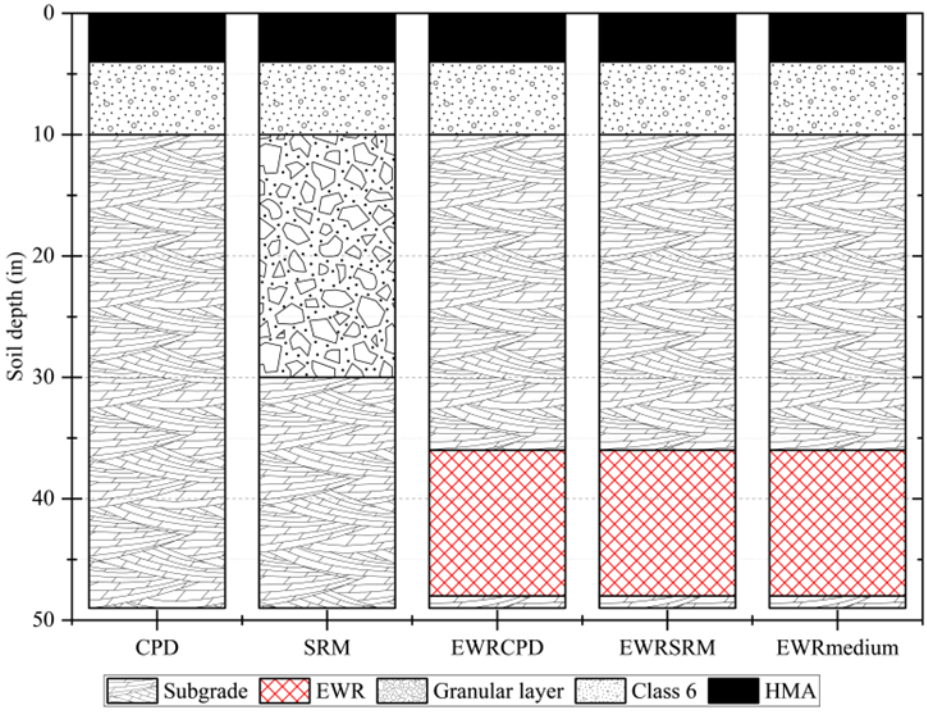

Figure 5.14: Pavement structures evaluated

Table 5-6: Subgrade and aggregate gradation.

Standard sieve no.	% Passing	
	Measured Subgrade	Specs. Limits Class 6
11/2 in	100	100
1 in	100	-
3/4 in	100	100-70
1/2 in	100	-
3/8 in	100	85-45
No.4	98.32	70-35
No. 8	91.64	-
No.10	90.64	55-20
No.40	82.5	30-10
No.60	75.37	-
No.100	66.55	-
No.140	61.563	-
No.200	57.9	7.0-3

Table 5-7: HMA volumetrics.

Item	Value
RAP (%)	20
Sand (%)	44
Granite (Crushed stone) Sand washed (%)	9
Granite (Crushed stone) unwashed (3/4) (%)	22
Granite (Crushed stone) unwashed (3/4) (%)	5
Density (lbs/ft^3)	149
New AC (%)	4.4
AC replacement (%)	19

For the purpose of this study, as shown in Figure 5.14, four alternatives have been considered:

- SRM (Soil Replacement Method) – This is another typical cross-section MnDOT utilizes for frost mitigation. The top 10” of the pavement structure have the same materials as the CPD test sections. However, the unbound base Class 6 is followed by 20” of “frost-free” granular material. This material is produced in accordance with the local technical specification 3149.2B.2, with 0-12% percent passing ratio No. 200/1 inch (MnDOT, 2020a). This pavement structure is typically assigned for traffic up to 7 million Flexible ESALs (BESALs). Hence, its performance is expected

to be better than that of the CPD structure. As such, the maintenance and rehabilitation activities follow a different pattern than CPD structures, based on the MnDOT pavement design manual, Chapter 7, (MnDOT, 2020b), hence labeled SRM.

- EWRCPD - The pavement cross-section of Cell 2306 replicates Cell 2305 down to 36" depth. At that location, the natural frost-susceptible subgrade was mixed with Terasill, a commercially available organosilane (OS) from Zydex Industries, to make the subgrade hydrophobic, i.e., water repellent. The OS is produced in India, shipped to the US in bulk, and transported to MnROAD from the nearest warehouse. The same maintenance and rehabilitation plan of the CDP section has been adopted for this alternative. Hence, this scenario has been named EWRCPD (Figure 5.14).
- EWRSRM – This scenario is similar to the previous one in terms of structure and materials, but the maintenance and rehabilitation activities follow the SRM pattern.
- EWRmedium – Likewise, pavement structure and materials are the same as the EWRCPD, but the maintenance pattern of this scenario is a mix of the one applied for SRM and the one for CPD, with patching not included in the maintenance stage.

Evaluating different maintenance and rehabilitation patterns is necessary since the EWR technology is a new approach to frost mitigation with little to no historical performance data. Table 5-8 provides details of the activities included in each maintenance and rehabilitation pattern.

Table 5-8: Maintenance and rehabilitation activities included in the study.

	CPD /EWRCPD		EWRmedium		SRM/EWRSRM	
Age	Activity	Mainline Quantity	Activity	Mainline Quantity	Activity	Mainline Quantity
0	Initial construction	Initial construction	Initial construction	Initial construction	Initial construction	Initial construction
8	Patching	10% Mainline Length	Mill Top lift and 3" overlay	100% Mainline Area	Crack treatment	16% Mainline Length
10	Mill Top lift and 3" overlay	100% Mainline Area	Crack treatment	32% Mainline Length		
12					Chip Seal	31% Mainline Length
13	Crack treatment	32% Mainline Length				
17	Chip Seal/ Patching	31% Mainline Length/10% Mainline Length	Chip Seal	31% Mainline Length		
20					Mill Top lift + ½" & Overlay Mill Thickness +1.5"	100% Mainline Area
23					Crack treatment	32% Mainline Length
27	Mill Top lift + ½" & Overlay Mill Thickness +1.5"	100% Mainline Area	Mill Top lift + ½" & Overlay Mill Thickness +1.5"	100% Mainline Area	Chip Seal	31% Mainline Length
35	End of 35-Year Analysis Period					

5.11.1 Analysis Methods

Figure 5.15 presents a graphical representation of the methodological framework adopted in this study. Primary data inputs for the LCA and LCCA modeling were gathered from MnROAD and MnDOT. FHWA LCA PAVE and MnDOT Excel-based LCCA tools were used in this study.

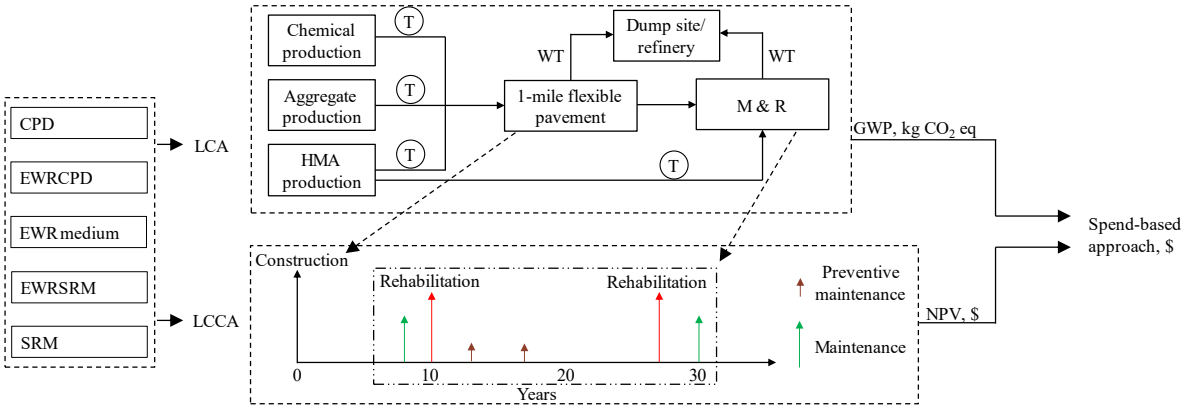

Figure 5.15: Methodological framework of the study

5.11.2 LCA Scope and System Boundaries

The functional unit for the LCA performed in this study is a 2-lane, 1-mile long, and 12-ft wide low-volume flexible pavement, with structures presented in Figure 5.14 above.

The system boundaries are presented in Figure 5.16. This study considered five life cycle stages: (1) raw material production, (2) material transportation, (3) construction, (4) maintenance, and (5) rehabilitation. The end-of-life stage is not considered. The top lift, in fact, is predicted to be reclaimed and utilized for subbase and base layers in other pavement structures, based on the growing sustainability drive by MnDOT to utilize less virgin material in road construction. Hence, the same end-of-life procedures are expected for all the scenarios considered, with the same environmental and financial impacts.

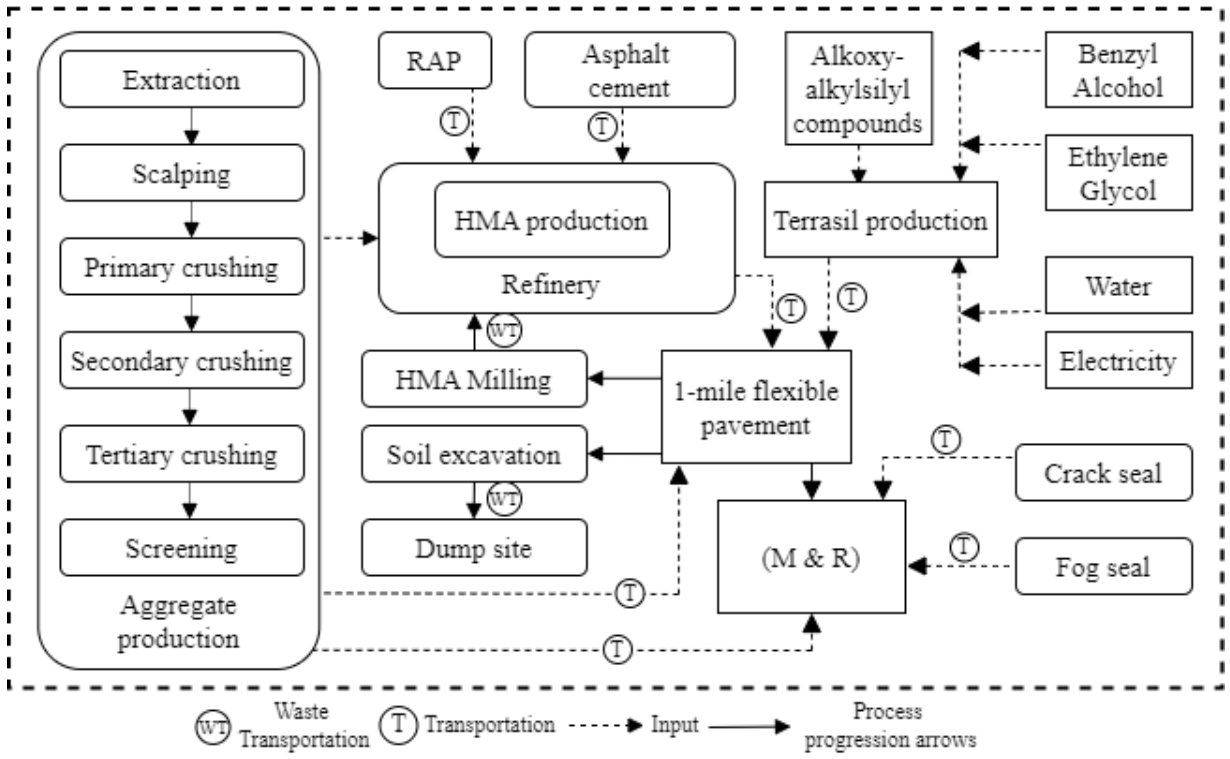

Figure 5.16: LCA system boundaries.

The analysis period is defined as 35 years because CPD and EWRCPD Cells at MnROAD were allowed to have an additional round of rehabilitation at Year 27 since the first rehabilitation was triggered by the expected reduction in international roughness index (IRI) caused by seasonal frost heave. Raw material production entails extraction and process used in all other stages (i.e., construction, maintenance, and rehabilitation). Likewise, material transportation encompasses all transportation activities for initial construction, maintenance, and rehabilitation cycles. The construction entails all equipment operation during initial construction. The maintenance stage considers preventive measures like crack treatment, chip seals for all pavement types, and small-scale repair and patching (applicable to only CPD and EWRCPD), as detailed in Table 5-8 above. Whereas the rehabilitation phase involves the reconstruction of the Mill Top lift + ½" & Overlay Mill Thickness +1.5". Supporting facilities such as streetlights, signs, drains, and structures are excluded.

5.11.3 Impact Assessment Methodology

The analysis presented in this study relied on the IPCC 2013 100a impact assessment methodology, which utilizes global warming potential (GWP) as the primary indicator to determine the environmental impacts over the 35-year analysis period. The GWP, expressed in kg CO_2 eq, measures how much a specific gaseous emission contributes to global warming relative to carbon dioxide.

5.11.3.1 Materials quantities and inventory

The LCA data utilized to model the foreground system were collected from MnROAD, MnDOT, together with the materials inventory included in the FHWA LCA PAVE tool. Quantities of HMA, aggregates, hydrophobic (OS) agents, and sealants were calculated according to the MnDOT specifications and summarized in Table 5-9. One of the main assumptions of this study concerns the environmental impacts of OS. Since no official EPD exists for this material, it was modeled as 392 kg CO_2 eq. However, to understand the impact of this assumption, a sensitivity analysis has been performed.

5.11.3.2 Transportation phase

This phase assesses the transportation of various raw (virgin aggregate and chemicals) to the construction site for initial construction, maintenance, and rehabilitation. All aggregates utilized in this study came from either Martin Marietta - Elk River South Pit or Hassan Sand & Gravel, Incorporated quarry 12 miles from the site. A 23-ton Double Bottom Dump Truck, Diesel (425 horsepower) was used, hence modeled as an off-highway truck, nonroad (300 < hp <= 600). The same truck type was utilized to transport HMA from the production plant, 59.2 miles from the site. The OS chemicals were obtained from the manufacturer's US warehouse and transported using a combination truck (diesel) to model the environmental burdens. The warehouse was 2,000 miles from the site. All equipment used in the construction was assumed to come from the contractor who constructed the model sections at MnROAD, with their equipment yard located 63.2 miles from the test site.

Table 5-9: Quantification of material used for each section (for 1-mile).

	Density (pcf)	CPD (ton)	EWRCPD (ton)	EWRmedium (ton)	EWRSRM (ton)	SRM (ton)
Material						
HMA (ton)	149	8,496	8,496	10,226	5,506	5,506
Class 6 (ton)	128	4,061	4,061	4,061	4,061	4,061
OS (ton)	69	0	15	15	15	0
Tack seal (ton)	61	14	14	13	6	6
Fog seal (ton)	79	2	2	2	5	5
Crack Sealant (ton)	75	14	14	14	11	11
Excavation						
Milled HMA (ton)	145	7,576	7,576	6,964	5,050	5,050
Subgrade (ton)	124	3,925	3,925	3,925	3,925	17,009

5.11.3.3 Construction phase

The fuel consumption of various construction machines, such as motor graders, trucks, rollers, wheel loaders, pavers, and tack trucks, causes environmental burdens during construction. All equipment utilized in this study is diesel-powered. Table 5-10 summarizes all emissions of each construction machine obtained from the FHWA LCA PAVE database.

Table 5-10: Construction equipment specification used.

Equipment	Model used (horsepower)	Equivalent Model	GWP (kg CO_2 eq) per hour
Paver	Caterpillar AP-1055D (224 hp)	Pavers, Nonroad Diesel Fuel, 175 < hp <= 300	68.71
Miller	Caterpillar PM-465 (500 hp)	Milling machine, Nonroad diesel Fuel, 300 < hp <= 600	131
Motorgrader	Moto grader 140/140 (250 hp)	Tractors/Loaders/Back hoes, Nonroad diesel Fuel, 175 < hp <= 300	25.82
Padfoot roller / Single drum roller	Bomag BW 211PD-5	Rollers, Nonroad diesel Fuel, 100 < hp <= 175	41.08
Smooth drum roller	Caterpillar CS563 (145 hp)	Rollers, Nonroad diesel Fuel, 100 < hp <= 175	41.08
Double drum steel	Caterpillar CB4.4	Rollers, Nonroad diesel Fuel, 40 < hp <= 50	15.8
Tack truck	Tack truck (200-360 hp)	Paving Equipment, Nonroad diesel Fuel, 175 < hp <= 301	71.53
Plug mill	Olympus Pugmill Plant 500TPH (100 hp)	Equipment operation, > 75 hp and < 750 hp	73.14
Road cutter	Husqvarna FS 5000d (45)	Equipment operation, > 25 hp and < 75 hp	13.83
Truck	Mack GR84F (425)	End dump truck/ off-highway truck, nonroad (300 < hp <= 600)	130

5.11.3.4 Maintenance and rehabilitation phases

Maintenance and rehabilitation routines were selected based on MnDOT pavement design office recommendations (Table 5-8). MnDOT suggests that typical preventive maintenance involves crack treatment and chip seal, while rehabilitation includes milling and overlaying. It should be noted that other routine activities, such as snow clearing, were not considered because they would be done irrespective of

pavement type. Apart from specialized equipment needed for specific activities, such as hot-applied sealant melters, air compressors, and asphalt crack-cleaning heat lances, the same equipment used in the construction phase was also adopted here. For the specialized equipment not included in the LCA PAVE database, generic equipment was used based on the specific horsepower. Materials were also modeled to come from the same source locations used in the construction phase.

5.11.3.5 Limitations of the LCA model

The analysis period of this study is 35 years, a relatively long period considering the rapid advancements in paving materials, construction equipment, power sources, and discount rates. With the ongoing shift toward sustainability, traditional diesel vehicles are expected to be partially phased out soon, leading to changes in global warming impact indicators (Qiao et al., 2022).

As mentioned above, there is a growing sustainability drive at MnDOT to utilize less virgin material in road construction. As such, one of the limitations initially recognized is relative to the limited RAP content in the HMA. Since this limitation is simple to overcome, a sensitivity analysis is presented considering different RAP contents, as indicated in Table 5-11.

Table 5-11: HMA mix ratios for different RAP contents included in the sensitivity analysis.

Item	**Value**			
RAP (%)	0	20	36	40
Sand (%)	30	44	39	25
Granite (Crushed stone) Sand washed (%)	10	9	5	13
Granite (Granite 1/2) (%)	20	0	0	22
Granite (Crushed stone) unwashed (3/4) (%)	40	22	20	
Granite (Crushed stone) unwashed (3/4) (%)	0	5	0	0
Density (lbs/ft^3)	148.5	149	149.3	156.1
New AC (%)	5.4	4.4	3.9	3.3
AC replacement (%)	0	19	28	39

5.11.4 Life Cycle Cost Analysis (LCCA)

The Life Cycle Cost Assessment (LCCA) procedure aims to determine the total economic value of a usable project segment by analyzing its initial costs and discounting future costs. Like the LCA, for which site-specific primary data were collected, the LCCA necessitates primary data, which was collected from

MnDOT and MnROAD. The analysis was carried out following the ISO 15686-5 framework and FHWA LCCA guide, summarizing the pavements' life cycle costs using Net Present Value (NPV).

The pavement cost was evaluated using the same analysis periods of 35 years of the LCA analysis. All inputs such as raw materials, construction schedule and methodology, and maintenance and rehabilitation plan used for LCA were utilized for LCCA (Walls, 1998; Airfield Asphalt Pavement Technology Program [AAPTP], 2011). The net present value (NPV) was utilized as the economic indicator to evaluate the economic impact using Equation 1 (Azadgoleh et al., 2024). NPV was selected because it utilizes a single value to specify the total cost throughout the analysis period while considering the time value of money. In this study, a conservative discount rate of 1% was considered.

$$NPV = \sum_{n=0}^{T} \left(\frac{(C_C + M_C + R_C) - Salvage\ value}{(1+d)^t} \right) \quad \text{(Equation 1)}$$

Where:

NPV = net present value of the pavement life cycle costs ($).

T = Analysis period (25 years).

t = Years after construction (year).

C_C = Construction costs in year t ($).

M_C = Maintenance cost in year t ($).

R_C = Rehabilitation Cost in year t ($).

d = Discount rate (1%).

When a road pavement reaches its service life, it will be recycled in place; hence, the remaining service life value is given by the salvage value (Equation 2) (Yan et al., 2023; Azadgoleh et al., 2024).

$$Salvage\ value = C_{Last\ Activity} \times \frac{N_{RL}}{N_{SL}} \quad \text{(Equation 2)}$$

$C_{Last\ Activity}$= Cost of the last rehabilitation activity, N_{RL}= Unused service life, in years, of the last activity at the end of the Analysis Period, and N_{SW} = Service life of the last activity in years.

5.11.5 LCA-LCCA Spend-based Integration.

A spend-based approach was utilized to integrate the LCCA and LCA calculations. This method was selected as appropriate because both LCCA and LCA employed the same data and assumptions for their respective analyses. Specifically, the GWP emissions were normalized into monetary costs by converting the GWP, in kg CO_2 eq values, to tons CO_2 eq and then assigning a price per ton of CO_2 as shown in Equation (3). A conversion rate of $185 per ton of CO_2 was used based on a study by Rennert et al. (2022). This monetary conversion enabled the integration of environmental impacts into the economic analysis. The resulting cost from the GWP emissions was then added to the calculated LCCA cost, allowing for a comprehensive assessment that incorporates both financial and environmental considerations.

The calculation for the spend-based cost is as follows:

$$Spend - based\ cost = \frac{GWP, kg\ CO_2\ eq}{1000} * \$185 \quad \text{(Equation 3)}$$

By integrating the GWP cost into the LCCA, the analysis provided a more holistic view of the project's overall impact, encompassing both economic and environmental dimensions. This approach ensures that decision-making processes consider not only the direct financial costs but also the broader environmental consequences, promoting sustainable development practices.

5.12 Results and Discussion

5.12.1 Life Cycle Assessment

Figure 5.17 shows the LCA results. The representation with primary and secondary vertical axes provides the overall GWP magnitude of the sections evaluated and the GWP values normalized based on the CPD results. Only EWRCPD had a higher emission than CPD, at +4% than the CPD option. Impacts below the CPD option were observed for SRM, EWRSRM and EWRmedium, at -3%, -25% and -8%, respectively. The high GWP obtained for CPD and EWRCPD is primarily due to the additional mill and overlay, and patching activities performed in both sections following the maintenance and rehabilitation pattern in Table 5-8.

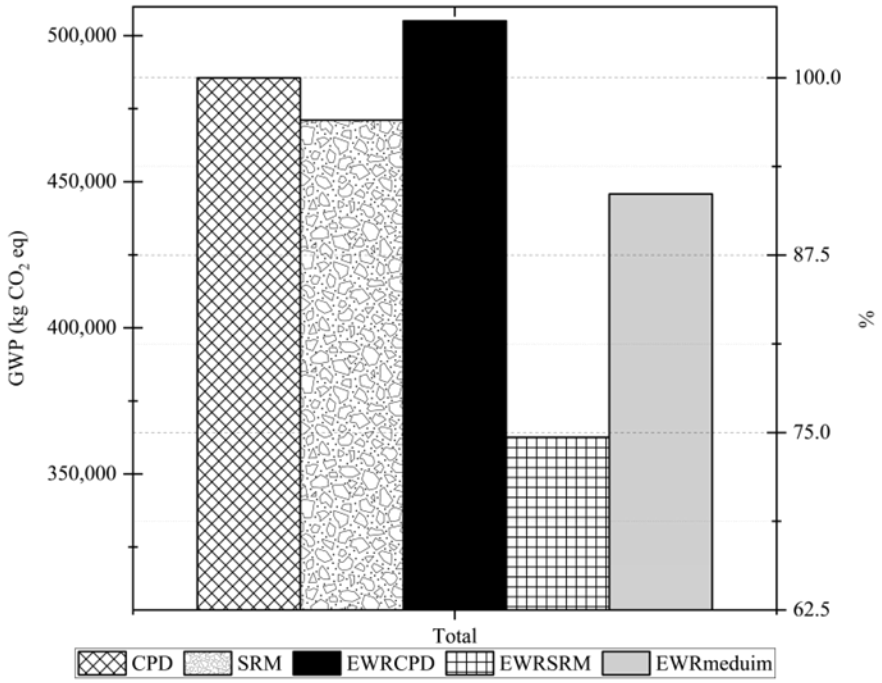

Figure 5.17: Normalized impact indicator values for each alternative to the soil replacement method

Figure 5.18 shows the breakdown of GWP emissions by life stage. Material production accounts for 55% to 69% of the total emissions, followed by material transportation at 11% to 20%. Specifically, material production accounts for 259,407 kg CO_2 eq (55%) in SRM, 241,973 kg CO_2 eq (67%) in EWRSRM, 307,983 kg CO_2 eq (69%) in EWRmedium, 328,905 kg CO_2 eq (66%) in EWRCPD, and 316,199 kg CO_2 eq (65%) in CPD. During the construction phase, the SRM section shows the highest GWP emissions at 89,176 kg CO_2 eq, while the CPD had the lowest at 42,921 kg CO_2 eq. Throughout their service

life, the production of a single 2-inch lift of HMA at 50,839 kg CO_2 eq is the main source of GWP, which makes up 10%, 11%, 10%, 14%, and 11% of CPD, SRM, EWRCPD, EWRSRM, and EWRmedium's total emissions, respectively. The combined activities for a single 2" lift of HMA (59,180 kg CO_2) account for 12% to 16% of the total emissions in all cases. In total, the HMA-related activities up to the construction stage contribute 122,727 kg CO_2 eq, making up 24-34% of the emissions. The second major source of emissions is found in the rehabilitation stage, with the material production for a 3" HMA overlay contributing 76,545 kg CO_2 eq (16% in SRM and CPD, 21% in the EWRSRM, 15% in EWRCPD, and 17% in EWRmedium). The breakdown of GWP emissions in Figure 5.19 shows that HMA activities account for more than 50%, regardless. Additionally, the 6" Class 6 base layer contributes 28,586 kg of CO_2 eq, with 16,623 kg CO_2 eq coming from its transportation to the site. Furthermore, chip seal contributes 22,728 to 45,456 kg CO_2 eq, while crack treatment contributes 8,880 to 11,574 kg CO_2 eq (2 to 3% of the overall emissions). Also, HMA milling accounts for 16,914 kg CO_2 eq (3 to 5% of the total emissions) across all cases.

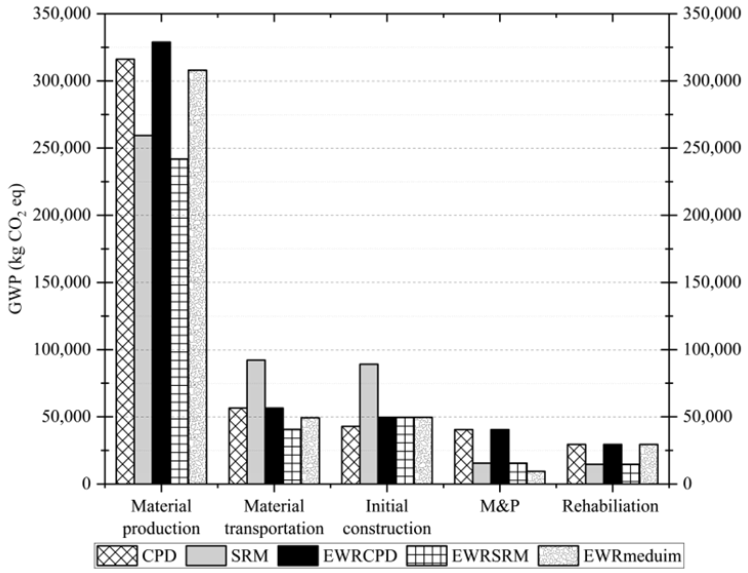

Figure 5.18: GWP breakdown by life cycle.

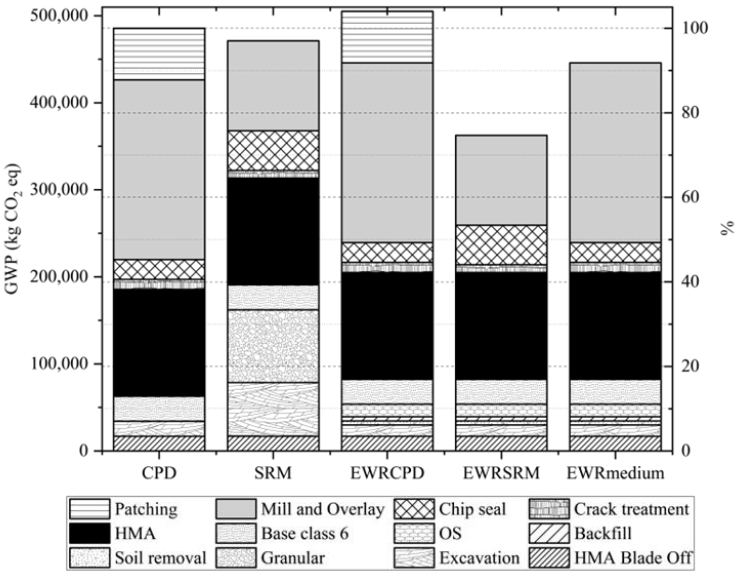

Figure 5.19: Breakdown of different activities leading to GWP (kg CO2 eq)

A 20-inch excavation contributes about 61,723 kg CO_2 eq, with 56,141 kg CO_2 eq coming from material haulage. Additionally, the input of granular material adds 83,546 kg CO_2 eq, with 51,544 kg CO_2 eq from material transportation. During the construction of the EWR variants, the use of OS accounts for 14,431 kg CO_2 eq (5,880 kg CO_2 eq from material production), assuming a global warming impact indicator (GWII) of 392 kg CO_2 eq. A GWII value of about 3,000 kg CO_2 eq for OS results in an increase in material production and an overall emission of 39,120 kg CO_2 eq. This increases OS's total contribution from less than 4% to about 9-13%. For the EWR variant methods, soil removal and later backfilling account for 4,414 and 4,867 kg CO_2 eq, respectively. Furthermore, the disposal of the 6" excavated material, including transportation, accounts for 13,090 kg CO_2 eq.

The rehabilitation stage contributes 22% (103,257 kg CO_2 eq) of the total GWP in SRM and 28% in EWRSRM. In other cases, the rehabilitation stage accounts for 41-47% (206,514 kg CO_2 eq) of the total GWP. Material production for rehabilitation makes up 77% (158,374 for the CPD rehabilitation plan and 79,187 kg CO_2 eq for the SRM rehabilitation plan) of total rehabilitation outputs, with material transportation at 9% and construction operation at 7% for all cases. In the maintenance stage, material production accounts for 48% (45,142 kg CO_2 eq) of the GWP in the CPD and EWRCPD cases and about 71% (24,220 to 37,397 kg CO_2) in other cases. Maintenance material production represents 8-11% of the

entire GWP emissions. The primary material driving GWP in the maintenance stage is chip seal, followed by crack sealants, while fog seal contributes little. Construction (equipment operation onsite), on average, accounts for 29% of the GWP in the maintenance stage.

This study evaluated the impact of different RAP contents in HMAs. As expected, the use of HMAs with no RAP results in a GWP emission increase of 30,876 to 47,326 kg CO_2 eq. A single 2-inch lift of HMA led to an emission increase of 8,984 kg CO_2 eq when comparing 0% RAP to 20% RAP (actually used at MnROAD). Additionally, for the 3-inch HMA overlay, the emission increased by 12,908 kg CO_2 eq. While the preferred RAP inclusion is 20%, some mixes meeting the minimum requirements incorporated higher AC replacement, such as 36% and 40% RAP inclusion. These mixes (see Table 5-11) (36% and 40% RAP) reduced total emissions across all cases by an average of 5% and 9%, respectively, as shown in Figure 5.20.

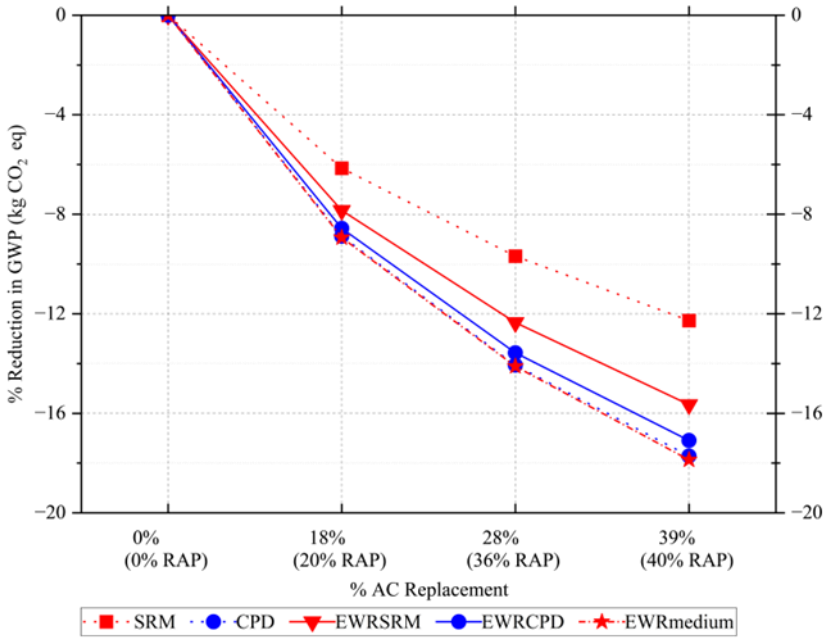

Figure 5.20: Direct contribution to GWP of different RAP contents

5.12.2 Life Cycle Cost Analysis

Figure 5.21a shows the total cost and breakdown of the various activities leading to the NPV of all cases pegged to CPD. EWRSRM had the lowest NPV compared to others, particularly EWRCPD. Furthermore, only EWRSRM and SRM were cheaper than the CPD due to lower maintenance and rehabilitation costs. EWRCPD and EWRmedium are the two most expensive, mainly because of higher construction costs and the two HMA overlays utilized during rehabilitation activities. The CPD section has the lowest initial construction cost of $550,521, accounting for 56% of the total cost, but is the most expensive to maintain. The initial construction cost of the EWR variants was $730,207, accounting for 63%, 73%, and 80% of the total cost of EWRCPD, EWRmedium, and EWRSRM, respectively (Figure 5.21b). The maintenance and rehabilitation plan costs $510,879 for the CPD, $348,351 for the EWRmedium, and $202,559 for SRM.

The EWRCPD, CPD, and EWRmedium have a salvage cost of -$74,134, while all other cases have -$22,089. The asphalt layer used during initial construction was the main cost driver across all cases ($360,886), accounting for 37%, 31%, 36%, 40%, and 38% of the total cost. Overall, HMA-related activities, including patching and overlay, account for $700,362 in CPD, EWRCPD, and EWRmedium, accounting for 71%, 60%, and 70%, respectively. In SRM and EWRSRM, HMA related activities cost $548,646, accounting for 60% and 58%, respectively. Across all cases, the class 6 base layer accounts for 10% of the cost, while initial milling accounts for less than 7%. In the EWR variants, OS-related activities, including purchasing, transportation, site construction, and application, added $141,008. In the SRM, the FFM granular material costs $111,329.19, accounting for 14% of the total. Overall, the findings suggest that EWRSRM is the most cost-effective option due to its lower initial construction, maintenance, and rehabilitation costs, making it a promising alternative to traditional methods. However, further field applications are recommended to validate and optimize this method and include actual maintenance and rehabilitation plans based on performance.

a

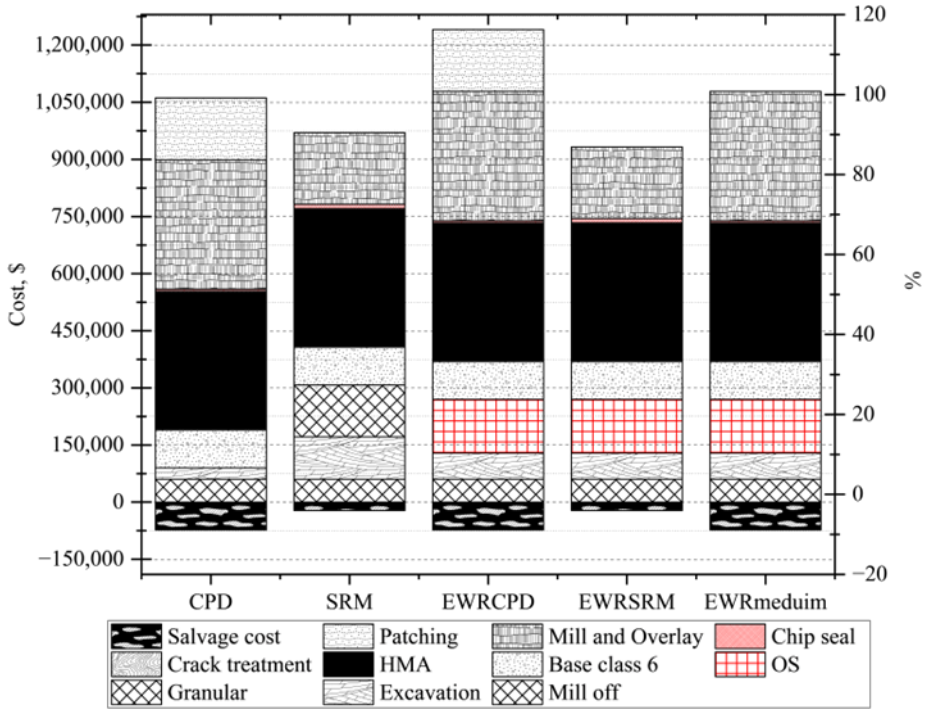

b

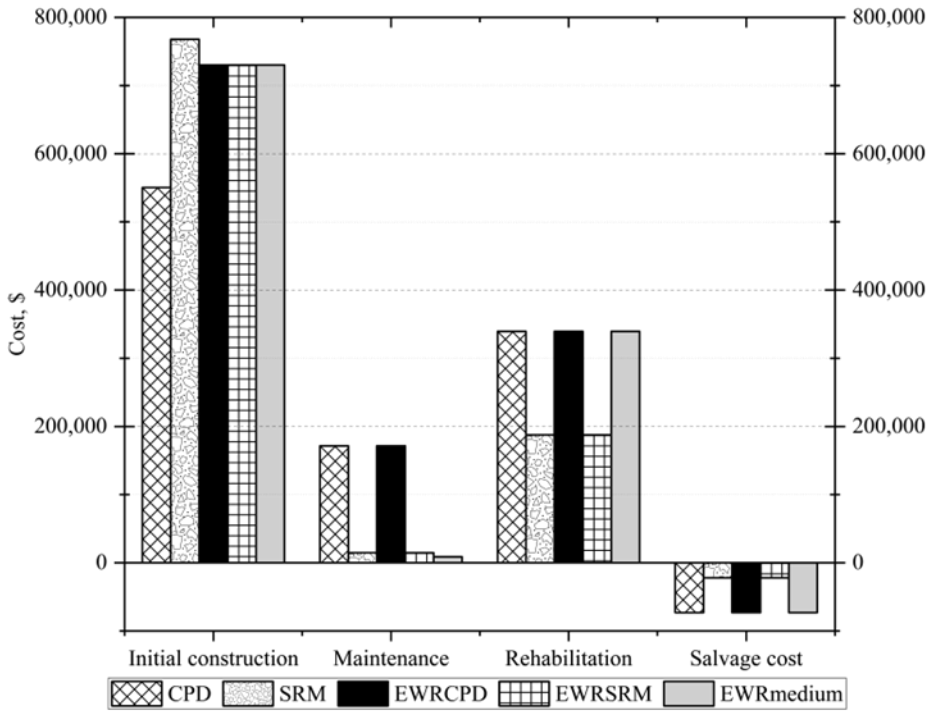

Figure 5.21: Breakdown of different activities leading to cost ($), b) LCCA Net Present Values (NPVs) results.

5.12.3 Spend-based Normalization of Environmental Impacts

This study used the spend-based approach to convert carbon tax the GWP values obtained through LCA evaluation and add them to the LCCA NPV. This approach was utilized as it is a simple, standardized approach that can be easily applied and modified as carbon tax changes in the future. From the analysis in Table 5-12Based on the carbon tax, the best alternative is the EWRSRM, with a GWP of 362,620 kg CO2 eq converted into $67,085 using 185 US$/t CO2. The corresponding NPV with integrated GWP equivalent monetized impact is $977,762. Hence, monetizing LCA results accounts for 6% of the total cost. From an overall cost point of view, the best option is the EWRSRM.

Table 5-12: Integration of LCA and LCCA through the spend-based approach.

	Best option	1st alternative	2nd alternative	3rd alternative	Worst option
LCA	EWRSRM	EWRmedium	SRM	CPD	EWRCPD
GWP, (kg CO_2 eq)	362,620	445,844	471,087	485,573	505,045
185 US$/t$CO_2$ eq ($)	67,085	82,481	87,151	89,831	93,433
% increase	0	23	30	34	39
LCCA Cost, ($)	EWRSRM	SRM	CPD	EWRmedium	EWRCPD
	910,677	948,332	988,263	1,005,422	1,167,950
% increase	0	4	9	10	28
Spend-based approach ($)	EWRSRM 977,762	SRM 1,035,483	CPD 1,078,094	EWRmedium 1,087,903	EWRCPD 1,261,383
% increase	0	6	10	11	29

5.13 Conclusions

The present study provides a thorough LCA and LCCA evaluation of different frost-resistant flexible pavements in Minnesota. Additionally, this study explores the monetary normalization of environmental impacts, GWP, to create a more holistic connection with LCCA results.

The key takeaways can be summarized as follows:

- EWRSRM is identified as the most sustainable and cost-effective method. The traditional soil replacement method (SRM) is approximately 4% more expensive and produces 30% more emissions than EWRSRM, assuming it performs as the SRM section during the service life.
- EWRCPD exhibited the highest emissions and the highest Net Present Value (NPV)
- Material production is the primary source of GWP emissions, accounting for 55% to 69% of total emissions, followed by 11% to 20% of material transportation. The primary emission source is HMA-related activities, contributing 58% to 71% of the total emissions.
- OS-related activities account for 10% of the total emissions in EWR variants. while FFM-related activities in SRM, including excavation and granular material, account for 30% of its emissions.
- Maintenance and rehabilitation activities, including associated material production and transportation, account for 33% (in SRM) to 62% (in CPD) of total emissions.
- OS-related activities account for 14% of the total cost, while FFM-related activities in SRM, including excavation and granular material, account for 14% of the total cost.

M&R accounts for 21% of the cost in SRM and 52% in CPD. A well-performing EWR variant using an SRM M&R plan would utilize 22% of the total cost for M&R, while an EWR variant mimicking a 10-inch pavement would require 43% of the total cost for M&R.

Similar to the LCA results, the HMA-related activities account for the most significant portion of the final NPV, accounting for 71% in CPD, 60%, and 70% in EWRCPD and EWRmedium, respectively. All HMA activities in EWR and EWRSRM account for 60% and 58%, respectively.

The spend-based approach did not impact the overall cost of all options since the LCA accounts for less than 6% of the spend-based approach.

Future research efforts should prioritize the collection of long-term performance data for the various pavement sections, particularly to validate the hypothesized maintenance and rehabilitation activities. Additionally, expanding the application of EWR variants in different climatic and traffic conditions will help to refine these methods and improve the accuracy of environmental and economic impact assessments in life cycle cost analysis. While the spend-based approach demonstrated minimal effects on the net present value, it is crucial to explore other methods for monetizing environmental impacts to enhance the comprehensiveness and applicability of sustainability assessments in pavement design.

5.14 References

AASHTO M145. (2021). AASHTO Soil Classification System," American Association of State and Highway Transportation Officials, Washington, D.C.

Airfield Asphalt Pavement Technology Program (AAPTP), 2011. Life cycle cost analysis for airport pavements. AAPTP 06-06, Applied Research Associates, Inc. 100 Trade Centre Drive, Suite 200 Champaign, IL 61820. efaidnbmnnnibpcajpcglclefindmkaj/https://eng.auburn.edu/research/centers/ncat/files/aaptp/Report.Final.06-06.pdf

American Association of State Highway and Transportation Officials. 1993 "AASHTO Guide for Design of Pavement Structures," Washington, D.C.

ASTM D2487-17. (2017) Standard practice for classification of soils for engineering purposes (unified soil classification system). ASTM international, West Conshohocken, PA.

ASTM D3282 – 24. (2024). Standard practice for classification of soils and soil-aggregate mixtures for highway construction purposes. West Conshohocken: American Society for Testing & Materials, 3282.," West Conshohocken, PA 19428-2959. United States.

Azadgoleh, M. A., Mohammadi, M. M., AzariJafari, H., Santos, J., Ahmadi, A., Alavi, M. Z., & Ayar, P. 2024. A comparative life cycle assessment (LCA), life cycle cost analysis (LCCA), mechanical and long-term leaching evaluation of road pavement structures containing multiple secondary materials. Journal of Cleaner Production, 458, 142484.

Barman, M., Dufalla, N., Li, Z., Mu, F., and Vandenbossche, J. M. (2013). Development of a rational mechanistic-empirical based design guide for thin and ultra-thin whitetopping., Climatic Considerations University of Pittsburgh Department of Civil and Environmental Engineering Pittsburgh, Pennsylvania 15261. Prepared for: FHWA Pooled Fund Project: TPF-5-165., 2013.

Christopher, B. R., Schwartz, C. W., Boudreaux, R., & Berg, R. R. (2006). *Geotechnical aspects of pavements* (No. FHWA-NHI-05-037). United States. Federal Highway Administration.

Doré, G., and Savard. Y. (1998). Analysis of seasonal pavement deterioration. In Transportation Research Board of the National Academies Preprint No. 981046, Washington, D.C.

Doré, G., & Zubeck, H. K. (2009). *Cold regions pavement engineering*. McGraw-Hill Professional and ASCE Press

Federal Highway Administration. (2105). Gravel roads: Construction & maintenance guide., US Department of Transportation, United States.

Janoo, V. C. (2002). Performance of base/subbase materials under frost action. In *Cold Regions Engineering: Cold Regions Impacts on Transportation and Infrastructure* (pp. 299-310).

Janoo, V. C., & Berg, R. L. (1990). Thaw weakening of pavement structures in seasonal frost areas. *Transportation Research Record*, (1286).

MnDOT. (2019). MnDOT Pavement Design Manual Chapter 4: HMA (Hot-Mix Asphalt). Minnesota Department of Transportation., 2019.

MnDOT. (2020). MnDOT standard specifications for construction., 2020 Edition, Volume 1," 2020.

MnDOT. (2019). MnDOT Pavement Design Manual: Chapter 3: Pavement Subsurface, Minnesota Department of Transportation, 2019.

MnDOT. (2019). MnDOT Pavement Design Manual: Chapter 7: Project-Type Selection, Minnesota Department of Transportation.

Newcomb, D., Willis, R., and Timm, D. H. (2010). Perpetual Asphalt Pavements, A Synthesis. Asphalt Pavement Alliance, Lanham, MD.

Oman, M. S., Lund, N. G., & Intertec, B. (2018). *Designing base and subbase to resist environmental effects on pavements* (No. MN/RC 2018-06). Minnesota. Dept. of Transportation. Research Services & Library.

Ovik, J. M., Birgisson, B., & Newcomb, D. (2000). Characterizing seasonal variations in pavement material properties for use in a mechanistic-empirical design procedure, Mn/DOT 2000-35, Minnesota Department of Transportation. https://hdl.handle.net/11299/701

Qiao, Y., Wang, Z., Meng, F., Parry, T., Cullen, J., & Liu, S. 2022. Evaluating the economic and environmental impacts of road pavement using an integrated local sensitivity model. Journal of Cleaner Production, 371, 133615.

Peterson, R. A., & Krantz, W. B. (2003). A mechanism for differential frost heave and its implications for patterned-ground formation. *Journal of Glaciology*, *49*(164), 69-80.

Rennert, K., Errickson, F., Prest, B. C., Rennels, L., Newell, R. G., Pizer, W., ... & Anthoff, D. (2022). Comprehensive evidence implies a higher social cost of CO2. *Nature*, *610*(7933), 687-692.

Saarelainen, S. and Gustavsson, H. (2001). Thaw weakening of subgrades in Finland, in In International Conference on soil mechanics and geotechnical engineering (pp. 2183-2186).

Salour, F., & Erlingsson, S. (2012). Pavement structural behaviour during spring thaw. *Swedish National Road and Transport Research Institute, Linköping, Sweden*.

St-Laurent, D., & Roy, M. (1995). *Evaluation structurale de chaussees souples dans un contexte climatique nordique*. Universite Laval.

U.S. Army. (1965). Soils and geology: Pavement design for frost conditions., US Army Corps of Engineers, Washington, DC.

U.S. Army Corps of Engineers. (1984). Pavement Criteria for Seasonal Frost Conditions, , EM 1110-3-138.

Walls, J. (1998). *Life-cycle cost analysis in pavement design: in search of better investment decisions*. US Department of Transportation, Federal Highway Administration.

White, T. D., & Coree, B. J. (1990). Threshold pavement thickness to survive spring thaw. Third international conference on bearing capacity of roads and airfields. Proceedings, Norwegian Institute Of Technology, Trondheim, Norway, July 3-5 1990. Volumes 1-2. *Publication of: tapir* publishers.

Yan, T., Marasteanu, M., Turos, M., Barman, M., Manikavasagan, V., & Chakraborty, M. 2023. Cost Estimate of B vs. C Grade Asphalt Binders (No. MN 2023-19). Minnesota. Department of Transportation. Local Road Research Board.

Zhang, W., & Macdonald, R. A. (1999). The Danish Road Testing Machine 1995–2000. In *Proceedings of the International Conference on Accelerated Pavement Testing*. Danish Road Institute.

CHAPTER 6: CONTRIBUTIONS AND RECOMMENDATIONS FOR FUTURE WORK

Research contributions

This dissertation has addressed key considerations for the field application of engineered water repellency (EWR), providing answers to questions frequently posed by stakeholders. These include the impact of organosilane (OS) treatment on the compaction curve, simplified design approaches, performance in resisting water pressure, and durability under extreme conditions. The research effectively addresses several field-related challenges, and the key contributions are summarized as follows:

Chapter 3: Performance Evaluation of Hydrophobic Soils

Article 1: Factors Affecting the Water Resistance of Frost-Susceptible Hydrophobic Soils

This study examines how soil density and clay content influence the water resistance of EWR-treated soils. Results indicate that increasing soil density can boost breakthrough pressure (BP) by up to three times compared to loose soils. Dense soils prevent preferential flow, making them ideal for field applications, as water must penetrate through compacted layers. Once BP is reached, water infiltration increases progressively. Loose soils, under similar water pressure, absorb more water than dense soils. Higher confining pressures further reduce voids and porosity, increasing BP. A 1.5-fold increase in clay content leads to a threefold increase in BP. Additionally, BP rises with increased molding moisture content until Maximum Dry Density (MDD) is achieved. However, higher loading rates reduce BP, suggesting a diminished ability to resist breakthrough under rapid pressure. EWR-treated soils demonstrated resistance to low hydrostatic pressures below BP for prolonged periods, but after repeated testing and soaking, BP values dropped significantly. After seven cycles of testing, BP reduced by 89%, and following seven days of soaking, it decreased by 81%. This reduction is attributed to microstructural changes in the soil, increased porosity, and the aggressive testing conditions unlikely to be encountered in the field.

Article 2: Investigation of the Compressive Strength of Engineered Water-Repellent Soils Under Varying Environmental Conditions

This study evaluates the hydrophobicity and mechanical strength of EWR-treated soils under different environmental conditions. EWR-treated soils showed contact angles greater than 90°, effectively resisting short-term water infiltration. These soils maintained their physical structure for extended periods, delaying water penetration. However, after 120 days of water exposure under a 30 mm water head, water infiltrated the samples due to increased porosity and crack formation. The OS-treated soils displayed favorable compaction properties, with lower Optimum Moisture Content (OMC) and minimal changes to MDD. Nonetheless, higher OS concentrations reduced mechanical strength, attributed to the organic components of OS that lower shear resistance. While moisture resistance improved, this reduction in strength may limit EWR applications in environments requiring high compressive strength. EWR samples exhibited greater resilience to wet-dry cycles, showing less degradation than untreated soils. The durability tests revealed that prolonged water exposure and repeated wet-dry cycles increased porosity and water absorption, leading to cracks and reduced water resistance over time.

Chapter 4: Field Evaluation of Engineered Water Repellency.

Article 3: Translating Laboratory Water Repellency Tests to Field Design: Developing a Capillary Break System for Frost Action Mitigation in Pavement Foundations at MnROAD

This article explores the optimization of organosilane (OS) applications for hydrophobic soil treatment under field conditions. Laboratory tests, including contact angle (CA) and breakthrough pressure (BP) testing, demonstrated that hydrophobicity ($CA > 90°$) was achieved at OS concentrations of 1:40 and higher, although soil mineralogy and fines content significantly impacted performance. The penetration depth of the OS treatment was influenced by the soil's initial moisture condition, with air-dried and oven-dried soils showing deeper OS penetration compared to soils at OMC. BP testing showed that higher OS concentrations applied via spraying resulted in better water resistance, although the penetration depth for sprayed

applications was limited to approximately 3.5 mm. In contrast, compacted samples achieved penetration depths of up to 70 mm. Field trials revealed limitations in achieving greater hydrophobic depth, as OS application volumes were capped at 227 liters for a 7.5 m by 23 m test section. The study concluded that BP values can be used to guide capillary barrier design for frost mitigation.

Article 4: Design and Construction of Engineered Water Repellency (EWR) at MnROAD

This study details the field test construction of EWR treatments for frost mitigation at MnROAD. The results indicate that while EWR impedes capillary rise, it may not fully prevent water from reaching ice lenses, particularly due to lateral moisture transport. Regardless of spray concentration, all samples achieved hydrophobicity with contact angles above 90° and effective penetration depths of approximately 7 mm. The study found that placing the EWR layer closer to the frost depth significantly reduces frost heave. For optimal performance, the deepest EWR layer should be placed at 75% of the frost depth, reducing frost heaving by 50%. While EWR limits capillary rise, side infiltration remains a challenge under certain conditions.

Chapter 5: Life Cycle Assessment and Cost Analysis of Frost Action Mitigation Methods (2 Articles)

Article 5: Comparative LCA and LCCA of Frost-Resistant Gravel Road Treatments in Rural Iowa

This study provides a comprehensive evaluation of different frost-resistant gravel road treatments using Life Cycle Assessment (LCA) and Life Cycle Cost Analysis (LCCA). Gravel roads with chemical treatments (GRWCT) emerged as the most sustainable and cost-effective option. Traditional regrade methods were 45% more expensive and generated 47% more emissions compared to GRWCT. The analysis revealed that material transportation is the largest source of emissions, accounting for 52% to 67% of the total, while raw materials contribute the most to the final Net Present Value (NPV), representing 67% to 80% of the cost.

Article 6: Environmental and Economic Assessment of Engineered Water Repellency for Frost Mitigation in Low-Volume Flexible Pavements in Minnesota

This study compares the environmental and economic impacts of various frost-resistant flexible pavements in Minnesota. EWR soil replacement methods (SRM) were found to be the most sustainable and cost-effective, producing 30% fewer emissions than traditional SRM methods, assuming similar performance over the service life. Material production, particularly related to hot-mix asphalt (HMA), was the largest contributor to global warming potential (GWP), accounting for 55% to 69% of total emissions. OS-related activities contributed approximately 10% to emissions and costs in EWR variants. The study provides important insights for optimizing the environmental and economic performance of EWR-treated pavements.

Recommendations for future research.

- For field application, many questions still need to be addressed, including optimizing organosilane (OS) to improve efficiency and reduce costs.
- Although OS-treated soils are expected to be non-leachable, further testing should include leaching experiments before and after activation to provide laboratory evidence supporting this claim.
- Drying time optimization for field applications should be explored to ensure effective EWR treatment.
- Future studies should investigate combining EWR with other methods, such as wicking fabrics, to manage near-surface moisture content more effectively.
- Additional field tests across different soil types and environmental conditions are necessary to further validate the performance and application of EWR treatments.